

Syracuse University

SURFACE at Syracuse University

Dissertations - ALL

SURFACE at Syracuse University

12-19-2022

CENOZOIC EXTENSION OF THE LAKE TANGANYIKA RIFT, EAST AFRICA: STRUCTURES, TECTONOSTRATIGRAPHY AND PALEOENVIRONMENTAL RECONSTRUCTION

Shaidu Shaban
Syracuse University

Follow this and additional works at: <https://surface.syr.edu/etd>



Part of the [Geology Commons](#), and the [Geomorphology Commons](#)

Recommended Citation

Shaban, Shaidu, "CENOZOIC EXTENSION OF THE LAKE TANGANYIKA RIFT, EAST AFRICA: STRUCTURES, TECTONOSTRATIGRAPHY AND PALEOENVIRONMENTAL RECONSTRUCTION" (2022). *Dissertations - ALL*. 1580.

<https://surface.syr.edu/etd/1580>

This Dissertation is brought to you for free and open access by the SURFACE at Syracuse University at SURFACE at Syracuse University. It has been accepted for inclusion in Dissertations - ALL by an authorized administrator of SURFACE at Syracuse University. For more information, please contact surface@syr.edu.

Abstract

Active continental rifts are ideal sites for understanding the break-up of continents, and long-lived rift lake environments are known as important reservoirs for endemic communities and biodiversity. The sedimentary fill of extensional continental rifts within the East Africa Rift System (EARS) records a long history of continental extension and variable tropical climate that is unparalleled in its duration and fidelity. Continental extensional basins are sensitive to variations caused by the interplay between tectonics, sedimentary processes, and climate change. However, to discern the sedimentary fill history and its related tectonostratigraphy, as well as for reconstructing past climate changes, high-fidelity data such as basin-scale high-resolution seismic reflection data and continuous drilling information from stratigraphic boreholes or exploratory wells are required.

Constraining the geometry of geological structures in extensional basins such as those within the EARS is important for studies of sedimentation, limnology, and hazards. Although previous studies have mapped geological structures of the Lake Tanganyika Rift in East Africa, many aspects of the geometry of the rift structures are still poorly known. Previous studies either used data with limited spatial coverage, with low resolution, or both. Much earlier rift basins of the Karoo Permo-Triassic system below the late-Cenozoic- Lake Tanganyika Rift sediments have been proposed to have acted as weak zones during the Cenozoic rifting, however this hypothesis has not before been explicitly tested.

Understanding the evolution of tectonic rift lakes is critical for studying continental breakup, recovering terrestrial climate histories, assessing hydrocarbon resources and biological evolution. Therefore, it is important to study how rift lakes evolve, interact and link in space and

time, as they are highly sensitive to tectonic processes and climate variability. For instance, recent studies speculate that in the past, Lake Rukwa flowed into Lake Tanganyika, East Africa during its high stands. Spectacular oversized deltaic prograding clinoforms, which may be linked to the outflow of Lake Rukwa, are observed in seismic reflection data within the Lake Tanganyika Rift on the Karema platform. In the absence of borehole data in this area, a numerical modelling approach may be required to test these lakes' connectivity.

Chapter 2 of this study uses recently acquired, state-of-the-art 2D seismic reflection data, together with reprocessed legacy data, to evaluate the evolution and distribution of sedimentary facies over the Lake Tanganyika Rift. Using seismic stratigraphic analysis, I reconstruct past depositional environments and the paleogeography of the lake and assess how tectonic-driven subsidence and hydroclimate variability modifies lacustrine basins. I identify six syn-rift seismic units overlying the acoustic basement and identify sedimentary units beneath the syn-rift sequence that suggest episodes of pre-rift sedimentation. This analysis suggests that the earliest - stage rift system is of low-relief that is usually dominated by alluvial, fluvial, and shallow lacustrine conditions. As the basin continued to evolve in space and time, the lacustrine environment increased in water depth, and catchment relief and accommodation increased, consistent with a more mature rift. Under these conditions, active extensional continental rifts exhibit extensive deltaic deposits and deep-water fans, and locally, canyons, channels, channel-levee complexes, turbidites, slumps and other mass flow deposits. In the latter part of continental rift lake history, erosional surfaces and abundant lowstand delta facies are observed, indicating periods of dramatic hydroclimate cycles. I assess the relative timing of key features of the rift, including the emergence of major structures and rift segment boundaries, and development of major drainages and linkages to upstream rift lakes. This study illustrates a shallow to deep

progression of rift valley environments and then restriction of littoral habitats that might have influenced the evolution of its unique endemic organisms.

Rift structures such as rift segments and accommodation zones, border faults, rift-parallel fault blocks, and transfer faults exert a first-order control on the spatial and temporal distribution of sedimentary facies and speciation of endemic species in continental rifts. The Western Branch of the EARS provides a natural laboratory to investigate how basement anisotropies assist in rupturing thick, strong continental crust in the magma-poor setting. Using the Lake Tanganyika Rift as a case study, chapter 3 of this dissertation integrates newly acquired, aeromagnetic and Full Tensor Gradiometry (FTG) data with 2-D seismic reflection data to assess the deep basin and underlying basement structure. I consider the evolution of the Kavala Island Ridge (KIR), a major rift segment boundary and assess the relationship of major structures around the KIR to inherited crustal anisotropies. Derivative-filtered aeromagnetic and gravity grids show a dominance of NW-trending structural fabrics at long wavelengths (>5km) corresponding to the deeper basement depths, and dominant NW-SE with a secondary NNE-SSW fabrics at shorter wavelengths (<3 km) representative of the shallower structures and intra-basinal structures. Long wavelength anomalies indicate that deep structures have a general NW-SE strike parallel to most of the regional basement structures. Short wavelength anomalies reveal that shallow subsurface structures are dominated by a NW-SE strike with a secondary NNE-SSW strike. The NW-SE striking structures are attributed to the inheritance of pre-existing basement structures. Seismically-constrained 2-dimensional forward modeling of the aeromagnetic and gravity data reveals: 1) an anomalously high-density (2.35-2.45 g/cc) deep-seated, fault-bounded wedge-shaped sedimentary unit that directly overlies the pre-rift basement, likely of Mesozoic rift (Karoo) origin; 2) a ~4 km-wide sub-vertical low-density (2.71 g/cc) structure within the 3.2 g/cc

basement, interpreted to be an inherited basement shear zone, 3) a large intra-basinal early-rift fault co-located with the modeled shear zone margins, defining a persistent intra-basin 'high', and 4) a shallow intra-sedimentary V-shaped zone of comparatively dense material (~ 2.2 g/cc), interpreted to be a younger axial channel complex confined between the intra-basin 'high' and border fault. The results provide insights on early-rift Tanganyika Rift architecture which was modulated by basement structure, and its influence on the subsequent rift structure. This study provides useful information for future research, especially on the evolution of juvenile rifts and how they transition into passive margins, as well as providing useful context for hydrocarbon exploration. Analysis of the stratigraphy on and around the KIR indicates that relief on the ridge was established early in rift history, and that it has been a persistent geographic boundary for much of the lifespan of Lake Tanganyika.

To test how juvenile active continental rifts and rift-lakes interact and link in space and time as they respond to slow tectonic processes and high-frequency climatic change, I employ a numerical modeling approach. In chapter 4, I integrate a FastScape algorithm that utilizes the stream power law to predict landscape evolution with the Linear Upslope Model for orographic precipitation to analyze and document the topographic evolution and hydrological connectivity of Lakes Tanganyika and Rukwa in the vicinity of the Rungwe volcano. The analysis suggests that as climate fluctuates, two active rift lakes that are in proximity and structurally linked may interact and connect, depending on the magnitude of precipitation. The models predict that Lake Rukwa overflowed into Lake Tanganyika causing the deposition of deltaic sediments along the Karema Platform. This implies that in the geologic past Lake Rukwa was a much larger lake than present; the small-sized underfilled condition of modern Lake Rukwa may be due to diminished precipitation and a regional rain shadow, produced by the growth of the Rungwe volcanic

edifice. This study provides background paleogeographic context for the LTR and Rukwa rifts and how tectonics modulates surface processes on the scale of large continental rifts, informative for understanding the origins of endemic species, water column exchanges and geo-resource exploration. However, understanding the details of changing hydrologic and water column chemistries over geologic time ultimately requires testing through scientific drilling.

To better constrain the timing nature of the identified seismic units as well as proving the hydrological connectivity between Lakes Tanganyika and Rukwa, deep scientific drilling intersecting the crystalline basement is required. Also, to prove the connectivity between Lake Rukwa to Lake Tanganyika over the past several hundred thousand years, core sampling of material from the Karema depression is required. Furthermore, to obtain a full picture of Cenozoic juvenile rifting, additional ‘infill’ multi-channel basin-scale seismic reflection or refraction data will be needed.

CENOZOIC EXTENSION OF THE LAKE TANGANYIKA RIFT, EAST AFRICA:
STRUCTURES, TECTONOSTRATIGRAPHY AND PALEOENVIRONMENTAL
RECONSTRUCTION

by

Shaidu Nuru Shaban

B.Sc., University of Dar es Salaam, 2010
M.Sc., University of Manchester, 2015

Dissertation

Submitted in partial fulfillment of the requirements for the degree of
Doctor of Philosophy in Earth Sciences

Syracuse University
December 2022

Copyright © 2022 Shaidu Nuru Shaban, December 2022
All rights reserved

Acknowledgements

We extend our acknowledgements to the Petroleum Upstream Regulatory Authority of Tanzania and the Tanzania Petroleum Development Corporation who provided an access to the commercial higher resolution 2D multichannel seismic data that were used for this study. The funds for this study were granted from Syracuse University (SU), TPDC and the NSF-supported EMPOWER Program. I would like to thank my advisor, Chris Scholz, for his courtesy, patience, guidance, and advice during my dissertation; Pete Cattaneo for all his help solving software related issues and encouragement; Liang Xue for his help solving coding related issues: Jacqueline Corbett for her help in the lab and proofreading my research work; Lachlan Wright, Nicholas Zaremaba, Laura Demott, and Nicholas Perezi for all their help in the lab. Committee members Rob Moucha, Jeffrey Karson, Christopher Junium, and Mike McGlue provided guidance, advice, criticism, and support throughout this project. Further, special thanks to all faculty, staff, and students in the department, especially Ruta Basijokaite, Amanda Campbell, Micah Wiesner, Laura Streib, McKenzie Brannon, He Ruliang, Christa Kelleher, Melissa Chipman and Greg Hoke for being a great group of people. Special thanks to my family for being so supportive, patient, and helpful during this process.

Table of Contents

Abstract	1
Acknowledgements.....	viii
Table of Contents.....	ix
List of Figures.....	xiii
CHAPTER 1: INTRODUCTION.....	1
Figures of Chapter 1.....	10
CHAPTER 2: THE STRATIGRAPHIC EVOLUTION OF THE LAKE TANGANYIKA RIFT, EAST AFRICA: FACIES DISTRIBUTIONS AND PALEO-ENVIRONMENTAL IMPLICATIONS	12
Abstract.....	13
1. Introduction.....	15
1.1. Background to the Lake Tanganyika Rift.....	16
1.1.1. Rift segmentation and structural provinces	18
1.1.2. Regional geology.....	20
1.1.3. Hydroclimate	21
1.1.4. Lake Tanganyika Rift fill	22
2. Data and methods.....	22
2.1. Data	22
2.2. Methods.....	23
3. Results.....	25
3.1. Seismic units.....	25
3.2. Central and southern basins (Kigoma, Kalemie, Marungu-Mpulungu).....	26
3.2.1. Seismic unit 1.....	26
3.2.2. Seismic unit 2.....	26
3.2.3. Seismic unit 3.....	27
3.2.4. Seismic unit 4.....	28
3.2.5. Seismic unit 5.....	29
3.2.6. Seismic unit 6.....	29
3.3. Ruzizi basin (North Lake Tanganyika Rift).....	30
3.3.1. Seismic unit 2.....	30

3.3.2.	Seismic unit 3.....	31
3.3.3.	Seismic unit 4.....	31
3.3.4.	Seismic unit 5.....	31
3.3.5.	Seismic unit 6.....	32
4.	Discussion.....	32
4.1.	Tectonic controls on evolving sedimentary facies distributions.....	32
4.2.	Hydroclimate controls on evolving sedimentary facies distributions.....	36
4.3.	The evolving paleogeography of the Lake Tanganyika Rift	40
4.4.	Model of rift basin evolution	41
4.5.	Habitat variability over time.....	43
	Conclusions.....	44
	Figures for Chapter 2	46
	Data availability	67
	Funding sources	68
	Acknowledgments.....	68
	CHAPTER 3: THE DEEP BASIN AND UNDERLYING BASEMENT STRUCTURE OF THE TANGANYIKA RIFT	69
	Key Points:.....	70
	Abstract	71
1.	Introduction	72
	Background	74
	1.1.1 The East Africa Rift System (EARS)	74
	1.1.2 Lake Tanganyika Rift	75
2.	Materials and methods	78
	2.1. Seismic interpretation.....	78
	2.2. Aeromagnetic data.....	79
	2.2.1. Reduction to the Equator	79
	2.2.2. Horizontal gradients and Total Horizontal gradients.....	80
	2.3. FTG data.....	80
	2.3.1. Rotational Invariants.....	81
	2.3.2. Upward Continuation.....	81

2.4 2.75-D Gravity and magnetic forward modeling	82
3. Data	83
3.1.1 Aeromagnetic data	83
3.1.2 Airborne-Full Tensor Gradiometry (Air-FTG®) data	84
3.1.3. 2-D Seismic reflection data	86
3. Results	86
4.1 Rift Structures	86
4.1.1 Shallow structural fabrics	87
4.1.2 Deeper structural fabrics	88
4.2 Updated fault map of the Tanganyika Rift	89
4.3 2.75-D Model of the Central Tanganyika Rift.....	89
5.Discussion	91
5.1 The Pre-rift Basement Structure Beneath the Tanganyika Rift	91
5.2 Incipient Stage of the Tanganyika Rift and the Controls of Structural Inheritance.....	92
5.2.1 The Presence of Karoo Sediments in the Kalemie-Marungu provinces	95
5.3 The Kavala Island Ridge and its implications	96
5.4 The Persistent Influence of Incipient Rift Structure on Subsequence Rift Phases	99
6 Conclusions	100
Acknowledgments	101
Data Availability Statement	102
Figures of Chapter 3.....	103
CHAPTER 4: THE PALEO-HYDROLOGIC CONNECTIVITY OF RIFT LAKES TANGANYIKA AND RUKWA, EAST AFRICA: INFLUENCE OF OROGRAPHIC PRECIPITATION."	119
Abstract	119
1. Introduction	120
1.1. The study area	124
1.1.1 The Tanganyika Rift	125
1.1.2 The Rukwa Rift.....	126
1.1.3 Hydroclimate.....	127
2. Data and methods	129

2.1 Data	129
2.2 Methods.....	129
2.2.1 Topographic analysis of the Karema depression erosion	129
2.2.2 Landscape evolution model (FastScape)	130
2.2.3 The linear model (LM) for orographic precipitation	131
2.2.4 Model setups	135
3.Results	137
3.1. Karema depression erosion	137
3.2. Precipitation distribution.....	137
3.4. Landscape evolution and hydro-connectivity	138
3.5. Lake depth evolution.....	139
3.6. Sensitivity analysis.....	139
4. Discussion	140
4.1. Karema depression erosion and incision analysis.....	140
4.2. Precipitation distribution and Rungwe Volcanic edifice	141
4.3. Hydrological connectivity of Lakes Tanganyika and Rukwa.....	144
4.4. Model limitations and further work	148
Conclusions	150
Figures for Chapter 4	152
CHAPTER 5: CONCLUSIONS AND FUTURE WORK.....	161
Data availability	167
Funding sources	167
Declaration of competing interest	168
Acknowledgements	168
Appendices.....	168
References.....	200
Vita (biographical data)	242

List of Figures

Figures for Chapter 1

Figure 1: (A) Lake Tanganyika Rift. Note five structural provinces of the rift from Ruzizi in the north to Mpulungu in the south demarcated by dashed red lines. Thick black lines represent the normal faulting trend within Lake Tanganyika, modified after Muirhead et al. (2019) (B) Inset shows the location of Lake Tanganyika within the Western Branch of the EARS. EB and WB are the Western and Eastern Branches respectively of the EARS.

Figure 2: Tanganyika-Rukwa Rift, part of the Western Branch of the East Africa Rift System. Chapter 3 focuses on the Lake Tanganyika Rift whereas Chapter 4 focuses on the area from a thick black rectangle, Lake Rukwa, and Northern part of Lake Nyasa (Malawi). The thick black rectangle represents the area where the deltaic deposits have been identified around the Karema Platform (Shaban et al., 2021).

Figure for Chapter 2

Figure 3: Study Area: A) Structural provinces of the LTR from Ruzizi in the north to Mpulungu in the south demarcated by dashed red lines (see text for details). Thick black lines show the normal faulting trend within Lake Tanganyika, modified after Muirhead et al. (2019). Inset shows the location of Lake Tanganyika within the Western Branch of the EARS. EB and WB are the Western and Eastern Branches respectively of the EARS. B) Locations of seismic data used in this study. The latest 2D seismic data tracklines are in green whereas the 1983/84 data tracklines are in blue.

Figure 4: A) Major structural features in the LTR that developed due to rift segmentation (see text for details). Colors indicate the depth to the Nyanja Event, the datum = lake surface (768 m above sea level). B) Geological map of the region surrounding the LTR (modified after Choubert

and Faure-Muret, 1968); note Karoo sediments are mainly observed on the Eastern side of the region. Bathymetry presented is derived from seismic reflection data set used in this study. Note the two major deep-water areas in the Kigoma and Marungu provinces.

Figure 5: Seismic facies and interpretations as identified and mapped in this study (after Mitchum et al., 1977; Posamentier and Vail, 1988; Baster et al., 2002).

Figure 6: Seismic dip profile, SW-NE south of the Kalya Platform. A) Interpreted (top) and B) uninterpreted (bottom) with six identified seismic units (1- 6), from oldest to youngest. Note the seismic characteristics change from S1 to S6. S2-S6 records a deeper lake as manifested by increasing the dominance of the high amplitude and parallel to semi-parallel reflections. S3-S5 records the facies variability with higher proportion of chaotic reflections and influence of alternating high- and low lake levels. S1-S6 represent the seismic depositional sequence in the central and southern basins of the LTR. Boxes a), b) and c) are selected areas for details as shown in the lowermost panels. C) 2012/2014 dip line showing the onlapping of S2 onto S1 as indicated by thick black arrows. The intra-rift faulting has disrupted the onlap pattern. D) PROBE dip line 210 showing seismic units across the Kigoma Province. The Ruzizi depositional sequences are shown in Figure 7.

Figure 7: A) Seismic dip profile, SW-NE south-west of the Karema Platform. Note the low-frequency high-amplitude, sub-parallel to parallel reflections below the Nyanja Event (green line) B) Inset map showing the extent of the Pre-Nyanja Event facies (within red line). The thick black line is the profile shown in (A), thick grey lines are the basement faults.

Figure 8: Seismic facies maps (A, B, E and F) and corresponding paleogeographic maps (C, D, G and H) as mapped in S2 through S5 in the southern provinces (Kigoma through Mpulungu)

constructed from ION-PROBE and latest commercial 2D seismic dataset. Note the significant changes in the paleogeography controlled by both tectonic and hydro-climate processes. MTDs and channels are pronounced in S3 onwards as a result of an increase in high relief. The onset of the Malagarasi River drainage is observed in S3.

Figure 9: Seismic dip profile, W-E from the northern basin (Ruzizi) of the LTR. A) Interpreted (top) and B) uninterpreted (bottom) with six identified seismic sequences (1- 6), from oldest to youngest. Only the Nyanja Event and S1 correlated with high confidence across the entire LTR, from the South Basin to the Central Basin to the North Basin.

Figure 10: Seismic reflection profile illustrating the deltaic facies. A) Strike seismic profile with sequence stratigraphic interpretations and prograding clinoforms (deltaic lobes), active canyons and stacked channels. Note the two different intervals, lower and upper interval, and each containing lobe-shaped clinoforms dipping towards the West. The fluvial-deltaic deposits record the continued subsidence, whereas the canyons manifest the uplifting of the Karema Platform or lake level drop due to hydroclimate changes. B) Uninterpreted section.

Figure 11: NW-SE seismic profile across Karema area in the Marungu Province. A) Interpreted seismic profile with interpretations of the migrating subaqueous delta fans characterized by highly chaotic seismic reflections in the distal part of the lake. The fan migrated towards the west then migrated towards the northwest (see also Figure 13). Note that the fans are evident in Sequence 4. Note the erosional surface at the base of S5b. The fault zone has been a conduit for sediments as noted in the channels at top of S5 as well as in S6. B) The lower panel is an uninterpreted section. For explanation colors see Figure 8.

Figure 12: A) W-E seismic profile in the Kigoma Province. C) N-S seismic profile in the same area as (A). The lower panels (B & D) are uninterpreted sections. The upper panels (A & C) are the seismic profiles ((40% transparency) with interpretations of the prograding clinoforms in seismic units 4 & 5. The thickness of the clinoform sets is ~200 ms in each sequence, the clinoforms are dipping towards the SW. The clinoforms are possible evidence for the southwestern progradation of the Ruzizi delta during a lake lowstand. For colors see Figure 8.

Figure 13: Seismic profile, SW-NE interpreted before flattening (A) and after flattening (C) showing the Ntiri High. When flattened on Seismic unit 4, profile suggests that the structure postdates Seismic unit 4. This is manifested by the erosional surface at the base of Sequence 5. Thick dark lines represent faults; note that most of the faults do not penetrate S5. Panels B) and D) are the uninterpreted seismic profile before and after flattening respectively.

Figure 14: Seismic facies maps (A, C, E, G and I) and corresponding paleogeographic maps (B, D, F, H, and J) as mapped in S2 through S6 in the Ruzizi Province constructed from ION-PROBE seismic data. Note the development of Ruzizi delta in S5, and more evident in S6. Note that following the formation of the Burton's Ridge, the basin experienced turbidites and MTDs as observed in S2, S3 and S4.

Figure 15: Seismic reflection line illustrating the deltaic facies in the Ruzizi Province. A) Interpreted profile of the southward prograding clinoforms (deltaic lobes), approximately 200 ms thick on average, because of the Ruzizi River influx. Note that the clinoforms emerge in Sequence 5 and onwards. B) Uninterpreted section.

Figure 16: Interpreted seismic reflection profiles across the Kigoma Province (A – D). Note the facies variations from high-continuity parallel seismic facies representing relatively low energy

deep water hemipelagic deposits, to wavy, discontinuous, and more chaotic facies indicating high energy channel complexes. The channels observed on PROBE 212 in Sequence 4 suggest the Malagarasi fan evolution during that time. The channel complex seen between 1200-1800 ms TWTT in S5 on section (A) is probably sourced from the North via the Ruzizi River through the narrow gap on the eastern part of the Burton's Bay Ridge (See Figure 13 for annotations).

Figure 17: Simplified conceptual schematic of the basin evolution as a result of rifting and hydroclimate processes. (A) Initial architecture of the crust with existing structural fabrics and pre-rift sedimentary deposits. Karoo group rocks occur within Permo-Triassic rift basins bounded by faults striking parallel with the inherited fabric in the basement terrains. During this time, the widely spaced network of drainages flowed towards the Karoo basins. (B) Rift initiation probably occurred in the mid-to-late Miocene through unlinked normal faults via the inherited basement anisotropies. The initial rift segments were possibly ~30 – 40 km wide and were composed of several half-grabens. Depositional sequence 1 was likely deposited in a fluvial and shallow lake environment. The footwall drainages delivered sediments in the hanging wall depocenters along border faults. The environment probably varied between wetland, savannah, and shallow lake. (C) Development of the Burton's Bay Ridge leading to the drainage separation of the Ruzizi Province from the rest of the rift. Faults began to link, and rifting focused onto the present border faults resulting in greater tectonic relief. Consequently, the sustained lake level developed leading to the deposition of S2. (D & E) Highstand (D) and lowstand (E). As the subsidence increased driven by extension, S3-S5 were deposited, and there is evidence of increased amplitude and frequency of lake level fluctuations. High relief developed during this time, leading to the deposition of MTDs and channel complexes. Both Ruzizi and Marungu

provinces saw the development of prograding deltas into the deep-water environments during lake level lowstand phases (E).

Figures for Chapter 3

Figure 18: Study area: (A) Digital Elevation Model of the East African Rift System (EARS) showing the location of Lake Tanganyika (red rectangle) along its Western Branch. WB and EB are the Western and Eastern Branches respectively. MER=Main Ethiopian Rift, LTr = Lake Turkana, LA = Lake Albert, LE = Lake Edward, LK = Lake Kivu, LT = Lake Tanganyika, LR = Lake Rukwa, LMr = Lake Mweru, LB = Lake Bangweulu, LM = Lake Malawi, and CB = Cahora Bassa dam. (B) Map of Tanganyika Rift syn-rift sedimentary thickness. Purple dashed lines show the boundary of structural provinces of the Lake Tanganyika Rift. Thick black lines show the basement-rooted normal faults (updated after Muirhead et al., 2019). Note the maximum of ~6 km thick sediments along the western border fault of the Kigoma Province. (C) Geological map of the region surrounding the LTR (modified after Choubert et al., 1968); note Mesozoic rift sediments (Karoo) on the western flank of the Tanganyika Rift. Delvaux (2001) suggested the extension of Karoo sediments into the Kalemie and northern part of the Marungu provinces of the Tanganyika Rift. CSZ = Chisi Shear Zone, MSZ = Mtose Shear Zone, Kate-Kipili Shear Zone. The red rectangular polygon shows the location of Figure 8A. The red ellipse in the central part of the Lake Tanganyika Rift represents a location of the Kaval Island Ridge. Bathymetry presented is derived from seismic reflection data set used in this study (maximum water depth = 1471 m). The two major deep-water areas are in the Kigoma and Marungu provinces.

Figure 19: (A) Locations of seismic data used in this study. The latest 2D seismic data tracklines are the 2014/2014 Multi-channel Seismic Survey (MCS), the 1983/84 data tracklines are PROBE

Multi-channel Seismic Survey (MCS). Note the profiles (in black colour) for figures 7 and 9. (B) The red polygon represents the FTG and Aeromagnetic survey area. The black rectangular polygon shows the location of Figure 8A (C - D). Example basin-scale seismic reflection NE-SW dip profile (2014), located south of the Kalya Platform in Lake Tanganyika Rift consisting of the uninterpreted (panel C) and interpreted (panel D) sections. The seismic images show six known seismic stratigraphic syn-rift units (S1, oldest, to S6, youngest). S2 - S6 generally records deeper rift lake sequences, manifested by increasing the dominance of the high amplitude and parallel to semi-parallel reflections. S3 - S5 records facies variability with higher proportion of chaotic reflections and influence of alternating high- and low lake levels (see also Shaban et al., 2021).

Figure 20: TMI reduced to the pole (RTP) anomaly exhibiting correct locations of the anomalies over the source. Note high magnetic anomaly in the southern part of the survey area (North Marungu Province) and low magnetic anomaly in the northern part of the survey area (North Kigoma Province). (B) Total Horizontal derivative (HG) of the RTP TMI anomaly. (C) Vertical derivative (Dz) of the RTP TMI anomaly. (D) Structures extracted from B. (E) structures extracted from C. The rose diagrams were created by measuring the general strike of each lineament then plotted using GeoRose software (Yong Technology Inc., 2014).

Figure 21: Butterworth bandpass filtered TMI RTP. (A) short wavelength, 5 - 12 km, (B) intermediate wavelength, 12 - 45 km, and (C) long wavelength, 45 - 205 km. The short wavelength reveals the magnetic bodies within less than 2 km below the surface, the intermediate wavelength reveals magnetic bodies within 2– 6 km below the surface, and the long wavelength reveals magnetic bodies within 6 – 14 km below the surface.

Figure 22: Rotational invariants anomaly showing high-to-medium frequency and short-to-intermediate wavelength anomaly lineaments (corresponding to shallow and intermediate depth intervals). A) R-1 and B) R-2, showing contacts, edges, and shapes of high-density geological bodies. Note NW-striking bodies (314° mean trend) in the central and southern parts and NNE-striking bodies (009° mean trend) in the northern part of the area. (C - D) Structural fabrics mapped in panels A and B respectively.

Figure 23: (A) Updated fault map of the Lake Tanganyika Rift from this study. MM and KKN represent the Mahale Mountains and Katenga - Kugulu - Ntengo lineaments respectively. The rose diagram shows the strikes of the mapped faults. Note that many faults mapped on the eastern part of the northern and central Lake Tanganyika are due to denser data coverage. (B – D) Previously published fault maps from Muirhead et al. (2019) in panel B, Rosendahl et al. (1992) in panel C, and Morley et al. (1988) in panel D. Note that our study has identified more faults within Lake Tanganyika and identified some NNE-SSW secondary fault trends in addition to the dominant NW-SE fault trend. Other structural strikes are NNW-SSE, NNE-SSW, and N-S. The inset map shows the data used during each study. The red and black polygons on panel A inset map demarcate the areas with Air FTG data, and the lines represent various 2D seismic profiles (refer to Figure 1).

Figure 24: A) NE-SW PROBE seismic profile 218 (see red line transect in the side-inset map in B and in Figure 2) located in the Central Tanganyika Rift (Kalemie Sub-basin). B) Forward model of the Gravity (Tz) and Magnetic (RMI) along the seismic profile 218. Modelled geology: each coloured polygon represents a block of distinct density and magnetic susceptibility from its neighbouring block. Note the high density (3.2 g/cc) basement and lower-density (2.71 g/cc) intra-basement shear zone along the margins of which a large intra-basinal fault localized. In the

sedimentary sections, the seismic shows a persistent intra-basin ‘high’ controlled by the footwall of the intra-basin fault. Also, the model suggests the possible presence of deep-seated high-density sedimentary rocks (2.45 g/cc), likely representing Mesozoic (Karoo) rift phase units. Note the channel complex (2.2 g/cc) within the younger sedimentary intervals (seismic units 3-4 in Shaban et al., 2021).

Figure 25: (A) Hillshade map of the eastern rift shoulder of the Tanganyika Rift (see location in Figures 2A-B), showing exposures of one of the exhumed NW-trending Precambrian basement shear zones in the region, the Chisi Shear Zone and its bounding basement terranes (modified after Kolawole et al., 2021b). The stereographic projections of published field measurements (circles: poles to gneiss foliation planes, diamonds: poles of mineral elongation lineation) show the dominant NW-SE trends of metamorphic fabrics within the shear zone and terranes. (B - C) Outcrop photograph and photomicrograph of eclogites in mylonitic garnet-clinopyroxene gneiss along the shear zone, indicating the presence of a suture zone along the mobile belt (source: Boniface et al., 2012). The photomicrograph shows reaction textures typical of eclogite facies metamorphism. Cpx: Clinopyroxene, Grt: Garnet, Di: Diopside, Pl: Plagioclase.

Figure 26: Seismic dip profile, SW-NE across the Kavala Island Ridge (KIR). A) Uninterpreted (top) and B) interpreted (bottom) with six identified seismic horizons, from oldest to youngest. Note that the KIR is devoid of sedimentary units except S1, implying the active nature of the ridge. The ridge is bounded by two major rift segment border faults with opposing polarities. Sedimentary packages thicken toward these faults implying syn-deposition. Note that across the profile there are two main fault trends. Contrary to seismic unit S1, seismic characteristics of S2-S6 display high amplitude and parallel to semi-parallel reflections suggesting a deeper lake environment.

Figure 27: Summary conceptual model illustrating the evolution of the KIR. (A) Initial stage before rifting. (B) Initial rifting stage triggered by two major faults with opposing polarities. During this stage, deposition of thicker units 1-2 was contemporaneous with the ridge evolution. (C) Mid-rifting stage. Seismic units 3-5 were deposited during this period contemporaneous with the ridge evolution (D) Late stage of KIR evolution. Note that the ridge was uplifted higher, and some of the sediments were eroded from the top of the ridge. E) Structure contour map (in depth) of the Nyanja Event horizon, the deepest, regionally mappable pre-rift surface (Rosendahl, 1987; Muirhead et al., 2019; Shaban et al., 2021). This horizon corresponds to the green reflector at the base of S1 in Figures 2C-D. F) Structure contour map (in depth) of the horizon at top of S3 unit, a syn-rift unit at intermediate depths.

Figure 28: A) Interpretation of paleo-topography of southwest Tanzania and eastern Congo during the Pre-Cenozoic phases of tectonic extension in East Africa (i.e., Karoo and Cretaceous). The map also shows the pre-rift basement shear zones (previously published ones and those mapped in this study) and rift-related faults. Paleo-extension direction is from Delvaux et al. (2012). (b) Present-day topography of the region showing faults along the evolving Tanganyika Rift. Note that the map includes both the currently active and dormant faults along the Tanganyika Rift. We interpret that the earliest faults in the central Tanganyika Rift (Kalemie Sub-basin) represent the south-eastern extension of the Luama Rift (see Figure 7 seismic section and forward model). Extension directions are from Delvaux (2001) and Delvaux and Barth (2010). Exhumed basement shear zones are from Daly (1988), Delvaux et al. (2012), and Kolawole et al. (2021b). CSZ: Chisi Shear Zone, KKSZ: Kate-Kipili Shear Zone, MSZ: Mtose Shear Zone. C) Cartoons illustrating the interpreted structural and landscape evolution of the

Central Tanganyika Rift, highlighting the persistent influence of the incipient rift structure (Stage 1) on the subsequent rift basin architecture (Stages 2 and 3).

Figures for Chapter 4

Figure 29: Study area covering the southern part of the Western Branch of the East Africa Rift System. The area of interest (red rectangle) is the southern part of Lake Tanganyika, Lake Rukwa, and northern part of Lake Nyasa (Malawi). Solid blue lines represent rivers. The thick black rectangle represents the area where the deltaic deposits have been identified around the Karema Platform (Shaban et al., 2021); for more details refer to the text. Notice the Rungwe Volcano just above Lake Nyasa. Inset map shows the East African Rift System (EARS, dashed line), EB= Eastern Branch, WB= Western Branch, and MER = Main Ethiopian Rift.

Figure 30: (a) Topographic map of the study area; black dotted line indicates the paleo-lake highstand of the Lake Rukwa at an elevation of ~962 m suggesting ~160 m above modern Lake Rukwa, the black solid arrow indicates the Lake Rukwa's overflow direction into the Lake Tanganyika via the Karema depression, and the red solid line indicates the position of the seismic profile of (b). (b) Interpreted 2D seismic reflection profile along the Karema Platform; note the spectacular prograding clinoforms and buried channel complexes (Shaban et al., 2021). Orange = deltaic clinoforms, yellow = shallow deposits, red = channel deposits, green = hemipelagic deposits, blue = mass transport deposits (MTDs). (c) Uninterpreted 2D seismic reflection profile along the Karema Platform.

Figure 31: Model processes. Model 1 used modern topography, whereas Models 2 and 3 used artificial topography. Model 2 was simulated with volcano for 5 Myr whereas Model 3 was simulated without volcano.

Figure 32: Analysis of the Karema depression (Ifumwe River) erosion. (A) 30 m SRTM DEM, the black solid polygon represents the Karema depression catchment. (B) Extracted 30 m SRTM DEM for the Ifumwe River catchment. (C) 30 m SRTM DEM capped 1200 m. (D) Estimated erosion for 200 kyr, obtained by subtracting the DEM in (C) from 1200 m datum.

Figure 33: Comparison of precipitation distribution between the satellite data (A) and Model 1 results (refer Model 1) (B). Satellite data are monthly averaged for the past 20 years (2000 - 2021) from the NASA Giovanni system (Huffman et al., 2019). Note the similarities in high precipitation between the satellite data and model predictions for Lake Rukwa and the Rungwe Volcano, and rain shadow between the southern part of Lake Rukwa and northwest of the Rungwe volcano. From both the observed and predicted results the precipitation is shown to increase from the southern parts of Lake Tanganyika to the northern parts of the lake.

Figure 34: Precipitation rates generated after 5 Myr for models 2 and 3 with similar rain base and wind speed parameters. (A) Model 2 was simulated with an uplifting volcano throughout model runtime. Note rain shadow northwest of the volcano, particularly around pseudo-Lake Rukwa. (B) Model 3 did not include a volcano. Note that the model predicts consistent precipitation rates distribution ranging from 1.9 m/yr to 2.05 m/yr with higher precipitation rates distributed in the western part of the model. Model 2 predicts a large range of values than Model 3 because of the orographic effect caused by the volcano and the overall topography generated at the end of the model (refer to Figure 8; section 3.4). It is evident that Model 2 simulates ‘mountainous range’ extending SW-NE connecting with the volcano.

Figure 35: Topography evolution after 5 Myr. (A) Scenario 1 of Model 1 used a rain-base of 1.5 m/y and a wind speed of 5 m/s and predicts the connectivity of Lakes Tanganyika and Rukwa. (B) Model 2 was simulated with volcano from time = 0 yr until the end of the model runtime. (C)

Model 3 did not include volcano. Note that all models predict the connectivity of Lakes Tanganyika and Rukwa. The obvious difference between models 2 and 3 is the elevation of the topography generated, whereby, Model 2 predicts higher elevation.

Figure 36: Lakes' depth predicted by models 1, 2 and 3 after 5 Myr. (A) Scenario 1 of Model 1 used the actual DEM of the area, a rain-base of 1.5 m/y, and a wind speed of 5 m/s. Note that contrary to the modern bathymetries, the model predicts shallower lake depth for Lake Tanganyika than Lake Rukwa. (B) Model 2 used an artificial DEM and included a volcano from time = 0 yr until the end of the model runtime, a rain-base of 1.5 m/y, and a wind speed of 5 m/s. (C) Model 3 used same model parameters as Model 2 but did not include the volcano. Note that while both models 2 and 3 predict pseudo-Lake Tanganyika deeper than pseudo-Lake Rukwa, Model 2 predicts greater depths for pseudo-lakes than Model 3.

Figure 37: Conceptual diagram of the connection between Lakes Tanganyika and Rukwa. (A) Lake connection stage: During this period, heavy precipitation caused Lake Rukwa to expand, fill to its spill point and overflow into Lake Tanganyika via the Karema depression. Wind flow from the southeast. (B) Today's condition: Dry conditions prevail around Lake Rukwa. Dry conditions were caused by diminished precipitation because of rain shadow possibly caused by the Rungwe Volcanic edifice. Wind flowed from the southeast.

Appendices

Figure S1: Sediment isochron maps across the Lake Tanganyika Rift for (a) Seismic unit 1 (b) Seismic unit 2 (c) Seismic unit 3 (d) Seismic unit 4 and (e) Seismic unit 5. Note the spatial and temporal variations and or depocenter migration across the Rift. Seismic units 1 and 2 record the thicker sediments. The basement involved faults are indicated by thick grey lines. Refer Figure 1 for sub-basins.

Figure S2. Vectors (in blue) and Tensors (in black) of the 3D Full Tensor Gradiometry field.

Note that three vectors of FTG produce nine component tensor field (T_{xy} , T_{xx} , T_{xz} , T_{yy} , T_{yx} , T_{yz} , T_{zy} , T_{zx} , and T_{zz}) of which when summed results into the five independent tensors, modified after Blake (1995).

Figure S3: (A) Analytical signal of the RTP TMI showing anomaly patterns associated with magnetised geology. Note a NW-SE striking magnetic body in the central part of the survey. (B) Tilt Derivative of a long wavelength (i.e., 6 km) low pass filtered RTP TMI showing shallow structures; negative values represent areas outside the source, zero values represent areas close to the edge of the source, and positive values represent areas over the source. Note a primary NW-SE strike and a secondary E-W strike of the lineaments. (D) Structures extracted from A. (E) Structures extracted from B.

Figure S4. (A) Adaptive Tilt Angle anomaly from the gravity anomaly (T_z). It combines three components: T_{xz} , T_{yz} and T_{zz} . Note the lineaments striking NW-SE in the central and southern part and NNE-SSW in the northern part of the survey area. (B) TDX exhibits lineaments like those from ATA anomaly, but more clearly delineated. (D) Structures extracted from A. (E) Structures extracted from B.

Figure S5: (A) First horizontal derivative of the Vertical Derivative of the Aeromagnetic data. (B) Zoomed in region of (A). Note the NW-SE striking structures; rift structures have strikes aligned with basement structures.

Figure S6: Analysis of the NNE-SSE lineament in the north-eastern part of the Kigoma Province from gravity anomaly. The prominent N-S lineament is not visible under the unfiltered T_z (A) and under the residual between the T_z upward continued by 6 km and the unfiltered T_z (B), but

it is not visible under long wavelength which is the Tz upward continued by 12 km (C). The absence of the prominent N-S lineament in the north basin in panel C, indicates the dominance of long wavelength content of the map, relative to panel B which dominated by intermediate wavelength anomalies. However, in panel A, the lineament becomes prominent, indicating the relatively shorter wavelength content of the data. Also note that the KIR is more prominent under shorter wavelengths, suggesting the dominance of basement material and absence of thick sedimentary material on the ridge. Note the Malagarasi River pathways in (A) as it delivers sediments to the offshore part of lake.

Figure S7: (A) Uninterpreted vertical derivative of 1-km resolution regional magnetic data, reduced to pole. (B) Interpretation of (A) overlaid with the interpreted faults. Note the CSZ extending from the Rukwa Rift to the Lake Tanganyika Rift modified after Kolawole et al. (2021). The thick black polygons are suggested to represent Pre-Cambrian fabrics.

Figure S8: An illustration of water budget on a windward slope with incoming moisture flux (F), upslope condensation source (S in the shaded region) and precipitation (P) modified after Smith & Barstad (2004). The top sketch is a multiscale rise scenario whereas the bottom represents a smooth rise.

Figure S9: A) Uplift rate and subsidence rates for Model 1. B) Uplift rates and subsidence rates for Model 2. C) Uplift rate and subsidence rates for Model 3. Note that in models 2 and 3, the subsidence rates of the pseudo-lakes are controlled by the slip rate border faults.

Figure S10: Wind speed sensitivity analysis on precipitation distribution. A) Scenario 1 of Model 1 with wind speed =5 m/s, B) Scenario 2 of Model 1 with wind speed =10 m/s, C) Scenario 2 of Model 1 with wind speed =15 m/s. Note that the precipitation rate increases as the wind speed

increases. A) Scenario 1 of Model 2 with wind speed =5 m/s, B) Scenario 2 of Model 2 with wind speed =10 m/s, C) Scenario 2 of Model 2 with wind speed =15 m/s. Note that the precipitation rate increases as the wind speed increases especially around the volcano.

Figure S11: (A) First horizontal derivative of the Vertical Derivative of the Aeromagnetic data. (B) Zoomed in region of (A). Note the NW-SE striking structures; rift structures have strikes aligned with basement structures.

Figure S12: Analysis of the NNE-SSE lineament in the north-eastern part of the Kigoma Province from gravity anomaly. The prominent N-S lineament is not visible under the unfiltered Tz (A) and under the residual between the Tz upward continued by 6 km and the unfiltered TZ (B), but it is not visible under long wavelength which is the Tz upward continued by 12 km (C). The absence of the prominent N-S lineament in the north basin in panel C, indicates the dominance of long wavelength content of the map, relative to panel B which dominated by intermediate wavelength anomalies. However, in panel A, the lineament becomes prominent, indicating the relatively shorter wavelength content of the data. Also note that the KIR is more prominent under shorter wavelengths, suggesting the dominance of basement material and absence of thick sedimentary material on the ridge. Note the Malagarasi River pathways in (A) as it delivers sediments to the offshore part of lake.

Figure S13: (A) Uninterpreted vertical derivative of 1-km resolution regional magnetic data, reduced to pole. (B) Interpretation of (A) overlaid with the interpreted faults. Note the CSZ extending from the Rukwa Rift to the Lake Tanganyika Rift modified after Kolawole et al. (2021). The thick black polygons are suggested to represent Pre-Cambrian fabrics.

Figure S8: An illustration of water budget on a windward slope with incoming moisture flux (F), upslope condensation source (S in the shaded region) and precipitation (P) modified after Smith & Barstad (2004). The top sketch is a multiscale rise scenario whereas the bottom represents a smooth rise.

Figure S14: A) Uplift rate and subsidence rates for Model 1. B) Uplift rates and subsidence rates for Model 2. C) Uplift rate and subsidence rates for Model 3. Note that in models 2 and 3, the subsidence rates of the pseudo-lakes are controlled by the slip rate border faults.

Figure S15: Wind speed sensitivity analysis on precipitation distribution. A) Scenario 1 of Model 1 with wind speed =5 m/s, B) Scenario 2 of Model 1 with wind speed =10 m/s, C) Scenario 2 of Model 1 with wind speed =15 m/s. Note that the precipitation rate increases as the wind speed increases. A) Scenario 1 of Model 2 with wind speed =5 m/s, B) Scenario 2 of Model 2 with wind speed =10 m/s, C) Scenario 2 of Model 2 with wind speed =15 m/s. Note that the precipitation rate increases as the wind speed increases especially around the volcano.

Figure S16: Wind speed sensitivity analysis on lake depth. A) Scenario 1 of Model 2 with wind speed =5 m/s, B) Scenario 2 of Model 2 with wind speed =10 m/s, C) Scenario 2 of Model 2 with wind speed =15 m/s. Note that as the wind speed increases, the lake depth decreases.

Figure S17: Model 2 sensitivity analysis. (A) and (D) represent topography and precipitation rate output respectively when the volcanic uplift rate is $1E-2$ m/yr. (B) and (E) represent topography and precipitation rate output respectively when the volcanic uplift rate is $1.5E-2$ m/yr. (B) and (E) represent topography and precipitation rate output respectively when the volcanic uplift rate is $2E-2$ m/yr. Note that, as the volcano uplift rate increases, the elevation of the topography increases as well as the maximum precipitation rate.

Figure S18: Model 2 sensitivity analysis. (A) and (D) represent topography and precipitation rate output respectively when the erodibility coefficient is $8E-4 \text{ m}^1\text{-}2 \text{ m yr}^{-1}$. (B) and (E) represent topography and precipitation rate output respectively when the erodibility coefficient is $8E-5 \text{ m}^1\text{-}2 \text{ m yr}^{-1}$. (B) and (E) represent topography and precipitation rate output respectively when the erodibility coefficient is $8E-6 \text{ m}^1\text{-}2 \text{ m yr}^{-1}$. Note that, as the erodibility coefficient increases, the elevation of the topography increases, however, there is no a clear relationship between the erodibility coefficient and precipitation rate.

Figure S19: Analysis of knickpoints from the Ifumwe tributaries extracted from a 30m resolution SRTM. (A) Ifumwe catchment with northern and southern branches identified. Note that several tributaries join the northern branch nearly at a right angle. (B) Stream profiles extracted from the Ifumwe catchment using the Topographic Analysis Kit (TAK) for TopoToolbox (MATLAB) tools (Forte and Whipple, 2019). The upper part and lower part are the southern branch and northern branch respectively. Red oval represents the Lake Rukwa spill point. (C) A schematic diagram of a longitudinal profile showing the knickpoint formation along stream channels due to different factors modified after Ahmed et al. (2019). Note that faulting or uplift causes steep knickpoints.

CHAPTER 1: INTRODUCTION

Processes controlling extension and hydroclimate variability play important roles in sedimentation in rifts, especially in lacustrine basins (Leeder and Gawthorpe, 1987; Burgess et al., 1989; Buck, 2004; Scholz et al., 2007). Continental rifts are structurally complex and are typically composed of a series of asymmetric fault-bounded sub-basins systems that flip polarity along-trend (McKenzie, 1978; Rosendahl, 1987; Morley, 1988; Lambiase, 1990; Logatchev and Zorin, 1992; Sherman, 1992; Muirhead et al., 2019). The spatial and temporal distribution of sedimentary facies in continental rifts are controlled by a variety of structures including accommodation zones that segment rifts into individual depocenters, uplifted border fault footwall blocks that direct drainages away from the rift basins, and rift-parallel fault blocks, transfer faults and jumps and gaps, which influence axial sediment transport (Lambiase and Bosworth, 1995; Morley, 1995). Also, rates of extension along strike influence changing depositional environments (Morley, 1988; Wright et al., 2020), and variability in extension may even influence the evolution and distribution of different sedimentary facies within the same depositional units. Rift-lake basins located at low latitudes such as those in the East Africa Rift System (EARS), are susceptible to dramatic climatic fluctuations (Lambiase, 1990; Scholz et al., 2007; McGlue et al., 2008; Tierney et al., 2010), which likely affect the nature and distribution of sedimentary facies. Accordingly, reconstructing paleo-environments and lake-level physiography provide insights into the basin evolutionary history and how active tectonism and hydroclimate changes affect lacustrine deposition (Cohen et al., 1997a; Lezzar et al., 2002). Furthermore, spatial, and temporal changes in rift basin depositional environments over the life history of a rift lake frame the habitats of unique endemic organisms.

Rift lake basins commonly persist for millions of years and behave as ‘island’ ecosystems, evolving complex endemic communities, and serving as model systems for evolutionary biology (e.g., McCune, 1987; Vadeboncoeur et al., 2011; Whiteside et al., 2011). The topographic morphology of active rifts basins, especially in humid climatic settings exert important controls on the transport pathways, character, and volume of sediments deposited in lacustrine basins (Leeder and Gawthorpe, 1987; Rosendahl, 1987; Burgess et al., 1989; Scholz et al., 1990; Buck, 2004; Scholz et al., 2007). Furthermore, rift architecture, fault dips and basin inversion have been suggested to impact the hydrocarbon accumulation (Morley, 1995). Therefore, deciphering the structural control on both the basin architecture and landscape evolution in such tectonic settings is of paramount importance for understanding the evolution of the Earth as well as solving problems in the applied fields of mineral and hydrocarbons exploration, hydrogeology, hydrology, surface CO₂ storage, and geothermal energy (Vasuki et al., 2014). Many ancient and modern extensional rifts host lacustrine basins (e.g., Rosendahl, 1987; Katz, 1990) that form archives of tectonic history, paleoclimate dynamics, and the maturation history of organic matter. Understanding the structural complexity of rift basins (McKenzie, 1978; Rosendahl, 1987; Morley, 1988; Lambiase, 1990; Logatchev and Zorin, 1992; Sherman, 1992; Muirhead et al., 2019) requires high-resolution, basin scale data sets. For instance, with time their structural geometry changes and they segment into sub-basins bounded by large offset border faults (Lavayssière et al., 2019). This along-trend segmentation of rift basins may occur on inherited pre-rift basement structures such as craton boundaries, terrane boundaries, and exhumed ductile shear zones that are rift-orthogonal or rift-oblique (e.g., Versfelt and Rosendahl, 1989; Corti et al., 2007; Laó-Dávila et al., 2015; Katumwehe et al., 2015; Wright et al., 2022; Kolawole et al.,

2022). Moreover, the tectonic rupture of continents often exploits ancient orogenic belts or long-lived crustal scale weakness zones (Vauchez et al., 1997).

On a basin scale, several studies have used seismic reflection data (e.g., Phillips et al., 2016) seismicity data (e.g., Kolawole et al., 2018a; Chisenga et al., 2023), remote sensing data (e.g., Hussein et al., 2006; Wilson et al., 2010; Laó-Dávila et al., 2015; Muirhead et al., 2019), or geological mapping (e.g., Beacom et al., 2001; Ring, 1994; Ring et al., 2005) to decipher rift structures and the effect of basement pre-existing structures on the evolution of extensional rifts. However, few studies have used high-resolution aeromagnetic data to analyze the impact of basement pre-existing structures in the evolution of continental rifts in the EARS (e.g., Kinabo et al., 2007; Katumwehe et al., 2015; Kolawole et al., 2018a, 2021, 2022). Few studies have used the integration of FTG, aeromagnetic data and seismic data for structural analysis (e.g., Malin, 2017; Peace et al., 2018; Jamaludin et al., 2021). Although several studies have promoted the notion that deep, large basins of the Western Branch, EARS, serve as examples for the evolution of half-graben basins in extensional settings, the geometry and kinematics of the earliest border and intrarift fault systems are poorly constrained (Ebinger et al., 2019; Kolawole et al., 2021).

The sedimentary records of tectonic lakes provide long-term archives of continental breakup, terrestrial climate, and biological evolution, and these basins also contain important hydrocarbon resources. However, their evolution is sometimes complicated by the interplay of controlling factors such as tectonics, climate, and local geology (Carroll and Bohacs, 1999). The location and timing of sedimentary facies in rift basins is driven by the interplay of basin accommodation (mostly tectonically controlled), and water plus sediment supply (mostly climate controlled) (Schumm, 1977; Surdam and Stanley, 1980; Kelts, 1988; Lambiase, 1990; Carroll and Bohacs, 1999). Thus, tectonic forces drive changes in the relief, drainage's baselevel,

erosion, and migration of depocenters; climate forcings affect elevation, erosion, and sediment flux. The effect of climate is more pronounced when it is modulated by orography (Smith and Bastard, 2004). Therefore, it is possible to use the nature and facies architecture of the syn-rift sedimentary fill to document any spatiotemporal variation in sediment production and infer potential feedback on surface mass transfer and tectonics and climate (Maniatis et al. 2009; Olive et al. 2014, 2022; Pechlivanidou et al. 2019).

Two proximal and structurally linked lakes have a possibility of ‘filling and spilling’ of the upstream lake into the downstream lake that is situated at nearly the same elevation above sea level. This condition is observed in several places such in the East African Rift where Lake Kivu overflows into Lake Tanganyika, which has important implications for solute loading and carbonate sedimentation in the downstream lake (e.g., Felton et al. 2007). This phenomenon is also possible for Lakes Tanganyika and Rukwa, which are structurally connected by the Chisi Suture Zone (Heilman et al., 2019, Kolawole et al., 2021) and the Karema depression, where Lake Rukwa is at a slightly higher elevation than Lake Tanganyika. Upstream lakes are important factors influencing lake hydrology, solute loading, and water column characteristics of downstream lakes (e.g., Haberyan and Hecky, 1987). When the upstream and downstream lakes connect, different regions of downstream lakes may have different water chemistries that can lead to speciation and potentially diversification (Simpson, 1953; Schluter, 2000; Ricklefs, 2003; Cardillo et al., 2005). There have been speculations that Lake Rukwa overflowed into Lake Tanganyika during its highstand in the geologic past (e.g., Delvaux and Williamson, 2008; Cohen et al., 2013). To test the possible connectivity of these two lakes requires subsurface information from drilling or numerical models.

The East African Rift System (EARS), more than 3000 km-long, is an ideal site to investigate processes of lacustrine basin evolution in an extensional setting (Figure 1). It initiated in the Oligocene corresponding with the opening of the Red Sea and Gulf of Aden (Omar and Steckler 1996; Menzies et al. 1997; Wolfenden et al., 2005). The EARS is composed of a series of rift segments, predominantly asymmetric half-graben basins (Rosendahl, 1987; Morley, 1989) of 100-150 km length, that mark the extensional history of the rift. The EARS splits into the Eastern and Western branches at the south terminus of the Main Ethiopian Rift, separated by the Archean Tanzania Craton (Rosendahl, 1987; Ebinger, 1989; Figure 1). The Western Branch of the EARS is magma-poor, with only a few volcanic centers such as the Virunga Volcanic Province positioned to the north of Lake Tanganyika, and the Rungwe Volcanic Province located south of the Lake Tanganyika Rift (Baker, 1971; Mohr and Wood, 1976; George et al., 1998; Furman, 2007; Biggs et al., 2009; O'Donnell et al., 2013).

This research focuses on the Lake Tanganyika Rift, situated in the Western Branch of the EARS (Figure 1). The Lake Tanganyika Rift contains an iconic lake, Lake Tanganyika, that has attracted the attention of various research communities including those focused on basin analysis, paleoclimatology, structural geology, limnology, paleontology, geochronology, geomicrobiology, evolutionary biology, biostratigraphy, and hydrocarbons exploration (Russell et al., 2020). It is endowed with one of the oldest and most continuous records of tropical climate on the continents (Russell et al., 2020). Lake Tanganyika is the deepest and most voluminous lake in Africa; it is ~645 km long and has a maximum water depth of 1470 m (Rosendahl, 1987; Shaban et al, 20021). The Lake Tanganyika Rift is composed of five main half grabens (typically ~80-140 km long and ~50-70 km wide) (Rosendahl et al., 1986; Rosendahl, 1987; Muirhead et al., 2019; Wright et al., 2020, Shaban et al., 2021).

A strong seasonal precipitation cycle over Lake Tanganyika is triggered by the Tropical Rain Belt (TRB) over central Africa whose migration path covers the Lake Tanganyika Rift (Coulter et al., 1991). When the TRB migrates over the southern tropics from October-May, precipitation occurs over the rift; when the TRB migrates northward during June-August, strong southerly monsoon winds flow over the lake causing a pronounced dry period. Precipitation over Lake Tanganyika averages ~1200 mm/year whereby its variations are primarily controlled by changes in the strength of the monsoon, as well as globally important climate phenomena such as the El Niño (Bergonzini et al., 2004; Tierney et al., 2008). Compared to the rest of equatorial Africa, the average precipitation over the Lake Tanganyika Rift is low, and these dry conditions are attributed to the zonal overturning circulation of the tropical atmosphere (i.e., the Walker Circulation) and topographic effects on the Indian monsoon circulation (Nicholson, 1996). However, although the temporal variation of these phenomena is known, their impacts to rift stratigraphy and landscape evolution on long-term changes in East African climate remain poorly known (Russell et al., 2020).

Little is known about the subsurface geology and stratigraphy of the Lake Tanganyika Rift. For instance, apart from shallow coring (less than 10 m) in the Holocene and Upper Pleistocene interval (Livingstone, 1965; Tiercelin et al., 1988, 1992; Scholz et al., 2003; Felton et al., 2007), there is no sampling of sedimentary section by deep drilling that penetrates the entire sedimentary section. The full sedimentary section at Lake Tanganyika Rift has been primarily inferred through examination of more than 6000 km 2-D seismic reflection data (Rosendahl, 1987; Rosendahl et al., 1988; Lezzar et al., 1996; McGlue et al., 2008) and only a few studies have analyzed the stratigraphy of the Lake Tanganyika (e.g., Rosendahl, 1987; Lezzar et al., 2002; McGlue et al., 2008).

My research analyzes the tectonostratigraphic evolution of the Lake Tanganyika Rift and considers implications for paleoclimate. It addresses several questions that can be grouped into three main sections:

a) Tectonostratigraphic evolution and paleoenvironmental reconstructions

This section addresses the following questions: (1) How did the structural and tectonic evolution of this multi-segment rift system affect the evolution and distribution of sedimentary facies along the length of the Lake Tanganyika Rift? (2) How did hydroclimate vary over the life-history of the Rift Lake, and how are those variations manifested in vertical and lateral facies variability? (3) What was the paleogeography of the Lake Tanganyika Rift from inception through modern times, and how did lacustrine habitats evolve?

b) The Deep Basin and Underlying Basement Structure of the Tanganyika Rift

This section addresses the following questions: (1) How does the structural strike of shallow rift structures differ from that of deep structures? (2) Do the Kalemie and Mpurungu provinces contain Karoo sediments? (3) What is the structural connection between the Kavala Island Ridge (KIR) and the Mahale Mountains and Katenga - Kugulu - Ntengo lineaments? (4) What is the effect of the KIR evolution on sediment dispersal, and on rift development?

c) Paleo-Hydrologic Connectivity of Rift Lakes Tanganyika and Rukwa in the vicinity of Rungwe Volcano

This section addresses the following questions: (1) Did Lake Rukwa overflow into Lake Tanganyika in the past and cause deposition of deltaic sediments around the Karema Platform? (2) Did the growth of the Rungwe Volcanic Province create a rain shadow around Lake Rukwa area? (3) What is the likely cause of the modern, underfilled condition of Lake Rukwa?

A robust investigation of the tectonostratigraphic evolution of the Lake Tanganyika Rift requires the use of high-fidelity geophysical data sets and drilling information. In chapter 2, I used recently acquired, state-of-the-art 2D seismic reflection data, together with reprocessed legacy data to evaluate the evolution and distribution of sedimentary facies over the rift lake (Shaban et al., 2021). The analysis in chapter 2 revealed six syn-rift seismic units that overlie acoustic basement and identified depositional units beneath the syn-rift sequence that suggest episodes of pre-rift sedimentation. Further, the analysis identified spectacular over-sized deltaic deposits around the Karema Platform, the southeastern part of the Rift (Figure 2). However, apart from speculations, the analysis did not clearly address the source of the deltaic deposits. The full source-to-sink analysis of these deltaic deposits is presented in chapter 4.

In chapter 3, I integrated FTG, aeromagnetic, 2-D seismic reflection data and SRTM DEM with 90m spatial resolution, to better characterize the deep-to-shallow basin structure of the Lake Tanganyika Rift, and the architecture of the pre-rift crystalline basement beneath its ~2-6 km-thick sedimentary fill (Figure 1). Chapter 3 reveals the shallow and deep rift structures, the control of pre-existing basement structures on rift evolution and tests the hypothesis of the presence of the Karoo sediments in the Kalemie and Mpurungu provinces suggested by Delvaux, 2001. Data presented in chapter 3 allow the identification of variations in strikes of the shallow and deep structures. Furthermore, the interpretation suggests a strong correlation between the deep rift structures and pre-existing basement structures. This study provides new insight into the earliest basin architecture of the Tanganyika Rift, controlled by inherited basement structure and provides evidence of their persistent influence on the subsequent basin evolution.

In chapter 4, I test the hypothesis of long-term hydrological connectivity between Lakes Tanganyika and Rukwa employing a landscape evolution model (Fastscape) (Braun and Willett,

2013) that utilizes a module that simulates orographic precipitation by means of a Linear Upslope Model (LM) (Smith and Barstad, 2004). The analysis reveals that Lake Rukwa overflowed into Lake Tanganyika via the Karema depression, and consequently caused the deposition of deltaic deposits around the Karema Platform.

Figures of Chapter 1

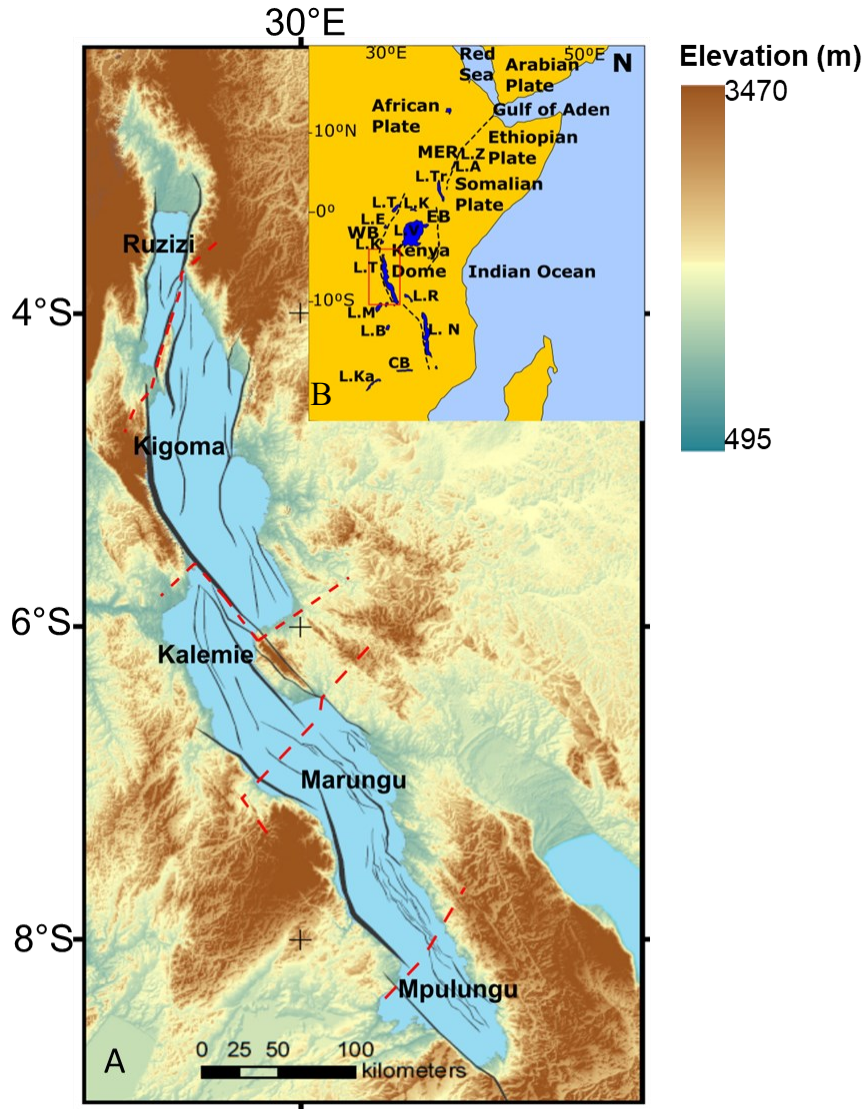


Figure 1: (A) Lake Tanganyika Rift. Note five structural provinces of the rift from Ruzizi in the north to Mpulungu in the south demarcated by dashed red lines. Thick black lines represent the normal faulting trend within Lake Tanganyika, modified after Muirhead et al. (2019) (B) Inset shows the location of Lake Tanganyika within the Western Branch of the EARS. EB and WB are the Western and Eastern Branches respectively of the EARS.

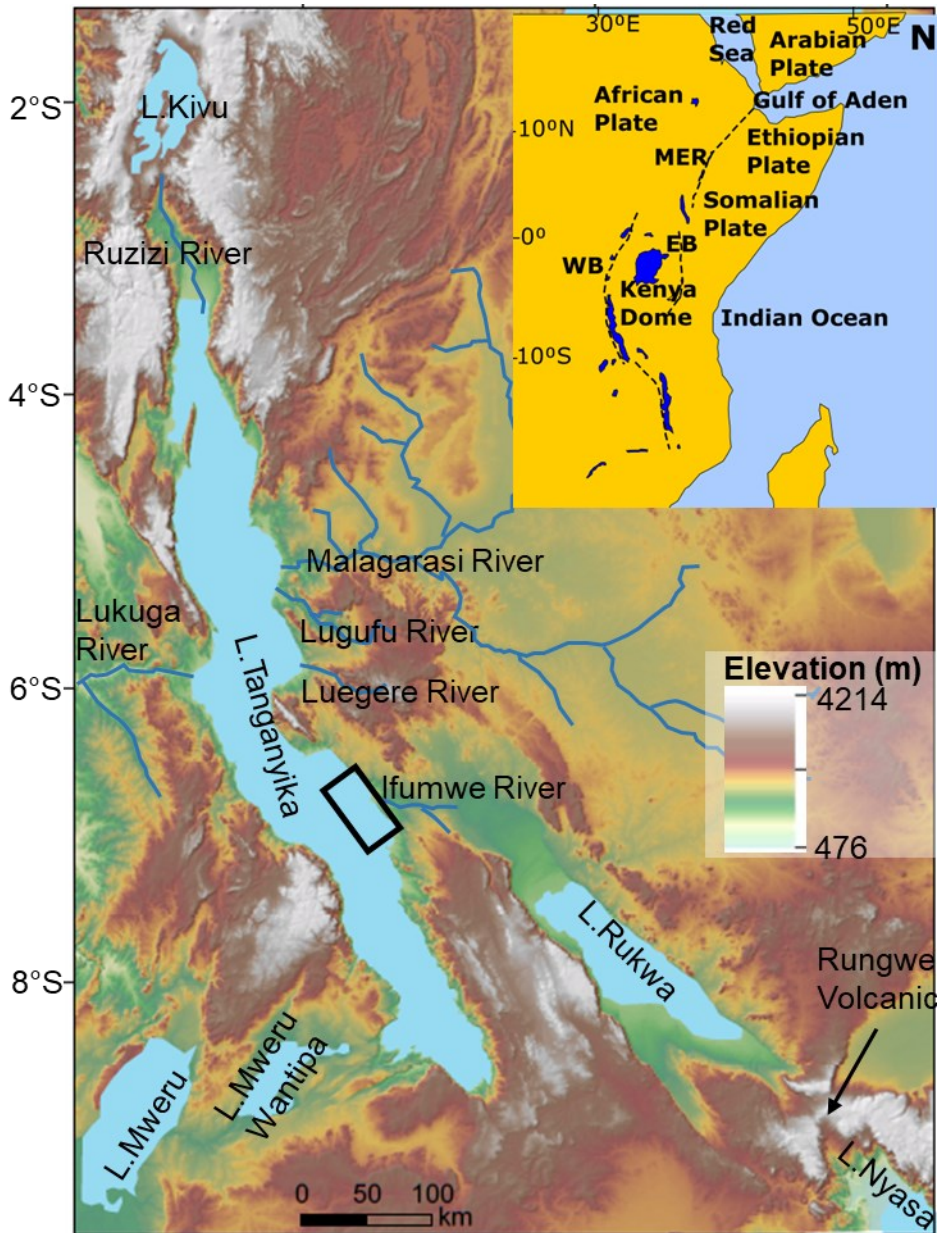


Figure 2: Tanganyika-Rukwa Rift, part of the Western Branch of the East Africa Rift System. Chapter 3 focuses on the Lake Tanganyika Rift whereas Chapter 4 focuses on the area from a thick black rectangle, Lake Rukwa, and northern part of Lake Nyasa (Malawi). The thick black rectangle represents the area where the deltaic deposits have been identified around the Karema Platform (Shaban et al., 2021).

**CHAPTER 2: THE STRATIGRAPHIC EVOLUTION OF THE LAKE
TANGANYIKA RIFT, EAST AFRICA: FACIES DISTRIBUTIONS
AND PALEO-ENVIRONMENTAL IMPLICATIONS**

This Chapter was published as:

Shaban, S.N., Scholz, C.A., Muirhead, J.D. and Wood, D.A., 2021. The stratigraphic evolution of the Lake Tanganyika Rift, East Africa: Facies distributions and paleo-environmental implications. *Palaeogeography, Palaeoclimatology, Palaeoecology*, 575, p.110474.

Abstract

Active continental rifts are ideal sites for understanding the break-up of continents, and long-lived rift lake environments are known as important reservoirs for endemic communities and biodiversity. The sedimentary fill of the Lake Tanganyika Rift records a long history of continental extension and variable tropical climate, that is unparalleled in its duration and fidelity. Recently acquired, state-of-the-art 2D seismic reflection data, together with reprocessed legacy data, are used to evaluate the evolution and distribution of sedimentary facies over the rift lake. Using seismic stratigraphic analysis, we reconstruct past depositional environments and the paleogeography of the lake and assess how tectonic-driven subsidence and hydroclimate variability modified the lake basin. We identify six syn-rift seismic units that overly the acoustic basement and identify depositional units beneath the syn-rift sequence that suggest episodes of pre-rift sedimentation. Based upon the seismic facies analysis, the earliest seismic stratigraphic unit is interpreted as deposited in an early-stage rift system of low-relief, that was dominated by alluvial, fluvial and shallow lacustrine conditions. Subsequent units exhibit attributes of a lacustrine environment of much greater water depth, enhanced catchment relief and accommodation, consistent with a more mature rift. In Seismic units 2-5, we observe extensive deltaic deposits and deep-water fans, and locally canyons, channels, channel-levee complexes, turbidites, slumps and other mass flow deposits. In the latter part of its history, erosional surfaces and abundant lowstand delta facies are observed, indicating the rift experienced dramatic hydroclimate cycles. We assess the relative timing of key features of the rift, including the emergence of major structures and rift segment boundaries, development of major drainages and linkages to upstream rift lakes. The evolving sedimentary facies of the rift illustrate a shallow-

to-deep progression of rift valley environments and the more limited littoral habitats that influenced the evolution of its unique endemic organisms.

1. Introduction

Processes driving extension and hydroclimate variability play important roles in sedimentation in rifts, especially in lacustrine basins (Leeder and Gawthorpe, 1987; Burgess et al., 1989; Buck, 2004; Scholz et al., 2007). Extensional rift basins, such as those within the East Africa Rift System (EARS), are structurally complex and are typically composed of a series of asymmetric rift segments (McKenzie, 1978; Rosendahl, 1987; Morley, 1988; Lambiase, 1990; Logatchev and Zorin, 1992; Sherman, 1992; Muirhead et al., 2019). The spatial and temporal distribution of sedimentary facies in continental rifts may be controlled by a variety of structures such as accommodation zones that segment rifts into individual depocenters, uplifted border fault footwall blocks that direct drainages away from the rift basins, and rift-parallel fault blocks and transfer faults, which influence axial sediment transport (Lambiase and Bosworth, 1995). Variable rates of extension along the basin length also likely promote changing depositional environments (Morley, 1988; Wright et al., 2020), and variability in extension may even influence the evolution and distribution of different sedimentary facies within the same depositional units. Rift-lake basins such as Lake Tanganyika, located at low latitudes, can experience dramatic climatic fluctuations (Lambiase, 1990; Scholz et al., 2007; McGlue et al., 2008; Tierney et al., 2010), which likely affect the distribution of sedimentary facies. Paleoenvironmental and lake-level reconstructions provide insights into the basin evolutionary history and how active tectonism and hydroclimate changes affect lacustrine deposition (Cohen et al., 1997a; Lezzar et al., 2002). Spatial and temporal changes in sedimentary facies distributions over the life history of a rift lake can reveal how depositional environments and rift valley habitats evolve.

Rift lake basins commonly persist for millions of years and behave as ‘island’ ecosystems, evolving complex endemic communities, and serving as model systems for evolutionary biology (e.g. McCune, 1987; Vadeboncoeur et al., 2011; Whiteside et al., 2011). The Lake Tanganyika Rift is also a world class site for evolutionary biology as it contains one of the most diverse collections of endemic species of any lake on the Earth (e.g., Salzburger et al., 2014; Ronco et al., 2021). Establishing its geological evolution provides additional environmental background for the evolution of aquatic and terrestrial organisms (Olsen, 1980; McCune, 1987,1996; Smith et al., 2002).

Here we investigate the tectono-stratigraphic evolution of a multi-segment rift, specifically examining the seismic stratigraphy of ~10 Ma Lake Tanganyika Rift using newly collected and reprocessed multi-channel reflection seismic data. We analyze the temporal and spatial distribution of seismic facies, and consider the following questions: (1) How did the structural and tectonic evolution of this multi-segment rift system affect the evolution and distribution of sedimentary facies along the length of the Lake Tanganyika Rift? (2) How did hydroclimate vary over the life-history of the rift lake, and how are those variations manifested in vertical and lateral facies variability? (3) What was the paleogeography of the Lake Tanganyika Rift from inception through modern times, and how did lacustrine habitats evolve?

1.1. Background to the Lake Tanganyika Rift

The Lake Tanganyika Rift (**Figure 3**) is one of the world’s largest and deepest active rift-lake systems and a site where processes of rift basin formation can be studied today. The Lake Tanganyika Rift contains one of the oldest and most continuous records of tropical climate on the continents (Russell et al., 2020).

The East African Rift System (EARS) initiated in the Oligocene coincident with the opening of the Red Sea and Gulf of Aden (Wolfenden et al., 2005), and produced a series of rift segments, mainly in the form of asymmetric half-graben basins (Rosendahl, 1987; Morley, 1989). Just south of the Main Ethiopian Rift (**Figure 3**), the EARS splits into the Eastern and Western Branches, which are separated by the Archean Tanzania Craton (Rosendahl, 1987; Ebinger, 1989). The Lake Tanganyika Rift is situated in the Western Branch and is occupied by Lake Tanganyika, the deepest and most voluminous lake in Africa, ~645 km long with a maximum water depth of 1470 m. The Western Branch of the EARS is magma-poor compared to the Eastern Branch with fewer than four volcanic centers, including the Virunga Volcanic Province to the north of Lake Tanganyika and the Rungwe Volcanic Province - south of the Lake Tanganyika Rift (Baker, 1971; Mohr and Wood, 1976; George et al., 1998; Furman, 2007; Biggs et al., 2009; O'Donnell et al., 2013). The start of Tanganyika rifting has been estimated at approximately 9-12 Ma (Cohen et al., 1993), or 7.8 - 5 Ma (Pasteels et al., 1989), although these estimates are based upon extrapolations and have considerable uncertainty. These estimates are younger than the 26-25 Ma initiation of the Western Branch of the rift proposed by Roberts et al. (2012), and the postulated Paleogene initiation of the western branch of the EAR as evidenced by the uplift of the Ruwenzori Mountain (Jess et al., 2020).

The Lake Tanganyika Rift is composed of a series of half grabens, each ~80-140 km long by 50-70 km wide (Rosendahl et al., 1986; Rosendahl, 1987; Muirhead et al., 2019; Wright et al., 2020). It is composed of three main bathymetric basins (Ruzizi, Kigoma and Marungu-Mpulungu basins) and several minor sub-basins as evidenced by the existing geophysical data. These sub-basins developed primarily through extension on both border and intra-rift faults (**Figure 3**). Depending on the rifted terrane-type (e.g., Archean vs Proterozoic lithosphere),

border faults accommodate upwards of 90% of the extensional strain (Muirhead et al., 2019; Wright et al., 2020) and, in contrast to basins in the Eastern Branch, rates of border fault slip are inferred to have increased as the system has evolved (Muirhead et al., 2019; Wright et al., 2020). All these normal fault systems influence sediment pathways into the basin (Rosendahl, 1987; Burgess et al., 1989, Gawthorpe et al., 1997; Gawthorpe and Leeder, 2008).

The Lake Tanganyika Rift extension direction is estimated to be E-W in the northern part and NE-SW in the south (Delvaux and Barth, 2010), with total estimated extension of ~3.75 km in the north, 7.07 -7.15 km in the central region, and 2.75 km in the southern section (Wright et al., 2020). The Lake Tanganyika Rift exhibits high topographic relief (>700 m above modern lake level) in several localities, including rift shoulder uplifts adjacent to border faults (Rosendahl, 1987; Wright et al., 2020) (e.g., Burton's Bay Ridge, Mahale Mountains) (**Figure 4**), which likely influence sediment accommodation and past lake morphometry.

1.1.1. Rift segmentation and structural provinces

The Lake Tanganyika Rift is segmented by nine major border faults (Rosendahl et al., 1986; Morley, 1988; Muirhead et al., 2019; Wright et al., 2020). From the north to the south end of the rift, the Lake Tanganyika Rift has been divided previously into five structural provinces (**Figure 3**) namely, the Ruzizi, Kigoma, Kalemie, Marungu, and Mpulungu Provinces (Rosendahl et al., 1988).

The Ruzizi Province is located between latitude 3.38°S and 4.36°S and is bounded by two the major border faults which strike NNE-SSW and SE-NW to the rift axis (Morley, 1988; Muirhead et al., 2019). The maximum lake depth here is ~320 m (TWTT depth of 450) (**Figure 4**). The province is bounded in the north by the South Kivu Volcanic Province and in the south the Burton's Bay intra-basinal ridge. This ridge marks a transfer zone (accommodation zone)

between the Ruzizi and Kigoma Provinces, has a maximum elevation of 1518 m above sea level, and forms an NNE-SSW-trending peninsula onshore (**Figure 4**).

The Kigoma Province, located between latitude 3.79°S and 6.05°S , is bounded by three major border faults that strike NNE-SSW in the north and the SE-NW in the south (Muirhead et al., 2019). The general trend of these faults may in part be controlled by NW-SE-trending structures of the Proterozoic Ubendian belt (Versfelt and Rosendahl, 1989; Klerkx et al., 1998). The maximum lake water depth in this basin is ~ 1230 m (TWTT depth of 1730 ms) (**Figure 4**). In the central area of the province there is a major anticline with \sim N-S striking hinge line (Rosendahl, 1987) and oil slicks have been reported at the lake surface above this structure (Simoneit et al., 2000). In the east, the province shallows onto two fault-controlled platforms, the Nyanza-Lac and Malagarasi platforms (Rosendahl, 1987). In the south, it is separated from the Kalemie Province by another topographic high, the Kavala Island Ridge accommodation zone (**Figure 4**).

The Kalemie Province is bounded by two major border faults in the south-west and north-east both striking NW-SE. This province is located between latitude 5.66°S and 6.65°S . The maximum lake water depth is 1074 m (TWTT depth of 1510 ms).

The Marungu Province is located between latitude 6.65°S and 8.18°S and is bounded by two major border faults on the western side that strike NNW-SSE. The deepest known part of Lake Tanganyika Rift (1470 m, TWTT depth of 1870 ms) is observed in this province (**Figure 4**). It contains major structural features (Rosendahl et al., 1986, 1988, 1992) such as the Moba structural high and the Ikola platform (**Figure 4**).

The Mpulungu Province is the southernmost structural province situated between latitude 8.18°S and 8.85°S . It is bounded by the east-dipping border fault striking NW-SE that follows the shoreline. The deepest water in this province is at ~ 520 m (TWTT depth of 740 ms) (**Figure 4**).

It exhibits two sets of faults, primary NW-SE striking and secondary ENE-WSW striking systems (Muirhead et al., 2019).

1.1.2. Regional geology

Lake Tanganyika is surrounded by Proterozoic and early Phanerozoic mobile belts of high-grade metamorphosed rocks (Choubert and Faure-Muret, 1968) that border the Archean Tanzania craton (**Figure 4**). In the north it is bounded by the Ubendian and Kibaran belts. The NNW-SSE-striking Ubendian belt is composed of gneisses, granites, and mica schists whereas the NE-SW–striking Kibaran Belt in the SW is composed of orthogneisses and high-grade metasediments and schists, quartzites and metaquartzites, and granites on the northeastern side (Fernandez-Alonso and Theunissen, 1998) (**Figure 4**).

Shallow coring of the Upper Pleistocene section encountered diatomaceous ooze-rich shale, siltstone, sands, and localized carbonates (Scholz et al., 2003, 2007; McGlue et al., 2008, 2020). Except for the shallow cores that sample the Holocene and late Pleistocene intervals (Livingstone, 1965; Tiercelin et al., 1988, 1992; Felton et al., 2007), the full sedimentary section at Lake Tanganyika has been primarily assessed through examination of seismic reflection data. Fault throws on border faults controlling accommodation development reach 8 km (Wright et al., 2020). Initial analysis of the Lake Tanganyika Rift suggest it contains more than 6 km of syn-rift lacustrine sediments (Rosendahl, 1987; Morley, 1988). Rosendahl et al. (1988) identified two major depositional units, namely the Magara and Kigoma sequences (oldest to youngest) in the comparatively low-resolution Project PROBE reflection seismic dataset; however, newly collected high-resolution 60-fold reflection seismic data, combined with reprocessed Project PROBE datasets, have since enabled more detailed subdivisions of the syn-rift stratigraphy in recent studies (Muirhead et al., 2019; Wright et al., 2020; this paper).

1.1.3. Hydroclimate

Lake Tanganyika is a meromictic lake, the second largest ($\sim 32,600 \text{ km}^2$) and the second deepest lake in the world and is set in a tropical climate. In the northern area, the lake experiences a moist tropical climate with approximately 1200 mm precipitation annually (Talling, 1991), with rainy seasons occurring between October and May (Stager et al., 2009). Rainfall fluctuations in the area are controlled by monsoon winds and the annual migration of the tropical rain belt (Nicholson, 1999). The modern lake experiences water loss through evaporation (Craig et al., 1974; Cohen et al., 2005; Dettman et al., 2005) and Lukuga River discharge (**Figure 4b**). Evaporation accounts for most lake water loss, 1530 – 2418 mm annually, which occurs mainly during the windy dry seasons ($\sim 250 \text{ mm/month}$, Savijarvi and Jarvenoja, 2000). The Lukuga River annual discharge is equal to 83 mm (Cohen et al., 1997a).

Lake Tanganyika experienced arid conditions in the past including during the late Holocene (Alin and Cohen, 2003) and the Last Glacial Maxima (LGM) from 34 ka to 14 ka (Felton et al., 2007). Earlier, water levels were reduced in the Pleistocene hundreds of meters because of climatic processes (Cohen et al., 1997a; Scholz et al., 2007). These large and rapid water volume variations pose a significant control on the deposition and distribution of sedimentary facies (Rosendahl and Livingstone, 1983) and had major impacts on the paleogeography of the rift valley.

The Lake Tanganyika catchment covers $\sim 238,700 \text{ km}^2$ (Gillman, 1993). Talling (1991) suggests that the Malagarasi River inflow and Lukuga River outflow are the only major pre-rift river systems. The Ruzizi River, which is the outflow of Lake Kivu, drains into the lake axially in the north (Figure 2b) (Haberyan and Hecky, 1987), but likely is far younger than other river drainages in the system (Brooks, 1950; Degens et al., 1973; this paper). Several other drainages

are present on the eastern part of the lake, including the Ugala and Ifume rivers (**Figure 3**), although their contribution to the overall sediment flux is unknown.

1.1.4. Lake Tanganyika Rift fill

Initial studies of the Lake Tanganyika Rift fill arose following seismic data acquisition by Project PROBE in 1983-1984 (Rosendahl et al., 1986). Rosendahl (1987) and Burgess et al. (1989) identified the base of syn-rift seismic units as a set of a distinct low frequency, high amplitude seismic reflections, referred to as the Nyanja Event. Lezzar et al. (1996), Cohen et al. (1997a) and McGlue et al. (2008) used high-resolution reflection seismic data to constrain the uppermost sedimentary strata in the Rift.

The high-relief accommodation zones are areas of basement highs, with only thin sedimentary strata deposited on top (Rosendahl, 1987; Burgess et al., 1989). The low-relief accommodation zones contain thick accumulations of syn-rift fill in some areas (Rosendahl, 1987; Burgess et al., 1989). These structures control the stratigraphic evolution and facies distributions by dictating drainage pathways and depositional environments (Burgess et al., 1989), which include alluvial, fluvial/shallow-water, littoral, deltaic and deep-water hemipelagic and turbidite depositional settings.

2. Data and methods

2.1. Data

This study is based on new and legacy reflection seismic data from Lake Tanganyika. The new data include twenty-one high resolution transects of 2D multichannel reflection seismic commercial data (**Figure 3**) acquired by Beach Petroleum Tanzania Ltd. and the Tanzania Petroleum Development Corporation (TPDC). These data were collected in the southeast part of

the Lake Tanganyika Rift. The 60-fold data have a frequency range of ~5-75 Hz and a vertical resolution of 8-10 m and were acquired using a 3 km-long streamer and a 500 cubic inch air gun array. The profiles are spaced ~ 3 km apart and cover 20% of the entire lake; due to the broadband nature of the data they provide more detailed information on syn-rift structure and stratigraphy than other existing seismic datasets in the area. The new data set is integrated with the legacy Project PROBE 2D seismic data originally acquired in 1983-84 and reprocessed in 2016 by ION Geophysical Company. The legacy data are 24-fold and widely spaced (up to ~28 km), but cover ~1900 line-km over the entire lake. That acquisition program used a 140 cubic inch single air gun and a 48-channel hydrophone streamer, with offsets up to 1450 m. Reprocessing details are contained in the Supplemental Information.

2.2. Methods

We use standard seismic stratigraphic and seismic analysis methods to characterize the Lake Tanganyika syn-rift package. The composition and mode of deposition (depositional setting, hydroclimate changes) impart a significant seismic facies and acoustic impedance variability to the sedimentary section. We use external and internal acoustic characteristics within the seismic units to interpret past depositional environments (**Figure 4**).

We first conducted seismic stratigraphic analysis by mapping of the key horizons bounding the main stratigraphic intervals, using DecisionSpace™ software. This includes identifying seismic reflection characteristics and terminations to recognize individual depositional units (Mitchum et al., 1977; Posamentier and Vail, 1988; Baster et al., 2003). We used stratal terminations such as truncation, onlap, and downlapping reflections to mark the boundaries of different depositional units. In some cases, wholesale changes in acoustic facies were used to discriminate depositional units. Secondly, we mapped seismic facies within each of

the identified depositional units based on seismic reflection attributes such as amplitude, reflection geometry, reflection continuity, and wavelet frequency. Mitchum et al. (1977) define seismic facies as a mappable, three-dimensional seismic units composed of groups of reflections whose parameters differ from those of adjacent facies units. Finally, by examining such acoustic facies we infer bed continuity, spacing, and thickness, lithological properties, and depositional processes (**Figure 5**). For instance, parallel, generally continuous reflections, which are commonly low amplitude and drape the pre-existing features are interpreted as hemipelagic and or pelagic deposits that accumulate mainly during high stand phases. Discontinuous, more or less parallel seismic reflections may represent turbidites. Chaotic, rumpled, and broken wavy seismic reflections are attributed to Mass Transport Deposits (MTDs). Prograding sigmoid clinoforms with steeply dipping seismic reflections with both toplapping and downlapping termination surfaces are associated with fluvial/deltaic inputs. These indicate higher sedimentation rates, limited subsidence, and lake level stillstands. Seismic reflections with an external form filling negative relief in the underlying strata are indicative of channel fills, trough fill, basin fill or slope-front fill (Mitchum et al., 1977; Posamentier and Vail, 1988; Baster et al., 2002).

We present the observations from each seismic unit in a series of seismic facies maps, and then present the interpreted paleogeography in a series of maps that infer the depositional environments of each seismic unit. To account for correlation difficulties, we present maps for the Ruzizi Province and central and southern basins (Kigoma-Kalemie-Marungu-Mpulungu) separately. We begin with the central and southern basins, as it has more coverage, then consider the Ruzizi Province.

3. Results

3.1. Seismic units

We identified six seismic units in the study area from the Nyanja Event acoustic basement to the lake floor, based on the downlap, truncation, incisions, overall reflection geometry and acoustic character (i.e. Muirhead et al., 2019; Wright et al., 2020) (**Figure 6**). Due to the complexity of geological structures along the extent of the lake (~650 km), the correlation of these seismic units from the southern end to the northern end of the lake is only possible with large uncertainties. Consequently, we treat the Ruzizi Basin north of the Burton's Ridge separately from the basins to the south after the deposition of Seismic unit 2. Hence, we present our facies analysis separately for these two areas (Mpulungu-Kigoma and Ruzizi). The Marungu Province is the best place to clearly assess the seismic units' evolution, as it is covered by the latest 2012/2014 seismic data set (**Figure 3**). Generally, all depositional units show thickening towards the bounding faults on structural dip-lines (Muirhead et al., 2019; Wright et al., 2020). Below the Nyanja Event we observe low-frequency high-amplitude, sub-parallel to parallel reflections in several locations, especially in the Marungu Province (**Figure 7**). These facies extend more than 100 km south-north on the eastern and north-eastern part of the Manda Graben. These deep facies are identified for the first time in the rift and are clearly observed using the latest 2012/2014 2D reflection seismic data set (e.g. only clearly observed in the Marungu Province). Previous studies (Rosendahl, 1987; Burgess et al., 1989) identified the Nyanja event as the contact between the syn-rift fill and pre-rift basement.

3.2. Central and southern basins (Kigoma, Kalemie, Marungu-Mpulungu)

3.2.1. Seismic unit 1

Seismic unit 1 is the oldest sedimentary package that overlies the Nyanja Event. This unit and the Nyanja Event exhibit relatively uniform seismic characteristics along the entire rift. Seismic unit 1 is characterized by low to moderate amplitude, low frequency, semi-continuous to continuous seismic reflections (**Figure 6, 8**). In the Marungu Province, tilted internal reflections of Seismic unit 1 dip towards the southwest throughout the seismic unit. Generally, seismic unit 1 thickness increases toward the border faults, westward in most provinces, with the thicknesses ranging from ~500 ms to ~1000 ms TWTT. The thickest section (~1000 ms TWTT) is observed in the Manda Graben of the Marungu Province (**Figure S1**) and it is generally thin in the Kalemie and Mpulugu provinces. Seismic unit 1 displays the least seismic facies variability except in parts of the Kigoma and Ruzizi provinces in which relatively minor high-amplitude reflectors are observed.

3.2.2. Seismic unit 2

Seismic unit 2 overlies Seismic unit 1 and shows considerable variability in acoustic response compared to Seismic unit 1 (**Figure 6**). It is because of this marked change in seismic reflection characteristics that we considered it as a separate depositional package. The seismic unit is mainly characterized by moderate amplitude, semi-continuous to continuous seismic reflections, with a slight wedge-shape external form thickening westward towards the faults (**Figure 6**). Parallel, continuous reflections dominate this unit from the Mpulungu area to the Kigoma Province. Sub-parallel, discontinuous, mixed amplitude reflections are only seen on the eastern margin around the eastern and north-eastern parts of Kigoma, and in the south-eastern

part of the Mpulungu Province (**Figure 8**). Chaotic, rumpled, broken, wavy reflections are localized in the Marungu and Mpulungu provinces (**Figure 8**). As observed in Seismic unit 1, Seismic unit 2 is thickest in the Marungu Province with a maximum thickness of ~1600 ms TWTT (**Figure S1**). The top of this unit is truncated by Seismic unit 3 seismic reflections, and it is missing on the shallow platform along the eastern (Marungu Province) and southern (Mpulungu Province) shore (**Figure 8**).

3.2.3. Seismic unit 3

Facies of Seismic unit 3 vary considerably compared to Seismic unit 2 (**Figure 8**). It is dominated by moderate amplitude, semi-continuous to continuous seismic reflections, with intervals of low-amplitude, chaotic seismic reflections. Clinoform features close to the margins are characterized by low amplitude to reflection-free discontinuous seismic reflections (**Figure 10**). Seismic unit 3 within the Kalemie and Kigoma Provinces is dominated by parallel, moderate-high continuity, high-amplitude and transparent to semi-transparent reflection facies with lens-shaped fills and external geometries. In the southeast of the Marungu Province, two stacked channels are observed, one cutting and filling the other (**Figure 9**). They are both characterized by low-amplitude to reflection-free, discontinuous seismic reflections. Similar to Seismic unit 2, sub-parallel, discontinuous, mixed-amplitude reflections are only seen on the eastern and north-eastern parts of Kigoma, and in the south-eastern part of Mpulungu Province; numerous small-scale incisions, and subtransparent-transparent reflections are observed on the eastern part of the Kigoma Province (**Figure 8**). In contrast to Seismic unit 2, Seismic unit 3 has sub-parallel, discontinuous, semi-transparent reflections in the Kalemie Province, southwestern and northeastern parts of the Kigoma Province, and the northern part of the Marungu Province (**Figure 8**). Seismic unit 3 unconformably overlies Seismic unit 2 in many localities (**Figure 6**).

On the Karema platform, an erosive top is suggested based on observed wavy reflections (**Figure 6**). Seismic unit 3 is thinner than the underlying seismic units with a maximum thickness of ~350 ms in the Marungu Province.

3.2.4. Seismic unit 4

Seismic unit 4 overlies Seismic unit 3 and is characterized by predominantly high amplitude, parallel to sub-parallel, and continuous to semi-continuous reflections (**Figure 6, 8**), although locally it shows lower amplitudes. Sub-parallel, discontinuous, mixed-amplitude reflections are observed in the southern part and northeastern parts of the Kigoma Province, the western part of the Kalemie Province, and in the southeastern part of Mpulungu Province (**Figure 8**). The prevalence of chaotic, discontinuous wavy reflections increases significantly in the southeastern part of the Marungu Province (**Figure 8**). As with Seismic unit 3, we observe fewer parallel, discontinuous, mixed amplitude reflections around the eastern and northeastern parts of Kigoma, and in the southeastern part of Mpulungu Province (**Figure 8**). Generally, in the Manda Graben, Seismic unit 4 is very similar to Seismic unit 3. In the northeast part of the Marungu Province, wavy seismic reflections are observed at the top of the unit. Compared to the other seismic units, in the Marungu Province the thickness of Seismic unit 4 is as much as ~1200 ms TWTT. In the Karema area in the Marungu Province and near Izinga in the Mpulungu Province, where there is a high density of profiles, we observe an increase in chaotic reflection packages and oblique-prograding clinoforms (**Figure, 8, 10, 11**). In the Kigoma Province, the prograding clinoforms are observed in the far west dipping towards the south-west (**Figure 8, 12**). On the eastern side of the Ntiri Block, there is a large lens-shaped package of transparent reflections that extends northward for ~20 km (**Figure 13**).

3.2.5. *Seismic unit 5*

Seismic unit 5 overlies Seismic unit 4 and is generally observed from the Kigoma to Mpulungu Province (**Figure 6**). It is marked by parallel, continuous reflections with small scale incisions, subtransparent-transparent facies, westward prograding clinofolds, chaotic reflections, and sub-parallel, discontinuous, mixed-amplitude reflections (**Figure 6**). Subparallel, discontinuous facies, with variable amplitude reflections are observed around the eastern margins of the Mpulungu, Marungu and Kigoma Provinces, and the western part of the Kalemie Province (**Figure 6**).

The base and top of Seismic unit 5 are marked by undulating seismic reflections (**Figure 4**). This seismic unit exhibits varying internal character depending on its position such as on the margin or in the distal parts. For example, around the Karema area, down-dip near the basin floor, Seismic unit 5 is marked by downlapping reflections towards the southwest. Compared to Seismic units 1-4, Seismic unit 5 is characterized by the increasing occurrence of both paleo- and modern canyons and incisions (**Figure 6**). For example, in the strike-line BST12-50, Seismic unit 5 is deeply incised by modern canyons and exhibits bi-directional downlap of the clinofolds, primarily near the inflow of the Ifume River (**Figure 8**). Seismic unit 5 has a maximum thickness (~ 400 ms) in the North Mpulungu Province and is generally less than ~200 ms thick elsewhere (**Figure S1**).

3.2.6. *Seismic unit 6*

Seismic unit 6 marks the uppermost depositional package in the study area, the top of which is the modern water-sediment interface. This unit is clearly observed in the Mpulungu and Marungu provinces. Seismic unit 6 is characterized by predominantly low amplitude, continuous,

parallel seismic facies (**Figure 8 and Figure 9**). These characteristics extend over the entire central and southern part of the basin, except in the Kigoma Province where it is marked by moderate-high amplitude continuous, parallel reflections. In the north-eastern part of the Karema area, its basal contact is marked by onlapping reflections overlying Seismic unit 5 (**Figure 4**). In the distal areas there is no evidence of onlapping reflections, and the reflections exhibit a draping geometry. Seismic unit 6 is the thinnest unit overall, varying between ~15 and ~50 ms TWTT with the thickest part observed in the South Mpulungu Province (**Figure 8**).

3.3. Ruzizi basin (North Lake Tanganyika Rift)

The Ruzizi basin contains syn-rift sediments that thicken towards the western border fault in the northmost part of the province to a maximum thickness of ~3100 ms TWTT. We identified six seismic depositional seismic units above the Nyanja Event, of which only Seismic unit 1 could be easily correlated with the seismic units identified in the central/southern basins of the Lake Tanganyika Rift (**Figure 7**). However, Seismic unit 1 in the Ruzizi Basin exhibits local occurrences of relatively higher amplitude reflections compared to the southern basins. It has an average thickness of ~300 ms and maximum thickness of ~400 ms TWTT, only ~40% of the maximum value observed in the southern basins. (**Figure 4**)

3.3.1. Seismic unit 2

Seismic unit 2 in the Ruzizi Province is characterized predominantly by nonparallel to sub-parallel mixed-amplitude reflections. Within this seismic unit, parallel continuous reflections are mainly observed in the eastern part of the basin (**Figure 7, 12**). Only localized sub-parallel, discontinuous, semi-transparent reflections are observed adjacent to the Burton's Ridge. Its thickness ranges from 200 -350 ms TWTT.

3.3.2. *Seismic unit 3*

Seismic unit 3 in the Ruzizi Province like other units, exhibits a wedge-shape geometry across the province. Its wedge-shape geometry thickens westward towards the faults. Seismic unit 3 characterized predominantly by parallel, medium-high-amplitude reflections. Other seismic facies observed within this seismic unit include sub-parallel, discontinuous semi-transparent reflections (**Figure 7, 12**). Seismic unit 3 has an average thickness of ~200 ms.

3.3.3. *Seismic unit 4*

Across the Ruzizi Province, Seismic unit 4 exhibits variable seismic facies, including sub-parallel, discontinuous semi-transparent reflections in the northern and eastern parts of the Province. Also, localized chaotic, broken, wavy reflections are observed in the northern tip of the province. The southern part is dominated by parallel medium-high amplitude reflections, and sub-parallel, discontinuous semi-transparent reflections. Seismic unit 4 is the thickest seismic unit in the Ruzizi Province overall, with an average thickness of ~ 400 ms (**Figure 7**).

3.3.4. *Seismic unit 5*

Seismic unit 5 in the Ruzizi Province is characterized by parallel, continuous medium-high amplitude reflections, and small-scale incisions, as well as moderately transparent reflections, as in Seismic unit 4. In the southern part of the basin, mixed amplitude, nonparallel to sub-parallel reflections dominate. In the north part of the Ruzizi Province, southward prograding clinoforms reflections are observed within Seismic unit 5 (**Figure 12, 13**). Seismic unit 5 ranges in thickness from 50 – 300 ms.

3.3.5. *Seismic unit 6*

Seismic unit 6 contains a collection of prograding clinoform reflections from the northern edge to the central part of the Ruzizi Province (**Figure 12**). About half of the seismic unit is dominated by parallel, continuous medium-high amplitude reflections. Other facies observed within Seismic unit 6 include sub-parallel, mixed-amplitude reflections and discontinuous semi-transparent reflections (**Figure 12**). It has an average thickness of ~200 ms.

4. Discussion

4.1. Tectonic controls on evolving sedimentary facies distributions

Seismic facies analysis of the latest reflection seismic datasets provides new insights into the evolution of the Lake Tanganyika Rift and its paleogeography over time. We have used the work by Mitchum et al. (1977) and Posamentier and Vail (1988) as a benchmark for the correlation and connection of seismic facies as well as the generation of palaeogeographical maps. However, due to the sparseness of the PROBE data set and the difference in vertical resolution of between the two seismic data sets used in this study, the correlations are prone to uncertainties. In order to minimize these uncertainties, we augmented the work by Muirhead et al. (2019), Wright et al. (2020) and the commercial potential field data.

The low-frequency high-amplitude reflections below the Nyanja Event (**Figure 6, 7**) may represent either Karoo rocks or possibly earlier Cenozoic deposits such as those described for the Rukwa Rift (e.g. Wescott et al., 1991; Morley et al., 1999; Roberts et al., 2012). We observe these reflections in the area adjacent to the Rukwa Rift, supporting the suggestion of deposits like those reported in the Rukwa Rift. The Nyanja Event has been attributed to either

sedimentary strata or lava-flows that cap pre-rift sediments (Rosendahl et al., 1988). However, we suggest that the Nyanja Event represents an old erosional or piedmont surface across most of the Lake Tanganyika Rift. In many places it is very irregular; the high-amplitude character suggests strong contrast between late-Cenozoic sediments to crystalline rocks.

The wedge-shaped geometry of all depositional seismic units above the Nyanja Event suggests that these packages are of syn-rift origin (e.g. Morley, 1989), and such geometries are recognized in other rifts around the world (e.g. Schlische and Olsen, 1990). A major shift in the seismic unit expansion toward the border faults (i.e. degree of “wedging” of the sedimentary section) from the lower to upper seismic units suggests a continued increase in fault-controlled subsidence with time (Muirhead et al., 2019; Wright et al., 2020). Thickening of seismic packages towards the border faults and other major intra-rift faults suggests that these faults accommodate most of the upper crustal extension in the basin (Muirhead et al., 2019). Our observation of low-moderate-amplitude, semi-continuous to continuous seismic reflections in Seismic unit 1 during the initial phase of rifting, suggests that early-rift sediments were deposited in either fluvial environments, shallow lake(s) or both. This is consistent with models for early rift evolution that propose initial rift deposits are composed of alluvial and fluvial basal sands and gravels and shallow lacustrine shales (Lambiase, 1990). Seismic unit 1 can be traced across the entirety of Lake Tanganyika Rift and exhibits little variation in external form. Accordingly, during this phase, the lake was either well-connected from north to south or only minor topographic highs were present that created major barriers. Although Seismic unit 1 is not preserved at the top of the Burton’s Bay Ridge, we attribute this to erosion as result of sub-aerial exposure. We observe evidence of erosion on top of the Burton’s Bay Ridge on seismic profile ION-PROBE 83-14 as marked by erosive top. The observation that Seismic unit 1 is relatively

thin in the northern area of the Lake Tanganyika Rift suggests that during this time the accommodation in this area was limited compared to the rest of the rift (**Figure 9**).

Reflection terminations of Seismic unit 2 onlap Seismic unit 1 in the northeast part of the Marungu Province, suggesting that this unit was deposited during a period of rising lake level (Figure 4). Its high continuity character extends from the Kigoma Province to the Marungu Province, suggesting that during this time the lake was longer and deeper than the earlier (Seismic unit 1) phase of the Lake Tanganyika Rift. As the accommodation increased with time, due to increased subsidence from both extension and sediment loading, more sediments were deposited.

The boundaries of seismic units 2-6 cannot be definitively correlated between these provinces. Accordingly, we interpret that during or just before the deposition of Seismic unit 2, a paleo-drainage divide developed that separated the Ruzizi Province from the rest of the rift zone. Though the exact timing of this event is not constrained, we suggest that the Burton's Bay Ridge has long been a sedimentary depositional divide between the Ruzizi and Kigoma provinces, except for a narrow gap on the eastern side of the ridge (**Figure 8**).

The Kavala Island Ridge is another important structural high in the Lake Tanganyika Rift that separates the Kigoma and Kalemie provinces (Figs. 1 and 2). Several authors have identified this structural feature as the primary paleo-drainage divide during past lake low-stands that produced distinctly different lakes (e.g. Brooks, 1950; Scholz and Rosendahl, 1988). This phenomenon may have directly forced the geographic separation of cichlid populations, resulting in unique clades (Sefc et al., 2007; Koblmüller et al., 2008; Vadeboncoeur et al., 2011; Danley et al., 2012).

Following development of the Burton's Bay Ridge, extensional deformation, basin subsidence and rift margin uplift accelerated between deposition of Seismic unit 1 and Seismic unit 5. This is supported by several lines of evidence for enhanced relief in the catchment over time. This evidence includes small-scale incisions indicative of channels, especially along the eastern margin of the rift; mass transport deposits (MTDs) and turbidites in the deep water; and progradational clinoforms along the eastern margin and the Ruzizi Province (**Figure 8, 10, 11, &12**). On the eastern side of the Marungu Province around the Karema area, the dominant seismic facies (seismic units 3 – 5) suggest abundant deltaic deposits, channel fills and turbidites, whereas in the Mpulungu Province the common facies suggest mass transport deposits (MTDs), shallow lake and/or fluvial, and channel fill deposits (**Figures 5, 6, 8, 10**). Wright et al. (2020) suggest that during the deposition of Seismic unit 1 and 2 70% of crustal extension was accommodated by border faults. During the deposition of Seismic units 3-6, however, extensional strain localized further on to border faults, which accommodated the majority of rift extension and would have subsequently enhanced the rate at which rift topography developed (Wright et al., 2020). An example of the evolution of high relief areas late in the evolution of the Lake Tanganyika Rift is the uplift of the Ntiri High; based on the erosional syn-deformational unconformity in the southern part of the structure and lack of asymmetric thickening, the Ntiri High likely postdates depositional Seismic unit 4 (**Figure 13**). The fault slip events that accommodated this uplift in conjunction with border faults in the eastern part of the province may have caused landslides that resulted in slumps and other MTDs in the deep-water areas in the northern and southern parts of the Ntiri High during deposition of Seismic units 4 and 5 (**Figure 8**). Additional evidence for increased relief includes channel deposits on the

Punda platform (Figure 2) within Seismic unit 5, as well as an increase in shallow lake/fluvial deposits in that area (**Figure 8**), which all together suggest an uplifted margin.

Other evidence of enhanced relief is the spatial and temporal distribution of depocenters. We observe the migration of depocenters with time to areas of maximum subsidence (**Figure S1**). For instance, at the end of Seismic unit 1 time, the thickest sedimentary packages for this unit in the Marungu Province are observed in the central part of the Province near the Ikola (Karema) Platform whereas at the end of the end of Seismic unit 3 time, the depocenter migrated towards the south-western part of province against the border fault (for details see Supplementary Material). Also, during the deposition of Seismic units 1-2, the depocenter is observed in in the central and south-western part against the border fault in the Kigoma Province, and in the southern part against a south-western border fault in the Kalemie Province. However, during the Seismic units 3-6 deposition there is an overall thickening of sediments towards the northern and eastern central parts of the Kigoma Province and the eastward shift in the Kalemie Province (Wright et al., 2020).

4.2. Hydroclimate controls on evolving sedimentary facies distributions

Lake Tanganyika Rift exhibits evidence of lake level drops that developed rapidly, over periods of a few thousand years, which has been attributed to hydroclimate variability rather than extensional deformation (Scholz and Rosendahl, 1988; Scholz et al.,2007; McGlue et al., 2008). The angular stratigraphic discordance and truncations at the basal contact of Seismic unit 3, coupled with highly variable seismic facies characteristics, suggest that this package may have been deposited during one or more lake level lowstands, also likely as a result of climate variability. As mentioned previously (Section 4.2.3), clinofolds in the Karema area observed

within Seismic unit 3 are clearly indicative of a westward prograding delta complex when lake levels were ~460 m lower than modern. Deltaic deposits are also found at the same approximate stratigraphic level in the Ruzizi Province (**Figure 14,15**), suggesting that the hydro-climatic event that controlled lake level and deposition was regional in nature. Severe arid climate episodes such as the mega-drought event proposed for the interval between 135 ka and 75 ka that reduced ~95% of the Lake Malawi's water volume have been suggested in the region (Scholz et al., 2007). Scholz et al. (2007) suggested that this aridity caused the lake level of the Lake Tanganyika Rift to drop by at least ~390 m relative to present. The arid climate followed by wetter conditions triggered abrupt lake-level rise in the Lake Tanganyika Rift and East Africa during the Pleistocene (Haberyan and Hecky, 1987; Gasse et al., 1989; Gasse, 2000; Scholz et al., 2007).

Deciphering the timing and nature of riverine inputs and large-scale fluvial sediment distribution in the rift is of paramount importance for understanding the lake's water balance, the biogeography of endemic populations, and past environments. Interestingly, a series of southwestward prograding clinofolds is also observed on the southeast side of the Burton's Ridge (**Figure 12**), more than 70 km from the northern tip of the Lake Tanganyika Rift. To account for these deposits, we suggest that during an arid interval the Ruzizi delta prograded far to the south through a narrow gap in the eastern side of the Burton's Ridge. Alternatively, during that time either the Mugara channel or Nyengwe channel may have been large enough to prograde to the offshore area, depositing these deltaic sediments. In the Karema area, the extent of deltaic deposition into the offshore area is markedly affected by intrabasinal faults. Similar delta deposits in the rift-lake basins have been documented in Lake Malawi (Scholz, 1995;

Lyons et al., 2011), Lake Edward (McGlue et al., 2006) and previously at Lake Tanganyika (McGlue et al., 2008).

Many continental margins with narrow shelves like the Lake Tanganyika Rift are characterized by deeply incised canyons that act as discharge-storage systems. These canyons force sediments to be deposited on the middle shelf and deeper parts of the basin via both surface plumes and bottom currents (Sømme, 2009). The well-studied eastern margin of the Lake Tanganyika Rift has canyons and marginal channels that deliver sediments beyond the margin edge. We suggest that deltas were deposited by both small and major drainage systems. Distal turbidite sedimentation in the deep parts of the basin was significant due to these canyons. However, due to the sparseness of the seismic data, only a limited number turbidite fan complexes were identified in this study, except for the southeast study area covered by the 2012/2014 seismic dataset (**Figure 3 and 8**). Around the Karema Platform, between the two major canyons, four stacked overlapping sets of clinoforms are observed (**Figure 10**). Except for these canyons and the Ifume River, the modern shoreline shows no evidence of active major rivers or drainage systems that could be responsible for the thick deltaic deposits observed around the platform. The modern Ifume River is a relatively small drainage, and seemingly is too small to feed the observed progradational delta packages. The volume of individual clinoform sets range from 2.81 km^3 to 38.5 km^3 whereby the mass ranges from 6.0 megaton to 82.0 megaton. A total of 7 deltaic units have been recognized with a gross volume more than 100 km^3 and an average surface area of $\sim 190 \text{ km}^2$ and $\sim 650 \text{ km}^2$ in the lower and upper intervals respectively. Using standard source-to-sink relationships (Coleman & Roberts, 1989; Milliman & Syvitski, 1992), these areas suggest drainage areas of $1.63 \times 10^3 \text{ km}^2$ and $1.77 \times 10^3 \text{ km}^2$ respectively. The average thickness of individual clinoforms at the Karema area is

approximately three-times that of the Dwanga (Lake Malawi) (Scholz, 1995) and Malagarasi Platform (Lake Tanganyika), and about four-times that of Lake Edward (McGlue et al., 2006). The Karema paleo-delta feature may have been formed during a time when Lake Rukwa was at a high-stand, outflowing into the Ifume River. The long-term water level history of Lake Rukwa is unknown, although it overflowed in the geological past, and as recently as the late Pleistocene and Holocene (Delvaux and Williamson, 2008; Cohen et al., 2013). One possible explanation for the deposition and then abandonment of the over-sized Karema deltas is that the once vigorous Rukwa outflow diminished when precipitation in the Rukwa catchment was reduced due to a rain shadow that developed north of the growing Rungwe volcanic edifice. Lake Rukwa is the only major lake in the western branch of the EAR that is hydrologically underfilled today. Whereas the evidence for magmatic activity in the Rungwe Volcanic Province suggest the Miocene age (Mesko et al., 2014), most documented Rukwa tephras date to the late Pleistocene (Thevenon et al., 2002). Further study of Lake Rukwa's hydrological record, and more details of the growth of the Rungwe Volcanic Province are required to test this hypothesis.

The Karema region (**Figure 3**) is especially well-constrained by new seismic data acquired in 2012/2014. Based on the dominance of high-amplitude continuous to semi-continuous seismic reflections on the Karema platform, we suggest that this area was dominated by near shore environments during Seismic unit 5 time (McGlue et al., 2008). Seismic unit 6 is dominated by hemipelagic sediment, as denoted by relatively parallel, weak- to moderate-amplitude, continuous, acoustically stratified seismic reflections. This is also supported by the work of Felton et al. (2007), who suggested profundal lithofacies, mainly organic-rich ooze and clay in the most recent sediments. The deposition of Seismic unit 6 is attributed to the latest major high stand phase in the Late Pleistocene (Felton et al., 2007; McGlue et al., 2008, 2020).

Units with moderate- to highly chaotic seismic reflections occurring mostly below the ‘Late Pleistocene’ deposits (**Figure 10**) are interpreted as slumps on the subaqueous fans. This suggests slope instability during this time. Erosional features observed mostly on flexural margins are attributed to tectonic uplift and to varying water levels driven by hydroclimate shifts.

4.3. The evolving paleogeography of the Lake Tanganyika Rift

Our analysis of the seismic facies of the Lake Tanganyika Rift provides new insights into the timing of the development of the major drainages into the lake. Deciphering the timing of the major drainages is key to establishing the sedimentary fill history and the paleolimnology of the basin. The major drainages developed gradually as the rift evolved.

The Malagarasi River may be the oldest major drainage to deliver sediments in the basin. Its initial impacts on the sedimentary section are observed in Seismic unit 3 (Central and Southern Basins) as manifested by turbidites and channel complexes (**Figure 8** and **Figure 16**). As extension progressed and topographic relief increased, the impact of the Malagarasi River was amplified, as observed in channel complexes extending more than 50 km north-south along the axis of the Kigoma Basin, and in turbidite facies (e.g. sub-parallel, discontinuous semi-transparent reflections) and submarine canyons in Seismic units 4 and 5 (**Figure 16**). Whereas the river flows east to west before it enters the lake, the observed offshore canyon and channel complex first extends southwest across the Malagarasi Platform, then bends to the north into the deep basin. We postulate that this sharp bend is due to footwall uplift of the eastern border fault in the Kigoma Province, and the thalweg extending around the fault’s southern tip (**Figures 4, 8**). Its depositional impact is observed beginning in the later stage of Seismic unit 3 deposition (Kigoma Province), as marked by complex sub-lacustrine fans (**Figure 16, 17**).

The first evidence of deltaic clinofolds attributed to the Ruzizi River is observed in Seismic unit 4 in the northwestern part of the Kigoma Province (**Figure 8 and 12**). During that time, the Ruzizi River may have prograded 70 km southwest of its modern mouth (section 5.2). However, the first clear evidence of clinofold facies in the Ruzizi Province is observed in Seismic unit 5 (Figure 12 and 13). This suggests that during Seismic unit 4 deposition, either the deltaic deposits formed thinner clinofolds that could not be resolved because of the low vertical resolution of the PROBE data set, or the province was under fluvial deposition and developed a broad delta plain.

Minor drainages such as Kapanza River and Mugara channel in the Ruzizi Province began delivering sediments during the deposition of Seismic unit 3, as manifested by turbidites and channels (**Figure 15**). By comparing the size of different deposits, we suggest that these two channels were previously larger drainages than observed today. These channels may have been later dammed by landslides or their baselevels were affected by tectonic uplift, and further investigation is warranted.

4.4. Model of rift basin evolution

Our suggested model for the development of structural-controlled stratigraphy in extensional rifts (**Figure 17**) is broadly consistent with and validates previous models of rift-infilling (Frostick and Reid, 1990; Lambiase, 1990; Morley et al., 1990; Tiercelin, 1990; Lambiase and Bosworth, 1995). For example, Lambiase (1990) proposed a tripartite model of rift evolution, with the initial rift stage dominated by alluvial, fluvial and or shallow-water lakes (**Figure 17**). As the faults continued to propagate and link, subsidence increased rapidly, allowing the deposition of deep-water facies (e.g Seismic unit 2 in Lake Tanganyika). This

introduced widespread lacustrine deposits, though in the case of Lake Tanganyika, high-relief accommodation zones, likely initiated during this time, may have acted as barriers to wide-sediment dispersal. Lambiase and Bosworth (1995) suggest that topographically high-relief accommodation zones can segment rifts into long structural half-grabens (50-150 km). Thus, each half-graben influences the distribution of sediments, causing spatial and temporal variations of discrete depocenters (e.g., **Figure S1**). We observe that the distribution of MTDs tends to be controlled mainly by hanging wall drainages (**Figure 8**). Also, the footwall uplift of some border faults is shown to direct some drainages away from the rift basin. As a result, the rift shoulders in the Lake Tanganyika Rift generally lack major drainages that flow directly into the basin (e.g., the western margin of the Rift), and most of the depocenters tend to be distributed adjacent to the border faults (**Figure 8, 14, and Figure S1**). The latest stages of the rift experienced expanded deltaic facies, shallow-water facies (e.g., Seismic units 3-5) and hemipelagic deposits in deeper lacustrine environments (e.g., Seismic unit 6). The deltaic facies are observed at the entry points of flexural margin drainages (e.g., Karema Platform and Malagarasi Platform). In the Lake Tanganyika Rift, the flexural margin is cut both by large drainages such as the Malagarasi River and smaller ones such as the Ifume River.

Parallel intrarift faults, that formed during the later stages of rifting, tend to block the continuity of sedimentary facies across the lake, resulting in compartmentalized sub-basins, like those described in other systems (Lambiase and Bosworth, 1995; Scholz, 1995). Unlike other rifts such as the Newark Group basins (Lambiase and Bosworth, 1995), the Lake Tanganyika Rift is marked by major intrarift normal faults that extend through the youngest parts of the sedimentary section, indicating ongoing activity (Rosendahl, 1987; Burgess et al., 1989; Muirhead et al., 2019; Wright et al., 2020). These faults act as barriers to sediment deposition,

subdividing half-graben basins into several minor depocenters, hence causing facies compartmentalization within the same rift segment (**Figure 8**).

Based on qualitative assessment of the geological terrains surrounding the Lake Tanganyika Rift (Figure 2) and the paleogeographic maps for seismic units 3 - 5 (Figure 6), we observe a greater abundance of mass transport deposits (MTDs) in the Bangweulu Block, and a preponderance of turbidites, channel complexes and deltaic deposits in part of the lake adjacent to the Ruzizian-Ubendian Belts (Figure 2, 6, and 12). Wright et al. (2020) demonstrate variations in the style of rifting and distribution of fault-related strain in these basement terranes of varying mechanical strength in the Lake Tanganyika Rift, which can ultimately lead to considerable variations in rift topography along this multi-segment rift basin. As such, one possible explanation for the abundant MTDs in Bangweulu Block segments is that the greater mechanical strength of the Bangweulu Block resulted in more steeply dipping border faults, and consequently steeper slopes on the lake margins that facilitated delivery of mass flows into the deeper reaches of the lake.

4.5. Habitat variability over time.

In large tropical lakes, water depth is the main control of the distribution of aquatic habitats (Olsen 1990). This is because the key aspects of lake's limnology such as light penetration, turbidity, currents, and mixing are a function of water depth. Most of the biodiversity in Tanganyika is highly restricted to the littoral zones (Cohen et al., 1997; Vadeboncoeur et al., 2011; McGlue et al., 2020; Russell et al., 2020). We envisage that at the end of Seismic unit 1 and early in Seismic unit 2-time, shallow conditions were widespread, and accordingly the water column was unstratified. However, as the rifting progressed and the lake

deepened (e.g., at the end of Seismic unit 2 through Seismic unit 3), habitats became restricted to the lake margins (littoral zones). It was only during this period that permanent stratification would have become possible, further inhibiting the biodiversity in deep waters. Complex seasonal chemocline dynamics would also have developed during these later intervals (Craig et al., 1974; Beadle, 1981; McGlue et al., 2020). With continuing border fault subsidence, the enhanced topography of several of the accommodation zones would have further served as geographic barriers, facilitating increases in speciation, especially in the latter intervals of rift development.

Conclusions

Six depositional seismic units were consistently identified in the Lake Tanganyika Rift based on the latest integrated commercial and reprocessed 2D multichannel reflection seismic datasets, indicating a complex history of extensional tectonics and hydroclimate variability. Seismic facies analysis reveals how the tectonics and hydroclimate processes controlled the facies distribution and the rift development. During the early stage of rift development, fluvial and or isolated shallow lakes dominated the landscape and sediment deposition (Seismic unit 1) as indicated by low-moderate-amplitude, semi-continuous seismic reflections. Border faults and topographically high accommodation zones segment the rift into long structural half-grabens, dictating sediment distributions. Burton's Bay Ridge acted as a significant sediment barrier between the Ruzizi and Kigoma Province resulting in contrasting depositional successions following the deposition of Seismic unit 1. As border faults continued to propagate and link, in conjunction with increased subsidence the rift focused onto the present border fault configurations and experienced sustained deep lake conditions (Seismic unit 2). This unit is characterized by the dominance hemipelagic deposits. During the later stages of the rift

development (e.g., Seismic units 3-5), the rift valley deepened, and regions of enhanced relief developed on the rift margins. The basin also experienced increased amplitude and frequency of lake level fluctuations, producing distinct highstand and lowstand stages, because of enhanced hydroclimate variability. During these later intervals, we observe increased rates of gravity-induced deposition, and spectacular prograding deltas developed during the lake lowstands. An extensive complex of large clinoform deposits, oversized for the current drainage, suggests a possible connection with Lake Rukwa through the Karema depression. The first evidence of the Malagarasi drainage is recorded in Seismic unit 3, as evidenced by deep water channel complexes and turbidites, whereas the first observation of sedimentation from the Ruzizi River is recorded in Seismic unit 3 time in the Ruzizi Province. Altogether, these observations demonstrate that the rift sedimentary fill architecture is a complex interplay of fault propagation and linkage, fault-controlled subsidence, hydroclimate processes, and evolving accommodation zones, drainage catchments and depositional pathways. Lake Tanganyika demonstrates that all these processes influence the distribution of rift valley habitats, and ultimately biodiversity and biological evolution in the rifts.

Figures for Chapter 2

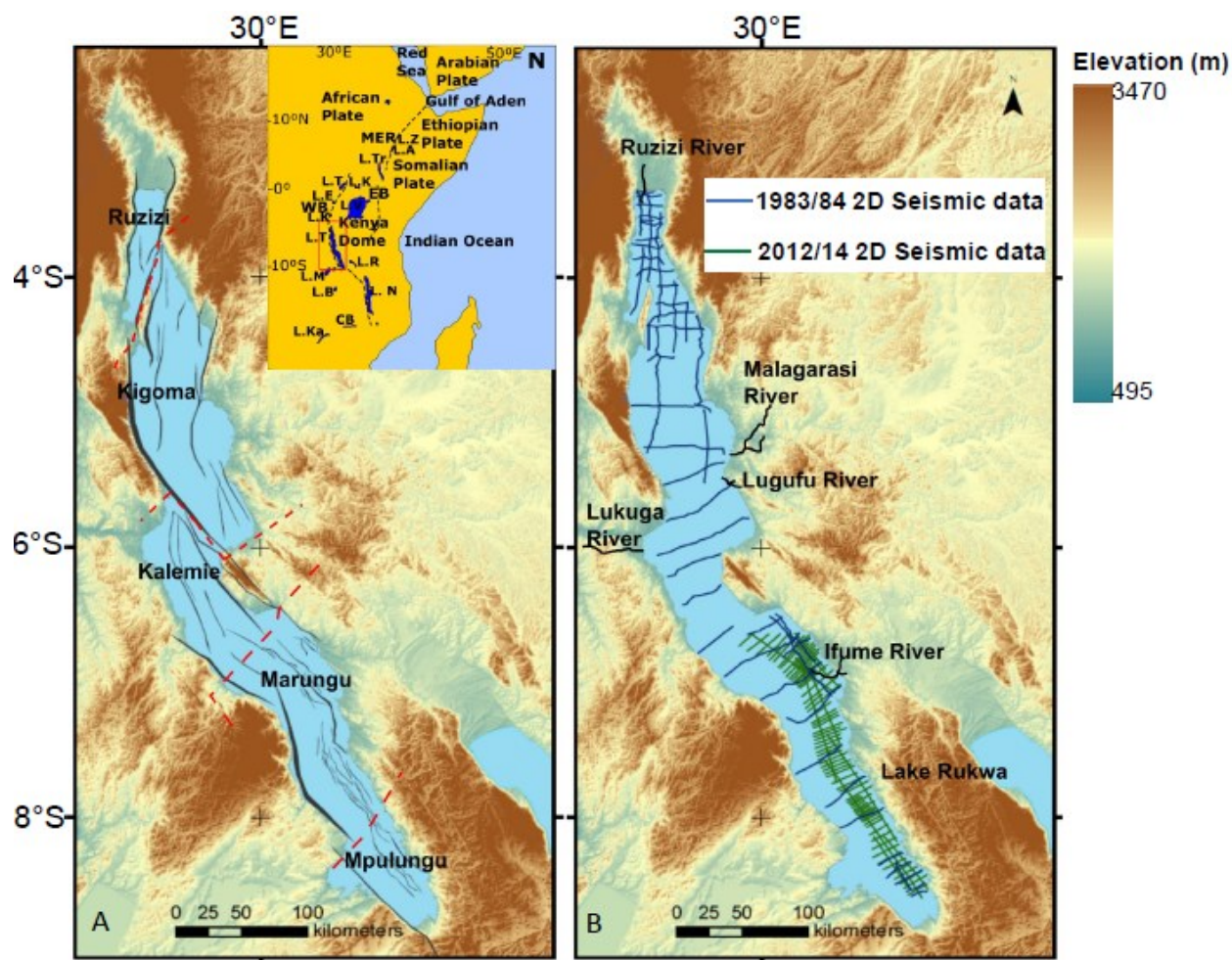


Figure 3: Study Area: A) Structural provinces of the LTR from Ruzizi in the north to Mpulungu in the south demarcated by dashed red lines (see text for details). Thick black lines show the normal faulting trend within Lake Tanganyika, modified after Muirhead et al. (2019). Inset shows the location of Lake Tanganyika within the Western Branch of the EARS. EB and WB are the Western and Eastern Branches respectively of the EARS. B) Locations of seismic data used in this study. The latest 2D seismic data tracklines are in green whereas the 1983/84 data tracklines are in blue.

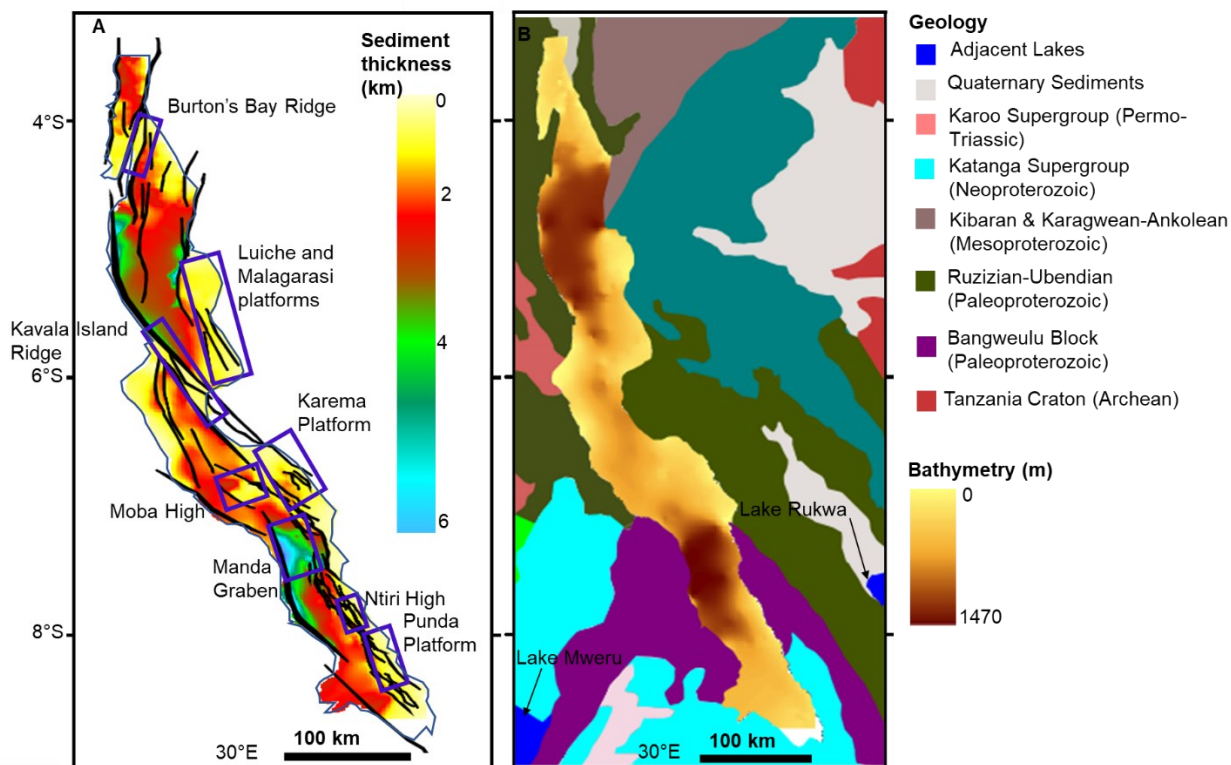
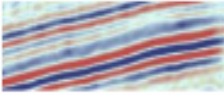
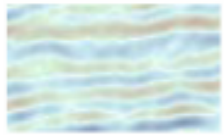

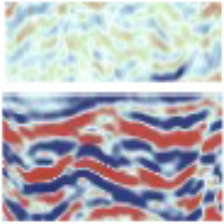
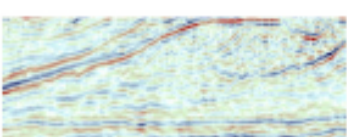
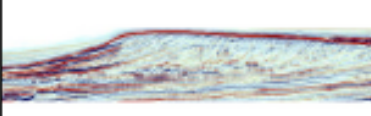
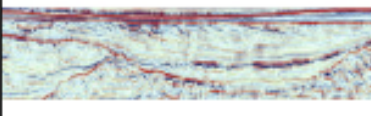


Figure 4: A) Major structural features in the LTR that developed due to rift segmentation (see text for details). Colors indicate the depth to the Nyanja Event, the datum = lake surface (768 m above sea level). B) Geological map of the region surrounding the LTR (modified after Choubert and Faure-Muret, 1968); note Karoo sediments are mainly observed on the Eastern side of the region. Bathymetry presented is derived from seismic reflection data set used in this study. Note the two major deep-water areas in the igoma and Marungu provinces.

Example Seismic Signature	Descriptions	Inference
	Parallel, generally continuous reflections, commonly low-amplitude; draping lake floor.	Hemipelagic deposits accumulate during high stand phases.
	Discontinuous reflections, more or less parallel.	May represent mud-turbidites deposited during lake level rise.
	Semi-transparent to transparent reflections; characteristics may vary based on geological setting and sediment type.	May indicate muddy turbidites, small slumps, debris flows and channel fill deposits (restricted within levees).
	Chaotic reflections, rumpled reflections, broken wavy reflections.	Indicates slumps, high density debris flows, sediment creep. Commonly onlapping, locally unconfined.
	Prograding sigmoid clinofolds; steeply dipping reflections with both toplapping and downlapping termination surfaces.	Associated with fluvial/deltaic inputs; indicative of higher sedimentation rate, limited subsidence and lake level stillstand.
	A combination of prograding sigmoid and oblique clinofold reflections.	Indicative of alternating sediment bypass and aggradational deposition under high energy environments. Indicative of deltaic environments.
	Fills: seismic reflections with an external form representing strata filling negative relief in the underlying strata.	Indicative of channel fills, trough fill, basin fill or slope-front fill. This image represents a distributary channel complex incised into a delta fringe.

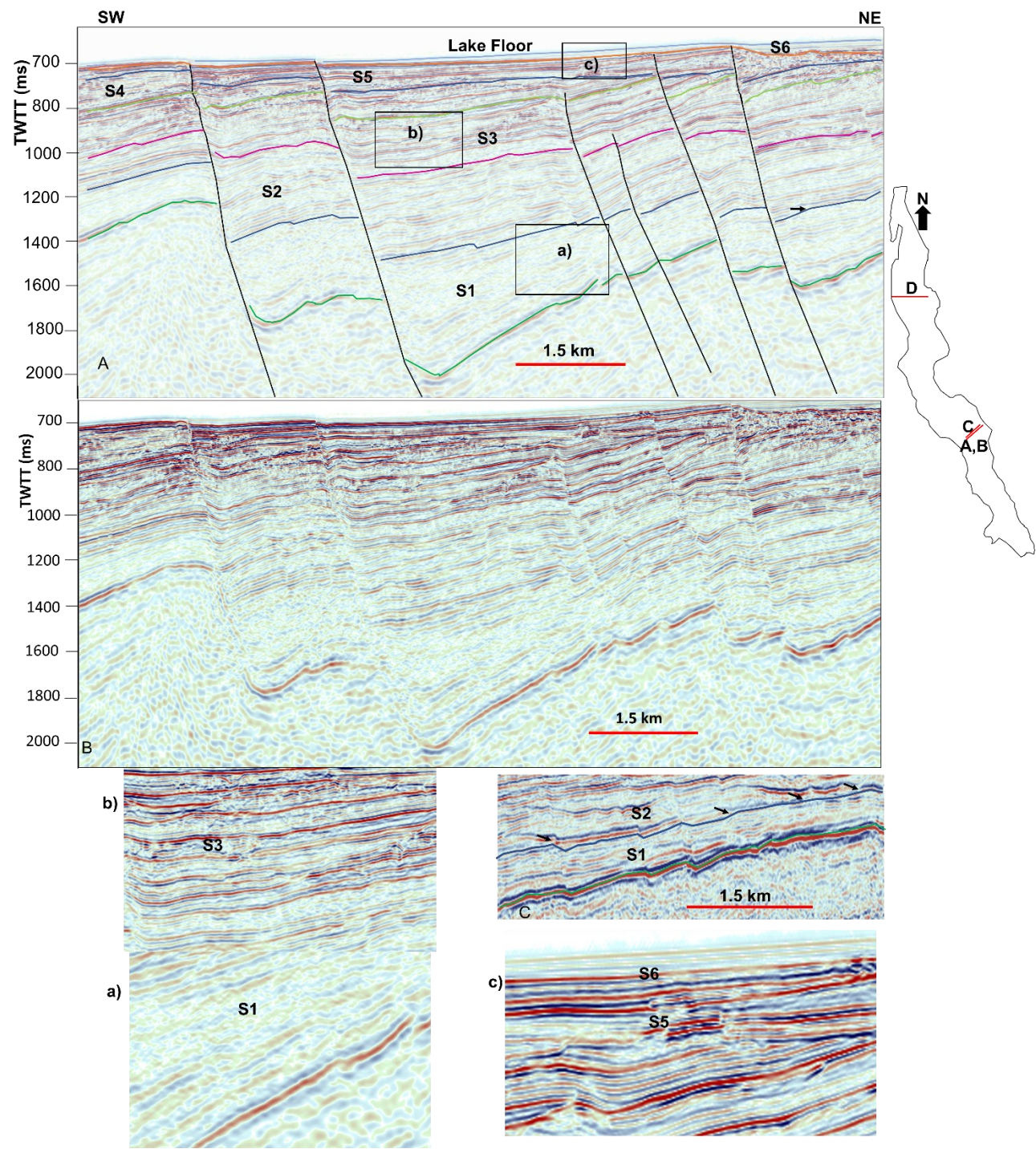


Figure 5: Seismic facies and interpretations as identified and mapped in this study (after Mitchum et al., 1977; Posamentier and Vail, 1988; Baster et al., 2002).

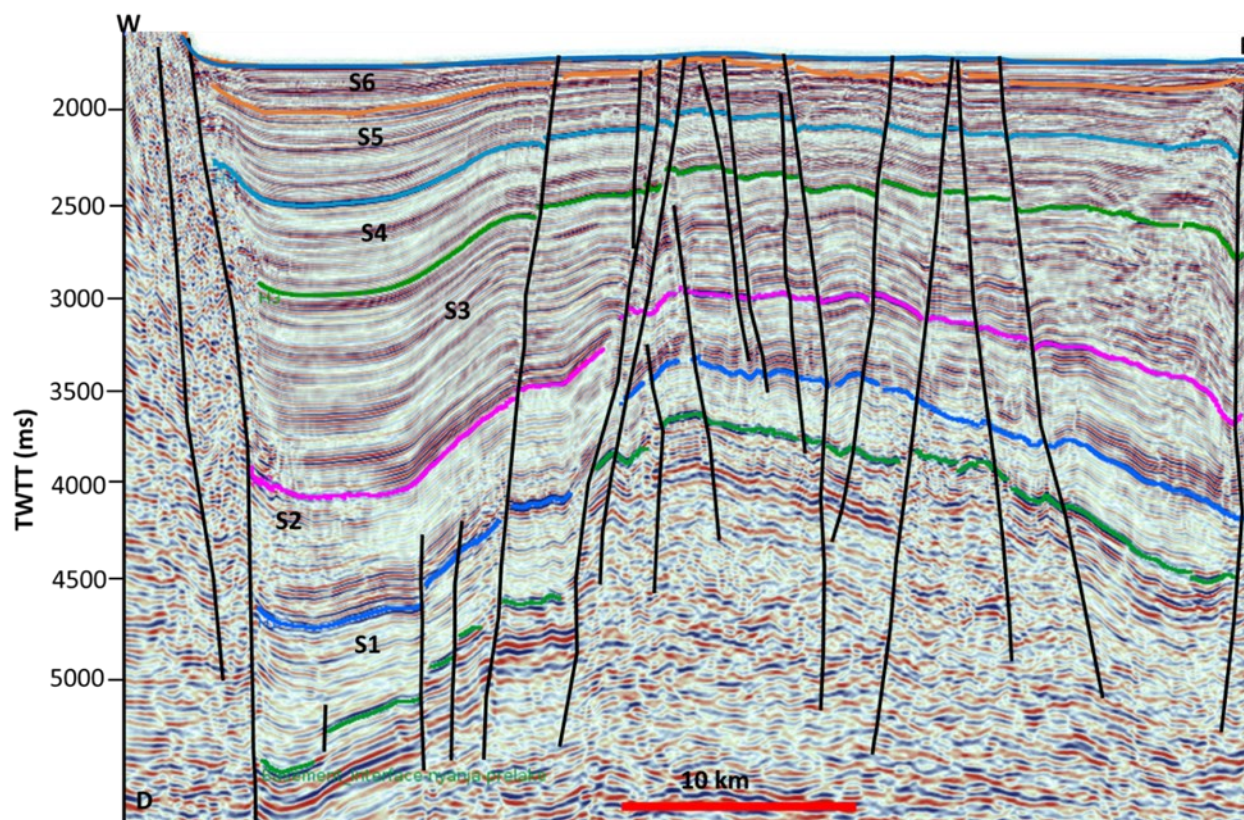


Figure 6: Seismic dip profile, SW-NE south of the Kalya Platform. A) Interpreted (top) and B) uninterpreted (bottom) with six identified seismic units (1- 6), from oldest to youngest. Note the seismic characteristics change from S1 to S6. S2-S6 records a deeper lake as manifested by increasing the dominance of the high amplitude and parallel to semi-parallel reflections. S3-S5 records the facies variability with higher proportion of chaotic reflections and influence of alternating high- and low lake levels. S1-S6 represent the seismic depositional sequence in the central and southern basins of the LTR. Boxes a), b) and c) are selected areas for details as shown in the lowermost panels. C) 2012/2014 dip line showing the onlapping of S2 onto S1 as indicated by thick black arrows. The intra-rift faulting has disrupted the onlap pattern. D) PROBE dip line 210 showing seismic units across the Kigoma Province. The Ruzizi depositional sequences are shown in Figure 9.

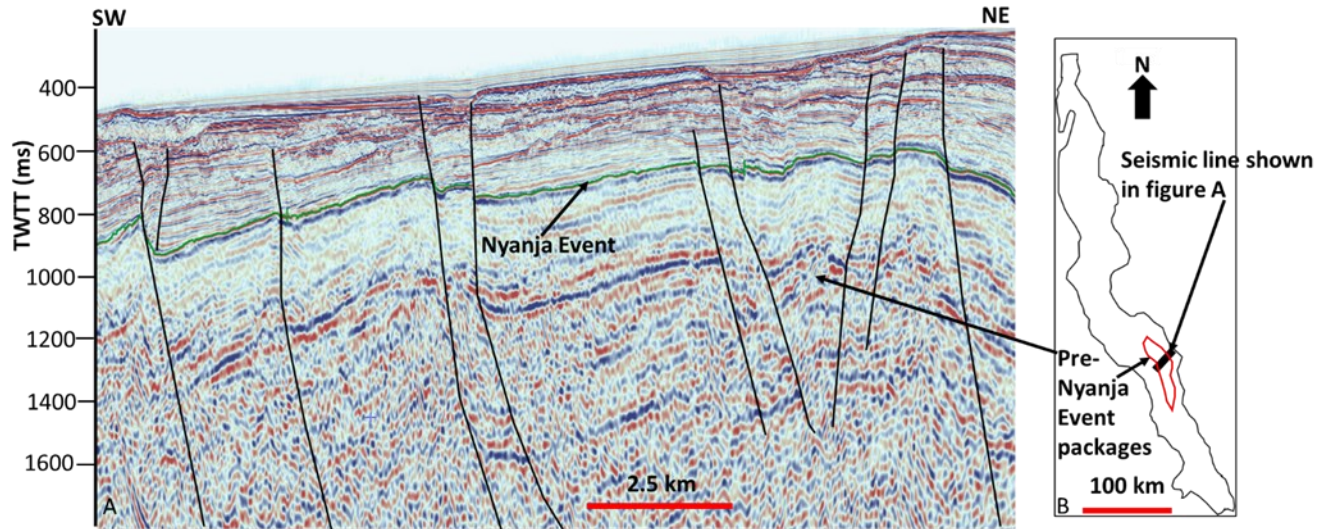
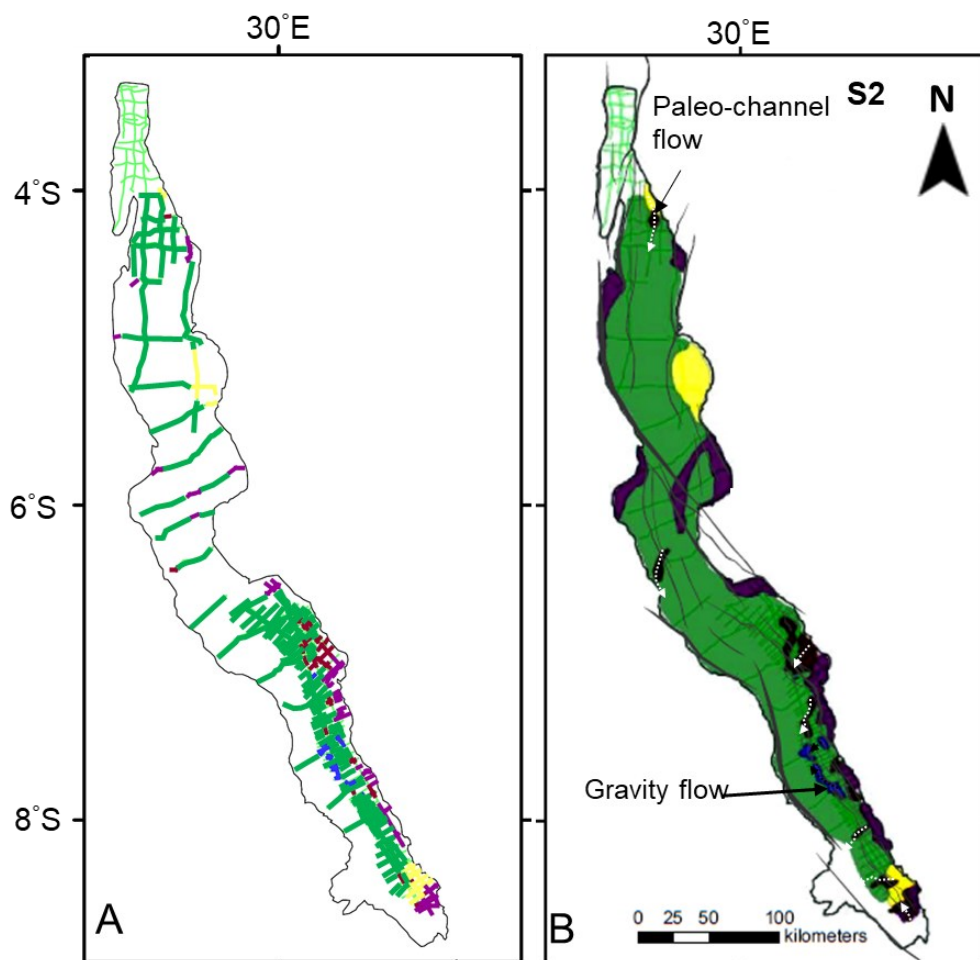
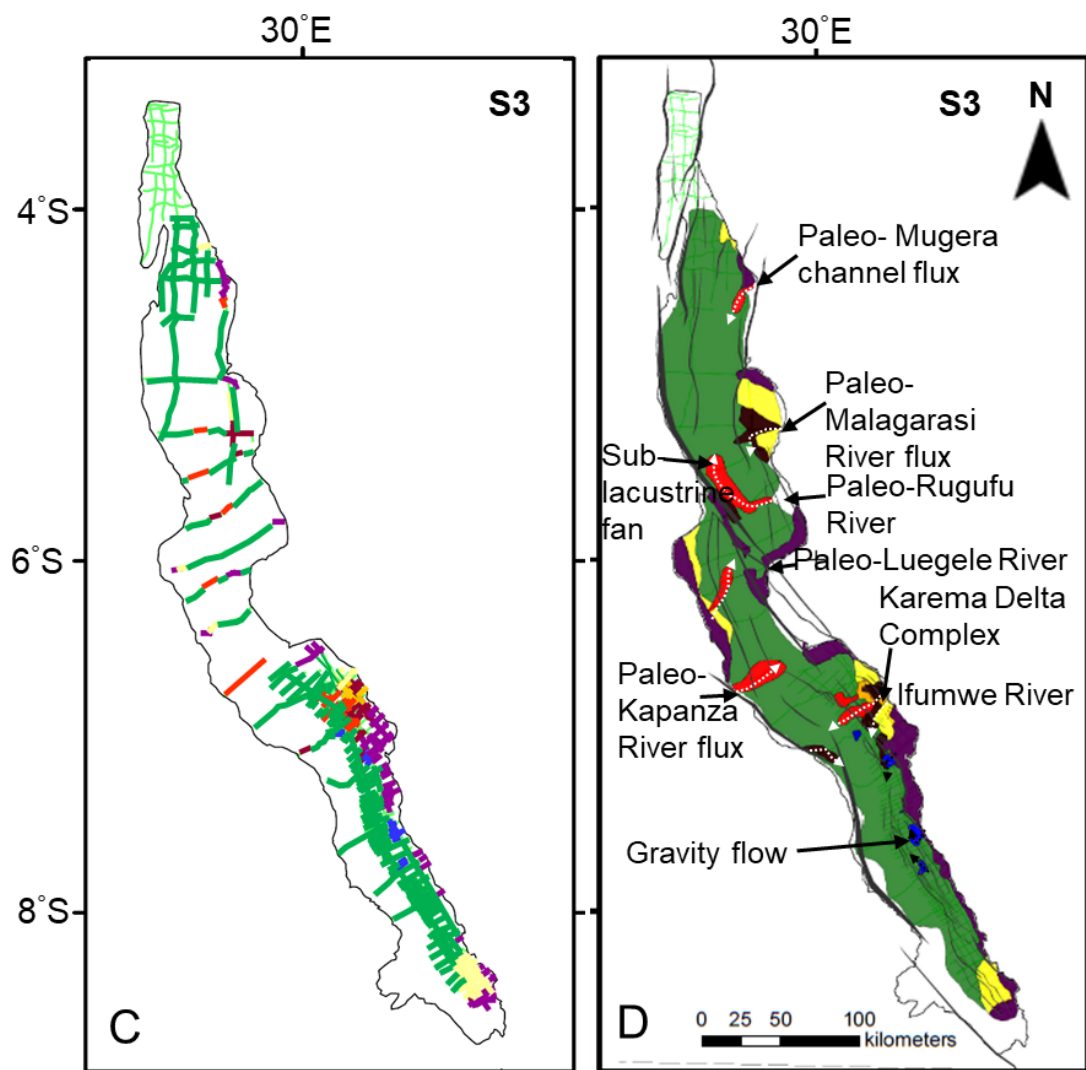
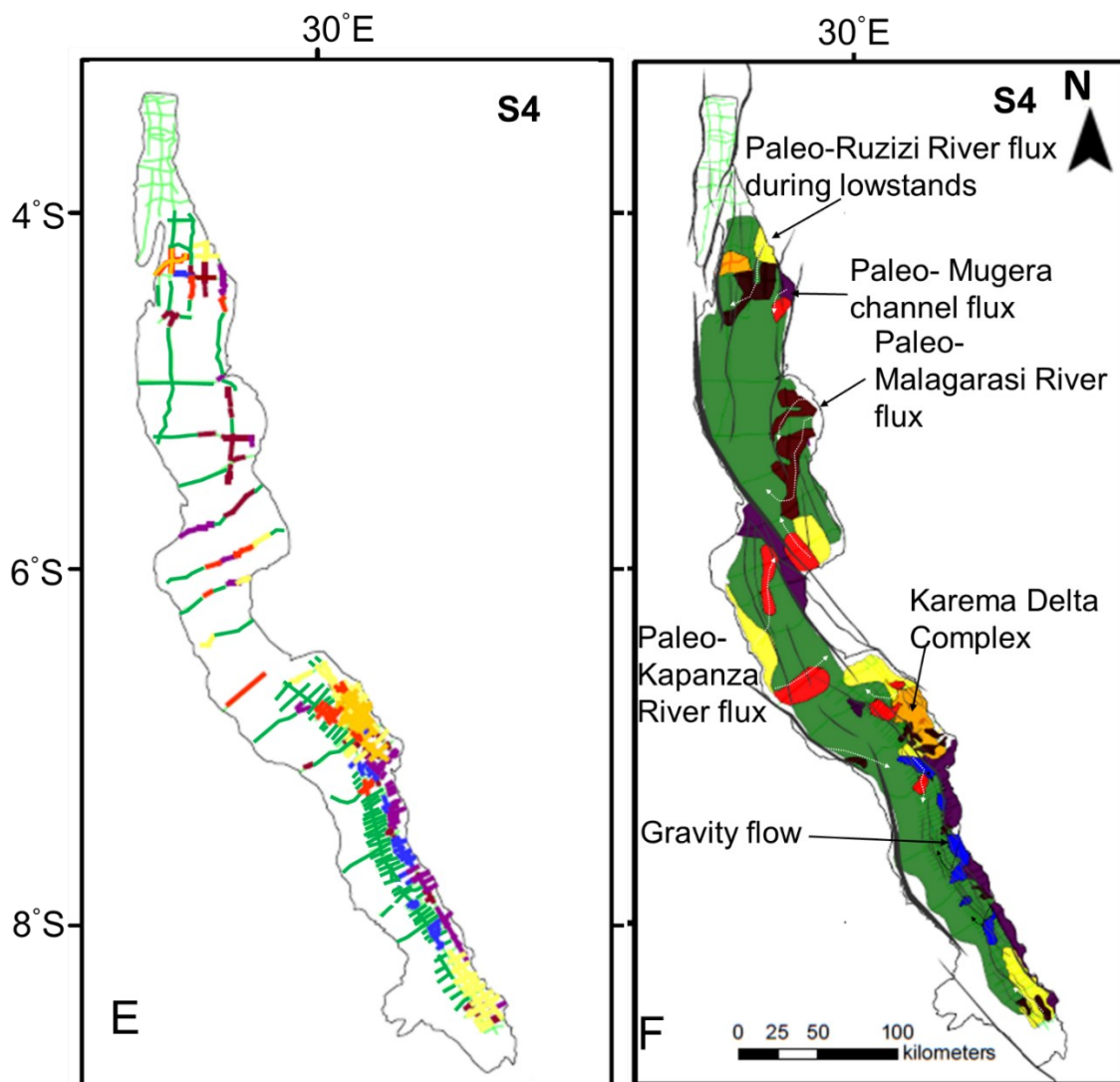
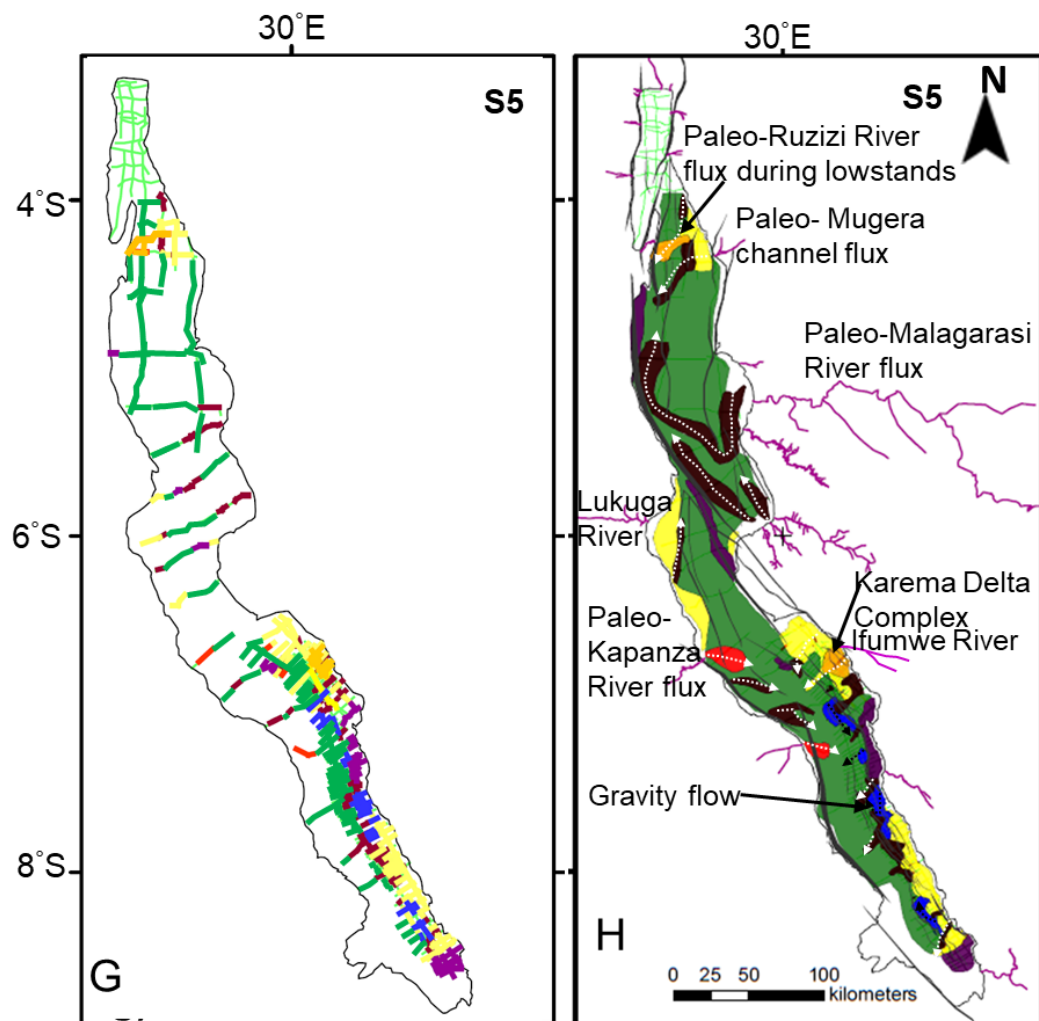


Figure 7: A) Seismic dip profile, SW-NE south-west of the Karema Platform. Note the low-frequency high-amplitude, sub-parallel to parallel reflections below the Nyanja Event (green line) B) Inset map showing the extent of the Pre-Nyanja Event facies (within red line). The thick black line is the profile shown in (A), thick grey lines are the basement faults.









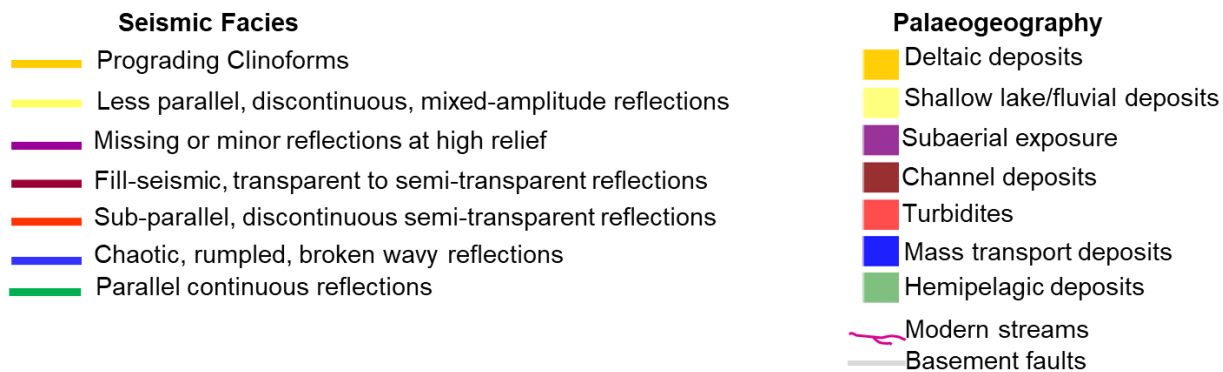


Figure 8: Seismic facies maps (A, B, E and F) and corresponding paleogeographic maps (C, D, G and H) as mapped in S2 through S5 in the southern provinces (Kigoma through Mpulungu) constructed from ION-PROBE and latest commercial 2D seismic dataset. Note the significant changes in the paleogeography controlled by both tectonic and hydro-climate processes. MTDs and channels are pronounced in S3 onwards as a result of an increase in high relief. The onset of the Malagarasi River drainage is observed in S3.

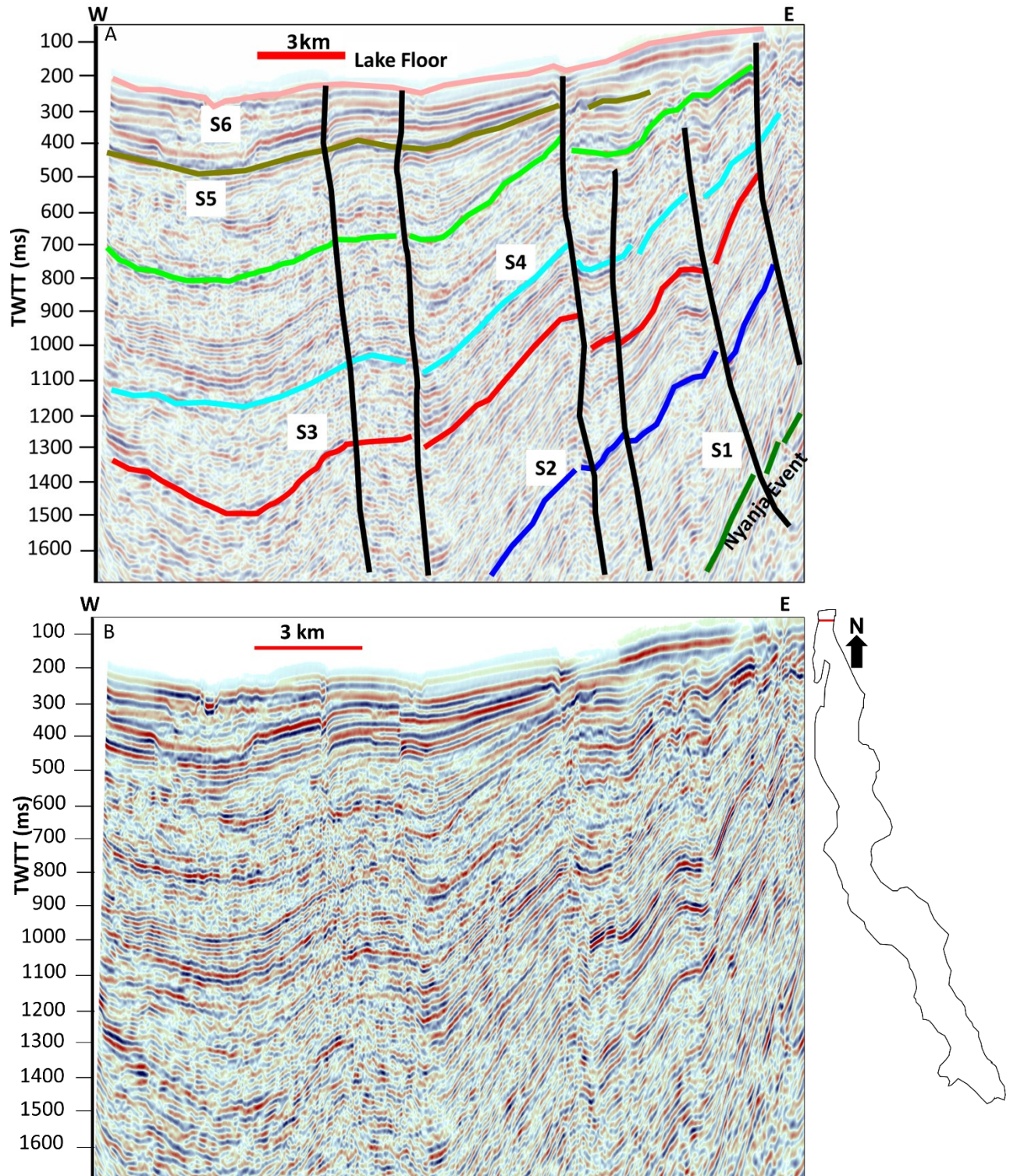


Figure 9: Seismic dip profile, W-E from the northern basin (Ruzizi) of the LTR. A) Interpreted (top) and B) uninterpreted (bottom) with six identified seismic sequences (1- 6), from oldest to

youngest. Only the Nyanja Event and S1 correlated with high confidence across the entire LTR, from the South Basin to the Central Basin to the North Basin.

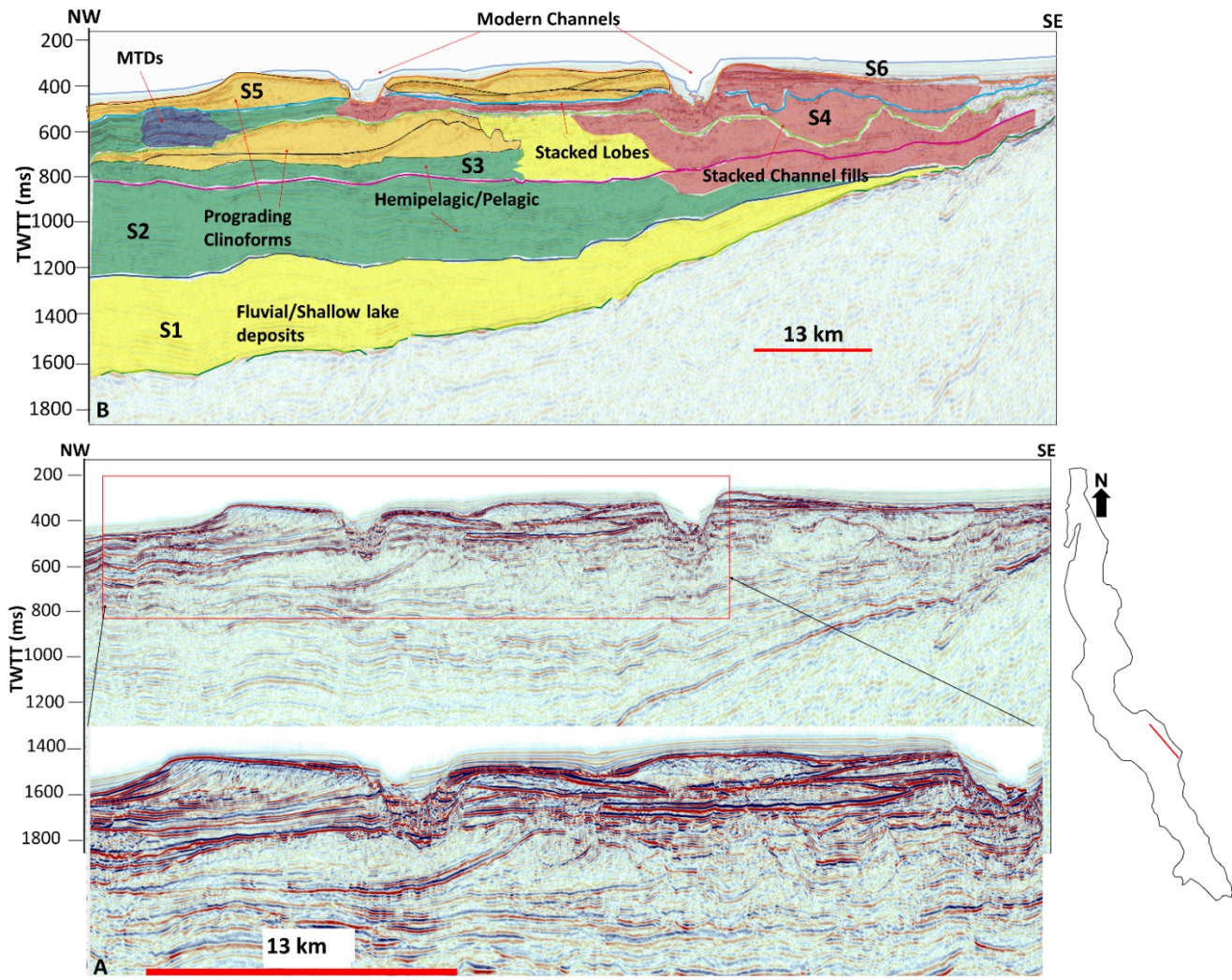


Figure 10: Seismic reflection profile illustrating the deltaic facies. A) Strike seismic profile with sequence stratigraphic interpretations and prograding clinoforms (deltaic lobes), active canyons and stacked channels. Note the two different intervals, lower and upper interval, and each

containing lobe-shaped clinoforms dipping towards the West. The fluvial-deltaic deposits record the continued subsidence, whereas the canyons manifest the uplifting of the Karema Platform or lake level drop due to hydroclimate changes. B) Uninterpreted section.

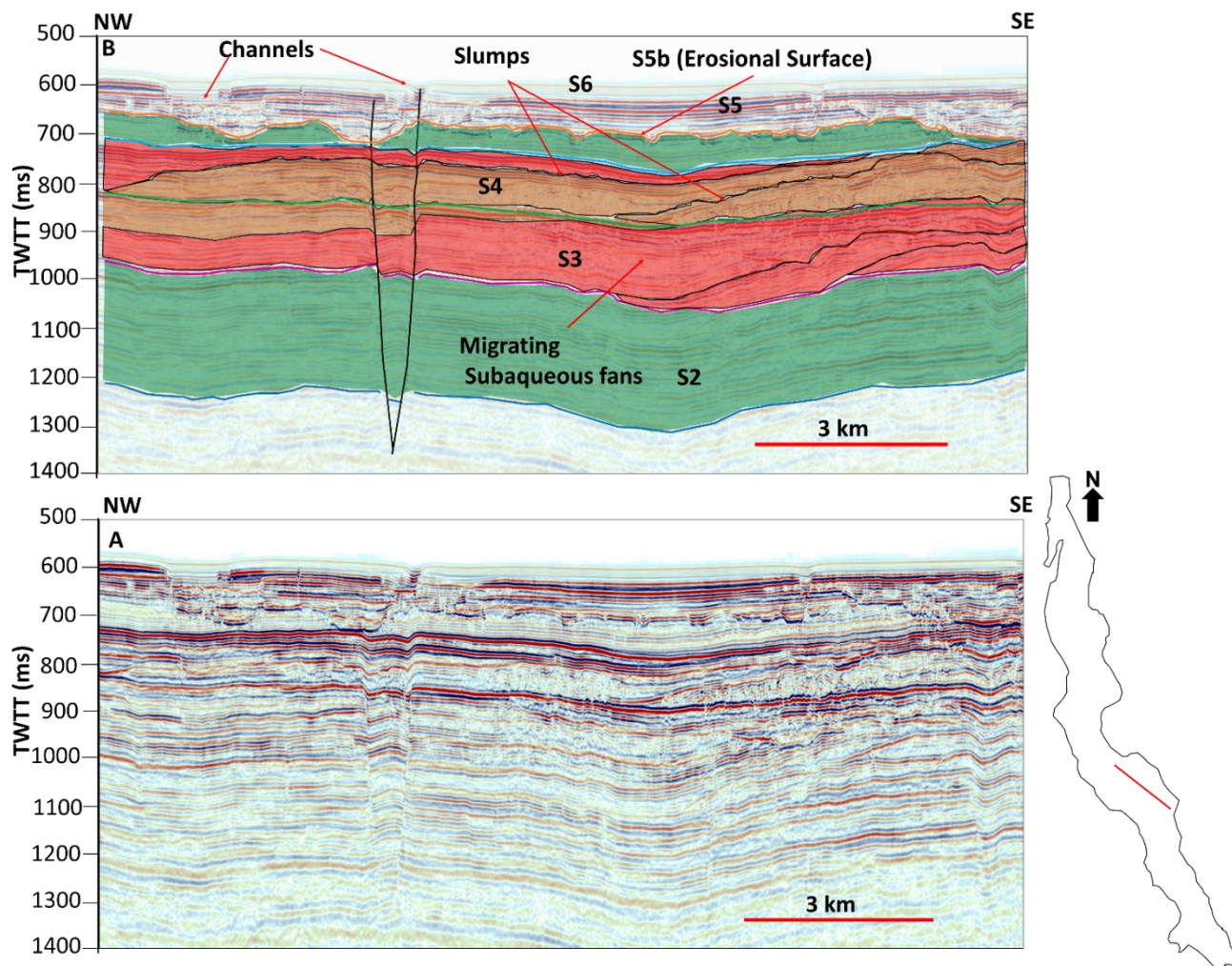


Figure 11: NW-SE seismic profile across Karema area in the Marungu Province. A) Interpreted seismic profile with interpretations of the migrating subaqueous delta fans characterized by highly chaotic seismic reflections in the distal part of the lake. The fan migrated towards the west then migrated towards the northwest (see also Figure 13). Note that the fans are evident in Sequence 4. Note the erosional surface at the base of S5b. The fault zone has been a conduit for sediments as noted in the channels at top of S5 as well as in S6. B) The lower panel is an uninterpreted section. For explanation colors see Figure 8.

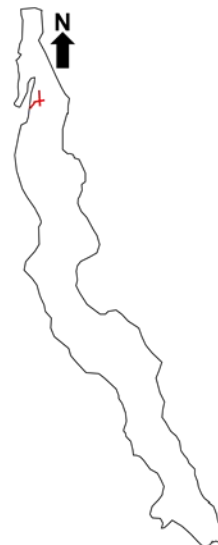
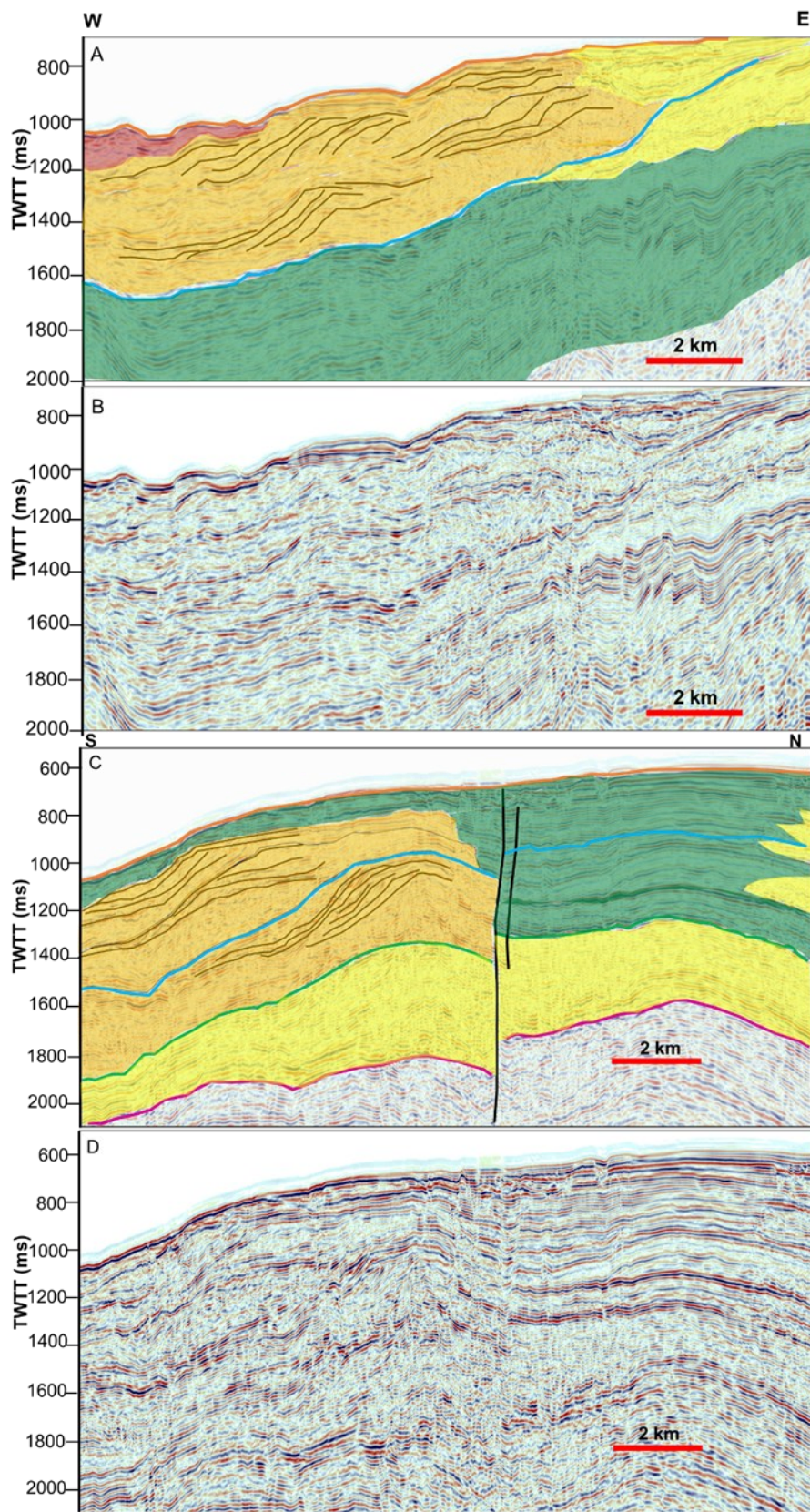


Figure 12: A) W-E seismic profile in the Kigoma Province. C) N-S seismic profile in the same area as (A). The lower panels (B & D) are uninterpreted sections. The upper panels (A & C) are the seismic profiles ((40% transparency) with interpretations of the prograding clinoforms in seismic units 4 & 5. The thickness of the clinoform sets is ~200 ms in each sequence, the clinoforms are dipping towards the SW. The clinoforms are possible evidence for the southwestern progradation of the Ruzizi delta during a lake lowstand. For colors see Figure 8.

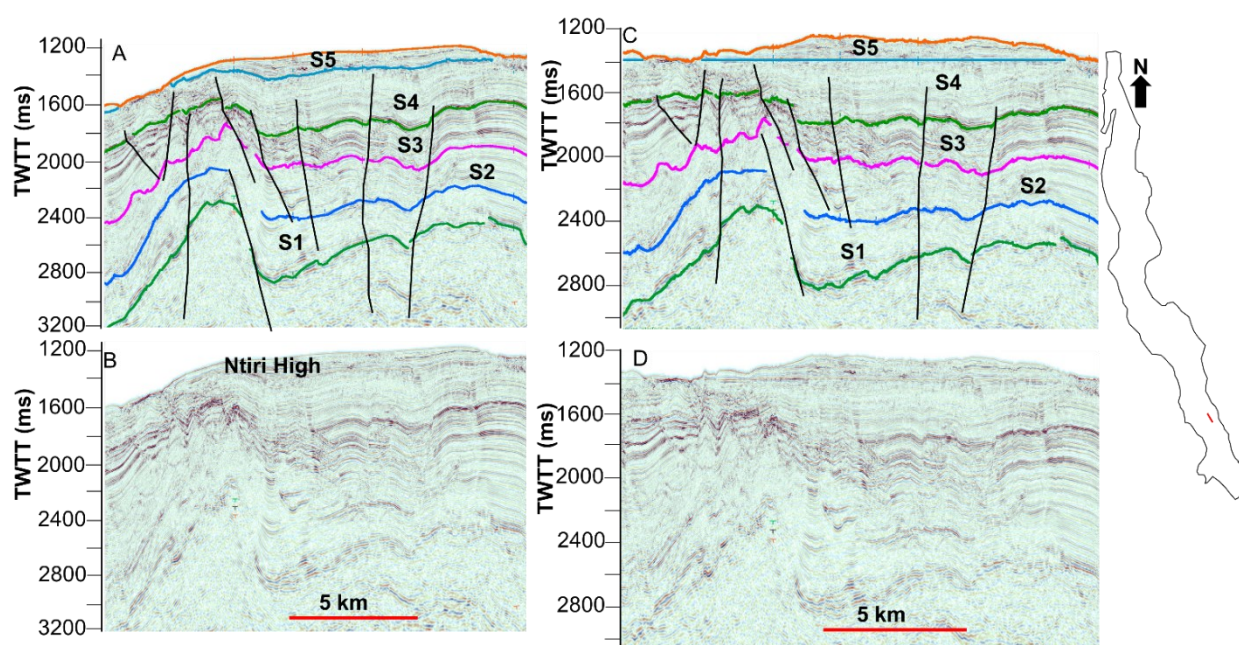


Figure 13: Seismic profile, SW-NE interpreted before flattening (A) and after flattening (C) showing the Ntiri High. When flattened on Seismic unit 4, profile suggests that the structure postdates Seismic unit 4. This is manifested by the erosional surface at the base of Sequence 5. Thick dark lines represent faults; note that most of the faults do not penetrate S5. Panels B) and D) are the uninterpreted seismic profile before and after flattening respectively.

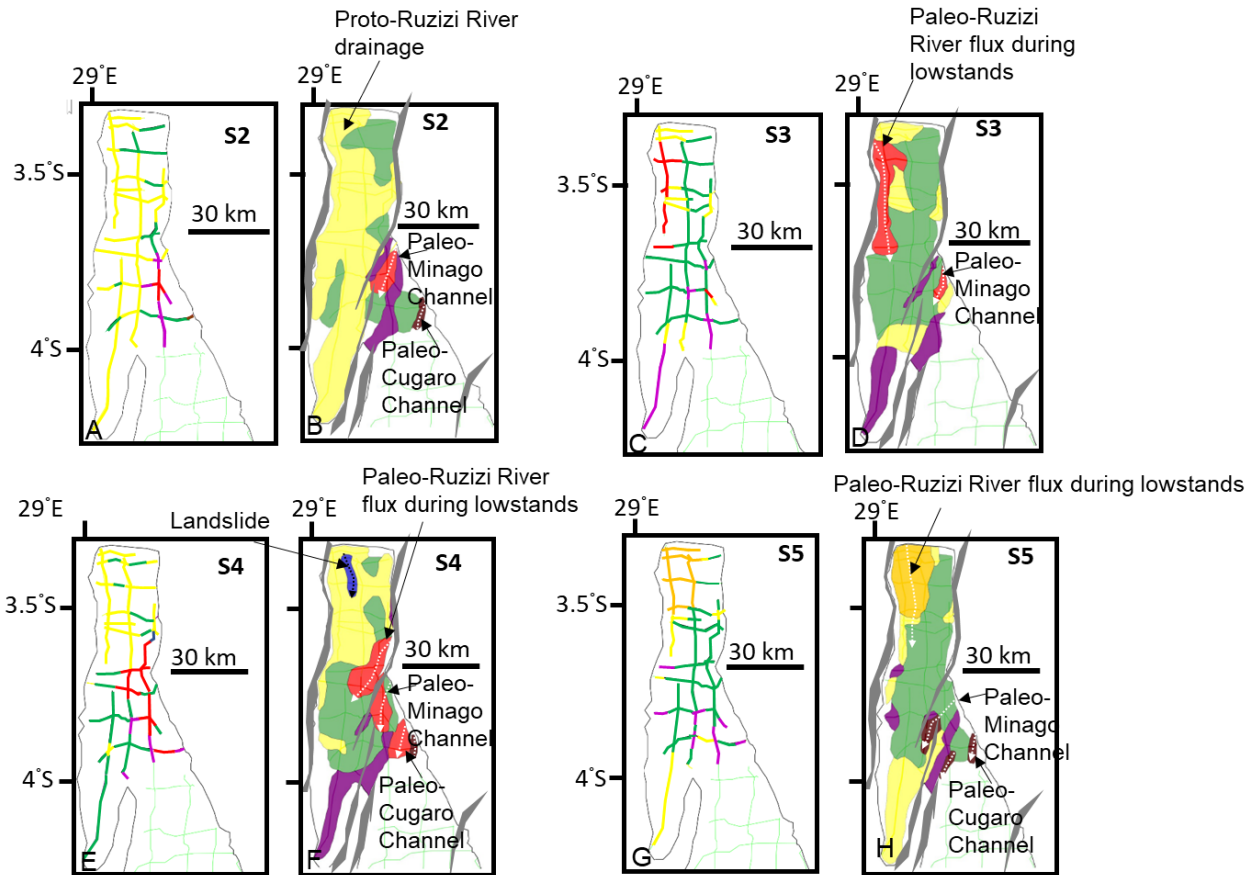


Figure 14: Seismic facies maps (A, C, E, G and I) and corresponding paleogeographic maps (B, D, F, H, and J) as mapped in S2 through S6 in the Ruzizi Province constructed from ION-PROBE seismic data. Note the development of Ruzizi delta in S5, and more evident in S6. Note that following the formation of the Burton's Ridge, the basin experienced turbidites and MTDs as observed in S2, S3 and S4.

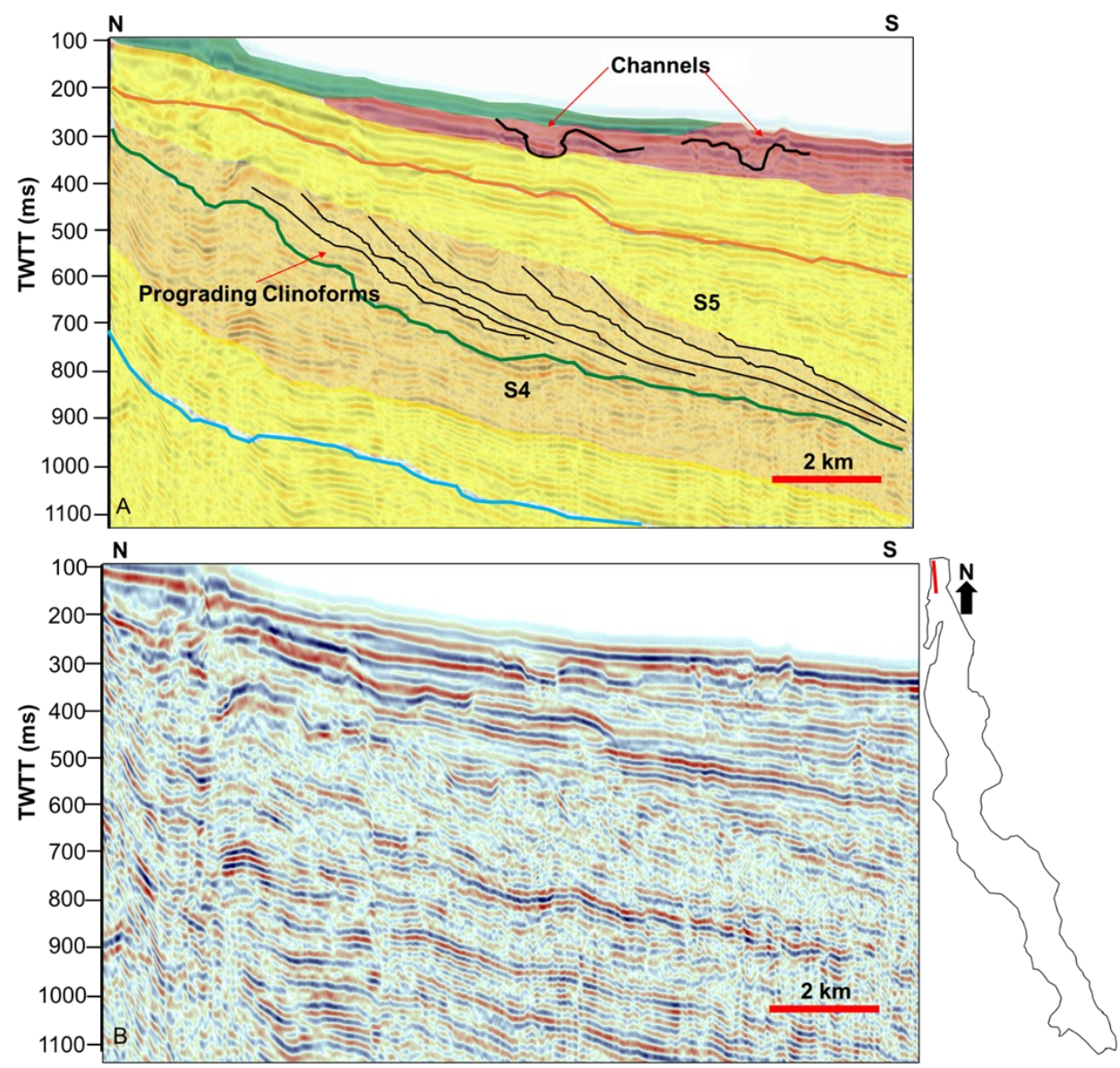


Figure 15: Seismic reflection line illustrating the deltaic facies in the Ruzizi Province. A) Interpreted profile of the southward prograding cliniforms (deltaic lobes), approximately 200 ms thick on average, because of the Ruzizi River influx. Note that the cliniforms emerge in Sequence 5 and onwards. B) Uninterpreted section.

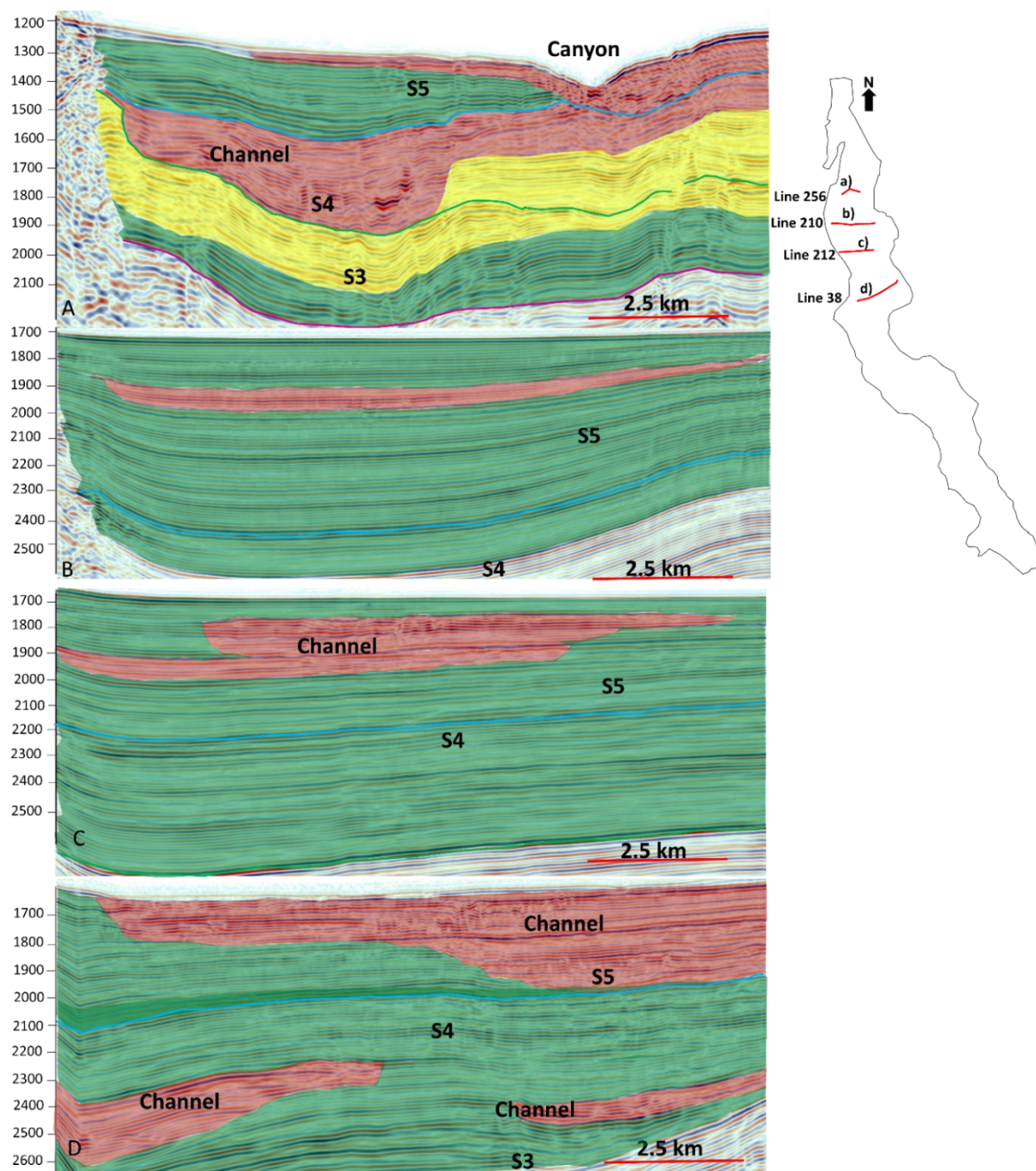


Figure 16: Interpreted seismic reflection profiles across the Kigoma Province (A – D). Note the facies variations from high-continuity parallel seismic facies representing relatively low energy deep water hemipelagic deposits, to wavy, discontinuous, and more chaotic facies indicating high energy channel complexes. The channels observed on PROBE 212 in Sequence 4 suggest

the Malagarasi fan evolution during that time. The channel complex seen between 1200-1800 ms TWTT in S5 on section (A) is probably sourced from the North via the Ruzizi River through the narrow gap on the eastern part of the Burton's Bay Ridge (See Figure 13 for annotations).

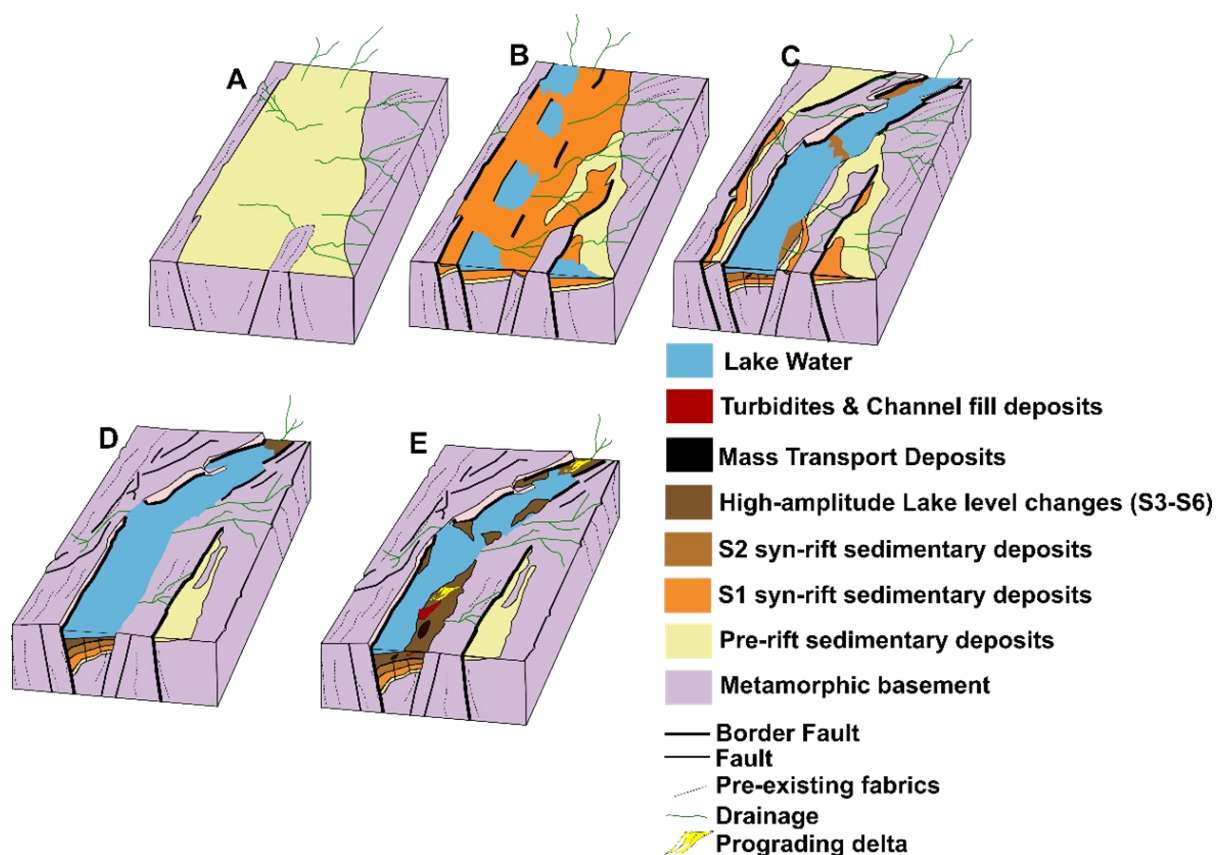


Figure 17: Simplified conceptual schematic of the basin evolution as a result of rifting and hydroclimate processes. (A) Initial architecture of the crust with existing structural fabrics and pre-rift sedimentary deposits. Karoo group rocks occur within Permo-Triassic rift basins bounded by faults striking parallel with the inherited fabric in the basement terrains. During this time, the widely spaced network of drainages flowed towards the Karoo basins. (B) Rift initiation probably occurred in the mid-to-late Miocene through unlinked normal faults via the inherited basement anisotropies. The initial rift segments were possibly ~30 – 40 km wide and

were composed of several half-grabens. Depositional sequence 1 was likely deposited in a fluvial and shallow lake environment. The footwall drainages delivered sediments in the hanging wall depocenters along border faults. The environment probably varied between wetland, savannah, and shallow lake. (C) Development of the Burton's Bay Ridge leading to the drainage separation of the Ruzizi Province from the rest of the rift. Faults began to link, and rifting focused onto the present border faults resulting in greater tectonic relief. Consequently, the sustained lake level developed leading to the deposition of S2. (D & E) Highstand (D) and lowstand (E). As the subsidence increased driven by extension, S3-S5 were deposited, and there is evidence of increased amplitude and frequency of lake level fluctuations. High relief developed during this time, leading to the deposition of MTDs and channel complexes. Both Ruzizi and Marungu provinces saw the development of prograding deltas into the deep-water environments during lake level lowstand phases (E).

Data availability

The latest commercial 2D multichannel reflection seismic datasets acquired in 2012 and 2014 are owned by the Government of the United Republic of Tanzania and can be accessed by the approval of the Petroleum Upstream Regulatory Authority (PURA). The Project PROBE 2D seismic data sets acquired in 1983-1984 were collected by Project PROBE of Duke University and reprocessed under the direction of Syracuse University; legacy data can be accessed through the Marine Geoscience Data System hosted by Lamont Doherty Earth Observatory at http://www.marine-geo.org/tools/search/Files.php?data_set_uid=26822 (DOI: 10.1594/IEDA/326822).

Funding sources

Support for this research was provided by the Syracuse University, National Science Foundation (NSF)-Empower Program and the Tanzania Petroleum Development Corporation.

Acknowledgments

We extend our acknowledgements to the Petroleum Upstream Regulatory Authority of Tanzania and the Tanzania Petroleum Development Corporation who provided an access to the commercial higher resolution 2D multichannel seismic data that were used for this study. The legacy reflection seismic data coupled in this study were reprocessed by ION Geophysical and were originally acquired by Project PROBE of Duke University, under the supervision of B.R. Rosendahl. The funds for this study were granted from Syracuse University (SU), TPDC and the NSF-supported Empower Program. Seismic analysis was carried out using Landmark Graphics Corporation DecisionSpace software, provided on a software grant to the Syracuse University. We thank the members of the Lacustrine Basin Research Group at SU for their assistance provided while completing this study, particularly, Lachlan J. M. Wright, Nicholas Zaremba, Peter Cattaneo and Jacqueline Corbett.

**CHAPTER 3: THE DEEP BASIN AND UNDERLYING BASEMENT
STRUCTURE OF THE TANGANYIKA RIFT**

This chapter has been submitted for publication in the Tectonics Journal as

The Deep Basin and Underlying Basement Structure of the Tanganyika Rift

Shaidu N. Shaban^{1*}, Christopher A. Scholz¹, Folarin Kolawole²

¹Department of Earth and Environmental Sciences, Syracuse University, Syracuse, NY 13244,
USA

²Department of Earth and Environmental Sciences, Columbia University, NY, USA

*Corresponding author, Email: snshaban@syr.edu

Key Points:

- Pre-rift basement fabrics beneath the Tanganyika rift are dominated by NW & NNE trends, parallel to the rift faults.
- Gravity-magnetic modeling of the basin reveals intra-basement shear zone exploited by large-offset early-rift intrabasin fault
- Although inherited basement structure modulated the earliest rift faulting, the effect cascaded through to subsequent phases of extension.

Abstract

The oldest structures in a rift basin define incipient rift architecture, and commonly modulate the patterns of landscape evolution, sedimentation, and associated hazards in subsequent phases of rift development. However, due to deep burial beneath younger, thick syn-rift sequences, and limited resolution of seismic imaging, critical early-rift processes remain poorly understood. In the Tanganyika Rift, East Africa, we augment existing 2-dimensional (2-D) seismic reflection data with newly acquired aeromagnetic and Full Tensor Gradiometry data to assess the deep basin and underlying basement structure. Aeromagnetic and gravity grids show a dominance of NW-trending long-wavelength (>5 km) structural fabrics corresponding to the deeper basement, and dominant NW- with a secondary NNE-trending shorter-wavelength (<3 km) fabric representing shallower, intra-basin structures. Seismically-constrained 2-dimensional forward modeling of the aeromagnetic and gravity data reveals: 1) an anomalously high-density (2.35-2.45 g/cc) deep-seated, fault-bounded wedge-shaped sedimentary unit that directly overlies the pre-rift basement, likely of Mesozoic rift (Karoo) origin; 2) a ~ 4 km-wide sub-vertical low-density (2.71 g/cc) structure within the 3.2 g/cc basement, interpreted to be an inherited basement shear zone, 3) large intra-basin early-rift fault co-located with the modeled shear zone margins, defining a persistent intra-basin 'high', and 4) a shallow intra-sedimentary V-shaped zone of comparatively dense material (~ 2.2 g/cc), interpreted to be a younger axial channel complex confined between the intra-basin 'high' and border fault. These results provide new insight into the earliest basin architecture of the Tanganyika Rift, controlled by inherited basement structure, and provide evidence of their persistent influence on the subsequent basin evolution.

1. Introduction

The topographic morphology of active rift basins, especially in humid climatic settings, exert important controls on the transport pathways, character, and volume of sediments deposited (Rosendahl, 1987; Burgess et al., 1989; Scholz et al., 1990; Gawthorpe and Leeder, 2000; Kolawole et al., 2021a). Accordingly, deciphering the structural controls on both the basin architecture and landscape evolution in such tectonic settings is of paramount importance for understanding the evolution of the Earth as well as solving problems in the applied fields of mineral and hydrocarbon exploration, hydrogeology, hydrology, subsurface CO₂ storage, and geothermal energy (Vasuki et al., 2014). Rift structures such as border and intra-basin faults, intra-basin fault blocks, accommodation zones, and transfer faults control the spatial and temporal distribution of sedimentary facies in continental rifts (Lambiase and Bosworth, 1995; Shaban et al., 2021). Many ancient and modern rift zones host lacustrine basins (e.g., Rosendahl, 1987; Katz, 1990) that form robust archives of tectonic history and paleoclimate dynamics.

Rift basins are structurally complex and are typically composed of a series of asymmetric fault-bounded sub-basins (McKenzie, 1978; Rosendahl, 1987; Morley, 1988; Lambiase, 1990; Logatchev and Zorin, 1992; Sherman, 1992; Muirhead et al., 2019; Scholz et al., 2020). The evolution of rift zones involves the development of regular along-axis structural segmentation into sub-basins that are bounded by large-offset border fault systems that flip polarity along-trend (Rosendahl, 1987; Ebinger, C.J., 1989; Laó-Dávila et al., 2015). This along-trend segmentation of rift basins may occur at inherited pre-rift basement structures such as craton boundaries, terrane boundaries, and exhumed ductile shear zones that are rift-orthogonal or rift-oblique (e.g., Versfelt and Rosendahl, 1989; Corti et al., 2007; Laó-Dávila et al., 2015; Katumwehe et al., 2015; Wright et al., 2022; Kolawole et al., 2022).

Inherited pre-rift basement structures are widely documented to exert prominent control on the evolution of continental rift zones. At continental scales, the tectonic break-up of continents generally occurs along ancient orogenic belts or long-lived crustal scale weakness zones (e.g., Vauchez et al., 1997). On the basin scale, studies have used seismic reflection data (e.g., Phillips et al., 2016), seismicity data (e.g., Kolawole et al., 2018a; Chisenga et al., 2023), remote sensing data (e.g., Hussein et al., 2006; Wilson et al., 2010; Laó-Dávila et al., 2015; Muirhead et al., 2019), or field geological mapping (e.g., Wheeler and Karson, 1989; Beacom et al., 2001; Ring, 1994; Ring et al., 2005; Wedmore et al., 2020) to decipher the influence of pre-existing basement structures on the evolution of rift zones. Studies have also used high-resolution aeromagnetic data to investigate the relationships between inherited basement structures and the localization and geometry of rift faults (e.g., Kinabo et al., 2007; Katumwehe et al., 2015; Kolawole et al., 2018a, 2021, 2022). However, using these various datasets in isolation often presents limitations, either in terms of spatial coverage, scale, imaging resolution, dimension (single or multi), and/or depth of investigation. Notably, a few studies have adopted the integration of Full-Tensor Gradiometry (FTG), aeromagnetic data, and seismic reflection data for the analysis of tectonic structures (e.g., Malin, 2017; Peace et al., 2018; Jamaludin et al., 2021). Although several studies have examined the evolving rift basins of the East African Rift System (EARS), the geometry and kinematics of the earliest fault systems are still poorly constrained (Ebinger et al., 2019; Kolawole et al., 2021b).

Here, for the first time, we integrate FTG, aeromagnetic, and 2-dimensional (2-D) seismic reflection data from a unique, biologically diverse, ecologically sensitive, resource-rich, and tectonically active Tanganyika Rift segment of the East African Rift System (**Figures 18A-B**), in order to investigate rift processes. The primary objective of this study is to better

characterize the deep-to-shallow basin structure of the Lake Tanganyika Rift, and the architecture of the pre-rift crystalline basement beneath its ~2- 6 km-thick sedimentary fill (**Figure 18B**). The extended objectives include: 1) updating the previously published fault map of the basin, and 2) assessing the possible presence of Pre-Cenozoic (i.e., Permo-Triassic age ‘Karoo’ and Cretaceous rift sediments), and 3) studying the subsurface structure of the Kavala Island Ridge (KIR), and its relationship with the Mahale Mountains and Katenga - Kugulu - Ntengo lineaments. The KIR is the most prominent structural high in the LTR separating the modern lake into distinct limnological domains (Scholz et al., 2003), and served as a paleodrainage divide during lowstands, and separates major faunal groups (Scholz and Rosendahl, 1988).

Background

1.1.1 The East Africa Rift System (EARS)

The EARS runs from the Red Sea and Gulf of Aden in the north to Mozambique and Botswana in the south, with a length of ~4000 km and width of 50-150 km (Morley et al., 1999; Chorowicz, 2005; Figure 1a). EARS rifting initiated in the Oligocene contemporaneously with the opening of the Red Sea and Gulf of Aden (Wolfenden et al., 2005). The EARS is composed of a series of rift segments (typically ~80-150 km long), predominantly in the form of asymmetric half-graben basins (Rosendahl, 1987; Morley, 1989). It is comprised of two branches, the Eastern Branch and Western Branch, separated by the Archean Tanzania Craton at the terminus south of the Main Ethiopian Rift (**Figure 18a**) (Rosendahl, 1987; Ebinger, 1989). The Eastern Branch has a series of volcanic centers along its strike spaced every ~20-100 km, and a long history of effusive magmatism. In contrast, the Western Branch is magma-poor, with

a few volcanic centers including the Virunga Volcanic Province and the Rungwe Volcanic Province to the north and south of Lake Tanganyika respectively (Baker, 1971; Mohr and Wood, 1976; George et al., 1998; Furman, 2007; Biggs et al., 2009; O'Donnell et al., 2013). Currently the Western Branch has a maximum crustal stretching rate of 2.9 mm/yr, whereas the Eastern Branch is stretching at rates up to 5.2 mm/yr (Saria et al., 2014).

1.1.2 Lake Tanganyika Rift

The Lake Tanganyika Rift (**Figure 18**) is situated in the Western Branch, and it holds the deepest and most voluminous lake in Africa (~645 km long and maximum water depth of 1470 m) (Capart 1952; Coulter, 1963; Rosendahl, 1987; Shaban et al, 20021). The timing of Lake Tanganyika Rift initiation is not well resolved due to the lack of information from the basal basin fill. Cohen et al. (1993) suggested an initial age of ~ 9-12 Ma based upon the extrapolation of near surface sediment cores, Pasteels et al. (1989) suggest 7.8 - 5 Ma, Roberts et al. (2012) suggest an age of 25-26 Ma based upon tephra ages within a nearby terrestrial rift sequence, whereas Jess et al. (2020) suggest that the age of initial rifting was coincident with the early uplift of the Ruwenzori Mountains (Eocene – Paleogene). The Lake Tanganyika Rift is one of the world's largest and deepest active rift-lake systems and a site where processes of rift basin formation can be studied today. It is endowed with one of the oldest and most continuous records of tropical climate on the continents (Russell et al., 2020). The Lake Tanganyika Rift is composed of a series of half grabens, typically ~80-140 km long and ~50-70 km wide (Rosendahl et al., 1986; Rosendahl, 1987; Muirhead et al., 2019; Wright et al., 2020, Shaban et al., 2021). Shaban et al. (2021) suggested three main bathymetric basins (Ruzizi, Kigoma and Marungu-Mpulungu basins) and several sub-basins from the northern end to the southern end of the Lake Tanganyika Rift (**Figure 18b**). These basins are bounded by nine border faults and are

kinematically linked by accommodation zones partitioning extension along strike (Rosendahl, 1987; Morley, 1988; Muirhead et al., 2019; Wright et al., 2020). Depending on the rifted terrane-type (e.g., Archean vs Proterozoic lithosphere), border faults accommodate upwards of 90% of the extensional strain (Muirhead et al., 2019; Wright et al., 2020) with the rates of normal border fault slip increasing with the system evolution (Muirhead et al., 2019; Wright et al., 2020). The normal fault systems influence sediment pathways into the basin (Rosendahl, 1987; Burgess et al., 1989; Shaban et al., 2021).

The Lake Tanganyika Rift exhibits two main extensional trends, NE-SW in the south and E-W in the northern part (Delvaux and Barth, 2010), with variable total extension (e.g., ~2.75 km in the south, 7.07 -7.15 km in the central region, and ~3.75 km in the north) (Wright et al., 2020). It exhibits high topographic relief in several localities such as the Mahale Mountains, including some rift shoulder uplifts more than 1500 m above the lake surface adjacent to border faults (Rosendahl, 1987; Wright et al., 2020; Delvaux, 2001). It is surrounded by Proterozoic and early Phanerozoic mobile belts of high-grade metamorphosed rocks (Choubert and Faure-Muret, 1968). These geological terranes wrap around the Archean Tanzania craton to the east, and the Congo craton to the west (**Figure 18c**). In the north, it is bounded by the NNW-SSE-striking Ubendian belt composed of gneisses, granites, and mica schists, and the NE-SW-striking Kibaran belt composed of orthogneisses and high-grade metasediments and schists, quartzites and metaquartzites, and granites (Fernandez-Alonso and Theunissen, 1998) (Figure 1c). At its southern extent, the Lake Tanganyika Rift continues into the Bangweulu cratonic block adjacent to Karoo structures (Daly et al., 1989; Klerkx et al., 1998; Lenoir et al., 1994; Morley, 2010).

Little is known about the sedimentary geology of the deepest parts of the rift; shallow coring of the Holocene and Upper Pleistocene sections penetrated diatomaceous ooze-rich shale, sands, siltstone, and localized carbonates (Livingstone, 1965; Tiercelin et al., 1988, 1992; Scholz et al., 2003; Felton et al., 2007; McGlue et al., 2008, 2020). The Lake Tanganyika Rift contains more than ~ 6 km of syn-rift lacustrine sediments in some areas, as evident in 2-D seismic reflection data (Rosendahl, 1987; Morley, 1988, Muirhead et al., 2019; Wright et al., 2020; Shaban et al., 2021; **Figure 18b**) distributed in at least six depositional units (Figures 2b-c; Muirhead et al., 2019; Shaban et al., 2021). The units consist of S1 (oldest) to S6 (youngest) deposits. S2 - S6 generally record deeper water rift lake sequences, manifested by increasing the dominance of the high amplitude and parallel to semi-parallel reflections. S3 - S5 records facies variability with higher proportion of chaotic reflections and influence of alternating high- and low lake levels (**Figure 19c**), indicating system with increasing relief (Shaban et al., 2021).

Following the geological mapping of Choubert and Faure-Muret (1968) and structural analysis of Muirhead et al. (2019), the inherited fabrics of the Lake Tanganyika Rift have two strong trends, NW-SE, and NE-SW as observed across the Proterozoic metamorphic terrains that the rift transects. For instance, there is a strong NW-SE trend of pre-existing lineaments in the Ruzizian-Ubendian belts, and a localized bimodal trend, NE-SW and NW-SE in the Bangweulu cratonic terrain (**Figure 19**). These pre-existing lineaments correlate well with the orientation of major shear structures that bound basement subterranean (e.g., Andersen and Unrug, 1984; Daly, 1988; Daly et al., 1989; Muirhead et al., 2019; Wright et al., 2020).

2. Materials and methods

To investigate the deep-to-shallow structure of the central Lake Tanganyika Rift (4.5° S to 7.5° S and 29° E to 31° E), we integrate aeromagnetic and FTG anomaly derivatives, the 2-D seismic reflection data, and a DEM. Our fault mapping approach follows standard practice, consistent with previous studies (e.g., Muirhead et al., 2019), albeit in the current study we augment Air-FTG® and aeromagnetic data to improve the lineament delineation, and we mostly focus on the central part of the rift (Kigoma, Kalemie and northern Marungu provinces) (**Figures 18 and 19**). The integration of FTG, magnetic data and seismic reflection data has proven to be an effective tool in both hydrocarbon and mineral exploration for structural mapping and delineating the size, shape, and thickness of the target bodies (Jackson et al., 2013; Jamaludin et al., 2021). Gravity anomalies are a function of density of the subsurface geology, thus, can be used to discriminate lithological bodies and gradients associated with faulting of those.

2.1. Seismic interpretation

We use seismic stratigraphic units (**Figure 19**) suggested by Muirhead et al. (2019) and Shaban et al. (2021) as stratigraphic markers to evaluate the structural characteristics. Using DecisonSpace™ Landmark software, we mapped major faults and minor faults respectively in the eastern-central part of the rift. We use the maps of stratigraphic markers (Nyanja Event and S3) offset by faults to discern the fault geometry. Fault mapping was augmented with the coherence seismic attribute extraction that reveals discontinuities. We project offsets on the seismic unit boundaries as fault heaves. We judge fault extents based on faults with the same strike on the adjacent seismic profiles, otherwise, in case of widely spaced profiles, we assume the fault extents terminate at the midpoint of two adjacent seismic profiles. The identification of fault extent in the strike direction also depends on the scale of the observation (Gillespie et al.,

1992). Thus, one fault trace on a map may be a combination of several trace segments when observed on a larger scale map (Lonergan et al., 1998). Also, the depth resolution limit of the acquisition method influences fault interpretation on seismic datasets inferred from displacement (Sheriff, 1977). We examine the fault orientations using rose diagram plots.

2.2. Aeromagnetic data

2.2.1. Reduction to the Equator

In the low magnetic latitudes, the shape of magnetic anomalies due to deep-seated vertical bodies undergoes distortion because of inclination and declination angles of the geomagnetic field. Consequently, it becomes cumbersome to correlate the observed magnetic anomalies and the positions of causative bodies (Baranov, 1957). To overcome this effect, the magnetic data are transformed as it would be measured at the magnetic poles by applying a reduction to pole (RTP) transformation (Baranov, 1957). When the magnetic survey area is located within magnetic latitude with an inclination angle less than 15° , the RTP fails to locate the anomalies exactly above the source bodies, hence, a reduction to the Equator (RTE) transformation is needed (Mono et al., 2018). Because our study area survey area is located within magnetic latitudes with magnetic inclination angle of between -20° and -40° below the Equator, to correctly locate the anomalies over the source, the TMI was reduced to the Pole (RTP) as shown in Figure 3

2.2.2. Horizontal gradients and Total Horizontal gradients

To aid structural mapping, subtle aeromagnetic and gravity anomalies can be better resolved using the mathematical derivatives of the total magnetic intensity and gravity data such as the vertical and total horizontal derivatives (Singh, 1994; Salem et al., 2008). In the case of aeromagnetic grid filtering, the total horizontal derivative resolves the rate of change of total magnetic intensity in the horizontal directions. Similarly, the vertical derivative resolves the rate of change of total magnetic intensity in the vertical direction. These derivatives generally resolve structures at shallow crustal depths (high wavenumber components of the data).

However, to resolve structures at intermediate and deeper crustal depths, we apply low-pass and high-pass filters on the RTP aeromagnetic grid. For this purpose, we adopted the Butterworth bandpass filter, which has the advantage of allowing the user to specify the desired mid-range wavelengths while attenuating the low and high extremes of the wavelength continuum (Butterworth, 1930). We applied a Butterworth bandpass filter of 5 - 12 km to resolve shallower (intra-sedimentary) structures, 12 – 45 km to resolve intermediate-depth (shallow basement) structures, and 45 - 205 km to resolve deeper intra-basement structures (**Figure 21**). A rule of thumb is that ca. one-third to one-quarter of the anomaly width is an estimate to the depth of the anomaly source. The structures were extracted manually by carefully tracing the lineaments. Furthermore, we used other derivatives such as tilt derivative, analytical signals and first horizontal derivative of the vertical derivative of the aeromagnetic data to delineate lineaments (refer to the Supplemental Information).

2.3. FTG data

We analyzed six tensor components of FTG data to delineate geological bodies and structures. The T_{zz} directly delineates the subsurface geology revealing major sub-basins and

structures, and T_{xz} delineates the axes of major structures in the north-south and east-west directions respectively, whereas T_{xx} and T_{yy} outline the edges of structures in the east-west and north-south directions.

2.3.1. Rotational Invariants

FTG invariants are effective for resolving complex subsurface structural trends in the upper crust (Mataragio and Kieley, 2009). The rotational invariants are powerful tools for identifying the density contrast between different geological features as well as visualizing all six tensor components from a single image (Mataragio and Kieley, 2009). These datasets commonly resolve high-frequency and short wavelength anomalies, corresponding to intra-sedimentary structures in basins. We use FTNR and filtered tensor data to compute rotational invariants. To remove non-geological high frequency signals, we applied a low-pass filter of 500 m to the FTNR data.

$$R-1 = \sqrt{(T_{xx}T_{yy} + T_{yy}T_{zz} + T_{xx}T_{zz}) - (T_{xy}^2 + T_{yz}^2 + T_{zx}^2)} \quad (5)$$

$$R-2 = (T_{xx}(T_{yy}T_{zz} - T_{yz}^2) + T_{xy}(T_{yz}T_{xz} - T_{xy}T_{zz}) + (T_{xz}(T_{xy}T_{yz} - T_{xz}T_{yy})))^{1/3} \quad (6)$$

The advantage of the rotational invariants (**Figure 22**) is the ability to retain the shape and orientation regardless of the rotation direction of the tensors about the z-axis (Mataragio and Kieley, 2009). The structures were extracted manually by carefully tracing the lineaments.

2.3.2. Upward Continuation

The observed Bouguer gravity anomaly is a sum of the regional and residual fields (Mickus et al., 1991). Thus, at any observation point, the gravity anomaly is a total of anomalies from large, deep-seated source bodies and small, localized source bodies close to the observation point. Thus, as a secondary approach for evaluating the relationship between shallow and deep

basement structures, we separated the regional and residual field by upward continuation of the gravity data set. This operation shifts the data by a constant height level above the Earth's surface (Jacobsen, 1987). According to Jacobsen (1987), if a potential field is upward continued to a height z , then sources situated at a depth greater than $0.5z$ can be imaged. Based on the 2D seismic data the crystalline basement in the Lake Tanganyika Rift is perceived within 5- 6 km (Rosendahl, 1987, Muirhead et al., 2019; Wright et al., 2020; Shaban et al., 2021); therefore, to remove the short wavelength anomalies corresponding to intra-sedimentary depth intervals, the data was upward-continued at 12 km. Furthermore, we used other derivatives such as adaptive tilt angle (ATA) and tilt derivative horizontal derivative (TDX) from the FTG anomaly (T_z) data to delineate lineaments (refer to the Supplemental Information).

2.4 2.75-D Gravity and magnetic forward modeling

To test the possible presence of Karoo sediments within the Lake Tanganyika Rift, we modelled two NW-SE profiles that run parallel to PROBE seismic profiles 83-216 (east of the KIR) and 83-218 (**Figure 19a**). Profiles were chosen to pass through the areas where Karoo sedimentary rocks were previously interpreted (Delvaux, 2001). 2.75-D modelling assumes a length of target (y -dimension) has a variable strike length in each of $+y$ and $-y$ direction. We assumed a general increase of density with increase of depth from the lake floor. We augmented this assumption with known densities from the shallow coring within the rift (e.g., Scholz et al., 2003) and analogues from the Malawi rift (e.g., Scholz et al., 2006). In deeper intervals where there is no possible analogue, so we used Gardner's equation (Eq.7) to predict lithological densities.

$$\rho = 0.31v^{0.25}$$

(7)

where ρ = predicted density, v = velocity obtained from seismic reflection data. We acknowledge however that the velocity information obtained from seismic data has inherent uncertainties, which we address the seismic processing section in Supplemental Information.

3. Data

3.1.1 Aeromagnetic data

The aeromagnetic data were collected in 2015 – 2016 alongside the Tanganyika Air-FTG® survey data over the east central part of the Lake Tanganyika Rift (**Figure 19b**) using a magnetometer system that is comprised of an airborne magnetometer and a base station. The total field was measured using the Geometrics 882 cesium vapor sensor mounted in a boom attached to the aircraft tail. The data were recorded at 10 Hz and compensated in real time by an RMS DAARC500 data acquisition system. To monitor diurnal variations in the background field, a GEM Systems GSM19 gradiometer base station was used, recording at 1 s intervals. This was backed up by a Geometrics G856 (proton precession magnetometer) base station recording at 10 s intervals. The aircraft was flown in the survey line headings (090°), and because at tropical latitudes the sensor's sensitivity weakens during turns, the figure of merit was split into partial calibrations.

The aeromagnetic data were processed by Bell Geospace Limited using Geosoft Oasis Montaj software to obtain the final measured residual magnetic intensity (RMI). Initial processing employed manual filtering to remove the interference noise from nearby artificial magnetic sources such as electrical equipment. Also, the Earth's regional magnetic field was removed from the survey data to separate local anomalies. The International Geomagnetic Reference Field (IGRF) tables corresponding to the time, date and acquisition height of the

survey were generated. Then, the calculated IGRF was subtracted from the recorded total magnetic intensity (TMI) and the statistical IGRF mean for the entire survey was added back in. Alken et al. (2021) defines the IGRF as a set of spherical harmonic coefficients that are used in a mathematical model to account for the large-scale, time-varying portion of Earth's internal magnetic field between epochs 1900 A.D. Other processing of the data included levelling (tie-line and micro) and de-meaning.

Aeromagnetic data detect subsurface geology that contains sufficient magnetic susceptibility to be magnetized by the passing of a magnetic sensor proximal to it. Therefore, high magnetic anomalies result from geology that is dominantly composed of minerals with magnetic affinities such as typically found in igneous and metamorphic rocks (crystalline basement). Consequently, the edges of sedimentary basins exhibit higher magnetic anomalies compared to the basins' axes due to their proximity to the basement rocks (Florio, 2018). Likewise, the vertical juxtaposition of basement rocks against sedimentary sequences along dip-slip faults creates prominent gradients in the aeromagnetic data (e.g., Grauch and Hudson, 2011; Kolawole et al., 2018a). Accordingly, we used aeromagnetic data mainly to discern basement structures.

3.1.2 Airborne-Full Tensor Gradiometry (Air-FTG®) data

The Air-FTG® data were acquired over the east central part of the Lake Tanganyika Rift (**Figure 19b**) alongside the aeromagnetic data (refer to section 2.2.1) using an FTG-1 unit owned by Bell Geospace Limited. The FTG system is comprised of three gravity gradient instruments (GGIs) mounted on a stabilized platform. The data were initially acquired in an internal coordinate system referenced to the axes of the three GGIs, which are the primary measurement components of the FTG. These data were later transformed into an East-North-Down (x, y, z)

coordinate system with x and y in the plane of the Earth's surface and z perpendicular to that plane downward towards the Earth. A total of 24,027-line kilometers of Air-FTG® data with 500 m in line spacing were acquired continuously throughout a flight at a ground speed of ~ 215 km/h over the period 18 November 2015 to 20 January 2016. The tie-lines were also acquired at 5000m intervals at 090° heading. A drape ranged between 929 m and 1875 m above sea level depending on the topography. Draping the survey is the process of projecting a flight height to a safer flyable constant terrain clearance, rather than at a constant elevation above sea level to optimize the survey pilots' flight path (Evjen, 1936; Pilkington and Roest, 1992). It improves the data fit at line intersections and reduces spurious variations in signal strength between survey lines.

The data were subjected to a series of processing steps to obtain the final measured gravity gradients used for interpretation. Specific processing methods included high-rate post-mission compensation (HRPMC), strip-average-reformat (SAR), bias and drift corrections, tie-line levelling, tensor components generation, full- tensor noise reduction (FTNR) and finally, terrain corrections. The processing was done by Bell Geospace Limited.

FTG measures the derivative of all the three gravity components in all three directions (G_x , G_y and G_z) (**Figure S2**), and enables the delineation of geology and geological structures (Dickinson et al., 2010). Conventional gravity measures only the changes in the G_z direction (i.e., the vertical component) whereas FTG enables measurement and detection of those changes in all directions (i.e., the vertical and two horizontal components). For a full swing, FTG assesses how each of the three components of the gravity vector varies in each of the three primary directions. This results in nine-component tensors (**Figure S2**). FTG can accurately measure the edges of anomaly sources and define their size, shape, and thickness. FTG data record short

wavelength signals generated by shallow to intermediate sources located within 10 km below the surface (Stuckless, 2008). These signals are not recorded in conventional gravity data, hence FTG exhibits greater resolution (Stuckless, 2008).

3.1.3. 2-D Seismic reflection data

This study augments the legacy Project PROBE 2-D seismic reflection data (PROBE) acquired in 1983-84 and reprocessed in 2016 by ION Geophysical Company. The PROBE multichannel, basin-scale seismic (MCS) data are 24-fold, widely spaced (up to ~28 km), but cover ~1900 line-km over the entire lake and image up to 6 km below the earth's surface. Its acquisition program employed a 140 cubic inch single air gun and a 48-channel hydrophone streamer, with offsets up to 1450 m (e.g., Rosendahl, 1987; Burgess et al., 1989; Muirhead et al., 2019; Wright et al., 2020; Shaban et al., 2021). Reprocessing details are contained in the Supplemental Information. We integrated the legacy data with state-of-the art commercial data acquired in 2012 and 2014 in the southern part of the lake within the Tanzania territory. The 2012/2014 data were acquired using a 3 km-long streamer and a 500 cubic inch air gun array and are 60-fold with a frequency range of ~5-75 Hz and a vertical resolution of 8-10 m.

3. Results

4.1 Rift Structures

The interpretation and integration of 2-D seismic reflection data, FTG, and aeromagnetic data reveal both shallow and deep structures along the Lake Tanganyika Rift.

4.1.1 Shallow structural fabrics

The total horizontal derivative, vertical derivative (**Figures 20a-c**), analytical signal, and tilt-angle derivative (**Figures S19a-b**) reveal structures with a general dominant trend of NW-SE (**Figures 20d-f**). However, we note that the tilt-angle derivative, which normalizes anomalies, resolves a secondary NE-SW trend (**Figure S3**). These derivatives generally reveal shallow upper crustal structures. Most of the resolved structures are within the south-eastern part of the Kigoma Province and the northern part of the Marungu Province (**Figures 20, 22, 23, S3**). In the southern part of the Kigoma Province, the horizontal gradient reveals lineaments of alternating magnetic polarities, with dominantly NW-SE trends.

The Butterworth filter for short wavelength anomalies in the aeromagnetic data (**Figure 21a**) also shows a dominance of NW-trending lineaments along the rift, with a prominent NE-trending lineament in the Kigoma Sub-basin, at the same location where the tilt-angle derivative shows NE-trending lineaments. The rotational invariants of the FTG data (**Figures 22a-b**) reveal high frequency lineaments along the rift basin, showing a dominance of a NW-SE ($\sim 315^\circ$) trend, with a prominent secondary NNE-SSW (20°) trend (**Figures 22c-d**). The maps show that the NNE-SSW lineaments dominantly occur in the northern sub-basins of the rift (Kigoma/Ruzizi Sub-basins). Overall, these inferred shallow lineaments, all dominantly trending NW-SE, are consistent with the regional trends of basement lineaments on the neighboring rift shoulder (see SRTM DEM hillshade map in **Figure 23, 25, S5**).

To better discern magnetic bodies, we compared RTP TMI to its AS, because the AS produces a positive anomaly for magnetic sources only. The AS exhibits high positive anomaly lineaments mostly in the central area and a few in the northern parts of the rift (**Figure S3a-b**). Moderate positive anomalies occur in the northern part of the Marungu Province. When

compared with the Tz data, the opposite is observed; the southern part of the survey (northern part of the Marungu Province) is marked by very low gravity anomalies. High gravity anomalies are observed at the KIR, northeast of the KIR and around the Karema/Ikola Platform (**Figure 6Sa-b**). Within the Mahale-KIR- Katenga - Kugulu - Ntengo corridor, the bandpass filtered RTP maps reveal ~E-W oriented lineaments with very high amplitudes (**Figures 21a-b**).

4.1.2 Deeper structural fabrics

High magnetic anomalies (>250 nT) in the intermediate- and long-wavelength Butterworth filtered-maps dominate the central and southern parts of the Tanganyika Rift and they dominantly trend NW-SE (**Figures 21a-c**). However, these Butterworth-filtered aeromagnetic maps and upward-continued gravity maps (**Figures S6a-b**) show N-S and NNE-SSW-trending gradients in the northern sub-basins of the rift. Moderate magnetic anomalies (20 to 250 nT) are predominantly observed in the northern sub-basins (north of the KIR). The NW-striking KIR is resolved in both long and short wavelength maps (**Figures 21b-c**). The lowest magnetic anomalies (0 -178 nT) are predominantly evident from the central part towards the northern part of the survey area (Kigoma Province). Both the analytical signal of the RTP total magnetic intensity and Tz component of the FTG maps show the NW-SE striking fabrics, possibly representing both the sedimentary and shallow basement fabrics. In addition, a similar structural trend is observed in the south of the Malagarasi Platform.

4.2 Updated fault map of the Tanganyika Rift

Based on the lineaments extracted from the filtered FTG and aeromagnetic data and their derivatives, we have updated the fault map of the Lake Tanganyika Rift (**Figure 23a**). There is a trend of faults consistent with that from recent works of Muirhead et al. (2019) and Rosendahl (1987). However, from this study we have confirmed the lateral extent of previous faults and added new faults, especially in the Kigoma Province.

Overall, the updated fault map shows that the Tanganyika Rift is dominated by NW-SE trending fault systems. However, a secondary fault set trending NNE-SSW is resolvable, mostly occurring in the northern sub-basins of the rift. The results show that the dominant fault trends closely correspond to the dominant structural trends in the rotational invariant of the FTG data, further validating the dominance of intra-sedimentary structures in the rotational invariant maps (compare **Figures 22c-d** with **Figure 23a** rose diagram).

4.3 2.75-D Model of the Central Tanganyika Rift

The 2.75-D forward modelling along seismic profiles 83-218 (**Figures 24a-b**) reveals previously unresolvable heterogeneities in the crystalline basement underlying the Tanganyika Rift as well as salient features in the sedimentary section. The model permits the inclusion of deep-seated sedimentary rocks with a density of 2.35 g/cc and 2.45 g/cc directly overlying the crystalline basement. Generally, the model predicts a sedimentary package with densities varying from 1.8 g/cc in the northeast part of the profile within the youngest unit, and 2.45 g/cc in the central and eastern part of the profile overlying the crystalline basement. It is revealed that sediments in both ends, the northeastern and southwestern parts of the profile, are characterized

by low densities. Within shallower seismic units 3-4 (Shaban et al., 2021), a prominent V-shaped intra-sedimentary unit with a density of 2.2 g/cc is resolvable; the discontinuous seismic facies pattern within this unit permits an interpretation of a large axial channel complex.

The model suggests an heterogeneous crystalline basement with density varying from 2.5 g/cc to 3.2 g/cc and magnetic susceptibility varying from 0.0001 to 0.001. At the basement level, the observed data can only be matched by the inclusion of 1) a laterally extensive shallow basement layer of very low density, possibly corresponding to a fractured weathered basement, and 2) a ~4 km-wide sub-vertical body of similarly low-density near the rift axis, which is flanked by basement of normal density. This central low-density sub-vertical basement body defines the footwall of a large intra-basinal fault that is synthetic to the SW-dipping border fault (**Figure 24b**). Generally, the basement exhibits an asymmetric geometry, high in the southwestern part, and deepens towards the northeast across the profile. Overall, the sediments thicken towards the east of the profile towards the intra-basinal fault. Also, the magnetic anomaly generally increases towards the east of the profile (in the direction of the eastern border fault).

Both gravity (T_z) and aeromagnetic (TMI) anomalies reveal long-wavelength low frequency anomalies across the profile whereas the T_{zz} anomaly exhibits a short-wavelength high frequency feature towards the southwestern part of the model profile, around the intra-basinal synthetic fault. The aeromagnetic data correlates well with the gravity data from the southwestern part of the profile up to a model distance ~5,880 m, then from this point southeastwards, these anomalies show a divergent pattern which may be due to the rotation of the transect from a rift-orthogonal trend.

5. Discussion

The augmentation of high-resolution potential field data with 2-D seismic reflection data has helped to constrain the structural characteristics of the central part of the Lake Tanganyika Rift. The potential field data sets help as an infill for areas with only widely spaced seismic reflection data coverage. Basin geometry and basement structures can be interpreted from FTG, and aeromagnetic grid enhancements enable good correlation between anomalies and large structures such as border faults imaged in the seismic reflection data. The analysis reveals faulted basement representing rift zone border faults and intra-basinal faults and reveals changes in the orientation of the lineaments at various depth ranges. This study provides a more precise and detailed structure delineation than previously available, especially in the Kigoma and Kalemie provinces (Tanzania side).

The integration of potential field and seismic data is however limited to the central eastern part of the Lake Tanganyika Rift due to data coverage constraints. Also, the petrophysical properties such as density and magnetic susceptibility used for 2.75D gravity and magnetic modeling have considerable uncertainties (refer to section 2.2.4).

5.1 The Pre-rift Basement Structure Beneath the Tanganyika Rift

The filtered FTG and aeromagnetic data have revealed the dominant NW-trending high density and magnetic fabrics at deeper structural levels, especially in the eastern part of the Kigoma Province, around the boundary between the Kigoma and Kalemie provinces, the eastern part of the Kalemie Province and the central and eastern parts of the Marungu Province (**Figures 21, 22, and S3**). These fabrics highlight the dominant fabrics in the Precambrian metamorphic

basement (intermediate and long-wavelength and derivative filters), consistent with the NW-trend of the previously mapped metamorphic fabrics on the rift shoulder onshore (Morley et al., 1988; Muirhead et al., 2019). The ~4 km-wide, sub-vertical, low-density high magnetic susceptibility body near the rift axis, which was modelled in the 2.75-D forward model, is a good example of the basement fabrics at deeper structural levels. We interpret the basement fabrics mapped in this study to represent metamorphic shear zones that bound the amalgamated basement terranes, as well as large-scale foliation of rocks within the basement terranes (e.g., Kolawole et al., 2021A, B). These basement shear zone and foliation trends in the terranes have also been studied on outcrops along the eastern shoulder of the Tanganyika Rift (Boven et al., 1999). The most prominent of the shear zones is the Chisi Shear Zone, a NW-trending >600-km long, 6–12 km-wide shear zone along which eclogite facies metamorphic rocks have been found, suggesting collisional suturing of the terranes (**Figures 25a-c**; Kolawole et al., 2021B; Boniface et al., 2012). These shear zones have been interpreted to have controlled the geometry and early-rift strain distribution along the neighboring Rukwa Rift (Kolawole et al., 2021b). In addition, the shear zones exert a persistent influence on Cenozoic rift faulting in the rift basins (Daly, 1988; Delvaux et al., 2012; Kolawole et al., 2021b) and in the zone of interaction between the Rukwa and Tanganyika Rifts (Kolawole et al., 2021a). Furthermore, we suggest that the revealed NW-SE and NNE-SSW basement fabric trends influenced the Cenozoic NW- SE and NNE-SSW fault trends within the Lake Tanganyika Rift.

5.2 Incipient Stage of the Tanganyika Rift and the Controls of Structural

Inheritance

Deciphering the impact of pre-rift structures on extension and determining causation is challenging (Versfelt and Rosendahl, 1989). This study integrates high-resolution FTG,

aeromagnetic data and basin scale 2-D MCS to evaluate the inheritance of pre-rift structures. The 2.75-D models clearly establish that the seismically defined top basement is heterogeneous, as indicated by variable densities (refer to section 4.6). There is no borehole or well information penetrating the crystalline basement in the region, thus this new information obtained from the FTG survey provides constraints on the deep subsurface that is not resolved from the available seismic reflection data. Basement density and susceptibility along both profiles are consistent with property values associated primarily with felsic crystalline rocks (2.6-2.75g/cc density and 100-2500 micro-cgs susceptibility) with some mafic rocks (density higher than 2.75g/cc and susceptibility above 3000 micro-cgs).

Our structural analysis indicates that high magnetic susceptibility basement is aligned with pre-existing geological structures, and that the basement is associated with the reactivation of pre-rift faults. This is supported by the general NNW-SSE and NNE-SSW trend identified from the regional basement as demonstrated in section 3.1. Also, the NNW and NW orientated structures are parallel to the Mahale Mountains and Katenga - Kugulu - Ntengo (Luama footwall) lineaments, and the Precambrian Chisi Shear Zone (CSZ) that extends from the Rukwa Rift (Kolawole et al., 2021b), supporting this hypothesis. Versfelt and Rosendahl (1989) suggested that the Cenozoic rifting followed Proterozoic mobile belts and bifurcated around the Tanganyika craton. Furthermore, they demonstrated that the NNW-SSE striking rift faults follow the Ubdendian and Ufipa foliation, whereas the NNE-SSW striking rift faults follow the Kibaride foliation. They defined the basement foliation as fabric of the pre-rift rocks including local faults and fractures, axial planar fabrics, strike of igneous bodies, metamorphic facies, schistosity and compositional layer boundaries. Furthermore, Versfelt and Rosendahl (1989) demonstrate that the Karoo and Cretaceous trough remnants run parallel to the KIR and sub-parallel to the west

Kigoma half graben as well as the southern half of the lake. Also, Heilman et al. (2019) suggested that the alignment of the Rukwa and Malawi rifts is strongly controlled by the configuration of the basement fabrics as demonstrated by the colinear alignment of the structures connecting the rifts with basement fabrics. Delvaux (2001) and Kolawole et al. (2021b) reached a similar conclusion, that the NW-SE trending Paleo-Proterozoic Ubende shear belt controls the basement morphology and overlying basins of the Tanganyika-Rukwa-Malawi rift segment. For instance, Kolawole et al. (2021b) suggest that the CSZ and adjacent terrane boundaries controlled the rift development as well as strain-distribution. According to Lenoir et al. (1994), the NW-SE trending structures of the Ubendian belt have been reactivated in several periods along the Paleoproterozoic sheared structures. Furthermore, the gravity and magnetic models predict that the intrabasinal normal fault in seismic profile 218 follows the western edge of the basement anomaly, a ~4 km wide structure, here interpreted as a paleo-shear zone, possibly representing a Precambrian terrane boundary (refer section 3.3 and 4.4). This phenomenon provides insight on the possible structural inheritance.

Our analysis suggests three generations of fault development: an older deep NW-SE, NNW-SSE, and NNE-SSW striking fault set controlled by pre-rift basement structures, and although the older set were subsequently reactivated, a younger, shallower ENE-WSW striking set may have later developed. The deep, older faulting occurred during the initial stages of the Rift development, possibly in the Early-mid Miocene. This is evidenced by these faults cutting across the Seismic units 1-5 (Shaban et al., 2021), and contributing to the total rift extension (Muirhead et al., 2019; Wright et al., 2020). The orientation of older, deep structures in the Lake Tanganyika Rift closely matches with some exhumed Precambrian mylonitic basement shear

zones and fold axes in the northern Malawi Rift (e.g., Kolawole et al., 2018a) and those in the Rukwa Rift (e.g., Wheeler and Karson, 1989; Kolawole et al., 2021b).

The significant magnetic anomaly observed in the southern part of the survey (northern part of the Marungu Province) suggests the presence of shallow crystalline basement of mafic affinity, possibly overlain by sediments with high magnetic susceptibilities (**Figure 20** and **S3**). This is supported by our modeling analysis that predicts a crystalline basement with density of 3.2 g/cc and magnetic susceptibility of 0.001, consistent with mafic intrusions possibly associated with Mesozoic Rifting. Given the proximity of the Rungwe Volcano and the presence of Precambrian basement terranes with abundant magnetic minerals, the sediments sourced from these areas are expected to be rich in magnetic minerals. However, it is assumed that the dominant magnetic basement in the rift fill is the pre-rift metamorphic basement. Mafic intrusions are common in the region especially in Archean Greenstone Belt in Tanzania, for example including the mafic metavolcanics in the Sukumaland Greenstone Belt (Borg and Shackleton, 1997; Manya, 2004) and mafic dykes reported in gold mines (e.g., Eberle, 1988).

5.2.1 The Presence of Karoo Sediments in the Kalemie-Marungu provinces

Delvaux (2001) suggested the presence of Permo-Triassic 'Karoo' sediments in the Kalemie-Marungu provinces within the Ubendian belt based on the interpretation of multichannel seismic profiles in the Lake Tanganyika Rift by Sander and Rosendahl (1989). They interpreted that the Karoo rift system in the Rukwa-Tanganyika rift was a precursor of the late Cenozoic rifting. However, apart from the outcropping sediments within the Lukuga depression along the Congolese side of Lake Tanganyika, there are no rock samples from the

Lake Tanganyika Rift to support the presence of Karoo sediments in the Kalemie-Marungu provinces. Our model predicts the possible presence of sediments below the Nyanja Event (**Figure 24**) with a density of 2.45 g/cc. This elevated density may be representative of the Karoo sediments buried at least 2.5 km in the subsurface, likely comprised of sandstones, shale, coal, siltstone, and conglomerates (Cahen and Lepersonne, 1978; Delvaux, 2001). Using an analogous density of the Malawi Karoo sediments (i.e., 2.4 g/cc, Bardwell et al., 1992), our calculated model response considerably matches the observed gravity anomaly (**Figure 24b**). In addition, our model indicates that the Karoo sediments in this area must have been significantly eroded prior to the Cenozoic rifting because the modelled thickness (i.e., ~300 m) is significantly lower than the Karoo sediments in the adjacent Rukwa Rift which has been estimated to be approximately ~ 3500 m thick (Wescott et al., 1991; Morley et al., 1992). However, the maps of Karoo half-grabens in this region show that they were very much restricted in size, suggesting limited accommodation for sediment deposition.

5.3 The Kavala Island Ridge and its implications

Although the modelled seismic section is located just south of the Kavala Island Ridge, being one of the persistent structurally controlled basement ridges in the Tanganyika Rift, we discuss the implications of the ridge for the tectonic and geomorphic evolution of the rift. The Kavala Island Ridge is the most prominent rift segment boundary in the entire Lake Tanganyika Rift and arguably the entire western branch of the EARS, and this high block has been an important physiographic and limnological barrier through much of the history of Lake Tanganyika. From our analysis, magnetic anomalies and FTG intermediate and long wavelength anomalies suggest that a major tectonic lineation intersects the rift around the KIR, parallel to

sub-parallel to the NNW striking regional basement foliation. (**Figures 20, 21, S3, and S6**). Kolawole et al. (2021b) suggested that to the northwest, the CSZ splays into two branches as it intersects the Tanganyika Rift in which one continues into the Luama Rift's northeast footwall via the KIR, and the other rotates northwards into the northern part of the Kigoma Province. However, based on our filtered aeromagnetic map (**Figure S7**), our preferred interpretation is that the CSZ extends into the northern part of the Kigoma province, and less likely into the footwall of the Luama Rift. Whereas the splay that continues into the Luama Rift's northeast footwall via the KIR is a different Precambrian Shear Zone, herein referred to as Mahale-Katenga Shear Zone.

Major shear zones are inferred to strongly control the structural evolution of the Lake Tanganyika Rift system. The oblique intersection of a laterally propagating rift tip at a pre-rift shear zone may induce stress redistribution at the rift tip (Crane and Bonatti 1987). We propose that the Tanganyika Rift was initially segmented across the exhumed Mahale- Katenga Shear Zone during which the southern tip of the Kigoma Province is deflected along the shear zone. This resulted in the formation of the Kigoma and Kalemie graben sub-basins and the KIR. We suggest that subsequent interaction and strain transfer between the Kalemie and Kigoma grabens across the KIR led to the linkage and coalescence of the rift basins and drowning of the KIR. Pre-rift crustal scale shear zones have been suggested to transiently arrest or deflect the lateral propagation of rift segments and associated faults. For instance, the rift-oblique/orthogonal Sanangoe and Lurio shear zones have been suggested to temporarily terminate and subsequently refract the lateral propagation of the Shire Rift Zone in the EARS, as evidenced by the termination of its early-phase rift tips near the shear zones (Kolawole et al., 2022). Also, the

NW-striking Precambrian Aswa Shear Zone terminates the Western Branch of the EARS north of the Albertine-Rhino grabens (Katumwehe et al., 2015, 2016).

Considering the long-term prominence of the KIR as a topographic high in the middle of this ancient lake, we highlight its evolutionary history. Displacement along the KIR is due to the southern and northern extensions of the Kigoma and Kalemie structural province border faults, respectively (**Figures 18a, 26 & 27**). Based on the seismic reflection data (**Figures 26**), the crest of the KIR is nearly devoid of sedimentary units except for a thin part of S1 unit and S6 units. The sedimentary units on either side of the ridge display a wedge-shape towards the ridge especially in S1, S3, S4, and S5, units, suggesting that the ridge was active during the deposition of these units. We suggest that the KIR growth initiated during the first stage of rifting, as major border faults in the Kigoma and Kalemie structural provinces attained nearly their full present length early in the Cenozoic rift history (Morley, 1989). During the deposition of S2 unit there was decrease in tectonic strain along the faults bounding the KIR, as evidenced by is relatively less significant thickening of the S2 unit toward the border faults. From S3 to S5 deposition period, the bounding faults of the KIR reactivated, as indicated by the thickening of the sedimentary packages towards the ridge (**Figure 27**). S6, which has a constant thickness away from the ridge, represents the sedimentary drape from the latest highstand phase of Lake Tanganyika (e.g., Scholz et al., 2007).

We attribute the large (~40 km long and 8 km wide) lineament striking almost N-S in the northeastern part of the Kigoma Province to high-density sedimentary rocks or shallow basement on the platform. Based on wavelength analysis on the Tz anomaly, the anomaly seems to have grown on top of the pre-existing basement high relief, and the platform is within 3 km of the lake surface (**Figure S6**). In conjunction with the KIR, these two lineaments together with the

Kigoma border fault control how the Malagarasi River delivers sediments into the lake. Consequently, the Malagarasi channel passes between these two lineaments, and eventually deposits sediments north of the KIR and west of the NNE-SSE platform. This interpretation is supported by the work of Shaban et al. (2021) that identified channel complex deposits in these localities attributed to the Malagarasi River processes. Drainages of the Malagarasi and Lugufu rivers indicate modern tilting of the Malagarasi Platform along the border fault of the Kigoma Province.

5.4 The Persistent Influence of Incipient Rift Structure on Subsequence Rift Phases

From our 2.75-D modelling we show that the interpreted axial channel complex is bounded by the localized intra-basinal high and the eastern border fault. The persistent intra-basin high block is observed adjacent to the early-rift intra-basin fault that bounds the western part of the interpreted ~4-km wide shear zone. This intra-basin high is also observed on the structural map of top of seismic deposition unit 3 (Shaban et al., 2021; **Figure 26**) and is co-located with the broad topographic high along the modern lake floor in the Kalemie Sub-Basin (**Figures 22, 28, and S6**). Based on the analysis of basement lineaments in this study, it is evident that topographic highs along the modern lake floor are associated with deep structural highs along the rift axis in the earliest syn-rift units (**Figures 27**). Prominent topographic highs, interpreted as accommodation zones are commonly associated with large border faults, including the KIR, the Burton's Bay Ridge that separates the Kigoma and Ruzizi provinces, and the Moba high that separates the Kalemie and Marungu province (Rosendahl et al, 1986; Rosendahl, 1987; Shaban et al 2021). We suggest that during the initial stage of the rift evolution, some of the pre-existing basement fabrics such as shear zones accommodate strain, and normal faulting occurs by

preferentially following the pre-existing weaknesses. During the middle stage of rift evolution, the intra-basinal fault that occurred due to pre-existing fabrics continued to grow. Then, during the latest stage of the rift evolution, as sediments deposition continued, the sediments covered the abandoned intra-basin fault, producing a subtle bathymetric high over the older footwall block (**Figure 28c**). Differential compaction of sediments on top of the buried intra-basinal fault likely contributed to the modern relief. Such topographic highs and differential compaction structures can form potential hydrocarbons traps in rift systems (e.g., Hao et al., 2009). These observations indicate that early Mesozoic rift structures can cascade and focus the later stage (Cenozoic) of the rift evolution.

6 Conclusions

Integrated aeromagnetic, Air-FTG, and seismic reflection data are used to assess the deep basin and underlying basement structure of the Lake Tanganyika Rift, East Africa. We use the short-wavelength, high-frequency components of the FTG and aeromagnetic data to delineate the shallow structural fabrics, corresponding to intra-sedimentary depth intervals, and the longer-wavelength, lower-frequency components to discern the deeper basement structural fabrics.

The results show a dominance of NW and NNE-trending fabrics within the shallow depths, consistent with the dominant trends of rift faults mapped in the seismic reflection data. The deeper basement is dominated by NW-trending fabrics, consistent with the dominant trend of exhumed basement shear zones and strike of metamorphic foliation in basement terranes along the rift shoulder. These results demonstrate the large-scale control of inherited basement fabrics on the geometry of rift faulting along the Tanganyika Rift.

These analyses support long held concepts that the KIR developed along a large and long paleo-ductile shear zone possibly connected to the Chisi Shear zone, and that paleo shear zone may have acted as locked zone during the south rift propagation. Seismic interpretations reveal that the relatively high relief of the KIR has been present since its bounding faults were fully established in the early stage of rifting; activity on those bounding faults increased in later stage of the rift evolution, although the high and frequent lowstand lake level exposures eroded most of the sedimentary section atop the crest of the ridge.

The results of a seismically constrained, full-tensor gradiometry and aeromagnetic forward model delineated the presence of a ~4 km-wide basement-bounded shear zone that controlled the location and down-dip geometry of a buried large-offset early-rift intra-basin fault. The strike and location of both the large-offset intra-basin fault and border fault, and density of the deepest sediments on their hanging walls suggest that incipient rifting in the central Tanganyika Rift may be Mesozoic in age. Furthermore, we find that the early-rift structural highs, commonly localized by large-offset rift faults that exploited exhumed pre-rift basement shear zones, persisted into the subsequent stages of tectonic extension, in some places continuing to displace the modern lake floor. We propose that although incipient rift structure is largely modulated by inherited basement fabrics and shear zones, their influence on basin morphology often cascades through to the subsequent stages of tectonic extension.

Acknowledgments

We extend our acknowledgements to the Petroleum Upstream Regulatory Authority of Tanzania and the Tanzania Petroleum Development Corporation (TPDC) who provided an

access to the commercial higher resolution 2D multichannel seismic data, FTG, aeromagnetic data that were used for this study. This work was supported by Syracuse University; National Science Foundation (NSF)-Empower Program; Chevron; Petrobras; and the Tanzania Petroleum Development Corporation. Decision-Space software was provided to Syracuse University through a software grant from Landmark-Haliburton to CAS. We thank the members of the Lacustrine Basin Research Group at SU for their assistance provided while completing this study, particularly Jacqueline Corbett.

Data Availability Statement

Data supporting this research are available at the Petroleum Upstream Regulatory Authority of Tanzania and the Tanzania Petroleum Development Corporation (TPDC) with restrictions that require agreements and are not accessible to the public or research community. The data can be accessed upon a formal request to the Petroleum Upstream Regulatory Authority of Tanzania and the Tanzania Petroleum Development Corporation (TPDC).

Figures of Chapter 3

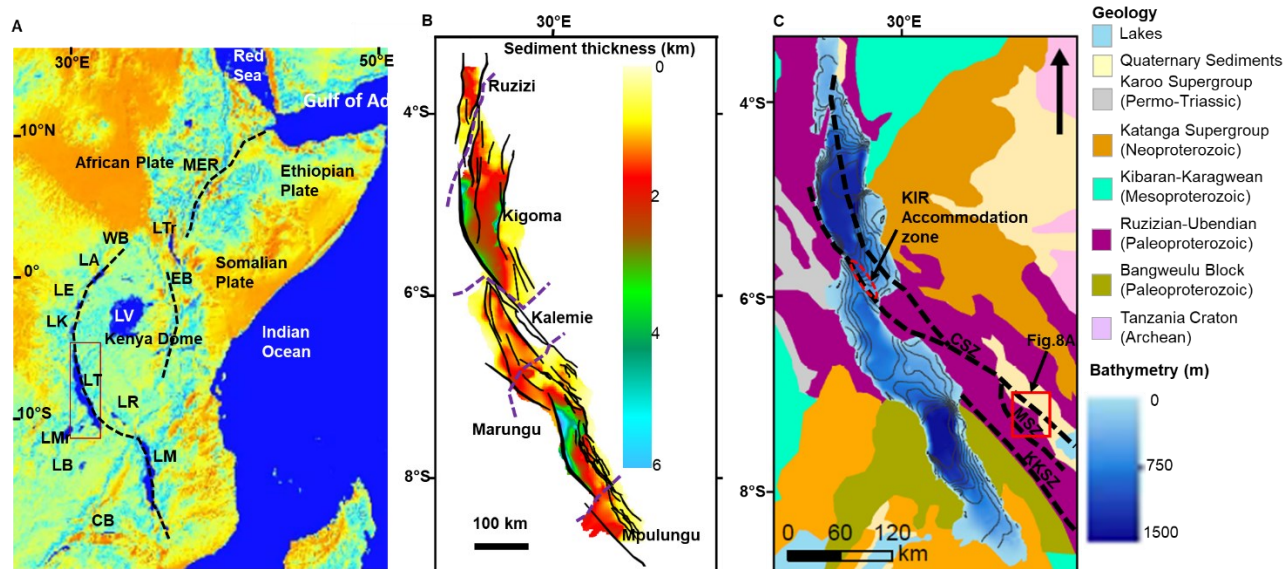


Figure 18: Study area: (A) Digital Elevation Model of the East African Rift System (EARS) showing the location of Lake Tanganyika (red rectangle) along its Western Branch. WB and EB are the Western and Eastern Branches respectively. MER=Main Ethiopian Rift, LTr = Lake Turkana, LA = Lake Albert, LE = Lake Edward, LK = Lake Kivu, LT = Lake Tanganyika, LR =Lake Rukwa, LMr = Lake Mweru, LB = Lake Bangweulu, LM = Lake Malawi, and CB = Cahora Bassa dam. (B) Map of Tanganyika Rift syn-rift sedimentary thickness. Purple dashed lines show the boundary of structural provinces of the Lake Tanganyika Rift. Thick black lines show the basement-rooted normal faults (updated after Muirhead et al., 2019). Note the maximum of ~6 km thick sediments along the western border fault of the Kigoma Province. (C) Geological map of the region surrounding the LTR (modified after Choubert et al., 1968); note Mesozoic rift sediments (Karoo) on the western flank of the Tanganyika Rift. Delvaux (2001) suggested the extension of Karoo sediments into the Kalemie and northern part of the Marungu provinces of the Tanganyika Rift. CSZ = Chisi Shear Zone, MSZ = Mtose Shear Zone, Kate-Kipili Shear Zone. The red rectangular polygon shows the location of Figure 8A. The red ellipse

in the central part of the Lake Tanganyika Rift represents a location of the Kaval Island Ridge. Bathymetry presented is derived from seismic reflection data set used in this study (maximum water depth = 1471 m). The two major deep-water areas are in the Kigoma and Marungu provinces.

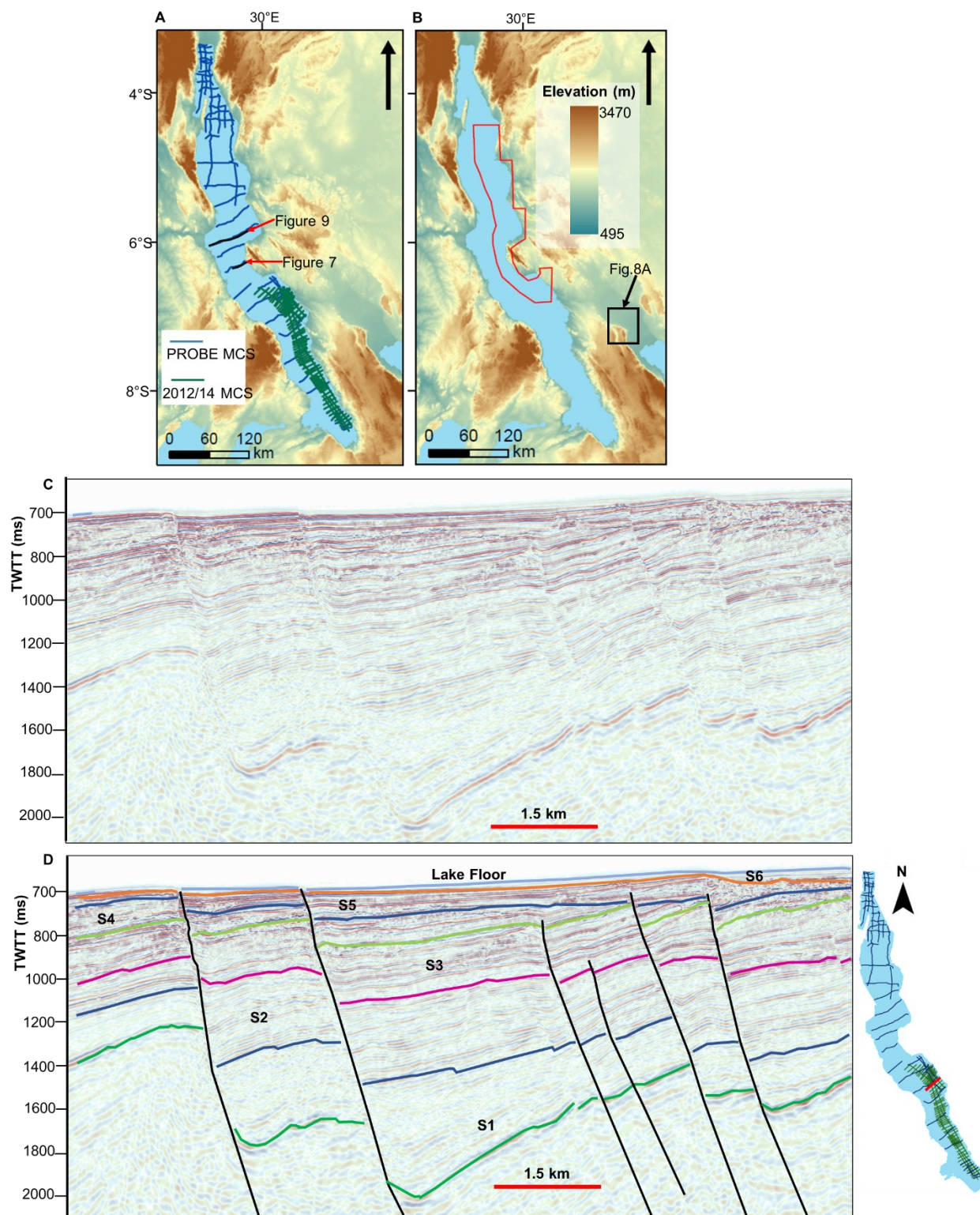


Figure 19: (A) Locations of seismic data used in this study. The latest 2D seismic data tracklines are the 2014/2014 Multi-channel Seismic Survey (MCS), the 1983/84 data tracklines are PROBE

Multi-channel Seismic Survey (MCS). Note the profiles (in black colour) for figures 7 and 9. (B) The red polygon represents the FTG and Aeromagnetic survey area. The black rectangular polygon shows the location of Figure 8A (C - D). Example basin-scale seismic reflection NE-SW dip profile (2014), located south of the Kalya Platform in Lake Tanganyika Rift consisting of the uninterpreted (panel C) and interpreted (panel D) sections. The seismic images show six known seismic stratigraphic syn-rift units (S1, oldest, to S6, youngest). S2 - S6 generally records deeper rift lake sequences, manifested by increasing the dominance of the high amplitude and parallel to semi-parallel reflections. S3 - S5 records facies variability with higher proportion of chaotic reflections and influence of alternating high- and low lake levels (see also Shaban et al., 2021).

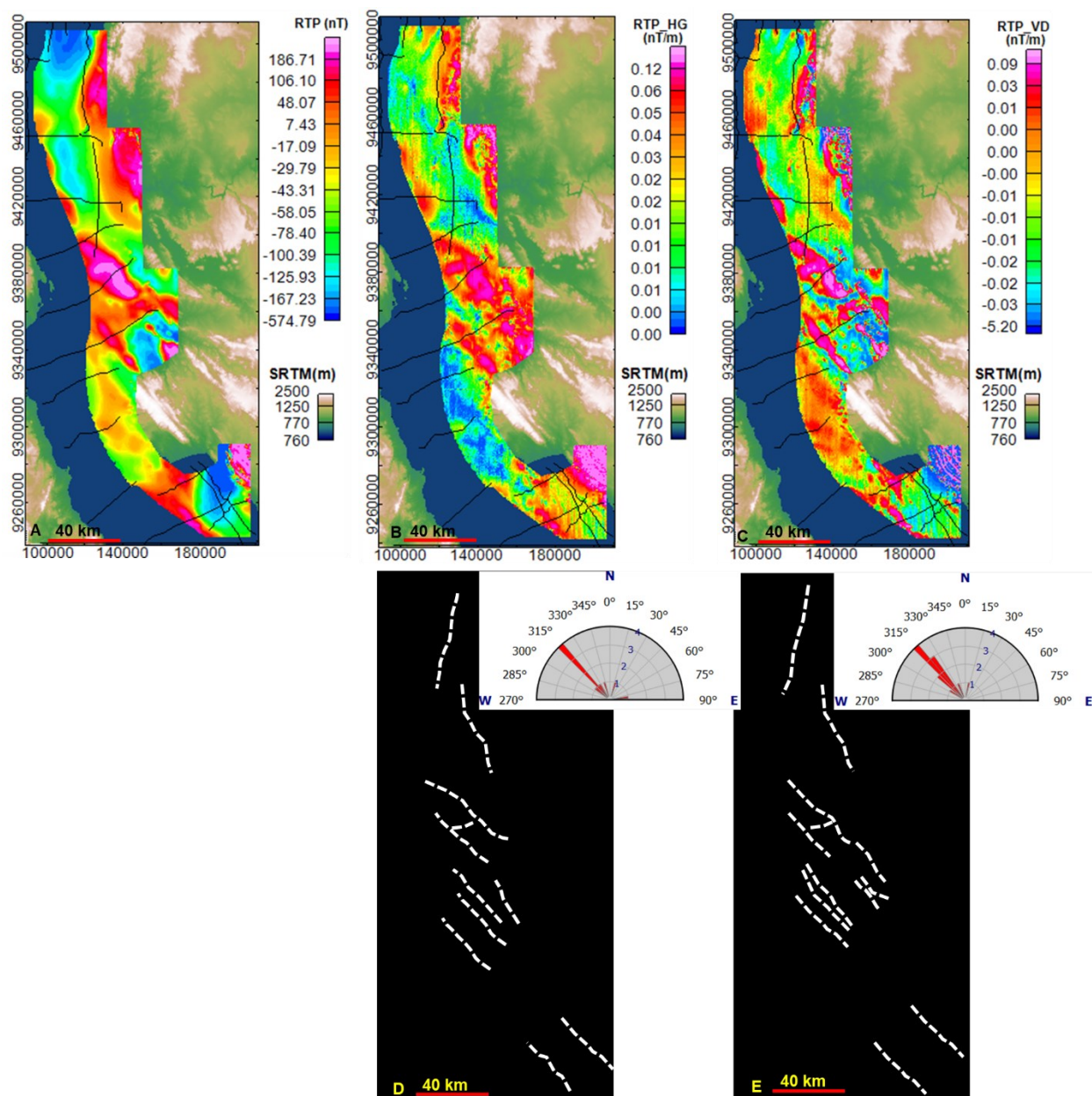


Figure 20: TMI reduced to the pole (RTP) anomaly exhibiting correct locations of the anomalies over the source. Note high magnetic anomaly in the southern part of the survey area (North Marungu Province) and low magnetic anomaly in the northern part of the survey area (North Kigoma Province). (B) Total Horizontal derivative (HG) of the RTP TMI anomaly. (C) Vertical derivative (Dz) of the RTP TMI anomaly. (D) Structures extracted from B. (E) structures

extracted from C. The rose diagrams were created by measuring the general strike of each lineament then plotted using GeoRose software (Yong Technology Inc., 2014).

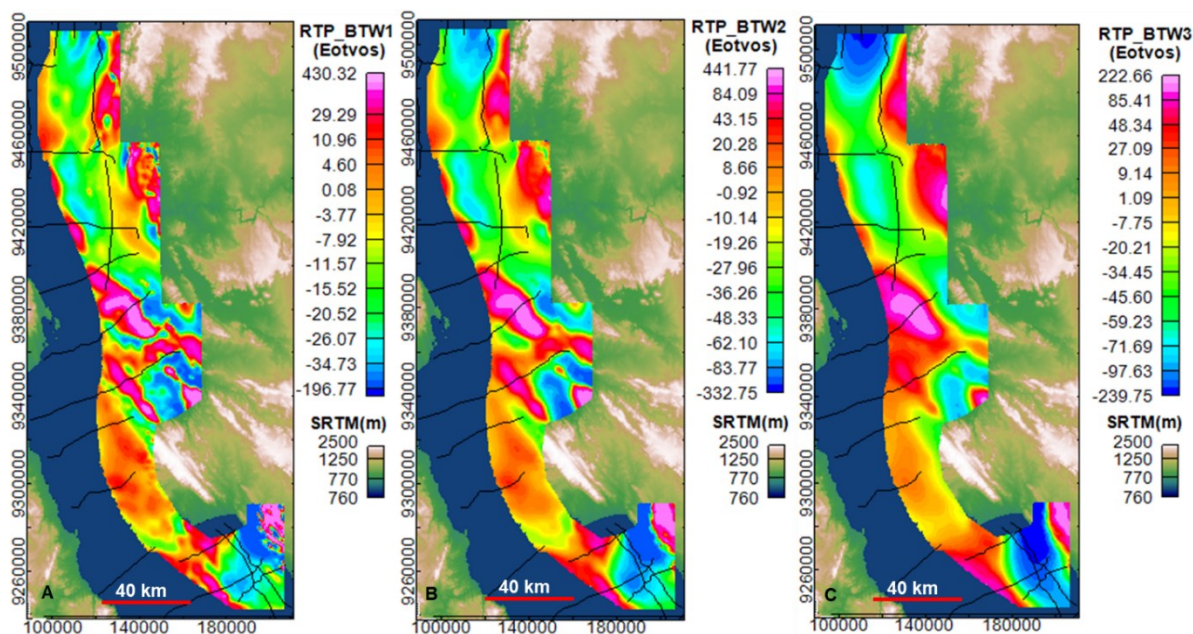


Figure 21: Butterworth bandpass filtered TMI RTP. (A) short wavelength, 5 - 12 km, (B) intermediate wavelength, 12 - 45 km, and (C) long wavelength, 45 - 205 km. The short wavelength reveals the magnetic bodies within less than 2 km below the surface, the intermediate wavelength reveals magnetic bodies within 2– 6 km below the surface, and the long wavelength reveals magnetic bodies within 6 – 14 km below the surface.

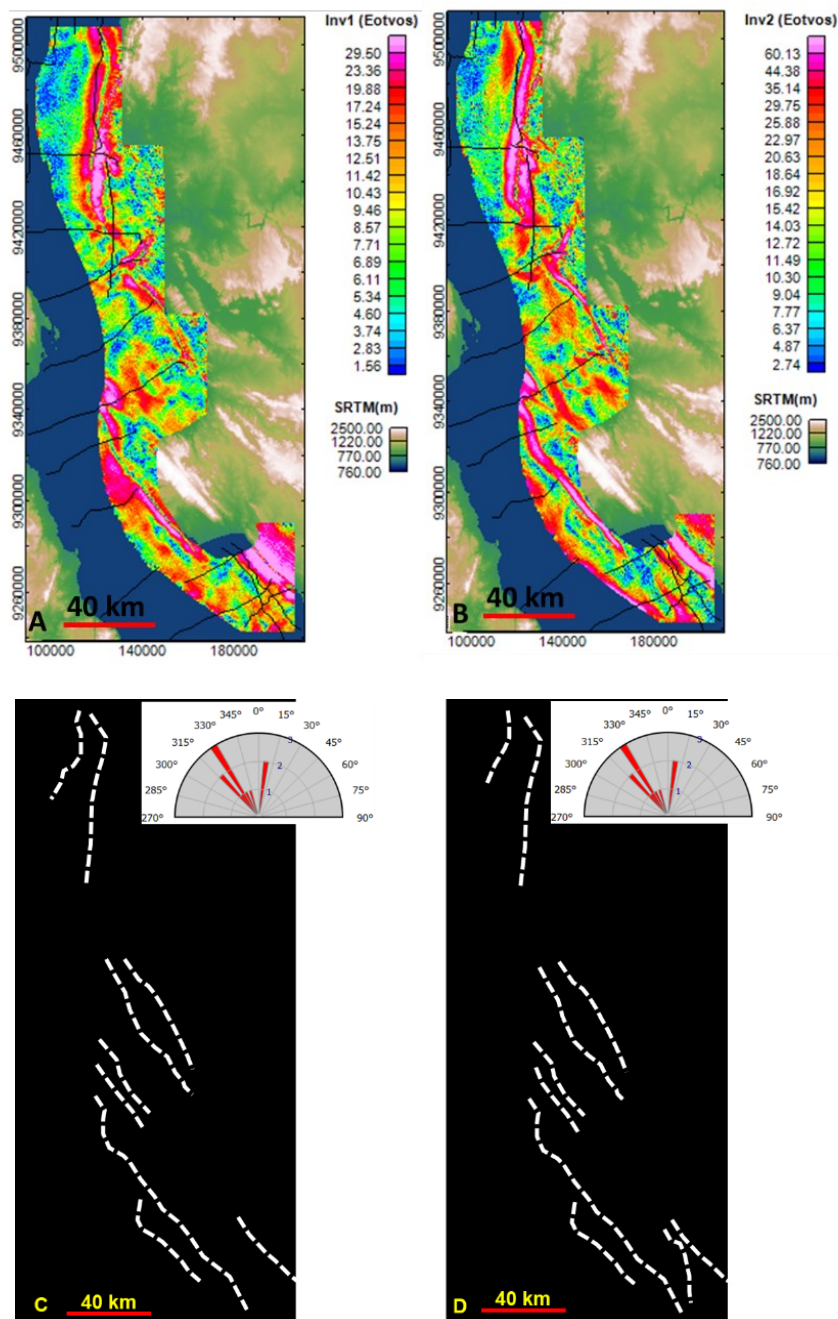


Figure 22: Rotational invariants anomaly showing high-to-medium frequency and short-to-intermediate wavelength anomaly lineaments (corresponding to shallow and intermediate depth intervals). A) R-1 and B) R-2, showing contacts, edges, and shapes of high-density geological

bodies. Note NW-striking bodies (314° mean trend) in the central and southern parts and NNE-striking bodies (009° mean trend) in the northern part of the area. (C - D) Structural fabrics mapped in panels A and B respectively.

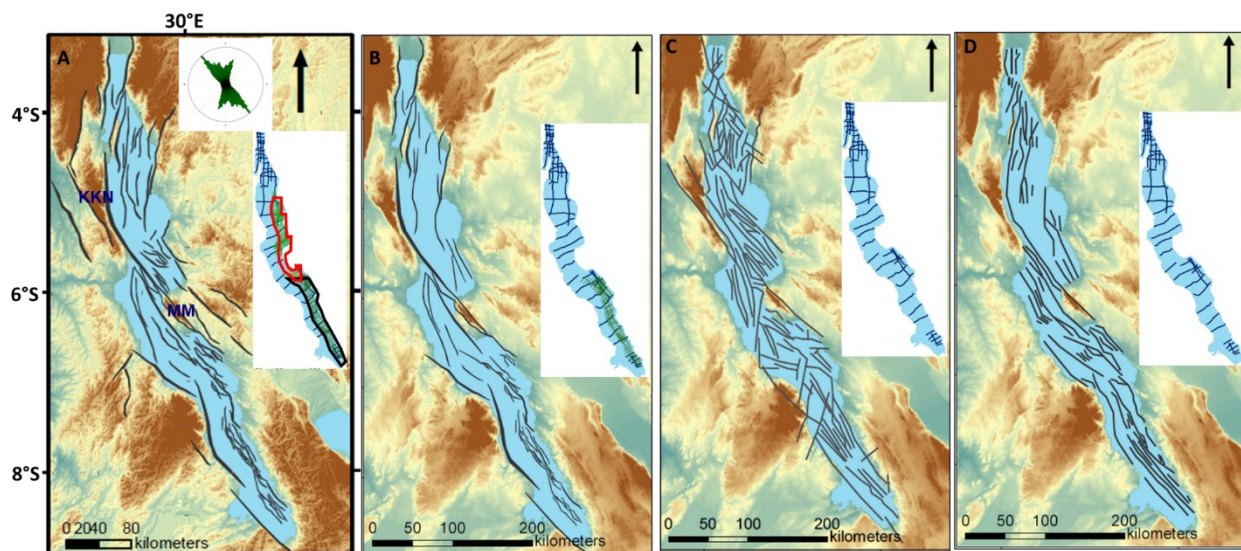


Figure 23: (A) Updated fault map of the Lake Tanganyika Rift from this study. MM and KKN represent the Mahale Mountains and Katenga - Kugulu - Ntengo lineaments respectively. The rose diagram shows the strikes of the mapped faults. Note that many faults mapped on the eastern part of the northern and central Lake Tanganyika are due to denser data coverage. (B – D) Previously published fault maps from Muirhead et al. (2019) in panel B, Rosendahl et al. (1992) in panel C, and Morley et al. (1988) in panel D. Note that our study has identified more faults within Lake Tanganyika and identified some NNE-SSW secondary fault trends in addition to the dominant NW-SE fault trend. Other structural strikes are NNW-SSE, NNE-SSW, and N-S. The inset map shows the data used during each study. The red and black polygons on panel A

inset map demarcate the areas with Air FTG data, and the lines represent various 2D seismic profiles (refer to Figure 1).

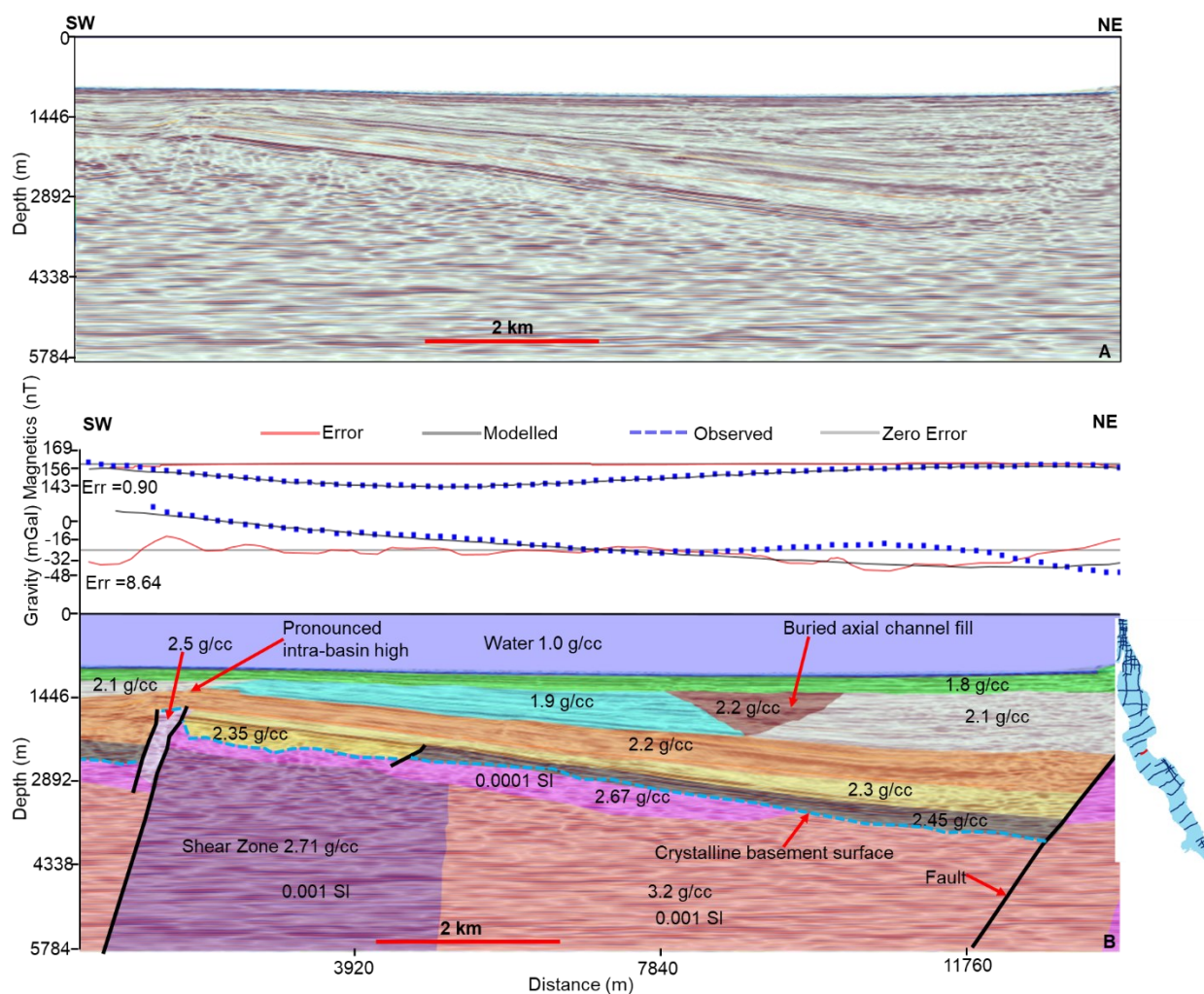


Figure 24: A) NE-SW PROBE seismic profile 218 (see red line transect in the side-inset map in B and in Figure 2) located in the Central Tanganyika Rift (Kalemie Sub-basin). B) Forward model of the Gravity (T_z) and Magnetic (RMI) along the seismic profile 218. Modelled geology: each coloured polygon represents a block of distinct density and magnetic susceptibility from its neighbouring block. Note the high density (3.2 g/cc) basement and lower-density (2.71 g/cc) intra-basement shear zone along the margins of which a large intra-basinal fault localized. In the sedimentary sections, the seismic shows a persistent intra-basin ‘high’ controlled by the footwall of the intra-basin fault. Also, the model suggests the possible presence of deep-seated high-density sedimentary rocks (2.45 g/cc), likely representing Mesozoic (Karoo) rift phase units.

Note the channel complex (2.2 g/cc) within the younger sedimentary intervals (seismic units 3-4 in Shaban et al., 2021).

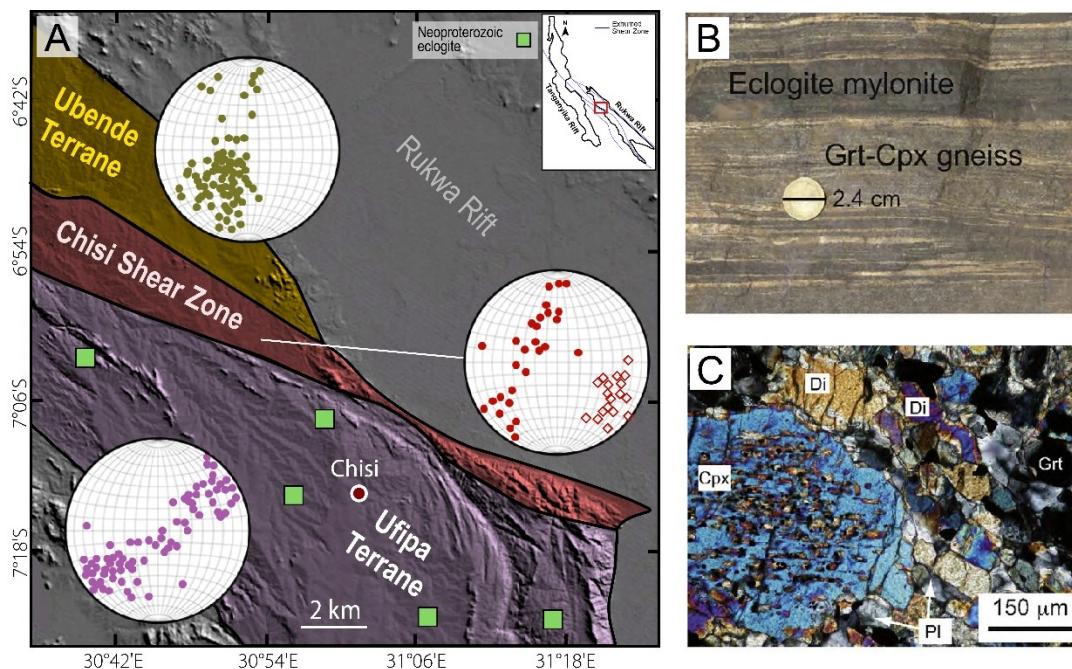


Figure 25: (A) Hillshade map of the eastern rift shoulder of the Tanganyika Rift (see location in Figures 2A-B), showing exposures of one of the exhumed NW-trending Precambrian basement shear zones in the region, the Chisi Shear Zone and its bounding basement terranes (modified after Kolawole et al., 2021b). The stereographic projections of published field measurements (circles: poles to gneiss foliation planes, diamonds: poles of mineral elongation lineation) show the dominant NW-SE trends of metamorphic fabrics within the shear zone and terranes. (B - C) Outcrop photograph and photomicrograph of eclogites in mylonitic garnet-clinopyroxene gneiss along the shear zone, indicating the presence of a suture zone along the mobile belt (source: Boniface et al., 2012). The photomicrograph shows reaction textures typical of eclogite facies metamorphism. Cpx: Clinopyroxene, Grt: Garnet, Di: Diopside, Pl: Plagioclase.

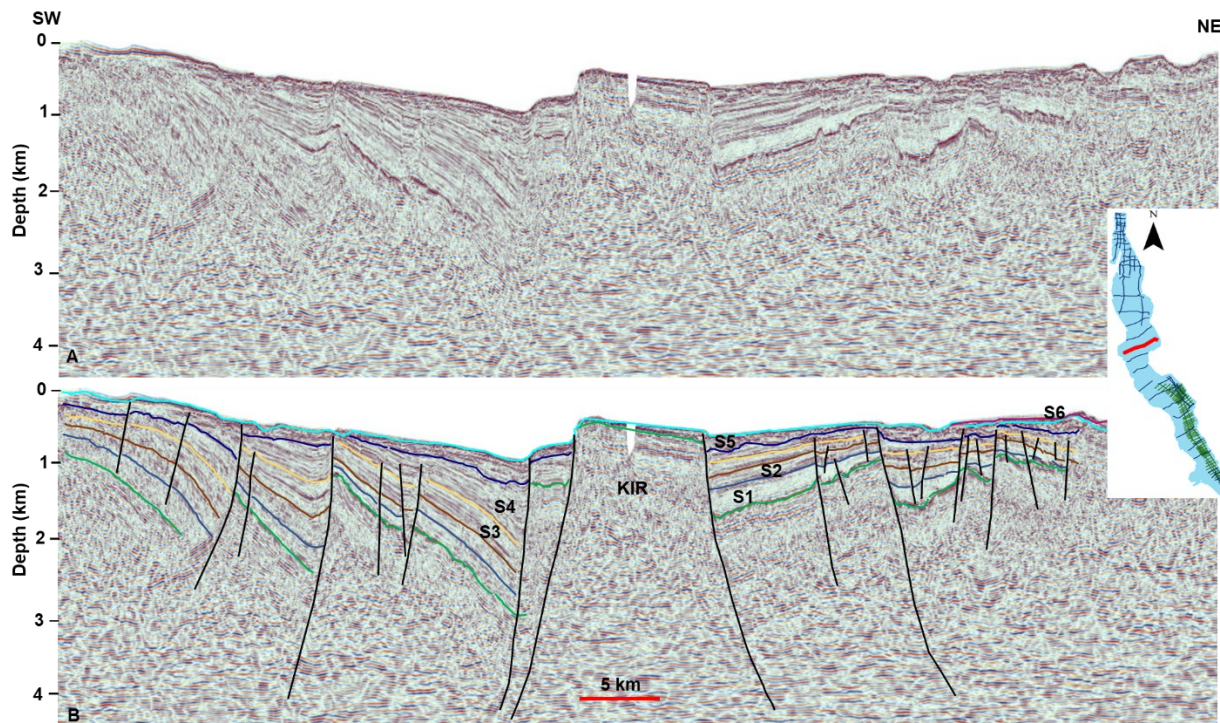


Figure 26: Seismic dip profile, SW-NE across the Kavala Island Ridge (KIR). A) Uninterpreted (top) and B) interpreted (bottom) with six identified seismic horizons, from oldest to youngest. Note that the KIR is devoid of sedimentary units except S1, implying the active nature of the ridge. The ridge is bounded by two major rift segment border faults with opposing polarities. Sedimentary packages thicken toward these faults implying syn-deposition. Note that across the profile there are two main fault trends. Contrary to seismic unit S1, seismic characteristics of S2-S6 display high amplitude and parallel to semi-parallel reflections suggesting a deeper lake environment.

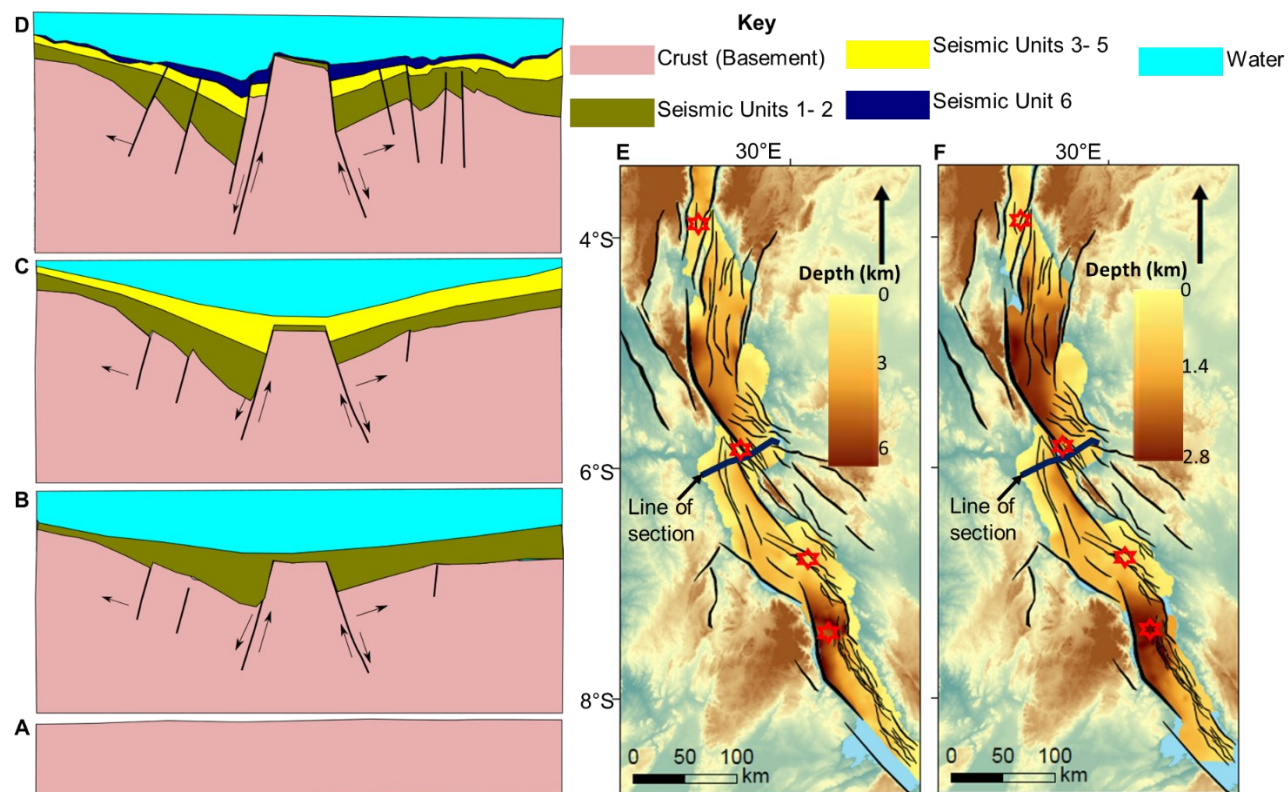


Figure 27: Summary conceptual model illustrating the evolution of the KIR. (A) Initial stage before rifting. (B) Initial rifting stage triggered by two major faults with opposing polarities. During this stage, deposition of thicker units 1-2 was contemporaneous with the ridge evolution. (C) Mid-rifting stage. Seismic units 3-5 were deposited during this period contemporaneous with the ridge evolution (D) Late stage of KIR evolution. Note that the ridge was uplifted higher, and some of the sediments were eroded from the top of the ridge. (E) Structure contour map (in depth) of the Nyanja Event horizon, the deepest, regionally mappable pre-rift surface (Rosendahl, 1987; Muirhead et al., 2019; Shaban et al., 2021). This horizon corresponds to the green reflector at the base of S1 in Figures 2C-D. (F) Structure contour map (in depth) of the horizon at top of S3 unit, a syn-rift unit at intermediate depths.

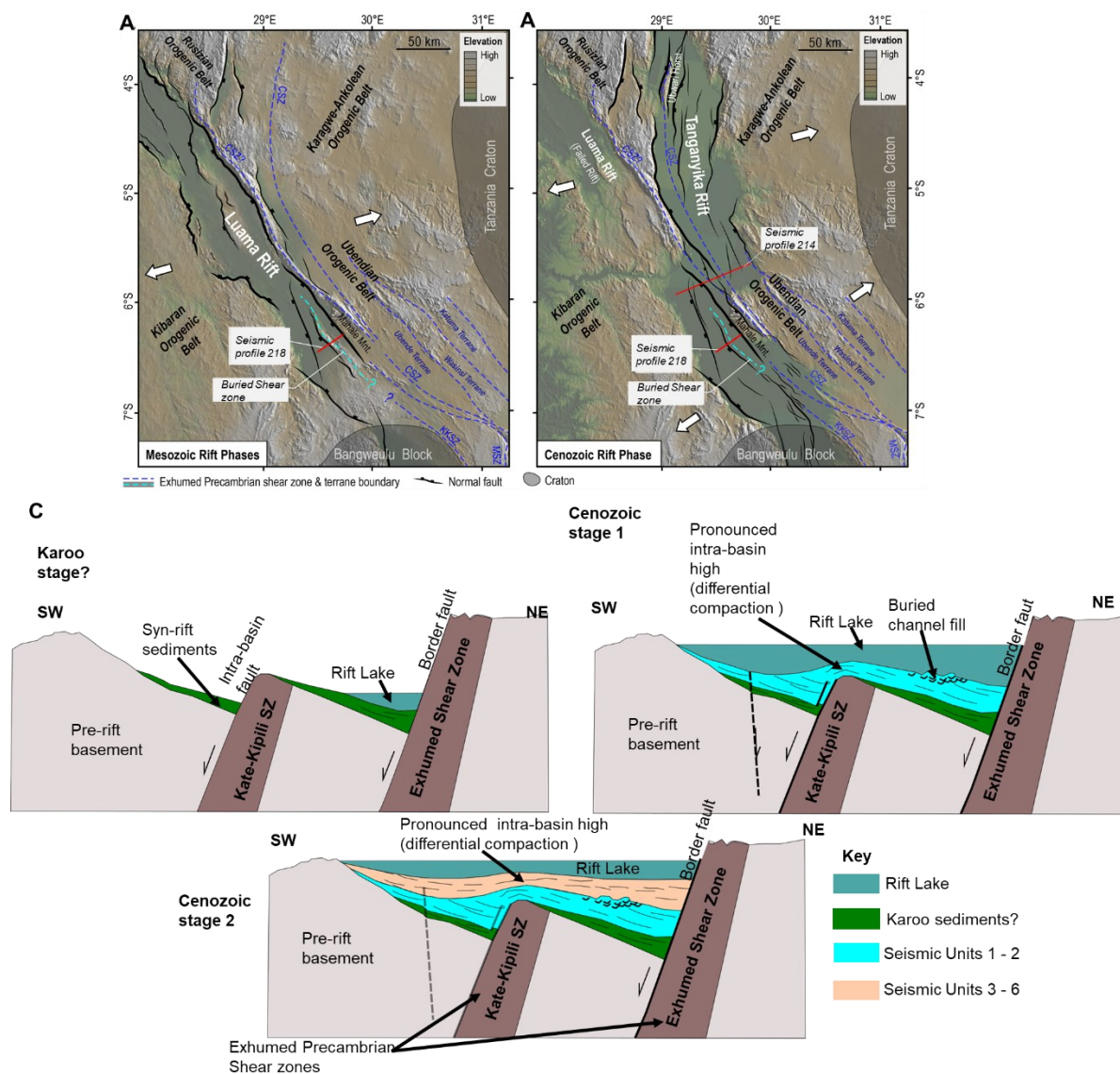


Figure 28: A) Interpretation of paleo-topography of southwest Tanzania and eastern Congo during the Pre-Cenozoic phases of tectonic extension in East Africa (i.e., Karoo and Cretaceous). The map also shows the pre-rift basement shear zones (previously published ones and those mapped in this study) and rift-related faults. Paleo-extension direction is from Delvaux et al. (2012). (b) Present-day topography of the region showing faults along the evolving Tanganyika Rift. Note that the map includes both the currently active and dormant faults along the Tanganyika Rift. We interpret that the earliest faults in the central Tanganyika Rift (Kalemie

Sub-basin) represent the south-eastern extension of the Luama Rift (see Figure 7 seismic section and forward model). Extension directions are from Delvaux (2001) and Delvaux and Barth (2010). Exhumed basement shear zones are from Daly (1988), Delvaux et al. (2012), and Kolawole et al. (2021b). CSZ: Chisi Shear Zone, KKSZ: Kate-Kipili Shear Zone, MSZ: Mtose Shear Zone. C) Cartoons illustrating the interpreted structural and landscape evolution of the Central Tanganyika Rift, highlighting the persistent influence of the incipient rift structure (Stage 1) on the subsequent rift basin architecture (Stages 2 and 3).

**CHAPTER 4: THE PALEO-HYDROLOGIC CONNECTIVITY OF RIFT LAKES
TANGANYIKA AND RUKWA, EAST AFRICA: INFLUENCE OF OROGRAPHIC
PRECIPITATION."**

This chapter has been submitted for publication in the *Global and Planetary Change*

Journal as:

Shaban, S. N., Scholz, C. A., Xue, L. The Paleo-Hydrologic Connectivity of Rift lakes
Tanganyika and Rukwa, East Africa: Influence of Orographic Precipitation., (in prep),
Journal of Global and Planetary Change.

Highlights

- Lake Tanganyika contains unusual oversized deltaic deposits whose source is evaluated.
- Numerical model demonstrates Lakes Tanganyika and Rukwa were connected over geologic time periods.
- The Karema deltaic deposits were mainly sourced from the Ifumwe catchment.
- The deltaic deposition occurred during Lake Rukwa's overflow into Lake Tanganyika.

Abstract

The evolution of continental rifts and their long-lived tectonic lakes is critical for understanding continental breakup, recovering terrestrial climate histories, revealing patterns of biological evolution, and assessing hydrocarbon resources. Recent studies suggest that Lake Rukwa, East Africa, flowed into adjacent Lake Tanganyika during its Holocene high stands. Spectacular oversized deltaic prograding clinoforms are also observed in seismic reflection profiles from the

Karema platform, which may be linked to the outflow of earlier phases of Lake Rukwa. We integrated a Landscape evolution model, FastScape, with the Linear Upslope Model for orographic precipitation, to analyze and document the topographic evolution and hydrological connectivity of the Lakes Tanganyika and Rukwa in the vicinity of the Rungwe volcano. The analysis suggests that Lake Rukwa overflowed into Lake Tanganyika causing the deposition of deltaic sediments along the Karema Platform. Ancient Lake Rukwa was apparently a much larger lake than the modern, underfilled lake. The underfilled condition of modern Lake Rukwa may be due to diminished precipitation and a regional rain shadow, produced by growth of the Rungwe volcanic edifice. The model simulates an artificial topography that reveals that a rain shadow around Lake Rukwa developed when the volcano was ~ 3500 m a.s.l., resulting in an underfilled Lake Rukwa basin. This study shows how tectonics modulates surface processes on the scale of large continental rifts, and how interactions between these two lakes produced oversized sand-prone deltas that may form potential hydrocarbon reservoirs and introduced pathways for biotic exchange and evolution.

1. Introduction

The sedimentary records of tectonic lakes provide long-term archives of continental breakup, terrestrial climate, and biological evolution, and these basins also contain important hydrocarbon resources. However, their evolution can be complex due to the interplay of controlling factors such as tectonics, climate, and local geology (Carroll and Bohacs, 1999). The spatiotemporal distribution of sedimentary facies in rift basins is a result of the interaction between basin accommodation (mostly tectonically controlled), and water plus sediment supply (mostly climate controlled) (Schumm, 1977; Surdam and Stanley, 1980; Kelts, 1988; Lambiase, 1990; Carroll and Bohacs, 1999). When two lakes are in proximity and structurally connected,

there is a possibility of ‘filling and spilling’ of the upstream lake into the downstream lake that is situated at nearly the same elevation above sea level (Hokanson et al., 2021). This condition is observed in the western branch of the East African Rift where Lake Kivu overflows into Lake Tanganyika, which has important implications for solute loading and carbonate sedimentation in the downstream lake (e.g., Felton et al. 2007). Similarly, Dagang et al. (2004) examined the evolution of an ancient lake in the southeast of the northern Tibetan Plateau, and found that the extant Nam Co, Siling Co, and Zhari Co lakes were components of a larger ancient lake system. Here, we hypothesize that this phenomenon may have developed between Lakes Tanganyika and Rukwa in the western branch of the East African Rift (Figure 1), which are structurally connected by the Chisi Suture Zone (Heilman et al., 2019, Kolawole et al., 2021) and the Karema depression.

This ‘filling and spilling’ of tectonic lakes can impact depositional environments and paleoecosystems. Upstream lakes are important factors influencing lake hydrology, solute loading, and water column characteristics of downstream lakes, as has been shown for Lake Kivu and Lake Tanganyika (Haberyan and Hecky, 1987). Consequently, different regions of downstream lakes may have different water chemistries that can lead to the opening of novel habitats and potentially diversification (Simpson, 1953; Schluter, 2000; Ricklefs, 2003; Cardillo et al., 2005). An example of faunal endemism and floral diversity influenced by adjacent basins is that of the modern hydrologically connected Malili lakes in Indonesia; outflow from the most upstream lake, Matano, influences processes in the downstream chain that terminates in Lake Towuti (Costa et al., 2015).

The Tanganyika-Rukwa connection was proposed by previous workers (Delvaux and Williamson, 2008; Cohen et al., 2013; Shaban et al., 2021). Shaban et al (2021) suggested the

possible connectivity between the two lakes in the geologic past via the Karema depression (**Figure 29**), based on the spectacular, thick, deltaic clinoform packages identified in 2-D seismic reflection data around the Karema Platform (**Figure 30**). Shaban et al. (2021) identified 7 deltaic units with a gross sediment volume of $\sim 100 \text{ km}^3$ and an average surface area of $\sim 190 \text{ km}^2$ and $\sim 650 \text{ km}^2$ in the old and young intervals, respectively. Based on standard source-to-sink relationships (Coleman & Roberts, 1989; Milliman & Syvitski, 1992), these paleo-deltas are predicted to have had drainage areas of $1.63 \times 10^3 \text{ km}^2$ and $1.77 \times 10^3 \text{ km}^2$, respectively. Shaban et al. (2021) suggested that the average thickness of these individual clinoform packages was approximately about four-times that of lowstand deltaic clinoforms observed in Lake Edward (McGlue et al., 2006), and three-times that of the Dwanga Delta (Lake Malawi) (Scholz, 1995) and a paleo-delta observed on the Malagarasi Platform, Lake Tanganyika (McGlue et al., 2006). Shaban et al. (2021) speculated that the deposition and subsequent abandonment of the oversized Karema deltas was a consequence of overflowing of Lake Rukwa, perhaps prior to the uplift of Rungwe volcanic edifice that formed a rain shadow, hence diminishing precipitation in the Rukwa catchment. The outflow of Lake Rukwa into Lake Tanganyika during its highstand has also been suggested by Delvaux and Williamson (2008) and Cohen et al. (2013); at its overflow stage, Lake Rukwa's maximum water depth was $\sim 176 \text{ m}$. Modern water depths for Lakes Tanganyika and Rukwa are $\sim 1471 \text{ m}$ (Shaban et al., 2021) and $\sim 6 \text{ m}$ (Barker and Gasse, 2003) respectively, with an surface elevation difference of 34 m . Notably, Lake Rukwa is the only large lake in the entire western branch of the East African Rift that is underfilled and hydrologically closed (**Figure 29**); combined with the observations of oversized paleo-delta deposits near Karema, and well-documented faunal exchange between Rukwa and other East African

bioprovinces (Cohen et al., 2013), there is clearly a long history of hydrological connectivity to other parts of the rift valley.

Here we hypothesize orography associated with Rungwe volcano played a role in the connection between Tanganyika-Rukwa connection, specifically inducing a rain shadow on the volcano's leeward side over the Rukwa catchment. Previous efforts suggested that the temporal and spatial distribution of precipitation can be highly influenced by orography. For example, based on the analysis of the influence of precipitation on bedrock river erosional efficiency and incision rate, Ferrier et al. (2013) emphasize the importance of including climate explicitly in landscape evolution models. Furthermore, the transport of subtropical humid air through extratropical cyclones can cause flooding, lake overfilling and landslide events (Lavers et al., 2011). The effect of above-normal atmospheric moisture levels is amplified by strong winds blowing across large orographic features (Sodemann, et al., 2009). To better understand the orography-precipitation relationship, modelling of the hydrological cycle and associated phenomena such as hydrological connectivity, sedimentation, floods, droughts, as well as climate variability, have been proposed (Daly et al., 1994; Weisse and Bois 2001; Kyriakidis et al., 2001; Drogue et al. 2002; Smith and Barstad 2004; Guan et al., 2005; Crochet et al., 2007).

The goal of this paper is to test the hypothesis of long-term hydrological connectivity between Lakes Tanganyika and Rukwa by 1) determining the provenance of the oversized Karema delta deposits, 2) determining the magnitude and duration of Rukwa overflow, and 3) assessing the drivers of the intermittent connection. We employed a landscape evolution model (Fastscape) (Braun and Willett, 2013) that utilizes a module that simulates orographic precipitation by means of a Linear Upslope Model (LM) (Smith and Barstad, 2004). Understanding orographic evolution is of paramount importance towards a better understanding

of water budgets and the hydrological connectivity of waterbodies such as Lakes Tanganyika and Rukwa. Using different tectonic scenarios in our models, we explore the lake footprints and changing paleo-lake conditions, landscape evolution, and sediment remobilization in Lakes Tanganyika and Rukwa.

1.1. The study area

Our study focuses on the southwestern part of the East African Rift System (EARS), the area on the southeastern part of the Lake Tanganyika Rift, the northern part of Lake Malawi (Nyasa), as well as the Lake Rukwa Rift (**Figure 29**). The elevated region in our study site includes the rift shoulders and the Rungwe volcano, where the modern precipitation patterns indicate heavy annual precipitation on its southern windward side relative to the leeward northern slopes (**Figure 30**).

The EARS, more than 3000 km-long, is an ideal site to investigate lacustrine basin evolution in an extensional setting. The EARS initiated in the Oligocene in parallel with the opening of the Red Sea and Gulf of Aden (Wolfenden et al., 2005). Extension produced a series of rift segments, predominantly asymmetric half-graben basins (Rosendahl, 1987; Morley, 1989) of 100-150 km length. South to the Main Ethiopian Rift (**Figure 29**), the EARS splits into the Eastern and Western Branches, separated by the Archean Tanzania Craton (Rosendahl, 1987; Ebinger, 1989). The Western Branch of the EARS is characterized as magma-poor, with only a few volcanic centers such as the Virunga Volcanic Province positioned to the north of Lake Tanganyika, and the Rungwe Volcanic Province located southeast of the Lake Tanganyika Rift (Baker, 1971; Mohr and Wood, 1976; George et al., 1998; Furman, 2007; Biggs et al., 2009; O'Donnell et al., 2013).

1.1.1 The Tanganyika Rift

The Tanganyika Rift (**Figure 30A**), ~645 km long with a maximum water depth of 1470 m, is one of the world's largest and deepest active rift-lake systems (Rosendahl, 1987; Burgess et al., 1988; Shaban et al., 20021). Lake Tanganyika contains one of the oldest and most continuous records of tropical climate on the continents (Russell et al., 2020), and due to its rich endemic faunas is an important study area for evolutionary biology (Meyer, 1993; Salzburger et al., 2002).

Lake Tanganyika rifting initiated at approximately 9-12 Ma (Cohen et al., 1993), or 7.8 - 5 Ma (Pasteels et al., 1989), however considerable uncertainty surrounds these estimates (Shaban et al., 2021). Roberts et al. (2012) proposed older ages (i.e., 26-25 Ma) for the initiation of the Western Branch of the EARS (East African Rift System), coincident with the uplift of the Rwenzori Mountain (Jess et al., 2020).

The Lake Tanganyika Rift is composed of five half graben basins, each ~80-140 km long by 50-70 km wide (Rosendahl et al., 1986; Rosendahl, 1987; Muirhead et al., 2019; Wright et al., 2020; Shaban et al., 2021), three main bathymetric basins (Ruzizi, Kigoma and Marungu-Mpulungu basins), and several sub-basins from north to south. In the Western Branch, depending on the rifted terrane-type (e.g., Archean versus Proterozoic lithosphere), border faults accommodate ~ 90% of the extensional strain (Muirhead et al., 2019; Wright et al., 2020). In the Lake Tanganyika Rift, the rates of normal border fault slip increased with the rift evolution (Muirhead et al., 2019; Wright et al., 2020), and intra-rift normal fault systems influence sediment pathways into the basin (Rosendahl, 1987; Burgess et al., 1989; Shaban et al., 2021).

The Lake Tanganyika Rift exhibits two main extension directions, E-W in the north and NE-SW in the south (Delvaux and Barth, 2010), with variable total extension (e.g., ~3.75 km in

the north, 7.07 -7.15 km in the central region, and 2.75 km in the southern section) (Wright et al., 2020). The Lake Tanganyika Rift exhibits high topographic relief, >700 m above modern lake level in several localities, including rift shoulder border faults (Rosendahl, 1987; Wright et al., 2020) (e.g., Burton's Bay Ridge, Mahale Mountains) (**Figure 31**).

1.1.2 The Rukwa Rift

The Rukwa Rift is a northwest-trending half-graben basin (~350 km by ~50 km) located in the southwestern part of the EARS along the Paleoproterozoic Ubendian belt, east of the Lake Tanganyika Rift (**Figure 29**). It contains approximately 8-11 km of syn-rift basin fill, thickening towards the north-east border fault (Lupa Fault), and is one of the thickest continental sedimentary sequences in Africa (Kilembe and Rosendahl, 1992). The Rukwa Rift initiation is controversial, with some researchers postulating a start in the Mesozoic (Morley et al., 1991) whereas others argue for Cenozoic rifting (Wescott et al., 1991). However, it is suggested that the Rukwa Rift Basin (RRB) contains Permo-Triassic Karoo sediments underlying the Cenozoic Lake beds (Wescott et al., 1991; Theunissen et al., 1996; Delvaux, 2001; Mtelela, 2018). Various lines of evidence support a pre-Neogene initiation. For instance, the analysis of kimberlites, which are important archives of crustal thermal perturbations associated with uplift or rift initiation, suggested a Late Paleogene origin (Batumike et al., 2008). Also, the low temperature thermochronology analysis of the Rukwa and Malawi rifts (Van der Beek et al., 1998), carried out for estimating the timing of uplift, erosion and associated rifting events, support a pre-Neogene initiation. Results from this analysis suggested that the Malawi and Rukwa rifts were subjected to regional cooling and denudation around ~40-50 Ma, much older than the Neogene rifting (Van der Beek et al., 1998). O'Connor et al. (2010), Roberts et al. (2010), and Stevens et

al. (2008) unequivocally suggested the presence of Cretaceous sediments confirming these thermal histories.

The Rukwa Rift opened sub-orthogonal to the regional NW-SE rift trend, with an E-W orientation similar to southern parts of the Lake Tanganyika rift (Ebinger 1989; Morley et al. 1990; Delvaux et al. 2012). Three major tectonic rifting episodes have been suggested for the Rukwa Rift: (1) a Permo-Triassic event that deposited Karoo Supergroup (Kilembe and Rosendahl 1992; Morley et al. 1999); (2) a Cretaceous rifting episode; and (3) late Oligocene rifting documented by the Red Sandstone Group deposits, which include the Galula and Nsungwe Formations, (Roberts et al., 2004, 2010, 2012). Modern Lake Rukwa, approximately 165-km-long, is located at the center of the basin (Kjennerud et al., 2001) (**Figure 29**).

1.1.3 Hydroclimate

Lake Tanganyika is a tropical and meromictic lake whereby below 100–200 m water depth the lake water is permanently anoxic and relatively rich in nutrients (Hecky et al. 1981; Edmond et al. 1993). In this lake, vertical mixing and southeasterly winds are primary sources of nutrients supplied through upwelling (Coulter, 1991), the process by which deep, anoxic waters rise and mineralize surface waters, accelerating phytoplankton biomass generation through photosynthesis (McGlue et al., 2020). The southeasterly winds push surface waters northward along the lake's axis and set up a deep current returning to the southern part of the lake, causing upwelling in the lake's southern sub-basins (Plisnier et al., 1999; McGlue et al., 2020). Along its axis, the lake has variable climatic conditions. For instance, in the northern part, Lake Tanganyika has a moist tropical climate with approximately 1200 mm precipitation annually (Talling, 1991), with rainy seasons occurring between October and April (Stager et al., 2009). The southern part has cool and dry seasons due to the strong trade winds from the southeast,

especially in May – September. During this time the tropical rain belt migrates to the northern hemisphere and Lake Tanganyika's local climate is predominantly controlled by the Indian Ocean monsoon (Plisnier et al., 1999; McGlue et al., 2020). During periods of weak monsoon winds, low-speed winds fail to cause strong seiches, and rainfall in the region is reduced (McGlue et al., 2020). During the rainy season the lake undergoes similar stratification along its axis, and the rates of vertical mixing are significantly reduced (Coulter, 1991).

The Lake Tanganyika catchment covers ~238,700 km² (Gillman, 1993). It receives water mainly through precipitation and inflow drainages including the Ruzizi River, the Malagarasi River, the Lugufu River, and the Ifumwe River (**Figure 29**). Talling (1991) suggests that the Malagarasi River was the only major pre-rift inflow river based upon biogeography of local fish fauna. The Ruzizi River is the outlet of Lake Kivu and drains into Lake Tanganyika axially at its northern tip (**Figure 29**) (Haberyan and Hecky, 1987). It is reportedly far younger than other river drainages in the system (Brooks, 1950; Degens et al., 1973; Shaban et al., 2021).

Evaporation and the Lukuga River discharge (**Figure 29**) explain the net water loss of modern Lake Tanganyika (Craig et al., 1974; Cohen et al., 2005; Dettman et al., 2005). Evaporation accounts for 1530 – 2418 mm of lake water loss annually, which occurs mainly during the windy dry seasons (~250 mm/month, Savijärvi and Jarvenoja, 2000). The Lukuga River discharge accounts for a water loss equal to 83 mm annually (Cohen et al., 1997a).

The Lake Tanganyika Rift has a dynamic climate history. During the late Holocene (Alin and Cohen, 2003) and the Last Glacial Maxima (LGM) from 34 ka to 14 ka (Felton et al., 2007) the lake was affected by arid conditions. About 60 ka the rift experienced warm climate attributable to the Northern Hemisphere insolation (Tierney et al., 2008). At several times in the Late Pleistocene, lake water levels were reduced by hundreds of meters, most likely attributable

to climatic processes (Scholz and Rosendahl, 1988; Cohen et al., 1997a; Scholz et al., 2007; McGlue et al., 2008). These large and rapid lake water volume variations commonly influence the deposition and distribution of sedimentary facies (Rosendahl and Livingstone, 1983; Scholz et al., 1990; Shaban et al., 2021) and the paleogeography of the rift valley (Shaban et al., 2021).

2. Data and methods

2.1 Data

This study used a 30 m resolution Digital Elevation Model (DEM) (NASA SRTM, 2013) for topographic analysis of knickpoints and landscape evolution model initial topography (**Figure 30**).

2.2 Methods

We used the integration of the FastScape algorithm (Braun and Willett, 2013) and the Linear Upslope Model for orographic rainfall (LM) (Smith and Barstad, 2004) to analyze and document the topographic evolution in response to orographic precipitation and hydrological connectivity of Lakes Tanganyika and Rukwa in the vicinity of the Rungwe volcanic field. The topographic analysis and FastScape model setup are in sections 2.2.1 and 2.2.2, respectively. The LM is briefly explained below in section 2.2.3, and for detailed methodology the reader is referred to Smith and Barstad (2004), Smith et al. (2005), Smith (2006), and Barstad and Smith (2005).

2.2.1 Topographic analysis of the Karema depression erosion

To test whether the Karema deltaic sediments were derived either from the Karema catchment via the modern Ifumwe River by normal processes or from overflow of Lake Rukwa, we estimate the total erosion of the Karema depression. We extracted the geophysical relief (e.g.,

Small and Anderson, 1998) to estimate the paleotopography of the Karema catchment. To generate the geophysical relief of the Ifumwe catchment, we capped its modern topography at 1200 m based on the general elevation of summits throughout the catchment. This was done to determine the possible maximum erosion that could have occurred within the catchment. We calculated erosion height as a difference in elevation between the paleosurface capped at 1200 m and the modern Ifumwe catchment topography. We estimated the volume of the eroded sediments by integrating the area under the curve (AUC) from the graph of erosion versus area. Furthermore, we used the Topographic Analysis Kit (TAK) for TopoToolbox (MATLAB) tools (Forte and Whipple, 2019) to analyse channel profile of the modern Ifumwe tributaries draining the Karema depression to gauge whether the channel incision was tectonically- or lithologically-driven (see Supplemental Material).

2.2.2 Landscape evolution model (FastScape)

We integrated the FastScape algorithm (Braun and Willett, 2013) and LM to predict landscape evolution following a set of tectonic and climatic forcings. FastScape solves the stream power law (Eq. 1 and Eq. 2) to parameterize bedrock incision by rivers in mountainous terrains:

$$\frac{\partial h}{\partial t} = U - KA^m S^n + \frac{G}{A} \int_A \left(U - \frac{\partial h}{\partial t} \right) dA \text{ for } h > \text{lake level} \quad (1)$$

$$\frac{\partial h}{\partial t} = Km \nabla^2 h + Qs \text{ for } h < \text{lake level} \quad (2)$$

where h is topographic height (elevation of the channel), t is time, U is uplift rate relative to a fixed or known base level (Whipple and Tucker, 1999), A is drainage area, K is erodibility coefficient, Km is the marine diffusion coefficient, G is deposition coefficient, S is channel slope in the direction of water flow, Qs is the sediment flux from continental domain to the lake, and m and n are empirical exponential constants. The values m and n are poorly constrained due to the

high variabilities and uncertainties associated with geomorphology, lithology, and climate (Snyder et al., 2003; Sklar and Dietrich, 2006; Lamb et al., 2015). In our models, we assumed the values of $K = 8.0 \times 10^{-6} \text{ m}^1 \text{ yr}^{-1}$, $m = 0.5$, and $n = 1$. Croissant and Braun (2014) proposed the values of $0 < m < 2$ and $0 < n < 4$. According to Eq.1, the landscapes will reach a steady state at $\frac{\partial h}{\partial t} = 0$. **Table S1** contains the parameters used for model setup in this study.

2.2.3 The linear model (LM) for orographic precipitation

The distribution of precipitation due to orography can be estimated using two methods: (1) the interpolation of rain gauge station data or (3) the upslope method (Smith and Barstad, 2004). The rain gauge data interpolation method involves calculations from sometimes sparse station data using inverse distance weighting or spline fitting (Daly et al, 1994; Hutchinson, 1998), whereas the upslope method uses the terrain slope and wind speed to estimate the condensation rate above the terrain (Collier 1975; Rhea 1977; Smith, 1979; Neiman et al., 2002). However, except for the few models such as quasi-analytical models (Hobbs et al., 1973; Bader and Roach, 1977; Alpert and Shafir 1989; Sinclair, 1994; Smith, 2003) and the modified Linear Upslope Model (LM) by Smith and Barstad (2004), neither model includes the influence of horizontal scale. Most models with the exception of LM assume that only upslope terrains control precipitation, thus with instantaneous fallout, the flat and leeward sides remain dry. This assumption ignores the evaporation of cloud water and hydrometeors due to descending air, and hence overestimates the precipitation (Smith and Barstad, 2004). The LM addresses the above-mentioned limitations by allowing delays and downstream advection, and by including condensed water conversion, airflow dynamics, advection and fallout, and downslope evaporation. The LM model seems to produce reliable estimates and complements rain gauge station data in data-sparse locations (Smith and Barstad, 2005; Barstad et al., 2007; Crochet et

al., 2007; Caroletti and Barstad, 2010). Also, the LM works better in the warm-rain systems without a need for including ice and snow components (Barstad et al., 2007).

The LM uses a simple set of equations that links condensed water advection, fallout, mean wind speed and precipitation. The backbone of this model is the consideration of a distributed source of condensed water $S(x, y)$ arising from forced ascent, and allowing delays and downstream advection (**Figure S8**). The source is the sum of the background rate of cloud water generation and local variations generated by orography-forced uplift. The two steady-state advection equations are described by equations (3) and (4):

$$U \cdot \nabla q_c = S(x, y) - \frac{\bar{q}_c(x, y)}{\tau_c} \quad (3)$$

$$U \cdot \nabla q_r = \frac{\bar{q}_c(x, y)}{\tau_c} - \frac{\bar{q}_r(x, y)}{\tau_f} \quad (4)$$

where \mathbf{U} = regionally averaged horizontal wind speed with eastward and northward components U and V ; τ_c = conversion time of cloud to hydrometeors, τ_f = hydrometeors fallout time; (x, y) = Cartesian coordinates; and $q_c(x, y)$ and $q_r(x, y)$ are vertically integrated cloud water and hydrometeor density respectively.

From equation (3), the source term $S(x, y)$ can be rewritten in the simple upslope model as:

$$S(x, y) = S_\infty + C_w U \cdot \nabla h(x, y) \quad (5)$$

where C_w = is an uplift sensitivity factor depending on surface humidity and lapse rate, S_∞ is the background non-orographic large-scale vertically integrated condensation rate, and $h(x, y)$ is the terrain. The equations (3) - (5), when the background non-orographic large-scale vertically integrated condensation rate and the conversion time are both zero, suggest the existence of cloud water over high terrain, but no precipitation. Another consideration is when

$S_\infty = 0$ and fallout time = infinity, indicating that the precipitation will form but will be stored in the air parcel until the hydrometeor evaporates.

By considering the source as vertically integrated condensation arising from forced ascent, the source term in equation (5) can be expressed as:

$$S(x, y) = \frac{C_w}{H_w} \int_0^\infty w(x, y, z) e^{-z/H_w} dz \quad (6)$$

Equation (5) assumes the air to be saturated with vapor such that $C_w =$ is an uplift sensitivity factor depending on surface humidity and lapse rate (equation (7)) and, H_w is the thickness of the ambient moist layer (equation (8)), and $w(x, y, z) =$ terrain-forced vertical air velocity. From equation (6), it is shown that the source declines with increasing thickness of the ambient moist layer.

$$C_w = \rho_{v0} \Gamma / \gamma \quad (7)$$

$$H_w = \frac{-R_v T^2}{L \gamma} \quad (8)$$

where ρ_{v0} = surface water vapor density, Γ = average moist-adiabatic lapse rate, and γ = environmental lapse rate, T = surface temperature, L = latent heat of vaporization, and R_v = gas constant for vapor. The terrain-forced vertical velocity at ground level, (i.e., $z = 0$) is a function of terrain slope and the horizontal wind:

$$w(x, y, 0) = U \cdot \nabla h(x, y) \quad (9)$$

Thus, from equation (5), in the absence of terrain $h(x, y)$, the uniform source creates constant values of cloud water column density, hydrometeor column density, and precipitation. Also, by considering equations (6) – (8), it is shown that notwithstanding the orography, the source term is controlled by wind speed, temperature, and moist stability. To gauge the

variations of vertical velocity with altitude, linear mountain-wave theory is used. The advantage of this theory is its ability to capture the 3D airflow pattern over complex terrains. For instance, the mountain width controls the wind speed and precipitation distribution indirectly by affecting the transient time (Crochet et al., 2007). Thus, narrow ridges have longer transient time than wide ridges, consequently, favour precipitation on the leeward side. Also, linear mountain-wave theory captures important features of the airflow such as an inverse relationship of vertical velocity and altitude (Crochet et al., 2007). As the vertical velocity dies with altitude, it forces the reduction of condensation, lateral airflow around topographic features, and the formation of gravity waves.

The general solution for orographic precipitation is obtained by Fourier transformation of equations (3) to (6) as in equation (10):

$$\hat{P}(k, l) = \frac{\hat{S}(k, l)}{(1+i\sigma\tau_c)(1+i\sigma\tau_f)} \quad (10)$$

where $\hat{S}(k, l)$ = Fourier transform of the source term ($S(x, y)$); k and l = horizontal components of the wavenumber, $i = -1$; and σ = intrinsic frequency given by $Uk + Vl$.

By rearranging equation (9), the source term $S(x, y)$ may be given as:

$$\hat{S}(k, l) = \frac{C_w i \sigma \hat{h}(k, l)}{(1 - imH_w)} \quad (11)$$

where $\hat{h}(k, l)$ = Fourier transform of the terrain, the denominator = airflow dynamics, and m = vertical wavenumber describing the depth and upwind tilt of the forced air ascent; it is governed by:

$$m = \left[\left(\frac{N_m^2 - \sigma^2}{\sigma^2} \right) (k^2 + l^2) \right]^{1/2} \quad (12)$$

where N_m = moist Brunt–Väisälä frequency. From equation (12), with weak stratification ($N_m^2 \ll \sigma^2$), the airflow becomes irrotational.

The combination of airflow dynamics, advection and time delays, thus combining equations (10) and (11), yields a single equation representing the LM:

$$\hat{P}(k, l) = \frac{C_w i \sigma \hat{h}(k, l)}{(1 - imH_w)(1 + i\sigma\tau_c)(1 + i\sigma\tau_f)} \quad (13)$$

From equation (11), we see that spatiotemporal variability of precipitation depends on orographic features, airflow dynamics (the first term in the denominator), surface temperature, advection (the second term in the denominator), cloud delay times (the third term in the denominator), wind, stability, and moist layer thickness. Thus, the negative sign in the dynamics factor shifts the precipitation upstream whereas the positive signs in the cloud-delay factors shifts the precipitation downstream.

To compute the total precipitation in the space domain, Crochet et al. (2007) suggested an inverse fast Fourier transform of equation (12) and adding the background or non-orographic precipitation (P_∞):

$$P(x, y) = \max\left[\iint \hat{P}(k, l) e^{i(kx+ly)} dkdl + P_\infty, 0\right] \quad (14)$$

2.2.4 Model setups

To test the orographic precipitation and formation of Karema depression, we setup three numerical cases incases in landscape evolution model as follows:

Model 1 setup (model with natural topography)

The overall modeling processes are illustrated in **Figure 31**. The Model 1 setup included the following characteristics: the modern DEM of the study area obtained from SRTM 30 m as

an initial topography of the area, the uplift rate was set based on elevation, and the uplift field of rift fault footwall uplift, hanging wall subsidence, and volcano uplift is shown in **Figure S9**. The DEM was smoothed to a factor of 10, causing the final resolution to be ~300 m. General model parameters were: wind direction = 120° (south-east), drainage area exponent = 0.5, slope exponent = 1, bedrock channel incision coefficient = 1E-3, soil (sediment) channel incision coefficient = 1E-5, detached bedrock transport or deposition coefficient = 2, soil (sediment) transport or deposition coefficient = 2, and soil and bedrock diffusion coefficients = 1. Then, three scenarios were simulated to for sensitivity analysis; scenario 1 employed the rain-base of 1.5 m/y and the wind speed of 5 m/s, scenario 2 employed the rain-base of 1.5 m/y and the wind speed of 10 m/s, and scenario 3 employed the rain-base of 1.5 m/y and the wind speed of 15 m/s. All scenario runs lasted 5 Myr at a time step of 10 kyr. Modelled outputs include topography, precipitation distribution, sediment thickness, lake depth, and drainages.

Models 2 and 3 setups (model with flat surface)

In models 2 and 3, we assumed a flat surface as the initial topography, however, the uplift rate was assigned based on regional geomorphic features and rift development (i.e., from high to low uplift rate, the preference was: the Rungwe volcanic field, rift shoulder and background), and the lakes were assigned the same subsidence rate (**Figure S9**). Pseudo-lakes simulating lakes Tanganyika, Rukwa and Nyasa were assumed to have different initial morphometry, and variable surface-water and groundwater interactions. Model 3 did not include the Rungwe volcano during the simulations. Like Model 1, all scenarios run for models 2 and 3 had a runtime of 5 Ma, and model outputs include topography, precipitation distribution, sediment thickness, lake depth, and drainages.

For sensitivity analysis, we simulated three scenarios for Model 2 by varying the volcano uplift rate, wind speed and cloud delay times (i.e., conversion and fallout times).

3.Results

3.1. Karema depression erosion

The analysis of the Karema erosion reveals a maximum erosion of ~390 m (**Figure 32**). From this analysis the total maximum possible volume of eroded sediments from the catchment is ~271.1 km³. This volume is comparable to 150 km³ of the Karema deltaic deposit estimated from the seismic analysis (Shaban et al., 2021).

3.2. Precipitation distribution

In Model 1, all three scenarios predict the orographic precipitation distribution due to the Rungwe Volcano, with higher precipitation centered in the southeastern part of the study area. Scenario 1 of Model 1 (i.e., with rain-base of 1.5 m/y and wind speed of 5 m/s) predicts high precipitation in the south and southeast of Lakes Tanganyika and Rukwa, and a rain shadow north and north-west of the Rungwe Volcano (**Figure 33B**). The only difference among the Model 1 scenarios is the increase in precipitation rate as the rain base and wind speed increases (Figure S3). Similarly, models 2 and 3 predict high precipitation rate in the south and southeast parts of the pseudo-lakes Tanganyika and Rukwa due to the wind from the southeast, whereas the maximum precipitation rate in Model 2 is higher than in Model 3 (**Figure 34**). However, in general Model 3 predicts higher precipitation rates which are almost evenly distributed, whereas in Model 2, the highest precipitation rate is localized around the volcano. Model 2 predicts the largest rain shadow northwest of the volcano across pseudo-Lake Rukwa. All models 1, 2, and 3

exhibit NW-SE and NE-SW trends as the primary and secondary precipitation distribution patterns due to the NW-trend of the rift basin and wind direction.

The effect of wind speed on precipitation distribution is demonstrated by scenarios 2 and 3 of models 1 and 2 (**Figure S11**). In general increase of wind speed would slightly increase the magnitude of rainfall on the windward side of the volcano/mountains. For instance, when the wind speed is increased from 5 m/s to 10 m/s, the maximum precipitation predicted by Model 1 increases from 1.49 m/yr to 1.497 m/yr with a change of 0.007 m/yr. Similarly, in Model 2, when the wind speed is increased from 5 m/s to 10 m/s, and 5 m/s to 15 m/s the maximum precipitation increases from 4.75 to 5.4 m/yr and 5.4 m/yr. respectively (**Figure S11**).

3.4. Landscape evolution and hydro-connectivity

The models reveal an important role of volcano development on the evolution of the landforms. For instance, in Model 1, the overall drainage incision increases as rain base and wind speed increases (**Figure 35**). All scenarios of Model 1 predict Lakes Tanganyika and Rukwa connectivity via the northwestern part of Lake Rukwa to the northeastern part of the Karema Platform. Models 2 and 3 predict the rapid growth of orography in the south and northeast of Lake Tanganyika (**Figure 36**). Both models 2 and 3 predict a connection between pseudo-lakes Tanganyika and Rukwa via the northwestern part of pseudo-Lake Rukwa. Model 2 predicts higher elevation than Model 3 and predicts steeper eastern border faults for both lakes compared to Model 3's predictions. Further, Model 2 predicts deformation in the southeastern corner of pseudo-Lake Tanganyika where it connects with pseudo-Lake Rukwa.

The effect of wind speed on landscape evolution is demonstrated in scenarios 1, 2, and 3 of Model 2. For instance, when the wind speed is increased from 5 m/s to 10 m/s, the elevation of the topography decreases by almost half as evidenced by elevation decrease along the footwall

part of the western border fault of the pseudo-Lake Tanganyika and the rift shoulder between the pseudo-lakes. Conversely, as the wind speed increases, the overall elevation is shown to increase and the deformation in the southeastern corner of pseudo-Lake Tanganyika where the two pseudo-lakes connect, smooths out (**Figure S12**).

3.5. Lake depth evolution

Model 1 predicts deeper lake depths in Lake Rukwa than in Lake Tanganyika. The predicted lake depths in Lake Tanganyika range between 50 – 150 m, whereas in Lake Rukwa the depths is >400 m. Because the basement subsidence rate is the same for pseudo-lakes, the difference in projected lake depth is due to the sediment deposited in the rift lakes. These results contrast with the modern bathymetries whereby modern Lake Tanganyika is much deeper than Lake Rukwa. There is no notable difference observed in lake depths from the predictions of all scenarios of Model 1 (**Figure 36 and Figure S13**). Model 3 predicts deeper lakes than Model 2, and its predictions mimic the modern bathymetries, whereby it predicts pseudo-Lake Tanganyika deeper than pseudo-Lake Rukwa (**Figure 36**).

3.6. Sensitivity analysis

Based on limited access and the lack of rain gauge stations in the study area, we could not calibrate the model with observed precipitation data. Consequently, we modeled several scenarios including varying the initial topography and varying key model parameters including rainfall to test the robustness of the modeled results. The sensitivity analysis covers parameters of erodibility coefficient, incision coefficients, volcano uplift rate, wind speed, rain-base, and conversion and fallout time. The sensitivity analysis (see also Supplemental Information) shows that erodibility coefficient, wind speed, conversion times and volcano uplift rate control the orographic precipitation and landscape evolution (**Figures S10, S11, S12, S13, and S14**).

4. Discussion

4.1. Karema depression erosion and incision analysis

The erosion analysis on the Karema depression suggests that overflow from a draining Lake Rukwa may have caused downstream erosion, producing additional sediment that formed the Karema deltaic deposits. This is supported by several lines of evidence. This includes the increase in steepness index of the Ifumwe River tributaries towards the trunk channel that suggests that the Ifumwe channel was extraordinarily widened by the overflow; the absence of evidence for erosion caused by local uplift from the knickpoint analysis (see Supplemental Material); and several tributaries joining the northern branch almost at a right angle suggest that the Ifumwe channel was widened by the overflow and later narrowed because of Lake Rukwa water level fall (**Figure S15**). However, other localized variations in channel gradients, for example along the midpoint of the southern main branch that transects within the NNW-SSE-striking Ubendian belt composed of gneisses, granites, and mica schists (Choubert et al., 1968), can be attributed to lithologic contacts between more and less competent rock masses (Walsh et al. 2012). Also, knickpoints may have been destroyed because of increasing channel depth, velocity, and bottom shear stress towards the knickpoint lip (Gardner, 1983). Steeper channels at junctions as exhibited by increasing K_{sn} of tributaries at junctions (**Figure S15**) could indicate incision to catch up with an incising north branch of the Ifumwe River during Lake Rukwa overflow stages.

The analysis of the Karema geophysical relief predicts the possible maximum erosion. As described in section 3.2, the estimated maximum possible volume eroded of $\sim 271.1 \text{ km}^3$ is of the

same order of magnitude as the estimated total volume of Karema deltaic sediments of ~ 100 km³, estimated from multi-channel 2-D seismic reflection data (Shaban et al., 2021). Assuming a decompaction factor of 1.5, the total volume of the Karema deltaic deposits approximates ~ 150 km³. This could explain that the Karema deltaic sediments were mainly sourced from Karema erosion with possible additional material from Lake Rukwa. Shaban et al. (2021) identified two intervals of deltaic deposits implying that the overflow of Lake Rukwa persisted for geologically significant periods, possibly lasting hundreds of thousands of years.

4.2. Precipitation distribution and Rungwe Volcanic edifice

Knowing the distribution of precipitation is fundamental for estimating river discharge that controls sediment transport and erosion of bedrock (Anderson and Anderson, 2010). In our models, we assume that paleorainfall is also controlled by a combination of trade winds and orography (e.g., section 2.2.3). Our modelling reveals that the pattern of precipitation is stronger at locations with major changes in the topographic slope (**Figures 33, 34 and 35**). For instance, all models with an uplifted volcano predict strong precipitation at the contact of the volcano and the Rukwa Rift and at high topographies south and northeast of Lake Tanganyika. The precipitation-slope relationship illuminates our understanding of how topography evolves under spatially variable precipitation, and how climate feedbacks influence continental evolution (Ferrier et al., 2013). The overall expansion of drainage networks with increasing rain base and wind speed in Model 1 sensitivity analysis suggests that as wind speed and precipitation increase, incision increases substantially. This is consistent with sensitivity analyses for Model 1 and Mode 2. Models 1 and 2 scenarios demonstrate that when wind speed increases the precipitation increases (**Figure S11**). This implies that as wind speed increases more moisture is brought in, generating large air mass saturation, hence more precipitation. However, for high

precipitation to occur, wind speed must not exceed the degree of air mass saturation, otherwise it will inhibit the growth of larger size droplets.

The local precipitation is modified and amplified by the presence of orography (Shestakova and Toropov, 2021). This effect is visible in the models, for instance, under models 1, 2, and 3, the precipitation magnitude across the study area is higher than the model with the volcano. However, because the precipitation decreases with increasing distance from the moisture source, the precipitation decrease becomes faster on the leeward side of the volcano, and even more when the volcano uplift rate is increased. This implies that at the volcano interface, the orographic precipitation consumes a significant amount of incoming moisture, causing higher precipitation on the windward side than the leeward side (Hergarten and Robl, 2021). This effect causes a rain shadow to develop on the northwestern parts of the volcano in all models, particularly, around Lake Rukwa. For instance, Model 2 predicts larger precipitation rate variability than Model 3 (**Figure 34**), and we attribute this to the orographic effect as explained above. Model 2 predicts higher topographies compared to Model 3 (**Figure 35**; section 3.4), hence rendering higher precipitation rate variability.

The higher precipitation in the southeastern part of the study area in Model 1 as well as the strong NW-SE pattern in models 2 and 3 are attributed to prevailing wind direction and the rift axis orientation (i.e., from the southeast) and the location of the Rungwe volcanic orography, consistent with the observed precipitation associated with wind direction and orography (Smith and Bastad, 2004). The study area receives seasonal precipitation mainly due to the seasonal monsoon winds flowing from the southeast (Plisnier et al., 1999; McGlue et al., 2020). The Model 1 predictions of precipitation distribution align well with the monthly average Global Precipitation Measurement satellite-derived precipitation distribution (Huffman et al., 2019)

(**Figure 33**). For example, Model 1 predicts higher precipitation around the Rungwe Volcano and low precipitation on Lake Rukwa, as does the satellite data. Also, Model 1 predicts a general increase in precipitation rates from south to north on Lake Tanganyika. However, the model predicts overall lower precipitation rates on Lake Tanganyika than the observed satellite data, and a smaller range of variability (1.448 – 1.490 m/yr) compared to the range of the observed satellite values (0.78 -2.30). The mismatch between the observed and predicted data is attributed to four main reasons: (1) the model did not utilize any actual input parameter other than actual DEM and latitude; (2) we simulated a forward model that uses the modern topography to predict the precipitation distribution in the next 5 Myr whereas the satellite data is the average of precipitation rates for the past 20 years; (3) the small size of the model limits the distance from the moisture source hence less variability in the predicted precipitation rates, because as the distance increases from the moisture source the rate of precipitation decreases, and an area exhibits larger range of variability; (4) uncertainties borne by multi-satellite global precipitation data because of meteorological and land surface features such as complex topography, soil moisture, land type, soil type, and temperature (Bhuiyan et al., 2018; Ehsan Bhuiyan et al., 2019a, 2019b).

Our models predict a strong control of precipitation rates on bedrock incision and rift basin deposition. The precipitation-river incision relationship is well depicted in Model 1, as evidenced by the drainage network evolution, including the Karema depression drainage (**Figure 35**). The comparison between Model 2 and 3, suggests that the Rungwe Volcanic Province played an important role on the local landscape evolution, including rift faulting, and relative uplift enhancing the axial drainage and erosion from the uplifted western flank (**Figure 35**). We attribute the Rungwe Volcanic construction to late Pliocene tectonic events (Ebinger et al., 1993;

Ivanov et al., 1999; Fontijn et al., 2010), although we acknowledge the initial eruptive timing is unknown. The height of the uplifted flanks and the basin's depth was shown to increase as the volcano uplift rate and the heave of the border fault increases.

4.3. Hydrological connectivity of Lakes Tanganyika and Rukwa

The surface-water and groundwater are envisaged to flow from regions and lakes at higher elevations to lakes at lower elevation under a common flow system (Hokanson et al., 2020, 2021). The models reproduce the connection between Lake (pseudo-lake) Rukwa to Lake (pseudo-lake) Tanganyika via the Karema depression (**Figures 33-36**). Lakes Tanganyika and Rukwa were connected, as a result of overflow of Lake Rukwa due to an increase in local precipitation which caused the Ifumwe River to attain a peak discharge (**Figures 34 and 38**). Because of increased precipitation around Lake Rukwa that caused the overflow, we interpret the delta morphology around the Karema Platform to have been modified by the flow regime of the Ifumwe River via the Karema depression. Deltaic sediments were possibly sourced from both Lake Rukwa and the Karema catchment (i.e., riverbank erosion). This is supported by forest dip angles as high as ~22 degrees and seismic attributes (non-parallel, steeply dipping low amplitude to transparent reflections with both toplapping and downlapping termination surfaces) of the deltaic clinoforms that suggest a coarse sediment composition (**Figure 31**). Coarse-grained sediments suggest a proximal source that can be attributed to both the Karema catchment and Lake Rukwa. Furthermore, our source-to-sink analysis of the relationship between the maximum possible erosion from the Karema depression or Ifumwe catchment (i.e., 271.1 km³) and the volume of Karema deltaic deposits (i.e., 150 km³) suggests that the Karema depression as the possible source. Assuming that the deltaic deposits were deposited in 200 kyr, this implies an

erosion rate of ~ 0.32 mm/yr within the Karema depression. However, this estimate is ten times that of Livingstone Mountains, adjacent to northern Lake Malawi (~ 0.02 mm/yr), suggested by Van der Beek et al. (1998) for the entire Mesozoic and Cenozoic eras. Therefore, this calls for another possible source apart from the Karema depression, which we suggest may be Lake Rukwa. As discussed under section 4.2, the overflow from a drained Lake Rukwa may have caused downstream erosion of the Karema depression (**Figure 38**). Accordingly, the southern parts of the Ifumwe catchment, including the rift shoulder between Lakes Tanganyika and Rukwa is marked by longitudinal lineaments, ridge-like, oriented parallel to the channel gradient. Although these features have been attributed to the shear zones (e.g., Choubert and Faure-Muret, 1968), we suggest that these features were amplified by the flooding event that resulted from Lake Rukwa overflow (e.g., Gupta et al., 2017). Furthermore, the 2D seismic reflection data reveal buried channel complexes around the Karema Platform adjacent to the deltaic clinoforms (e.g., **Figure 30**; Shaban et al., 2021). We attribute these buried channel complexes to submarine canyons that incised the drainage across a former flood plain because of base level lowering. Floods accelerated by breaching of overfilled basins can produce large-scale sediment deposition and long-term landscape evolution (O'Connor et al., 2009, 2020), for example the Ebro Basin (NE Spain) (Garcia-Castellanos et al., 2003), the Sichuan Basin (Richardson et al., 2008), the Colorado Plateau (Dickinson, 2012), and the Dover Strait (Gupta et al., 2017).

Our modeled lake connectivity aligns with previous observations, such as Lakes Nam Co, Siling Co and Zhari Co in the southeast of the northern Tibetan Plateau (Dagang et al., 2004). Also, thick deltaic sediments have been identified in Lake St. Clair; these sediments are attributed to the connectivity of Lakes St. Clair and Huron via the St. Clair River (Holtschlag and Koschik, 2002). It has been estimated that the average discharge of the St. Clair River is 5×10^3

m^3/s (Holtschlag and Koschik, 2002) whereby $\sim 2 \times 10^5 \text{ km}^3$ of sediments are transported by the St. Clair River from the Lake Huron to the Lake St. Clair shoreline via five distributaries (Holtschlag and Koschik, 2002).

In lacustrine deltaic settings, the lake controls the base level of a river and the location of the shoreline; therefore, deltaic systems can be used to infer the paleo-lake level changes and paleo-climate variabilities (Machlus et al., 2000; Shaban et al., 2021). Consequently, it is important to consider how a Lake Tanganyika lowstand occurred contemporaneously with a Lake Rukwa highstand overflow, when the two lakes are separated only by $\sim 50 \text{ km}$. The Lake Tanganyika catchment is ~ 6 times the size of the Rukwa catchment, and for example receives hydrologic inputs from as far north as the Virunga highlands via Lake Kivu overflow, more than 600 km from the study area. The Lake Rukwa water level signal in contrast is reflective of conditions near the modern lake. It is possible that Lake Tanganyika low lake stage conditions during deposition of the Karema oversized deltas were reflective of a hydroclimate environment far from the study site, and possibly quite different from the region near Lake Rukwa. A thorough analysis of lake level forcings in both Tanganyika and Rukwa requires an alternative modeling approach, such as a hydrologic energy balance model, that fully captures not only precipitation but also evaporation from the lake surface of these large lake systems.

Mountainous regions exert a strong control on the magnitude and distribution of precipitation and drainage runoff (Sodemann, et al., 2009). We suggest that the lake level drop of Lake Rukwa is related to the extended dry periods coupled with the Rungwe volcano development (**Figure 38**). Results from Model 3 implies that before development of the Rungwe volcano both the lakes received similar rates of precipitation, but the growth of volcano topography blocked most of the incoming moisture from southeast, hence, causing higher

precipitation rates on its windward side and rain shadow on its leeward side. Model 2 predicts that the rain shadow across pseudo-Lake Rukwa began when the height of the volcano was ~3500 m, almost half of its height at the end of the model. The volcano height at the end of the Model 2 run is more than twice that of the actual modern Rungwe volcano. Such high uplifted rate is adopted because we develop the high elevated volcanic topography from an initially flat surface. Also, a combination of uplift and subsidence rates controls the height of the topography generated by the model. Previous studies have reported records of extended dry periods such as the Last Glacial Maximum (LGM), ~20 ka in the Tanganyika-Rukwa rift system (e.g., Barker and Gasse, 2003; Felton et al., 2007; McGlue et al., 2008). For example, Vincens et al. (2005) used pollen to infer that during the LGM, Lake Rukwa was under cooler and drier climatic conditions than today and that an aridification trend intensified ca. 3500 yr toward modern conditions. Also, Kennerley (1962) suggests that Lake Rukwa occupied almost the entire basin during the early Holocene but was almost dry in the 1980s.

The topography, basin area and basin elevation control the size and shape of a delta. Thus, larger rivers depositing sediments along a passive margin with a gentle slope form larger deltas than those formed by small rivers depositing sediments along a continental margin with a steep slope (Milliman and Syvitski, 1992). An alternative explanation for the Karema delta formation is the possible presence of a large paleo-river, with a drainage area intermediate between that of the Malagarasi River and Ruzizi River. This is based on the comparison of the thickness of the Karema deltaic deposits with that of the Malagarasi and Ruzizi deltaic deposits that shows that while the thickness of the Karema deltaic deposits is less than that of the Ruzizi deltaic deposits, it is almost four-times that of the Malagarasi River deltaic deposits (refer to section 1). We cannot completely rule out the possibility that rather than delta construction due

to Rukwa overflow, the large Karema paleodeltas were formed by Malagarasi River flow into Lake Tanganyika via the Ifumwe River in the geologic past (**Figure S16**). For this to have occurred the Malagarasi must have shifted its course to the modern location (i.e., via Kigoma) through basin capture. Such capture could have been caused by the local uplift of the topography that is located between the modern Ifumwe and Malagarasi Rivers, and the northwestwards propagation of the Lupa border fault (**Figure S16**).

4.4. Model limitations and further work

Modeling lake connectivity requires robust information such as rain gauge station data, drainage discharge data, temperature, paleotopography, and high-resolution models. However, our models lack many of these constraints, and the paleo-topography was only assumed. Also, none of our models predicted the very shallow lake level of Lake Rukwa as it is today. This is likely due to the model extent in terms of its size and the failure to predict the paleotopography at the start of simulation.

The main challenges of orographic precipitation modelling are twofold: i) the model resolution needed to properly resolve all important precipitation processes in complex orographic regions is of high order (in single-digit kilometers or a few meters) (Smith, 1979) and ii) due to topographic complexity, results of such numerical modelling may be difficult to reproduce accurately (e.g., Bousquet and Smull, 2003; Georgis et al., 2003; Rotunno and Ferretti, 2003; Smith, 2003). For instance, in our models the main limitation is the simplification of the vertical structure of the atmosphere using vertical integration and a linearization of the fluid and cloud dynamics, and an assumption of a horizontally uniform background flow and atmospheric properties. Thus, the temperature, wind vectors, static stability, and cloud delay times are assumed to be constant in space. Furthermore, the atmosphere is assumed to be saturated. Also,

nonlinear effects such as flow blockings are not captured by the model. Additionally, the model is not suitable to unstable atmospheric conditions (Crochet et al., 2007). Furthermore, in our models we use a constant K , whereas estimates of the value of the erosion coefficient are prone to variations up to four orders of magnitude depending on lithology and climate (Stock and Montgomery, 1999).

To evaluate the effects from unconstrained parameters, we carried out a series of sensitivity analyses on the erodibility coefficient, wind speed, conversion times and volcano uplift rate (Figures S3-7). Our results reveal the significance of wind speed, erodibility coefficients and rain base in controlling the spatial landscape evolution as elaborated under section 2.2.3. Such results agree with recent analysis of orographic models (Morales et al., 2021). By using Monte Carlo analysis, Morales et al. (2021) showed significant parameters were found to be horizontal wind speed, relative humidity, surface potential temperature, and fallout time.

Further work such as core sampling of material over the past several hundred thousand years from Lake Rukwa to Lake Tanganyika along the Karema depression is required to constraint the timing and paleoenvironments associated with the hydrological connectivity. Dating sedimentary units, analyzing mineral assemblages for provenance and analyzing isotopic variability of stratigraphic units will aid in constraining the connection histories of the two lakes. Also, alternative models such as climate models (e.g., Jaeger et al., 2013; Huziy and Sushama, 2016) or energy balance hydrologic models (e.g., Lyons et al., 2011) will contribute additional information on the connectivity of Lakes Tanganyika and Rukwa.

Conclusions

We present an integration of landscape evolution and orographic precipitation modelling to illustrate how rift tectonics and magmatism coupled with climate forcing caused the connectivity of Lakes Tanganyika and Rukwa. From this modelling we show that:

1. The modelling results suggest a Lake Rukwa overflow into Lake Tanganyika through the Karema depression and provides constraints on the climate and tectonic conditions required for the overflow as demonstrated by models 1, 2, and 3.
2. Karema deltaic deposits were deposited during Lake Rukwa overflow into Lake Tanganyika, and sediments were sourced from the Karema depression and Lake Rukwa shoreline as supported by seismic character of the deltaic deposits, and the Karema depression erosion analysis including the longitudinal profile analysis of the Ifumwe River tributaries.
3. Orography has a strong control on the magnitude and distribution of precipitation and further bedrock incision and rift basin deposition. In addition to dry periods, the Rungwe volcanic edifice likely produced rain-shadow on its leeward side leading to diminished precipitation and distribution around Lake Rukwa, as indicated by the underfilled modern Lake Rukwa.
4. Results from sensitivity analysis suggest that in addition to precipitation rate, wind speed and wind direction also play a major role in the development of orographic precipitation as evidenced by precipitation increase with wind speed increase in Model 1.
5. When two lakes are in proximity and structurally connected, overflowing of one of them that is spatially located above the other adjacent lake may lead to the overflow into the other as

evidenced by the interconnectedness of Lakes Tanganyika and Rukwa via the Karema trough.

6. Tectonics could modulate surface processes on the scale of large continental rifts, and the interactions between two proximal lakes can produce oversized sand-prone deltas that may form potential hydrocarbon reservoirs and introduce pathways for biotic exchange and evolution.

This study provides a benchmark for scientific studies focusing on juvenile rift lake interactions, sediment provenance, and biotic exchange and evolution.

Figures for Chapter 4

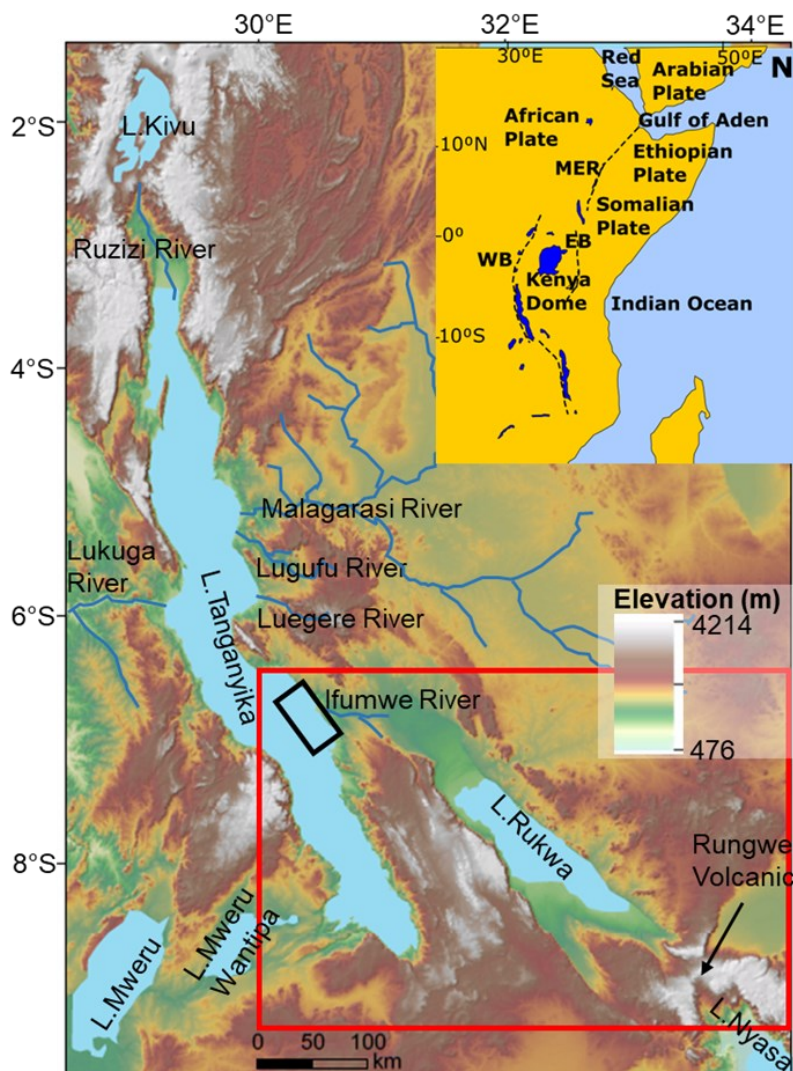


Figure 29: Study area covering the southern part of the Western Branch of the East Africa Rift System. The area of interest (red rectangle) is the southern part of Lake Tanganyika, Lake Rukwa, and northern part of Lake Nyasa (Malawi). Solid blue lines represent rivers. The thick black rectangle represents the area where the deltaic deposits have been identified around the Karema Platform (Shaban et al., 2021); for more details refer to the text. Notice the Rungwe Volcano just above Lake Nyasa. Inset

map shows the East African Rift System (EARS, dashed line), EB= Eastern Branch, WB= Western Branch, and MER = Main Ethiopian Rift..

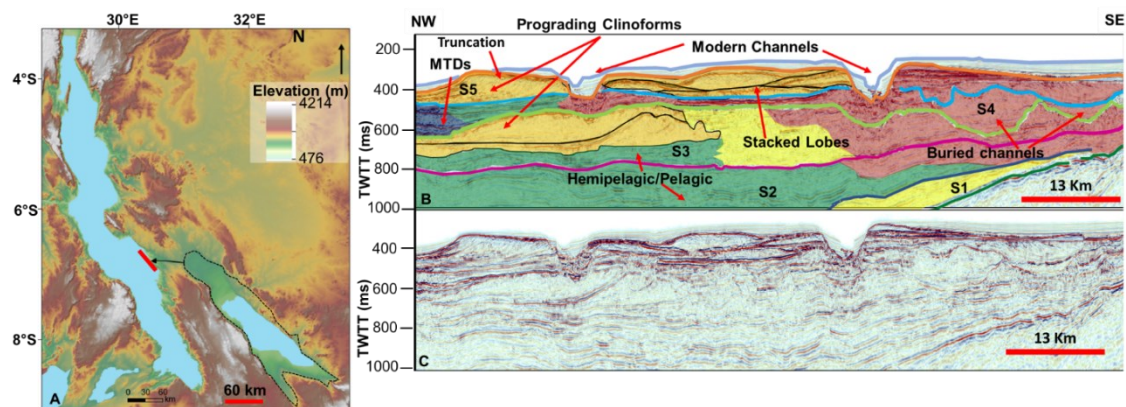


Figure 30: (A) Topographic map of the study area; black dotted line indicates the paleo-lake high-stand of the Lake Rukwa at an elevation of ~962 m suggesting ~160 m above modern Lake Rukwa, the black solid arrow indicates the Lake Rukwa's overflow direction into the Lake Tanganyika via the Karema depression, and the red solid line indicates the position of the seismic profile of (B). (B) Interpreted 2D seismic reflection profile along the Karema Platform; note the spectacular prograding clinoforms and buried channel complexes (Shaban et al., 2021). Orange = deltaic clinoforms, yellow = shallow deposits, red = channel deposits, green = hemipelagic deposits, blue = mass transport deposits (MTDs). (C) Uninterpreted 2D seismic reflection profile along the Karema Platform

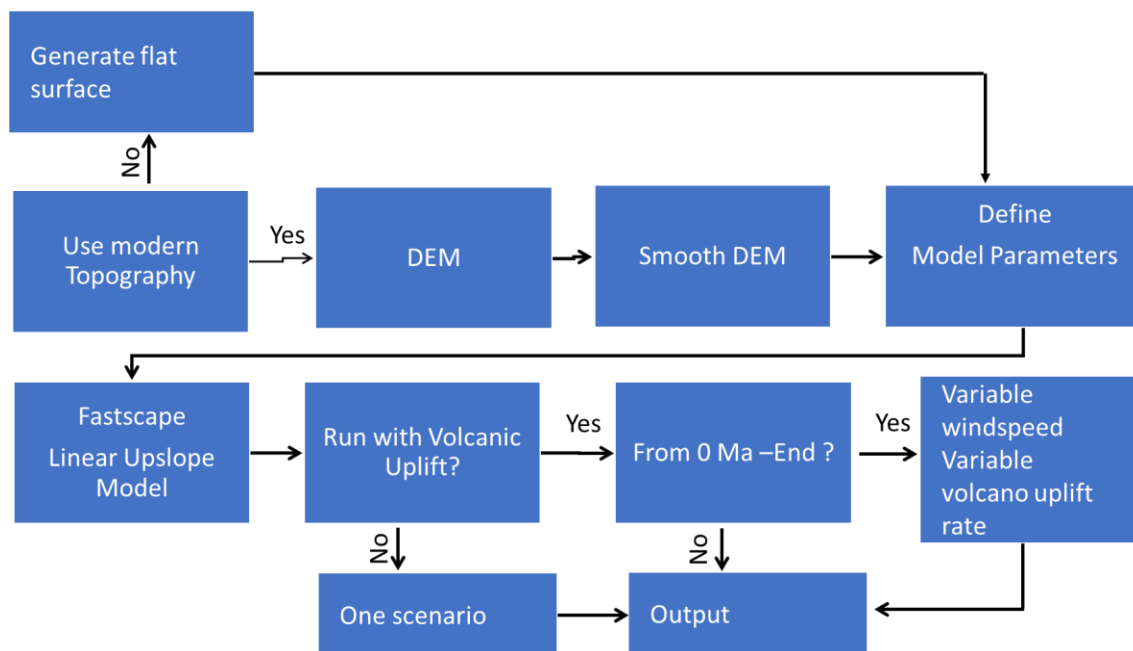


Figure 181: Model processes. Model 1 used modern topography, whereas Models 2 and 3 used artificial topography. Model 2 was simulated with volcano for 5 Myr whereas Model 3 was simulated without volcano.

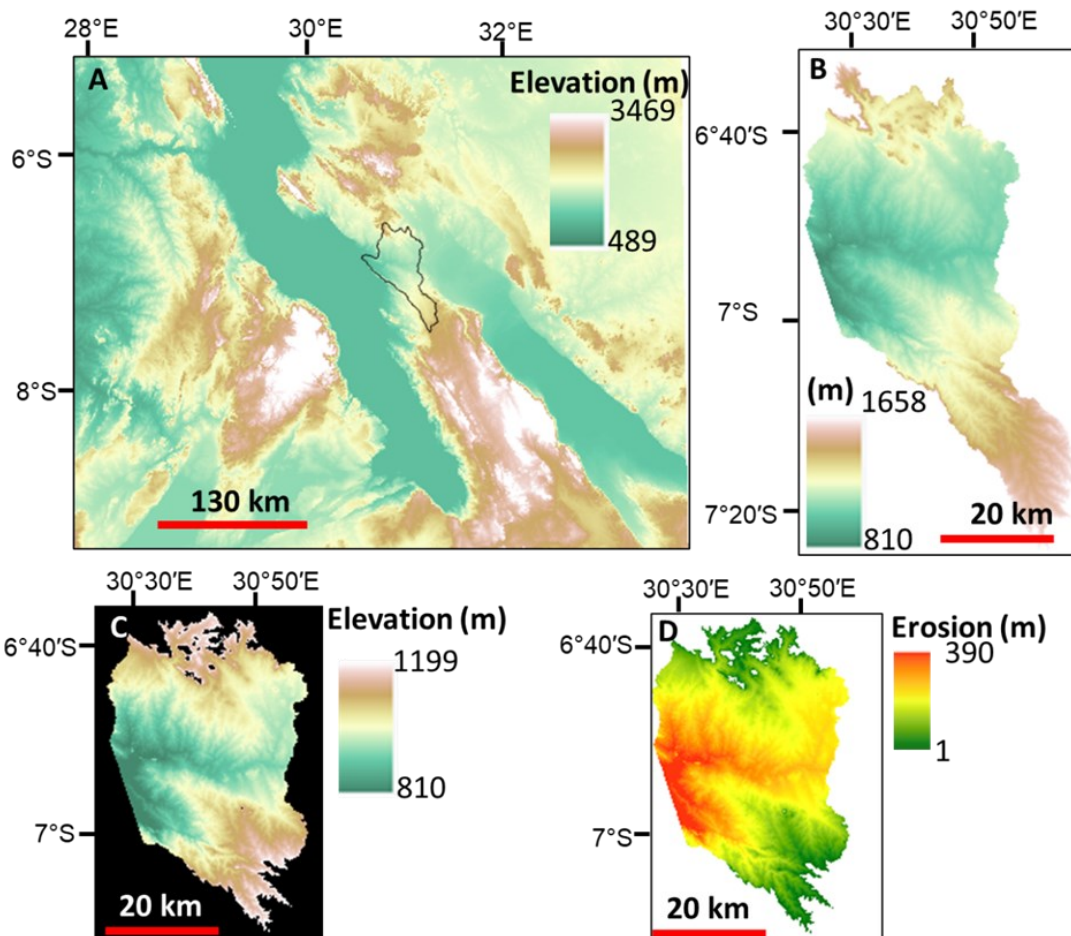


Figure 32: Analysis of the Karema depression (Ifumwe River) erosion. (A) 30 m SRTM DEM, the black solid polygon represents the Karema depression catchment. (B) Extracted 30 m SRTM DEM for the Ifumwe River catchment. (C) 30 m SRTM DEM capped 1200 m. (D) Estimated erosion for 200 kyr, obtained by subtracting the DEM in (C) from 1200 m datum.

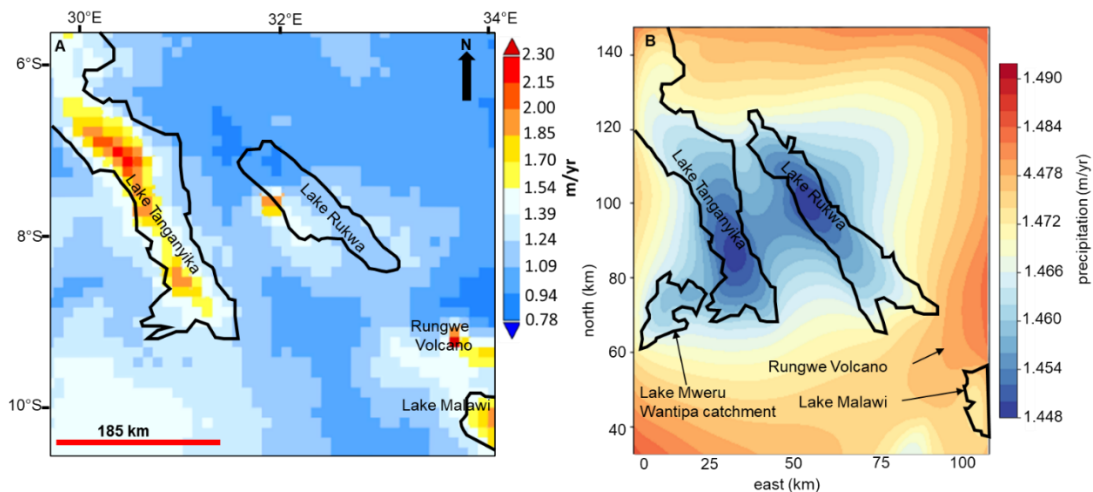


Figure 34: Comparison of precipitation distribution between the satellite data (A) and Model 1 results (refer Model 1) (B). Satellite data are monthly averaged for the past 20 years (2000 -2021) from the NASA Giovanni system (Huffman et al., 2019). Note the similarities in high precipitation between the satellite data and model predictions for Lake Rukwa and the Rungwe Volcano, and rain shadow between the southern part of Lake Rukwa and northwest of the Rungwe volcano. From both the observed and predicted results the precipitation is shown to increase from the southern parts of Lake Tanganyika to the northern parts of the lake.

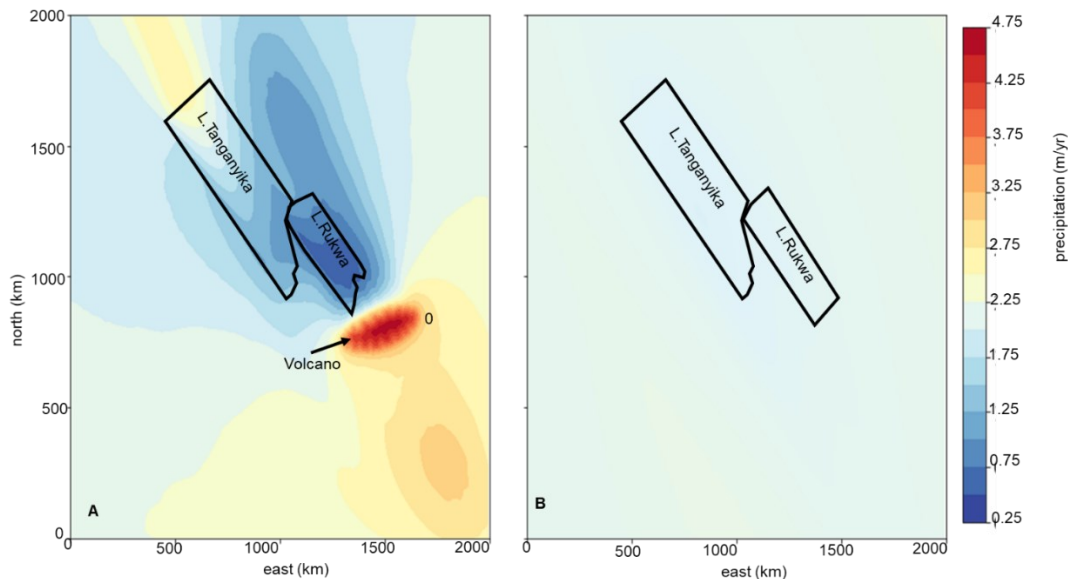


Figure 35: Precipitation rates generated after 5 Myr for models 2 and 3 with similar rain base and wind speed parameters. (A) Model 2 was simulated with an uplifting volcano throughout model runtime. Note rain shadow northwest of the volcano, particularly around pseudo-Lake Rukwa. (B) Model 3 did not include a volcano. Note that the model predicts consistent precipitation rates distribution ranging from 1.9 m/yr to 2.05 m/yr with higher precipitation rates distributed in the western part of the model. Model 2 predicts a large range of values than Model 3 because of the orographic effect caused by the volcano and the overall topography generated at the end of the model (refer to Figure 8; section 3.4). It is evident that Model 2 simulates ‘mountainous range’ extending SW-NE connecting with the volcano.

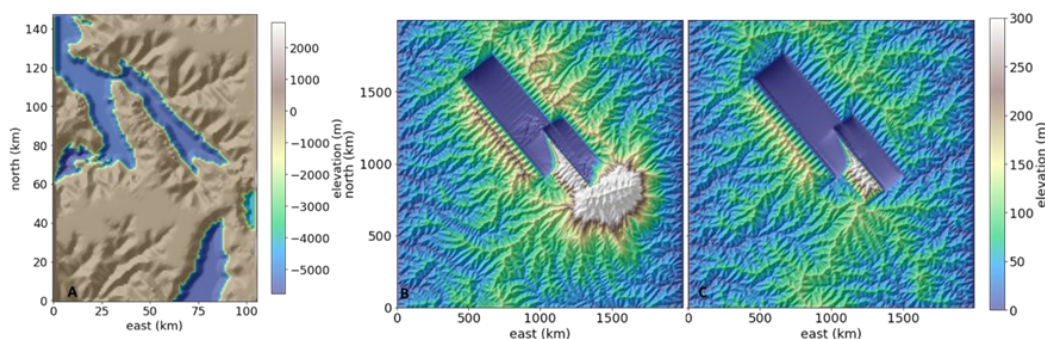


Figure 36: Topography evolution after 5 Myr. (A) Scenario 1 of Model 1 used a rain-base of 1.5 m/y and a wind speed of 5 m/s and predicts the connectivity of Lakes Tanganyika and Rukwa. (B) Model 2 was simulated with volcano from time = 0 yr until the end of the model runtime. (C) Model 3 did not include volcano. Note that all models predict the connectivity of Lakes Tanganyika and Rukwa. The obvious difference between models 2 and 3 is the elevation of the topography generated, whereby, Model 2 predicts higher elevation.

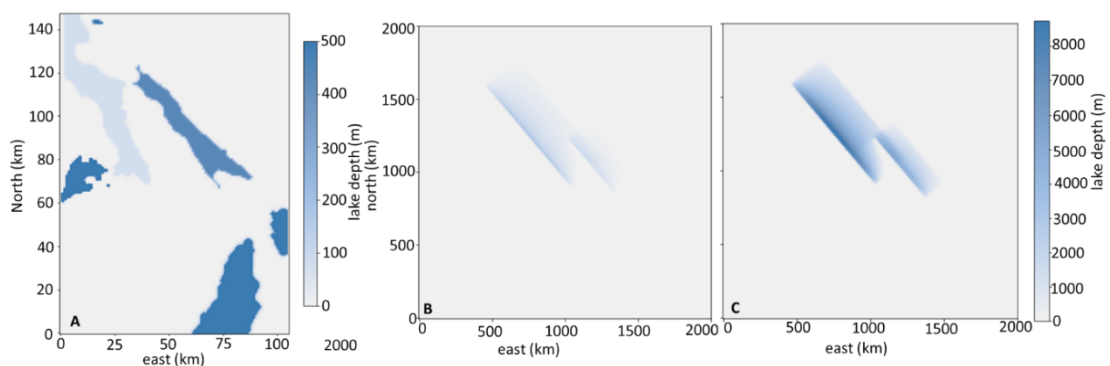


Figure 37: Lakes' depth predicted by models 1, 2 and 3 after 5 Myr. (A) Scenario 1 of Model 1 used the actual DEM of the area, a rain-base of 1.5 m/y, and a wind speed of 5 m/s. Note that contrary to the modern bathymetries, the model predicts shallower lake depth for Lake Tanganyika than Lake Rukwa. (B) Model 2 used an artificial DEM and included a volcano from time = 0 yr until the end of the model runtime, a rain-base of 1.5 m/y, and a wind speed of 5 m/s. (C) Model 3 used same model parameters as Model 2 but did not include the volcano. Note that while both models 2 and 3 predict

pseudo-Lake Tanganyika deeper than pseudo-Lake Rukwa, Model 2 predicts greater depths for pseudo-lakes than Model 3.

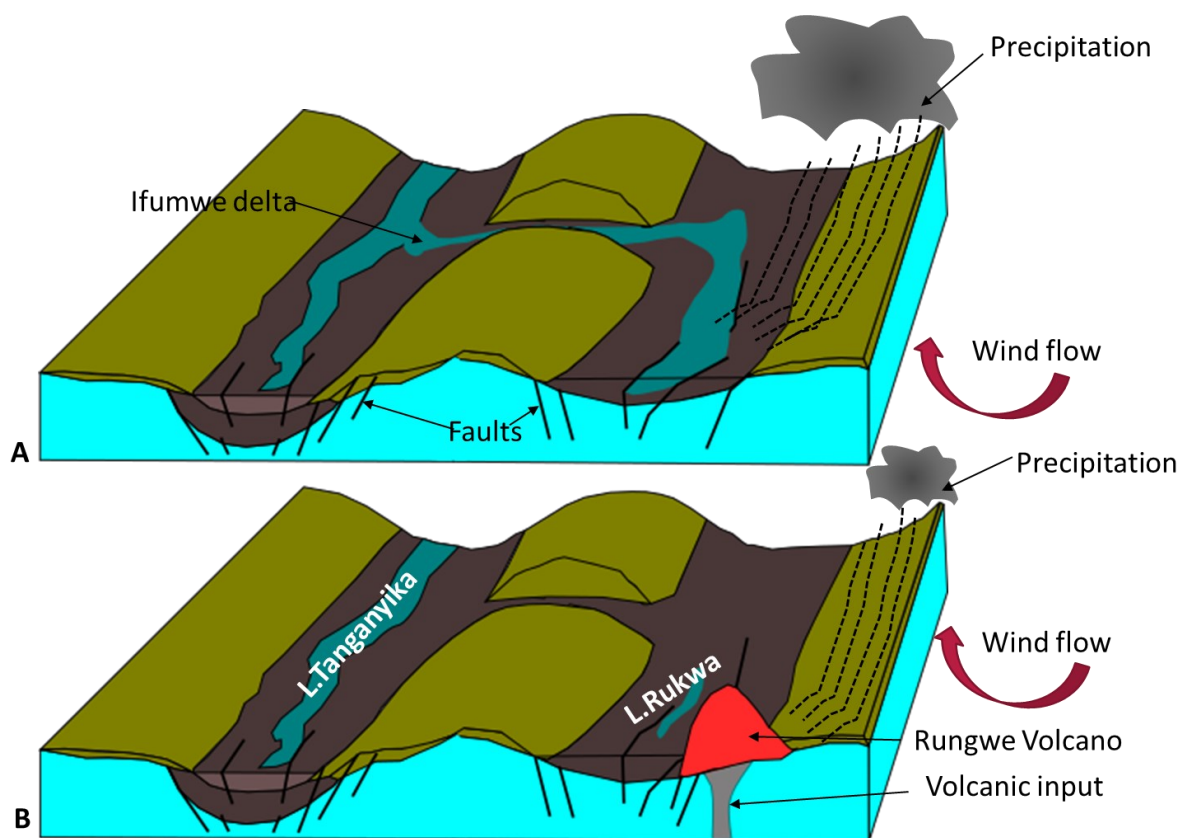


Figure 3819: Conceptual diagram of the connection between Lakes Tanganyika and Rukwa. (A) Lake connection stage: During this period, heavy precipitation caused Lake Rukwa to expand, fill to its spill point and overflow into Lake Tanganyika via the Karema depression. Wind flow from the southeast. (B) Today's condition: Dry conditions prevail around Lake Rukwa. Dry conditions were caused by diminished

precipitation because of rain shadow possibly caused by the Rungwe Volcanic edifice.

Wind flowed from the southeast.

CHAPTER 5: CONCLUSIONS AND FUTURE WORK

To decipher the tectonostratigraphic evolution of the Lake Tanganyika Rift and paleoclimate of the area, I integrated 2-D seismic reflection data, potential field data and satellite data. This study has addressed several aspects of the rift including:

- (1) The impacts of structural and tectonic evolution of this multi-segment rift system on the evolution and distribution of sedimentary facies along the length of the Lake Tanganyika Rift,
- (2) Spatial and temporal hydroclimate variability over the life-history of the rift lake,
- (3) The paleogeography of the Lake Tanganyika Rift from inception through modern times, and its impacts to lacustrine habitats,
- (3) The structural strikes of shallow and deep structures of the Rift,
- (4) The control of crustal anisotropies and Mesozoic structures on the Cenozoic rifting,
- (5) The presence of Karoo sediments within the Lake Tanganyika Rift,
- (6) The structural connection between the Kavala Island Ridge (KIR) and the Mahale Mountains and Katenga - Kugulu - Ntengo lineaments (Luama footwall),
- (7) The effect of the KIR evolution on the sediment dispersal and rift development,
- (7) The paleoflow of Lake Rukwa into Lake Tanganyika and its control on the deposition of deltaic sediments around the Karema Platform.

Chapter 2 reaffirmed that six depositional seismic units are in the Lake Tanganyika Rift, suggesting a complex history of extensional tectonics and hydroclimate variability. As

revealed by seismic facies analysis, the tectonics and hydroclimate processes controlled the facies distribution and the rift development. For instance, the manifestation of low-moderate-amplitude, semi-continuous seismic reflections within the Seismic unit 1, during the early stage of rift development, show the rift was dominated by fluvial and or isolated shallow lakes. Because of border faults and topographically high accommodation zones that segment the rift into long structural half-grabens, sediment distributions were highly impacted. For example, following the deposition of Seismic unit 1, the Burton's Bay Ridge acted as a significant sediment barrier between the Ruzizi and Kigoma provinces causing a contrasting depositional succession. Seismic unit 2 suggests that as border faults continued to propagate and link, in conjunction with increased subsidence, the rift focused onto the present border faults and experienced sustained deep lake conditions as indicated by the dominance of acoustic signatures typical of hemipelagic deposits. As the rift continued to develop (e.g., Seismic units 3-5), the rift valley deepened, and regions of enhanced relief developed on the rift margins. This was accompanied by an increase in the amplitude and frequency of lake level fluctuations, a consequence of enhanced hydroclimate variability. During these later intervals, the rates of gravity-induced deposition increased, and spectacular prograding deltas developed during the lake lowstands. Although in different parts of the seismic unit, the first evidence of both the Malagarasi River and Ruzizi River drainage is recorded in Seismic unit 3, as evidenced by deep water channel complexes and turbidites. Chapter 2 concludes that the rift sedimentary fill architecture results from fault propagation and linkage, fault-controlled subsidence, and hydroclimate processes, which all control the evolving accommodation zones, drainage catchments, and depositional

pathways. Furthermore, we learn that all these processes influence the distribution of rift valley habitats, and ultimately biodiversity and biological evolution in the rifts.

Using short wavelength, high frequency and long wavelength, low frequency gravity and aeromagnetic anomalies, and gravity and aeromagnetic forward modelling in chapter 3, I was able to assess the deep basin and underlying basement structure of the Lake Tanganyika Rift, East Africa. Using longer-wavelength, lower-frequency components I delineated the shallow structural fabrics corresponding to intra-sedimentary depth intervals, and used the longer-wavelength, lower-frequency components to delineate the deeper basement structural fabrics. The analysis has revealed that shallow syn-rift structures are within a depth of ~1-3 km, whereas pre-rift basement structures are within a depth of ~5-8.5 km. The results reveal that shallow structures strike predominantly NW-SE consistent with the dominant trends of rift faults mapped in the seismic reflection data. The long wavelength gravity and magnetic anomaly analysis indicates that deep structures predominantly strike NW-SE consistent with the dominant trend of exhumed basement shear zones and strike of metamorphic foliation in basement terranes along the rift shoulder. This implies that they developed during the initial stages of the rifting and were controlled by the preexisting basement fabrics. Furthermore, the results support long held concepts that the KIR developed along a large and long paleo-ductile shear zone possibly connected to the Chisi Shear zone, and that paleo shear zone may have acted as locked zone during the south rift propagation. Based on seismic interpretations it seems that the high relief of the KIR has been present since its bounding faults were fully established in the early stage of rifting; activity on those bounding faults increased in later stage of the rift evolution,

although the high and frequent lowstand exposures eroded most of the sedimentary section atop the crest of the ridge.

The 2.75D gravity and aeromagnetic modelling reveals the presence of an anomalously high-density (2.35-2.45 g/cc) deep-seated, fault-bounded wedge-shaped sedimentary unit that directly overlies the Pre-rift metamorphic basement in the Kalemie Province attributable to the Karoo origin. However, we argue that drilling information that intersects the crystalline basement is required to confirm this interpretation. Furthermore, the gravity and aeromagnetic modelling delineated the presence of a ~4 km-wide basement-bounded shear zone that controlled the location and down-dip geometry of a buried large-offset early-rift intra-basin faults. Also, the modelling demonstrates that magma-poor margins may host significant volumes of extension-related high magnetic susceptibility rocks, something that is unlikely to be resolved by seismic data only. Furthermore, we find that the early-rift structural highs, commonly localized by large-offset rift faults that exploited basement shear zones, persisted into the subsequent stages of tectonic extension, in some places continuing to displace the modern lake floor. Furthermore, chapter 3 concludes that although incipient rift structure is largely modulated by inherited basement fabrics and shear zones, their influence on basin morphology often cascades through to the subsequent stages of tectonic extension. These results provide new insight into the earliest basin architecture of the Tanganyika Rift, controlled by inherited basement structure, and provides evidence of their persistent influence on the subsequent basin evolution.

In chapter 4, I integrated landscape evolution modeling with an orographic precipitation modeling component to illustrate how rift tectonic processes in conjunction with climate forcing might have caused the connectivity of Lakes Tanganyika and Rukwa.

This modeling supports the interpretation that Lake Rukwa overflowed into Lake Tanganyika through the Karema depression and provides constraints on the climate and tectonic parameters required for the overflow. Consequently, Karema deltaic deposits were possibly deposited during Lake Rukwa overflow whereby the sediments were eroded from the Karema depression and the Lake Rukwa shoreline as indicated by seismic character of the deltaic deposits as well as erosion and longitudinal profile analysis. This demonstrates that when two lakes are in proximity and structurally connected, there may be important long-term consequences for the sedimentary fill in the downstream system. Tectonics modulates surface processes on the scale of large continental rifts, and the interactions between two proximal lakes can produce oversized sand-prone deltas that may form potential hydrocarbon reservoirs in the downstream lake and introduce pathways for biotic exchange and evolution.

The models suggest that the Rungwe volcanic edifice may have produced a rain-shadow on its leeward side, leading to diminished precipitation amount and distribution around Lake Rukwa, a reason for the small size of the modern Lake Rukwa. This study provides a benchmark for scientific studies focusing on juvenile rift lake interactions, sediment provenance, and biotic exchange and evolution.

Despite the in-depth analysis of this study, the age and nature of the depositional units and the top of the crystalline basement remain unconstrained in the Lake Tanganyika Rift. Only the work of Cohen et al. (1993) attempted to resolve this but was limited to the uppermost section of the Rift, less than 10 m, in the Holocene and Upper Pleistocene interval. A lack of deep section age information limits our ability to constrain the temporal evolution of the tectonostratigraphy of the Rift and the timing of various paleoclimatic

events that modulate the rift evolution. Scientific drilling, including a drill core intersecting the crystalline basement may help provide age constraints as well as information on the characteristics of the syn-rift fill. Furthermore, a deep core of the basement will provide information on the nature of the crystalline basement and confirm the nature of the ‘Nyanja Event’ previously identified in seismic reflection data. The drilling information will also constrain the timing of the deltaic deposits reported in chapter 2 and 4 this study. In chapter 4, I explained the possible source of the Karema deltaic deposits and concluded that Lake Rukwa overflowed into Lake Tanganyika, however, I did not provide the time constraints for these events. Therefore, this also calls for drill core that intersects the bottom surface of the Karema deltaic deposits which can provide the age constraints. Also, core sampling of material along the Karema depression over the past several hundred thousand years, for dating sedimentary units, analyzing mineral assemblages for provenance and analyzing isotopic variability will aid in constraining the connection histories of Lake Rukwa and Lake Tanganyika.

The 2-D seismic reflection data and potential field data used in this study as presented in chapters 2, 3, and 4 are not bias free. For instance, the 2-D seismic data faces the challenges of coverage and resolution. The PROBE data set are the only 2-D basin scale seismic reflection data that transect all territory water bodies of Lake Tanganyika; however, they are very widely spaced, limiting the ability to constrain the spatial extent of rift structures and syn-rift fill along the strike of the rift. The latest commercial 2-D basin scale reflection data are restricted to the southeastern parts of the lake within Tanzania territory. Similarly, the potential field data sets are restricted to the half of the lake within Tanzania territory, limiting our ability to elucidate the full picture of the rift structures along and

across the strike of the rift. Therefore, a new tight ‘infill’ seismic reflection or refraction data set akin to the commercial data set in the Tanzania side or the SEGMENT project in Lake Malawi that transects the whole lake would help provide a full story of the Cenozoic juvenile rifting.

Furthermore, to test the long-term connectivity between Lakes Tanganyika and Rukwa, a thorough analysis of lake level forcings in both Tanganyika and Rukwa requires an alternative modeling approach. One approach would be a hydrologic energy balance model, that fully captures not only precipitation but also evaporation from the lake surfaces of these large lake systems.

Data availability

The latest commercial 2D multichannel reflection seismic datasets acquired in 2012 and 2014 are owned by the Government of the United Republic of Tanzania and can be accessed by the approval of the Petroleum Upstream Regulatory Authority (PURA). The Project PROBE 2D seismic data sets acquired in 1983-1984 were collected by Project PROBE of Duke University and reprocessed under the direction of Syracuse University; legacy data can be accessed through the Marine Geoscience Data System hosted by Lamont Doherty Earth Observatory at http://www.marine-geo.org/tools/search/Files.php?data_set_uid=26822 (DOI: 10.1594/IEDA/326822).

Funding sources

Support for this research was provided by Syracuse University, National Science Foundation (NSF)-Empower Program, grants from Chevron and Petrobras to CAS, and the Tanzania Petroleum Development Corporation.

Declaration of competing interest

The authors have no competing interests to declare.

Acknowledgements

We extend our acknowledgements to the Petroleum Upstream Regulatory Authority of Tanzania and the Tanzania Petroleum Development Corporation (TPDC) who provided an access to the commercial higher resolution 2D multichannel seismic data that were used for this study. The funds for this study were granted from Syracuse University (SU), grants from Chevron and Petrobras to CAS, TPDC and the NSF-supported EMPOWER Program. Orographic precipitation modeling was carried out using the model after Smith and Barstad (2004). We thank the members of the Lacustrine Basin Research Group at SU for their assistance provided while completing this study, particularly Jacqueline Corbett.

Appendices

Supplemental Material for Chapter 2

Introduction

This Supplementary Information provides additional explanation to the methodologies used for the analysis presented in the main paper. It presents 1) background context to Project PROBE; 2 & 3) Project PROBE data reprocessing and 2012/2014 data processing; 4) Spatial and temporal distributions of depocenters.

1) Project PROBE background

Project PROBE, based at Duke University, carried out reconnaissance seismic reflection surveys of Lake Tanganyika in 1983- 1984. under the direction of B.R Rosendahl.

The project collected ~1900 line-km of 2D basin-scale, multichannel seismic reflection data from the North to the South of the Lake Tanganyika Rift. These data were acquired aboard the R/V NYANJA, using a 48-channel hydrophone streamer and a single, 140 cubic-inch airgun, with offsets up to 1450 m. Seismic data were processed at project PROBE's computing facility using DIGICON software. Due to the large extent of the rift, the seismic profiles were shot at spacing of 12-28 km between dip lines, with closer spacing in the northern part of the Rift (Ruzizi and part of the Kigoma Basin). The 24-fold profiles were later reprocessed by ION Geophysical Company. Due to the short seismic streamer employed, this data set was challenged with problems of multiples especially in the northern part of the Ruzizi Province.

2) Project PROBE data reprocessing

Following renewed interest in hydrocarbon exploration in the rift valley, the Project PROBE data set were reprocessed in 2016 in order to minimize noise and improve the resolution at the basin scale. ION Geophysical used the following procedures during reprocessing. It undertook pre-processing data validations such as Geometry QC and line tie analysis, residual bubble energy removal, zero phase conversion, and velocity analysis. Then it carried the following routines during processing: spherical spreading correction, noise attenuation, multiple attenuation, SRME (free surface multiple attenuation), time variant filter (water bottom-dependent), F-X deconvolution, residual noise attenuation, prestack time and depth migration. Post-processing workflows involved the following: post-Migration Radon de-multiple, mute, deconvolution, time variant band-pass filter, gain application, time-to-depth conversion, and coherency filter.

3) 2012/2014 data processing

The commercial data sets were processed on board the MV Mwongozo using the Fugro UniSeis seismic processing package. The onboard processing was conducted twice (preliminary and full). The pre-processing included reformatting from SEG-D format, gain application, noise analysis, multiple attenuation, and stacking. The data were then sorted into 80-fold CMP gathers. The initial processing used the following workflow: Offset check; inverted channels check; missed shot check; Near Trace display; each 50th shot display; noise analysis for whole line in a “before first arrival” window; auxiliary channel check; top mute picking; brute velocity analysis; and brute stack. Then the full processing onboard was undertaken by using the following workflow: conversion into FSI internal format (Floating point); Butterworth Filter 8 Hz 18dB/oct 100 Hz 53dB/oct; T² gain compensation; instrumental delay correction 1 ms; surface relative multiple elimination; velocity analysis: 1 km interval; parabolic radon demultiple based on above mentioned velocity analysis; dip move out; sorted to CDP gather 80 fold; navigation merged with CDP position from P1/90; NMO correction; outer mute in CDP gather; stack: offset weighted; FX Deconvolution; KIRCHHOFF migration 100/200 traces half width; time variable filter: Time: LOW_filter-HI_filter = 0:16-300; 750:12-250; 1250:8-200; 1500:8-150; gun and cable compensation, final amplitude scaling: Gain (dB) = 4.0t; conversion to SEG-Y format; resample to 4 ms; minimum phase; American Polarity; navigation referenced to CDP position; water bottom referred to MSL; CDP X, Y coordinates at bytes: 73-76, 77-80; Shotpoint at byte 17-20; and DP at byte 21-24.

Fugro performed the final full processing in its office, and the following routine was used: processing and parameter tests; seismic data and observers’ logs from the survey

review; transcription; Recording System Delay and Amplitude Recovery; bulk time shift of 1 ms; T2

amplitude gain recovery; trace editing and acquisition noise removal; bad shot removal and channel editing; Surface Related Multiple Attenuation; CDP Sorting (sorted into 80 fold CDP gathers); navigation assignment; Velocity analysis; NMO; Mute: outer mute in CDP gather; Parabolic Radon Demultiple; Dip Move Out; The Poststack included the following: FX and FK parameters; Kirchoff Migration of 100/200 traces half width; Time variable filter; gun and cable compensation; band pass filters; Final amplitude scaling: GAIN (db) = 4.0; Conversion to SEG-Y format, resample to 4 ms; minimum phase; American Polarity; and navigation referenced to CDP position, water bottom referred to MSL.

4) Spatial and temporal distributions of depocenters

From **Figure 2**, the modern geometry, we observe the thickest (~ 6 km) sedimentary packages in the Marungu Province against the western bounding fault. The Kigoma Province records ~ 4-5 km of sedimentary packages against the western and eastern bounding faults whereas the Ruzizi Province records ~ 3 km of sedimentary packages against the western bounding fault. The Kalemie Province records the minimum thickness of the sedimentary packages, ~2 – 3 km against the south-western and eastern border faults.

Going back into the geological time, we observe varying spatial and temporal distribution of depocenters (**Figure S1**). For instance, at the end of Seismic unit 1 time, the thickest sedimentary packages for this unit in the Marungu Province are observed in the central part of the Province near the Ikola (Karema) Platform. In the Kigoma province, the depocenter is restricted to the western border faults and the southern parts of the two central

basement faults. In the Ruzizi Province, we observe the depocenter in the northernmost part of the province between two basement faults, whereas the Burtons 'Bay Ridge records the minimum thickness of sedimentary packages. The depocenter in the Kalemie Province is observed in the southern part of the Province.

At the end of deposition of Seismic unit 2, the depocenter is shown to extend across the central and western part of the Marungu Province, marking the thickest sedimentary packages of the Seismic unit 3 (**Figure S1**). In the Kigoma Province, the depocenter migrated towards the south-western part of the province against the bounding fault. Also, we observe the spatial changes in the Kalemie Province, two small depocenters are restricted to the northern and south-eastern parts of the province.

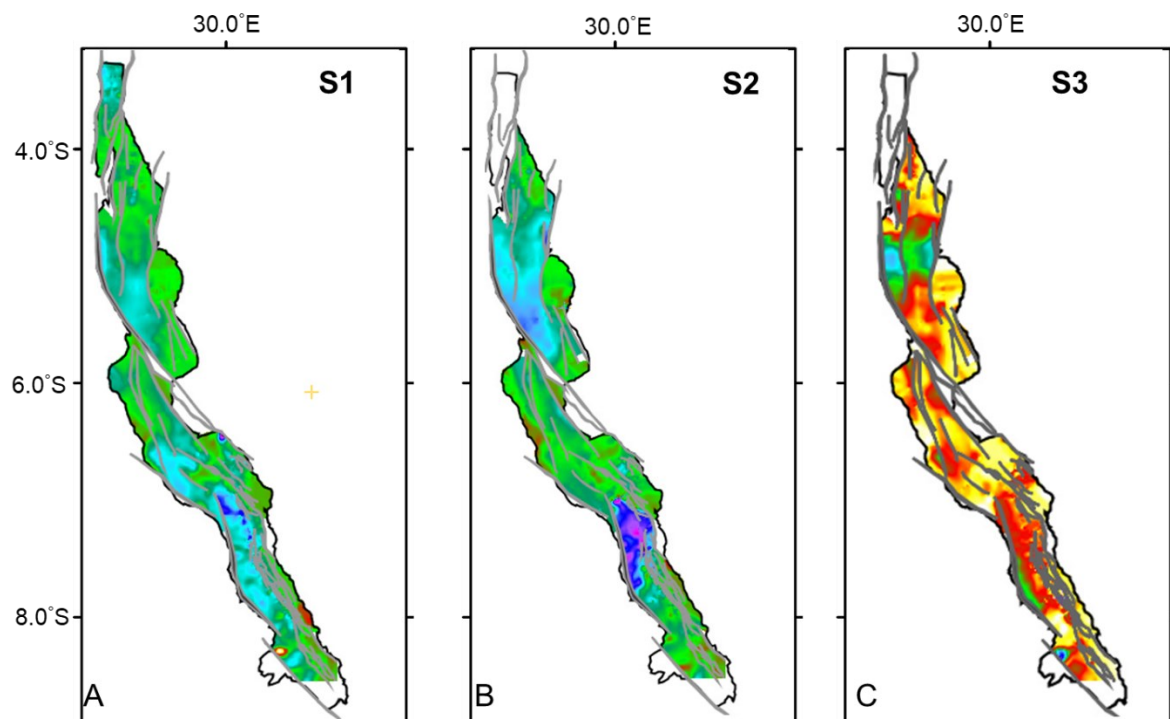
As the rift continued to evolve, at the end of Seismic unit 3, the Kigoma Province is shown to have the thickest sedimentary packages for Seismic unit 3 (**Figure S1**). The depocenter is observed in the central part of the province. In the Marungu Province, the depocenter migrated towards the south-western part of province against the border fault.

The isochron of Seismic unit 4 suggest that the Marungu Province has the thickest sedimentary packages of the Seismic unit 4 (**Figure S1**). The depocenter is observed in the central and southern part against the western bounding fault. In the Kigoma Province, we observe two depocenters in the south-western and north-eastern parts of the province suggesting a migration from that observed during the Seismic unit 3 time. However, no spatial variation of depocenters is observed in the Kalemie Province during this time.

During the deposition of Seismic unit 5, we do not observe spatial variation of depocenters in the Marungu and Kalemie provinces in comparison to what was observed at

the end of Seismic unit 3 (**Figure S1**). However, we observe a migration of hypocenters in Kigoma Province; one hypocenter is observed in the western part against the bounding fault, and one observed in the north-western part of the province against a bounding fault.

Supplementary Figure (Figure S1)



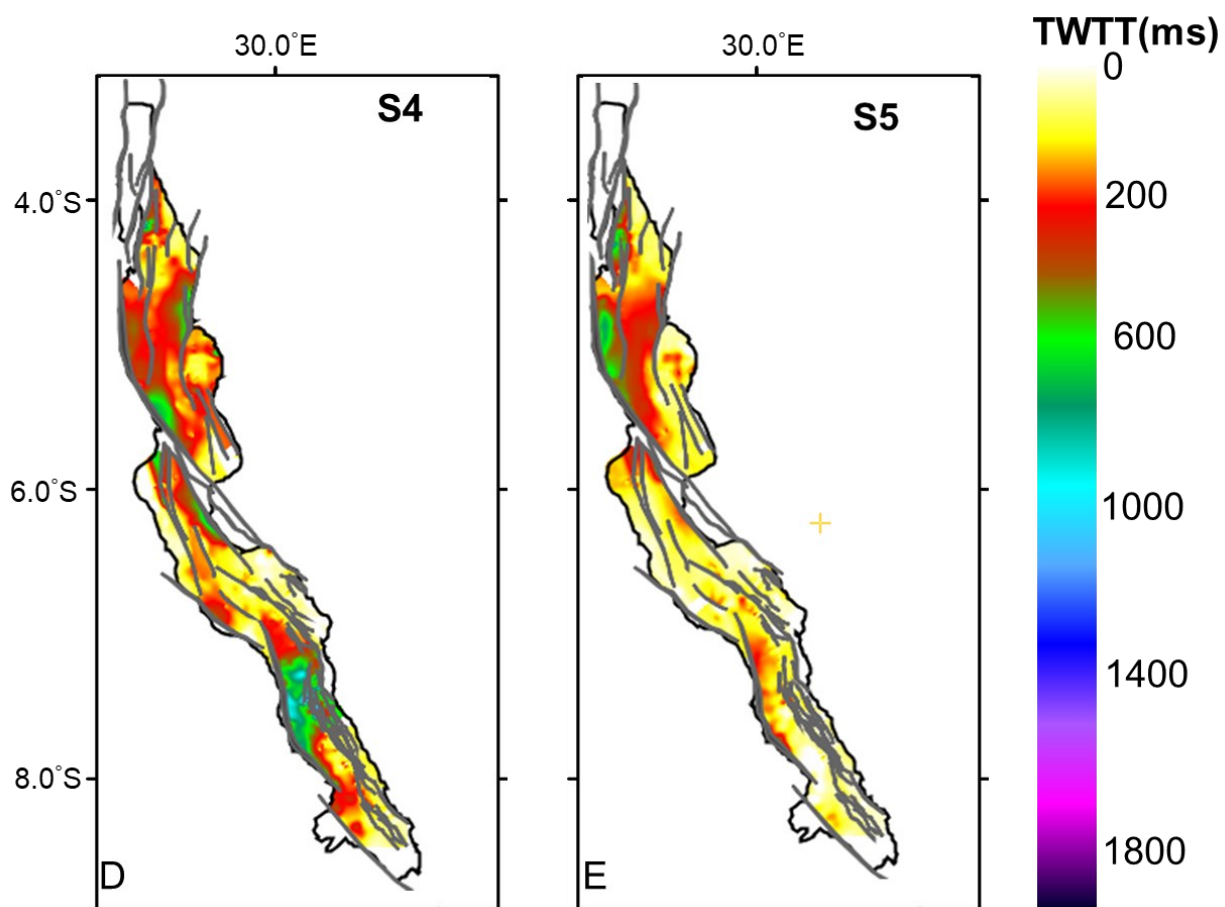


Figure S1: Sediment isochron maps across the Lake Tanganyika Rift for (a) Seismic unit 1 (b) Seismic unit 2 (c) Seismic unit 3 (d) Seismic unit 4 and (e) Seismic unit 5. Note the spatial and temporal variations and or depocenter migration across the Rift. Seismic units 1 and 2 record the thicker sediments. The basement involved faults are indicated by thick grey lines. Refer Figure 1 for sub-basins.

Supplemental Material for Chapter 3

Introduction

This Supplementary Information provides additional explanation to the methodologies used for the analysis presented in the main paper. It presents 1) background context to Project PROBE; 2 & 3) Project PROBE data reprocessing and 2012/2014 data processing; 4) Spatial and temporal distributions of lineament using Butterworth bandpass filtering analysis.

1) Project PROBE background

Project PROBE, based at Duke University, carried out reconnaissance seismic reflection surveys of Lake Tanganyika in 1983- 1984. under the direction of B.R Rosendahl. The project collected ~1900 line-km of 2D basin-scale, multichannel seismic reflection data from the North to the South of the Lake Tanganyika Rift. These data were acquired aboard the R/V NYANJA, using a 48-channel hydrophone streamer and a single, 140 cubic-inch

airgun, with offsets up to 1450 m. Seismic data were processed at project PROBE's computing facility using DIGICON software. Due to the large extent of the rift, the seismic profiles were shot at spacing of 12-28 km between dip lines, with closer spacing in the northern part of the Rift (Ruzizi and part of the Kigoma Basin). The 24-fold profiles were later reprocessed by ION Geophysical Company. Due to the short seismic streamer employed, this data set was challenged with problems of multiples especially in the northern part of the Ruzizi Province.

2) Project PROBE data reprocessing

Following renewed interest in hydrocarbon exploration in the rift valley, the Project PROBE data set were reprocessed in 2016 in order to minimize noise and improve the resolution at the basin scale. ION Geophysical used the following procedures during reprocessing. It undertook pre-processing data validations such as Geometry QC and line tie analysis, residual bubble energy removal, zero phase conversion, and velocity analysis. Then it carried the following routines during processing: spherical spreading correction, noise attenuation, multiple attenuation, SRME (free surface multiple attenuation), time variant filter (water bottom-dependent), F-X deconvolution, residual noise attenuation, prestack time and depth migration. Post-processing workflows involved the following: post-Migration Radon de-multiple, mute, deconvolution, time variant band-pass filter, gain application, time-to-depth conversion, and coherency filter.

3) 2012/2014 data processing

The commercial data sets were processed on board the MV Mwongozo using the Fugro UniSeis seismic processing package. The onboard processing was conducted twice (preliminary and full). The pre-processing included reformatting from SEG-D format, gain application, noise analysis, multiple attenuation, and stacking. The data were then sorted into 80-fold CMP gathers. The initial processing used the following workflow: Offset check; inverted channels check; missed shot check; Near Trace display; each 50th shot display; noise analysis for whole line in a “before first arrival” window; auxiliary channel check; top mute picking; brute velocity analysis; and brute stack. Then the full processing onboard was undertaken by using the following workflow: conversion into FSI internal format (Floating point); Butterworth Filter 8 Hz 18dB/oct 100 Hz 53dB/oct; T² gain compensation; instrumental delay correction 1 ms; surface relative multiple elimination; velocity analysis: 1 km interval; parabolic radon demultiple based on above mentioned velocity analysis; dip move out; sorted to CDP gather 80 fold; navigation merged with CDP position from P1/90; NMO correction; outer mute in CDP gather; stack: offset weighted; FX Deconvolution; KIRCHHOFF migration 100/200 traces half width; time variable filter: Time: LOW_filter-HI_filter = 0:16-300; 750:12-250; 1250:8-200; 1500:8-150; gun and cable compensation, final amplitude scaling: Gain (dB) = 4.0t; conversion to SEG-Y format; resample to 4 ms; minimum phase; American Polarity; navigation referenced to CDP position; water bottom referred to MSL; CDP X, Y coordinates at bytes: 73-76, 77-80; Shotpoint at byte 17-20; and DP at byte 21-24.

Fugro performed the final full processing in its office, and the following routine was used: processing and parameter tests; seismic data and observers’ logs from the survey

review; transcription; Recording System Delay and Amplitude Recovery; bulk time shift of 1 ms; T2

amplitude gain recovery; trace editing and acquisition noise removal; bad shot removal and channel editing; Surface Related Multiple Attenuation; CDP Sorting (sorted into 80 fold CDP gathers); navigation assignment; Velocity analysis; NMO; Mute: outer mute in CDP gather; Parabolic Radon Demultiple; Dip Move Out; The Poststack included the following: FX and FK parameters; Kirchoff Migration of 100/200 traces half width; Time variable filter; gun and cable compensation; band pass filters; Final amplitude scaling: GAIN (db) = 4.0t; Conversion to SEG-Y format, resample to 4 ms; minimum phase; American Polarity; and navigation referenced to CDP position, water bottom referred to MSL.

Analytical signals

Commonly, magnetic anomaly patterns are affected by a combination of variations in the Earth's background field as well as potential remnant magnetization present in magnetic source bodies (Kebede and Mammo, 2021). To overcome this challenge, we use the analytical signal defined by Eq. 1(Beiki, 2010).

$$|As(x, y, z)| = \sqrt{\left(\frac{\partial M}{\partial x}\right)^2 + \left(\frac{\partial M}{\partial y}\right)^2 + \left(\frac{\partial M}{\partial z}\right)^2} \quad (1)$$

whereby M is the TMI-RTP. The AS enables the identification of anomaly patterns associated with magnetized geology regardless of the positivity or negativity of a magnetic

anomaly (**Figure S3**). Long wavelength AS data captures deep seated, regional magnetic sources, whereas short wavelength, residual AS data represents shallow seated, local magnetic sources (Al-Ibiari et al., 2018). The structures were extracted manually by carefully tracing the lineaments.

Tilt-Derivative

The tilt-derivative method considers a magnetic tilt angle that is a normalized derivative according to the ratio of the vertical and horizontal derivatives of the RTP field. The tilt angle was first derived by Miller and Singh (1994), then refined by Verduzco (2004) and later modified by Salem et al. (2007). The tilt angle is computed as the arctangent of ratio of the first vertical derivative to the first horizontal derivatives of the magnetic/gravity field (Salem et al., 2007; 2008; 2013). It ranges between -45° and 45° whereby zero contours locate the edges of the source (**Figure S3**). However, its amplitude varies between -90° and 90° , and it has three rates: negative (outside the source), zero (close to the edge of the source), and positive (over the source) (Ibraheem et al., 2018). This technique overcomes the noise effect by discriminating the shallow sources from the intermediate sources, however, it fails to image sources buried at considerable depths (Arisoy and Dikmen 2013; Kebede and Mammo, 2021). The tilt-angle derivative detects edges of geological bodies and structures by normalizing all the edges in a data set (Kolawole et al., 2018a) (**Figure S3**).

Adaptive Tilt Angle (ATA) and Tilt Angle from analytical signal

FTG data are often underutilized because many interpreters rely more on the vertical gravity gradient anomaly (T_{zz}) component while ignoring the horizontal component data. A better approach is to combine all or partial sets of FTG components into new tensor variables as suggested by Murphy (2004) and Murphy and Brewster (2007). This approach simplifies the identification of the shape, size, and orientation of target structures within the sub-surface geological complexity (Kebede and Mammo, 2021). For instance, Salem et al. (2013) proposed the approach so called “Adaptive Tilt Angle” that combines three components: T_{xz} , T_{yz} and T_{zz} as shown below.

$$\theta_a = \tan^{-1} \left[a \frac{T_{zz}}{\sqrt{T_{xz}^2 + T_{yz}^2}} \right] \quad (2)$$

where a is structural index and θ_a is ATA.

The ATA is like the Tilt Derivative for the case of magnetic data as described above. Thus, the zero contours correspond to the edges of source bodies and are used to delineate lineaments (**Figure S4**).

Kebede and Mammo (2021) proposed another tilt angle (TA) that is computed using the analytic signal generated from the FTG data components T_{zz} , T_{xx} and T_{yy} as described in Eq.3. The advantage of the TA is its ability to decipher structural features of the area more accurately while overcoming the problem of noise sensitivity that is often encountered when using conventional analytical signal maps (Kebede and Mammo, 2021).

$$\theta = \tan^{-1} \left[\frac{\frac{\partial |As(x,y,z)|}{\partial z}}{\sqrt{\left(\frac{\partial |As(x,y,z)|}{\partial x}\right)^2 + \left(\frac{\partial |As(x,y,z)|}{\partial y}\right)^2}} \right] \quad (3)$$

where θ is Tilt Angle and $|As(x, y, z)|$ is Analytic Signal.

To delineate lineaments, we first extract zero contours from the TA maps, and then extract the lineaments from zero contours. To validate the method, we plotted both the existing and extracted lineaments on the same map (**Figure S4**).

Automatic edge detection on tilt derivative horizontal (TDX)

Tilt Derivative Horizontal (TDX) is the amplitude of the horizontal gradient that is normalized to the absolute value of the vertical derivative (Cooper and Cowan, 2006). It is defined by Eq.4.

$$TDX = \tan^{-1} \left[\frac{\left(\frac{\partial M}{\partial x}\right)^2 + \left(\frac{\partial M}{\partial y}\right)^2}{\left|\frac{\partial M}{\partial z}\right|} \right] \quad (4)$$

where $\partial M/\partial x$, $\partial M/\partial y$, and $\partial M/\partial z$ are the first derivative of the gravity field (M) in the x, y, and z directions. It is advantageous over the conventional Tilt Derivative in delineating both deep and shallow sources (**Figure S4**).

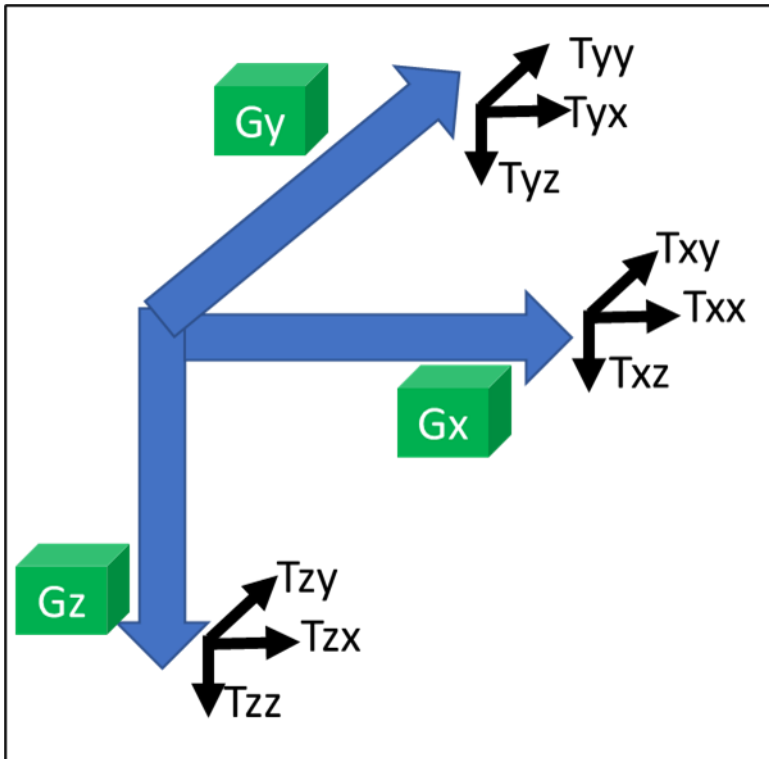


Figure S2. Vectors (in blue) and Tensors (in black) of the 3D Full Tensor Gradiometry field. Note that three vectors of FTG produce nine component tensor field (T_{xy} , T_{xx} , T_{xz} , T_{yy} , T_{yx} , T_{yz} , T_{zy} , T_{zx} , and T_{zz}) of which when summed results into the five independent tensors, modified after Blake (1995).

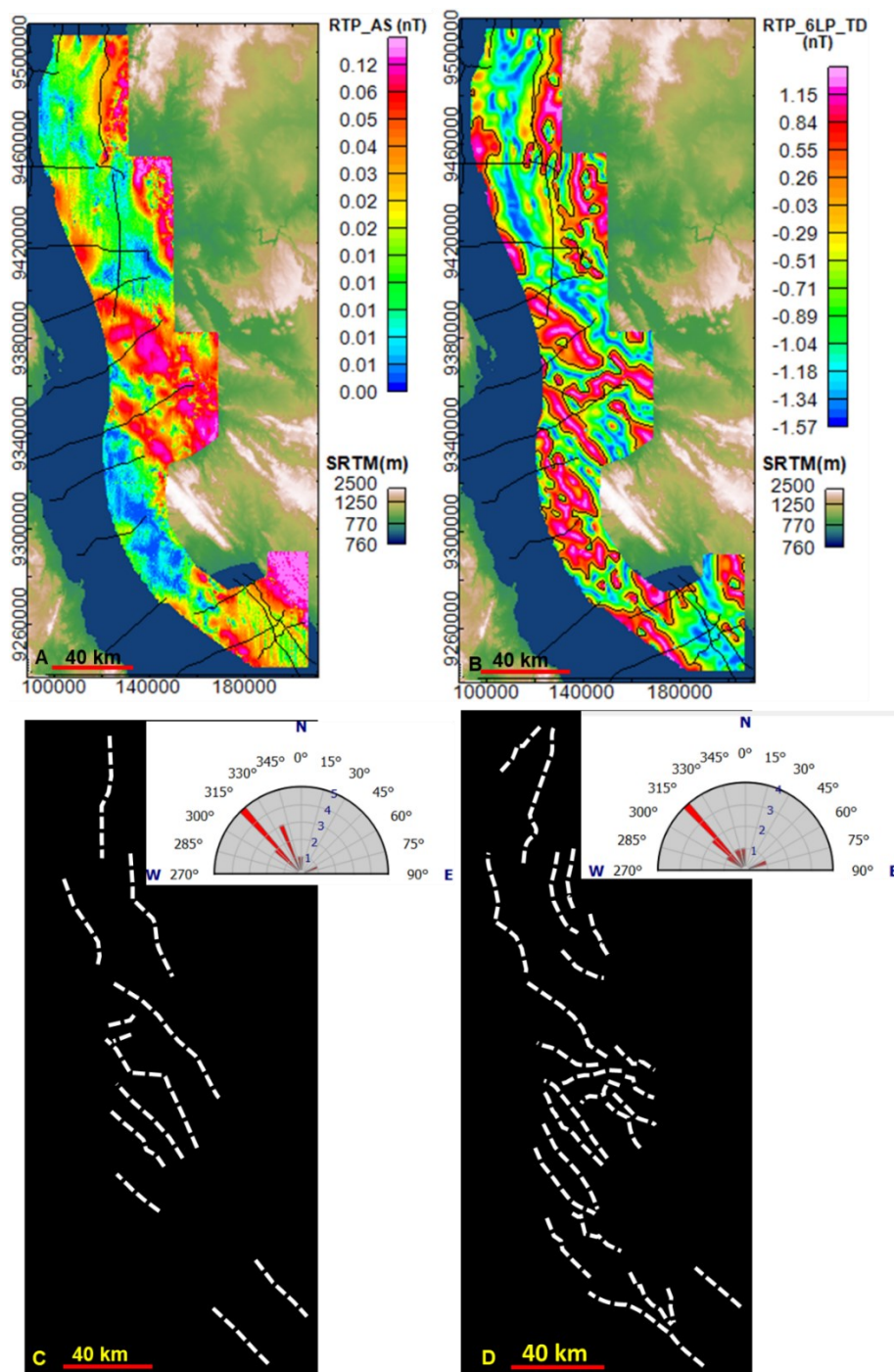


Figure S3: (A) Analytical signal of the RTP TMI showing anomaly patterns associated with magnetised geology. Note a NW-SE striking magnetic body in the central part of the survey. (B) Tilt Derivative of a long wavelength (i.e., 6 km) low pass filtered RTP TMI showing shallow structures; negative values represent areas outside the source, zero values

represent areas close to the edge of the source, and positive values represent areas over the source. Note a primary NW-SE strike and a secondary E-W strike of the lineaments. (D)

Structures extracted from A. (E) Structures extracted from B.

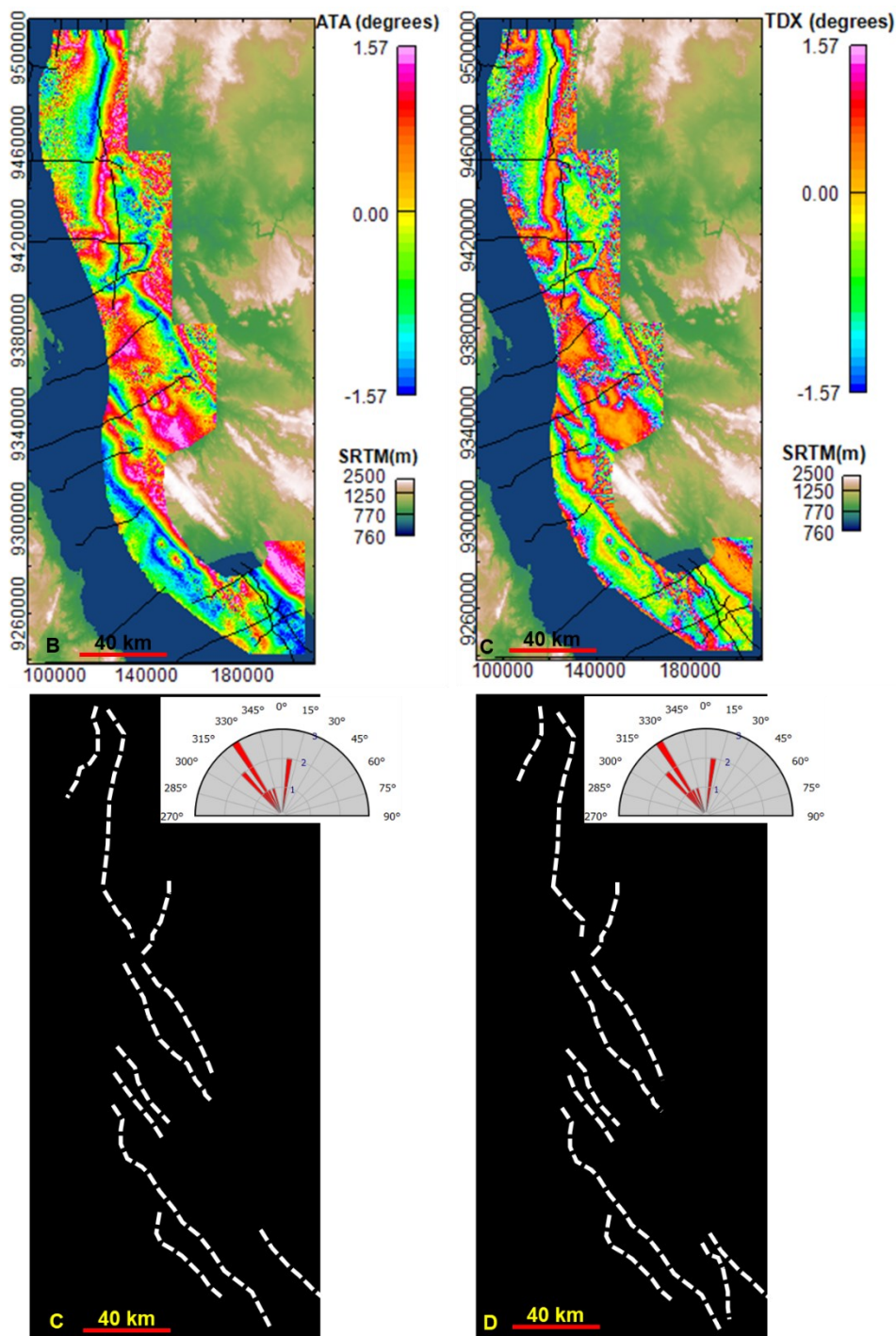


Figure S4. (A) Adaptive Tilt Angle anomaly from the gravity anomaly (T_z). It combines three components: T_{xz} , T_{yz} and T_{zz} . Note the lineaments striking NW-SE in the central and southern part and NNE-SSW in the northern part of the survey area. (B) TDX exhibits

lineaments like those from ATA anomaly, but more clearly delineated. (D) Structures extracted from A. (E) Structures extracted from B.

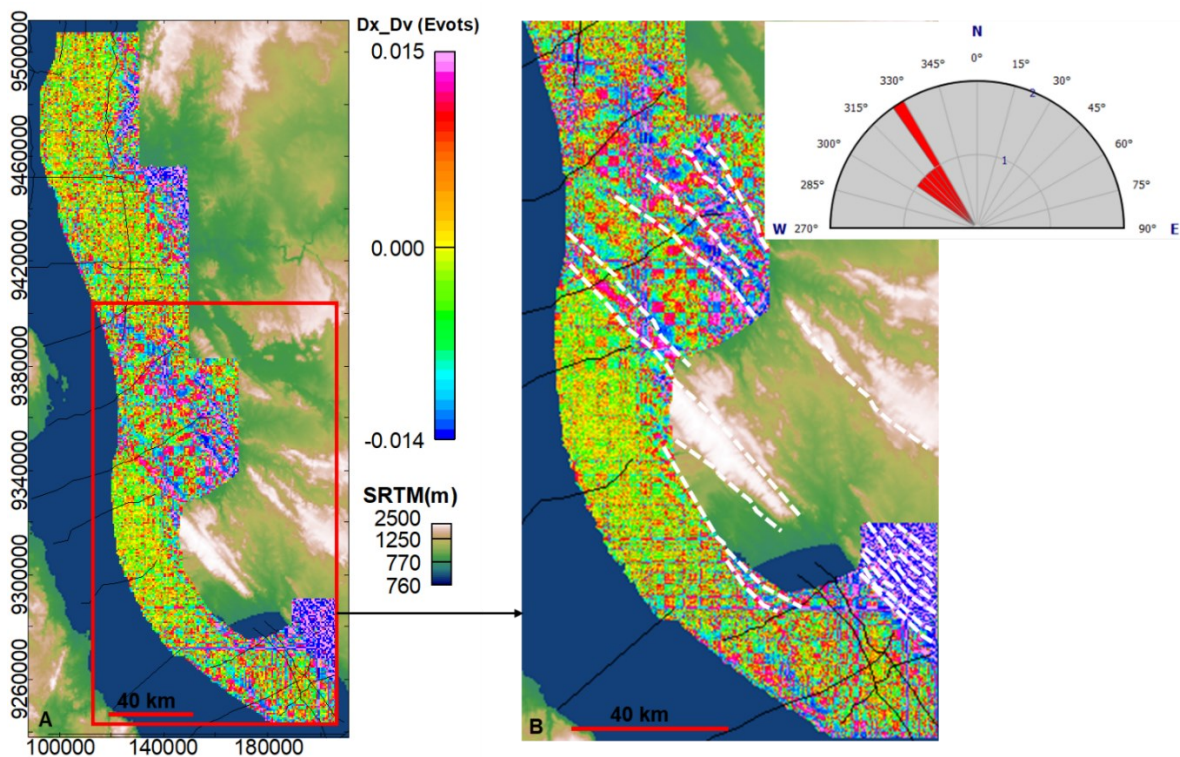


Figure S5: (A) First horizontal derivative of the Vertical Derivative of the Aeromagnetic data. (B) Zoomed in region of (A). Note the NW-SE striking structures; rift structures have strikes aligned with basement structures.

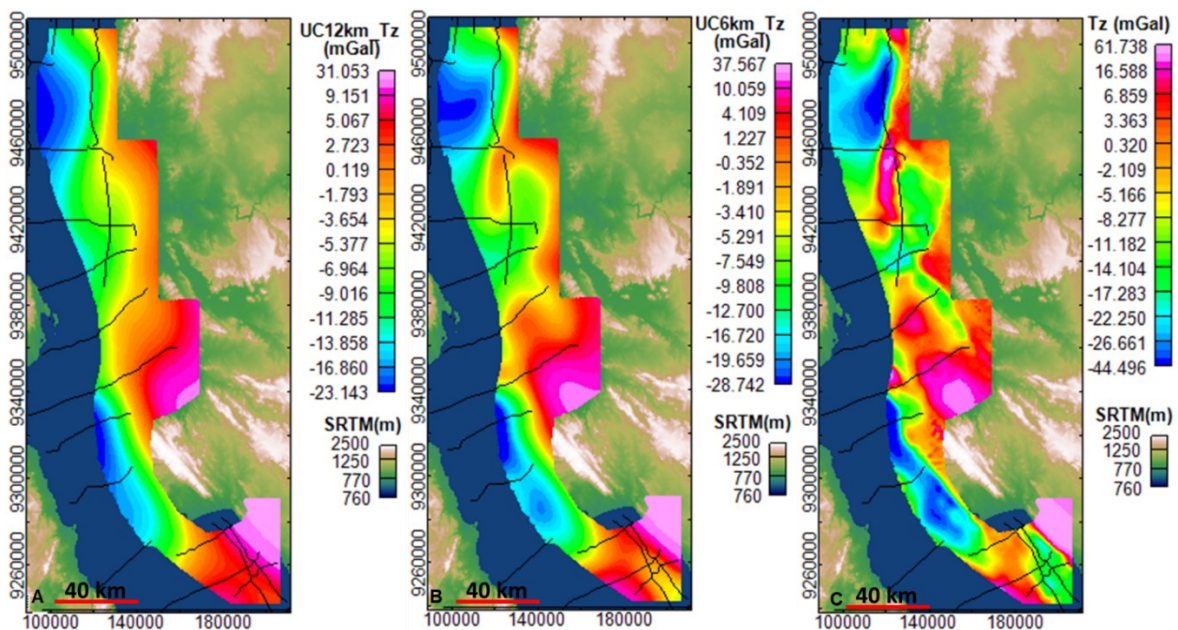


Figure S6: Analysis of the NNE-SSE lineament in the north-eastern part of the Kigoma Province from gravity anomaly. The prominent N-S lineament is not visible under the unfiltered Tz (A) and under the residual between the Tz upward continued by 6 km and the unfiltered TZ (B), but it is not visible under long wavelength which is the Tz upward continued by 12 km (C). The absence of the prominent N-S lineament in the north basin in panel C, indicates the dominance of long wavelength content of the map, relative to panel B which dominated by intermediate wavelength anomalies. However, in panel A, the lineament becomes prominent, indicating the relatively shorter wavelength content of the data. Also note that the KIR is more prominent under shorter wavelengths, suggesting the dominance of basement material and absence of thick sedimentary material on the ridge. Note the Malagarasi River pathways in (A) as it delivers sediments to the offshore part of lake.

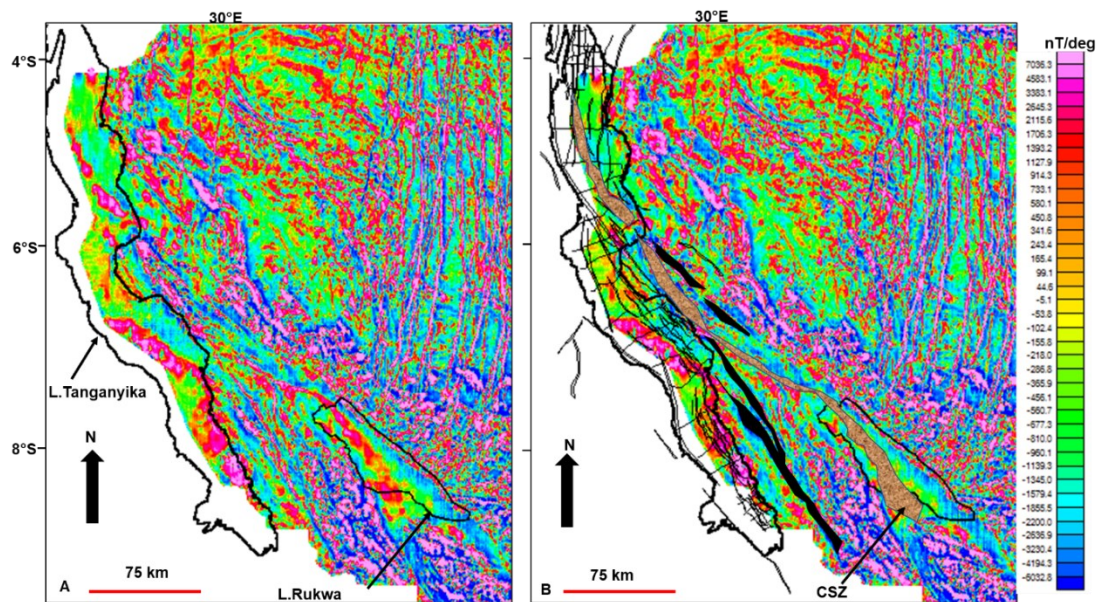


Figure S7: (A) Uninterpreted vertical derivative of 1-km resolution regional magnetic data, reduced to pole. (B) Interpretation of (A) overlaid with the interpreted faults. Note the CSZ extending from the Rukwa Rift to the Lake Tanganyika Rift modified after Kolawole et al. (2021). The thick black polygons are suggested to represent Pre-Cambrian fabrics.

Supplemental Material for Chapter 4

Introduction

This Supplementary Information provides additional explanation to the model parameters and outputs presented in the main paper.

1) Modelling parameters

We have integrated the FastScape algorithm (Braun and Willett, 2013) that solves the stream power law to predict landscape evolution, and the Linear Upslope Model (LM) (Smith and Barstad, 2004) to analyse and document the topographic evolution and hydrological connectivity of the lakes Tanganyika and Rukwa in the vicinity of the Rungwe volcanic. The model parameters are presented in **Table S1**.

Table S1: Model parameters

Input Parameter	Range	Input Parameter	Range
DEM		Uplift rate	0.1 to 100 mm/yr
Latitude		Lapse rate	-1 to -7 °C /km
Precipitation base	10 to 80 mm	Drainage area exponent	0.5 to 1.02
Wind speed	1 to 100 ms ⁻¹	Slope exponent	0.0005-0.00005
Wind direction		Soil deposition coefficient	0.0005-0.00005
Conversion time	200 to 2000 s	Bedrock deposition coefficient	0.0005-0.00005
Fallout time	200 to 2000 s	Soil (channel) incision coefficient	0.0005-0.00005
Moist stability frequency	0 to 0.01 s ⁻¹	Bedrock (incision) incision coefficient	0.0005-0.00005
Water vapor scale height	1 to 5 km	Background precipitation rate	0 to 5 mm/h
Moist adiabatic lapse rate	-5 to -9°Ckm ⁻¹	Vertical wavenumber	0.01 to 0.0001
Reference density	0.001 to 0.02 kg/m ⁻³	Volcano uplift rate	1 cm/yr
Sub-uplift ratio	1.5	Maximum slip rate	1 cm/yr
Extension rate	1E-4 m/yr	Fault tip growth	1E-6 m/yr

1) Additional model output figures

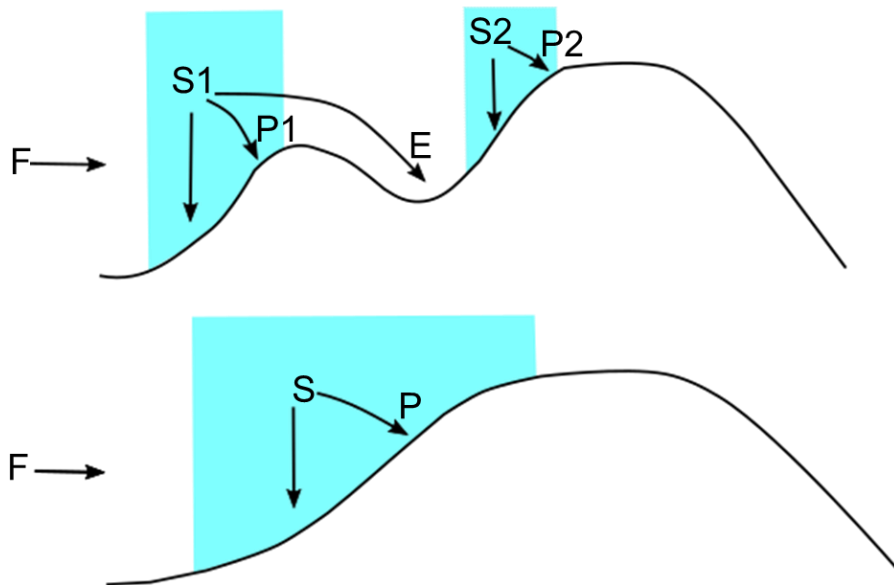


Figure S8: An illustration of water budget on a windward slope with incoming moisture flux (F), upslope condensation source (S in the shaded region) and precipitation (P) modified after Smith & Barstad (2004). The top sketch is a multiscale rise scenario whereas the bottom represents a smooth rise.

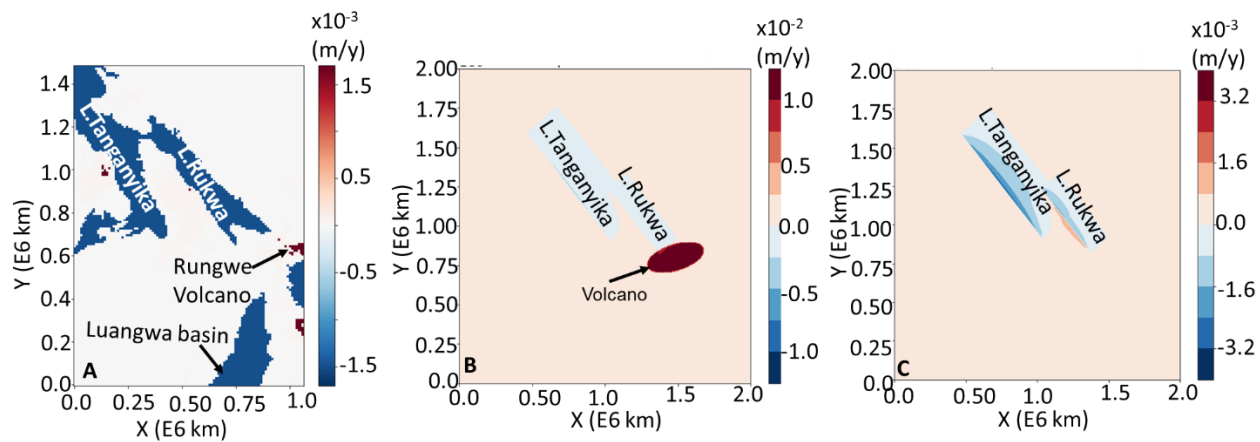


Figure S9: A) Uplift rate and subsidence rates for Model 1. B) Uplift rates and subsidence rates for Model 2. C) Uplift rate and subsidence rates for Model 3. Note that in models 2 and 3, the subsidence rates of the pseudo-lakes are controlled by the slip rate border faults.

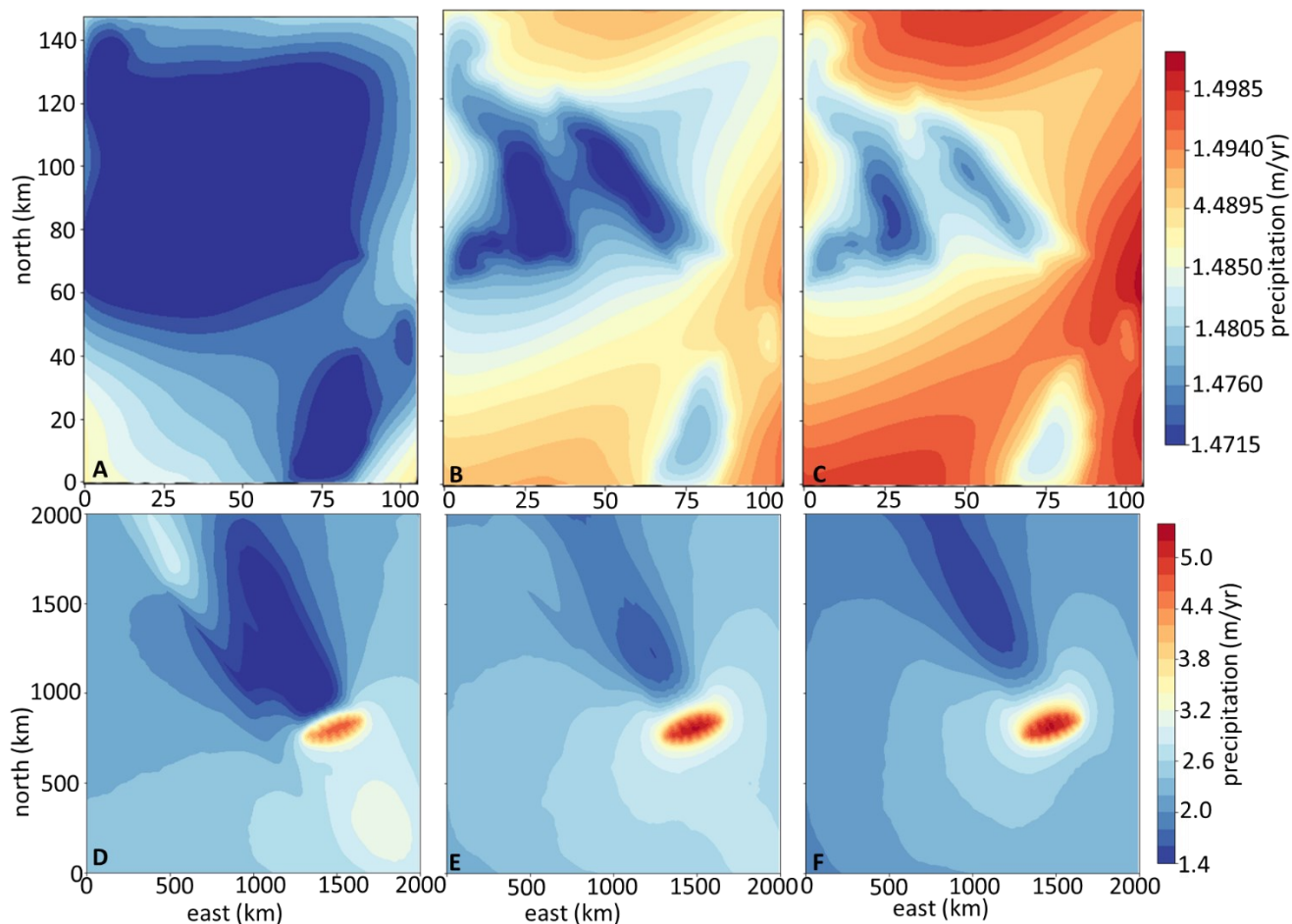


Figure S10: Wind speed sensitivity analysis on precipitation distribution. A) Scenario 1 of Model 1 with wind speed =5 m/s, B) Scenario 2 of Model 1 with wind speed =10 m/s, C) Scenario 2 of Model 1 with wind speed =15 m/s. Note that the precipitation rate increases as the wind speed increases. A) Scenario 1 of Model 2 with wind speed =5 m/s, B) Scenario 2 of Model 2 with wind speed =10 m/s, C) Scenario 2 of Model 2 with wind speed =15 m/s. Note that the precipitation rate increases as the wind speed increases especially around the volcano.

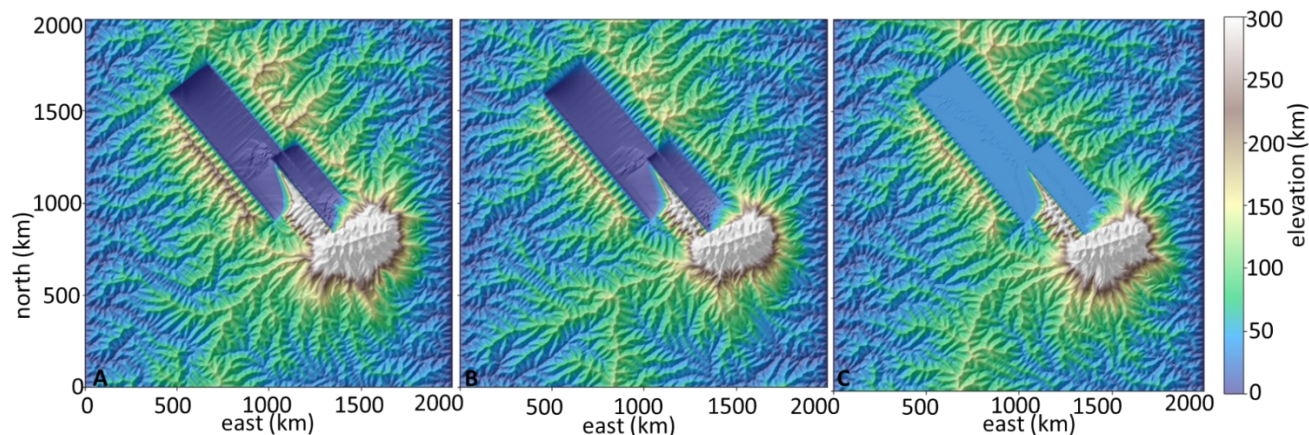


Figure S11: Wind speed sensitivity analysis on topography evolution. A) Scenario 1 of Model 2 with wind speed =5 m/s, B) Scenario 2 of Model 2 with wind speed =10 m/s, C) Scenario 2 of Model 2 with wind speed =15 m/s. Note that the elevation changes as the wind speed increases. Note how the deformations around the connection between the lakes smoothens out with wind speed increase. However, it is shown that the elevation of the footwall of western border fault of Lake Tanganyika decreases as the wind speed increases.

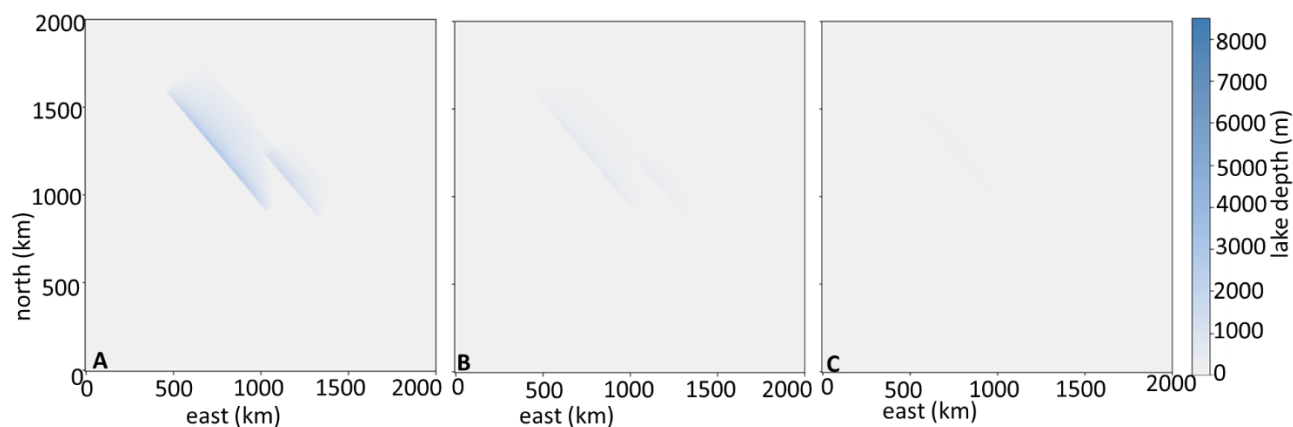


Figure S12: Wind speed sensitivity analysis on lake depth. A) Scenario 1 of Model 2 with wind speed =5 m/s, B) Scenario 2 of Model 2 with wind speed =10 m/s, C) Scenario 2 of Model 2 with wind speed =15 m/s. Note that as the wind speed increases, the lake depth decreases.

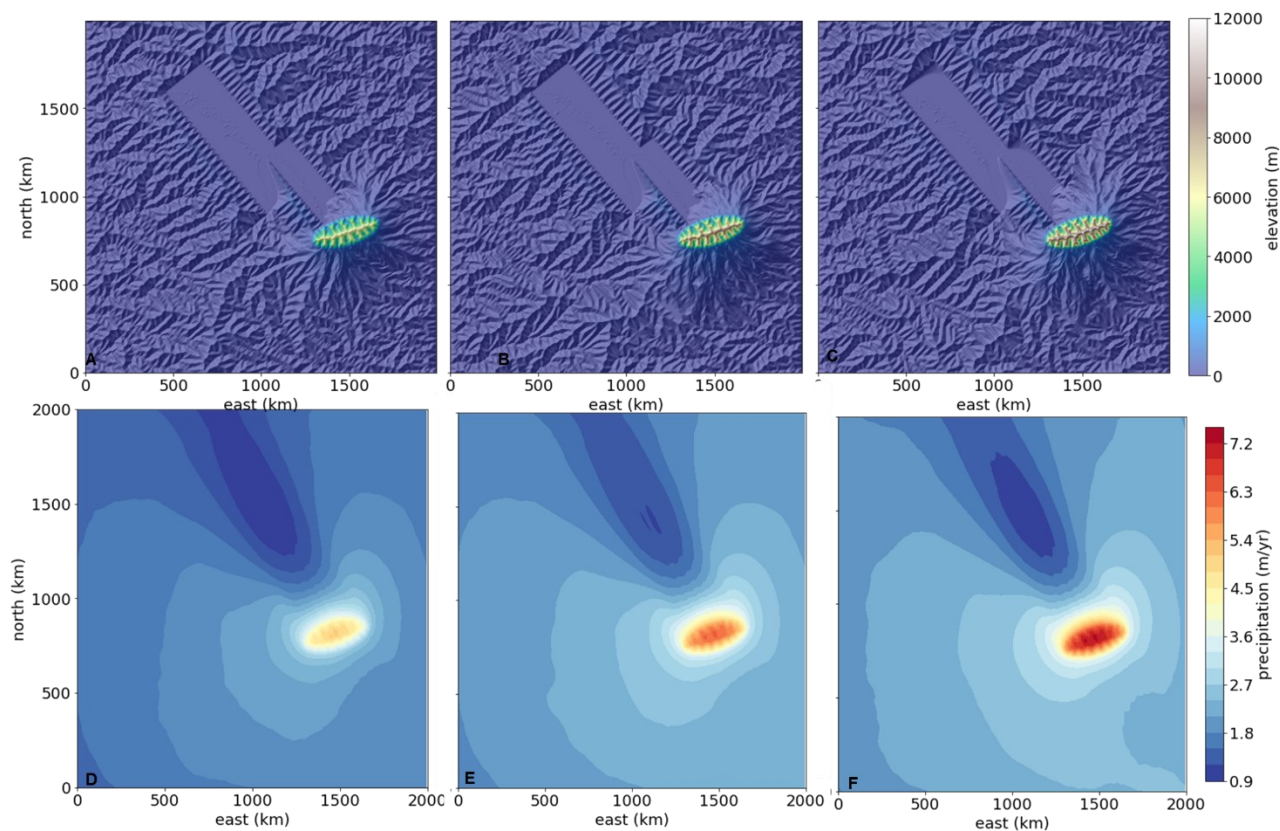


Figure S13: Model 2 sensitivity analysis. (A) and (D) represent topography and precipitation rate output respectively when the volcanic uplift rate is 1×10^{-2} m/yr. (B) and (E) represent topography and precipitation rate output respectively when the volcanic uplift rate is 1.5×10^{-2} m/yr. (C) and (F) represent topography and precipitation rate output respectively when the volcanic uplift rate is 2×10^{-2} m/yr. Note that, as the volcanic uplift rate increases, the elevation of the topography increases as well as the maximum precipitation rate.

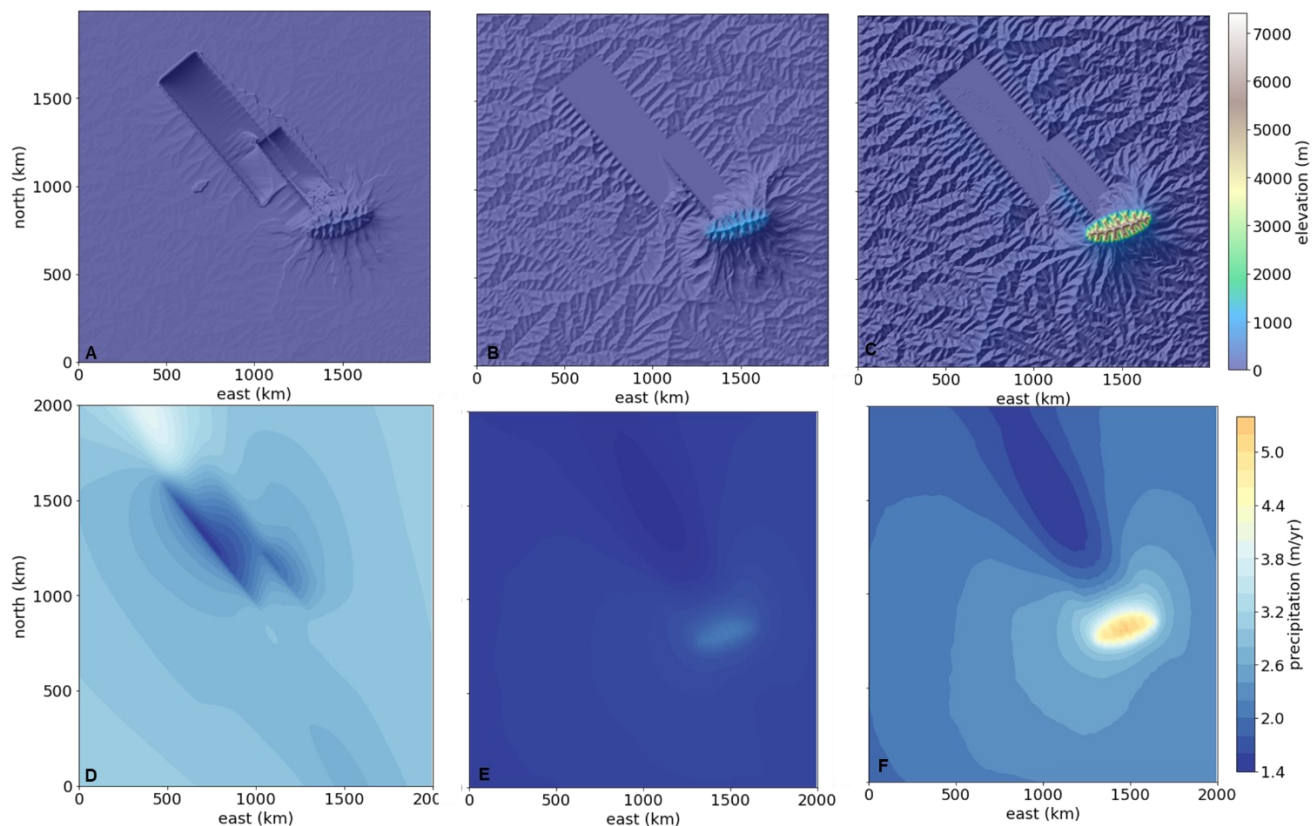


Figure S14: Model 2 sensitivity analysis. (A) and (D) represent topography and precipitation rate output respectively when the erodibility coefficient is $8E-4 \text{ m l}^{-2} \text{ m yr}^{-1}$. (B) and (E) represent topography and precipitation rate output respectively when the erodibility coefficient is $8E-5 \text{ m l}^{-2} \text{ m yr}^{-1}$. (C) and (F) represent topography and precipitation rate output respectively when the erodibility coefficient is $8E-6 \text{ m l}^{-2} \text{ m yr}^{-1}$. Note that, as the erodibility coefficient increases, the elevation of the topography increases, however, there is no a clear relationship between the erodibility coefficient and precipitation rate.

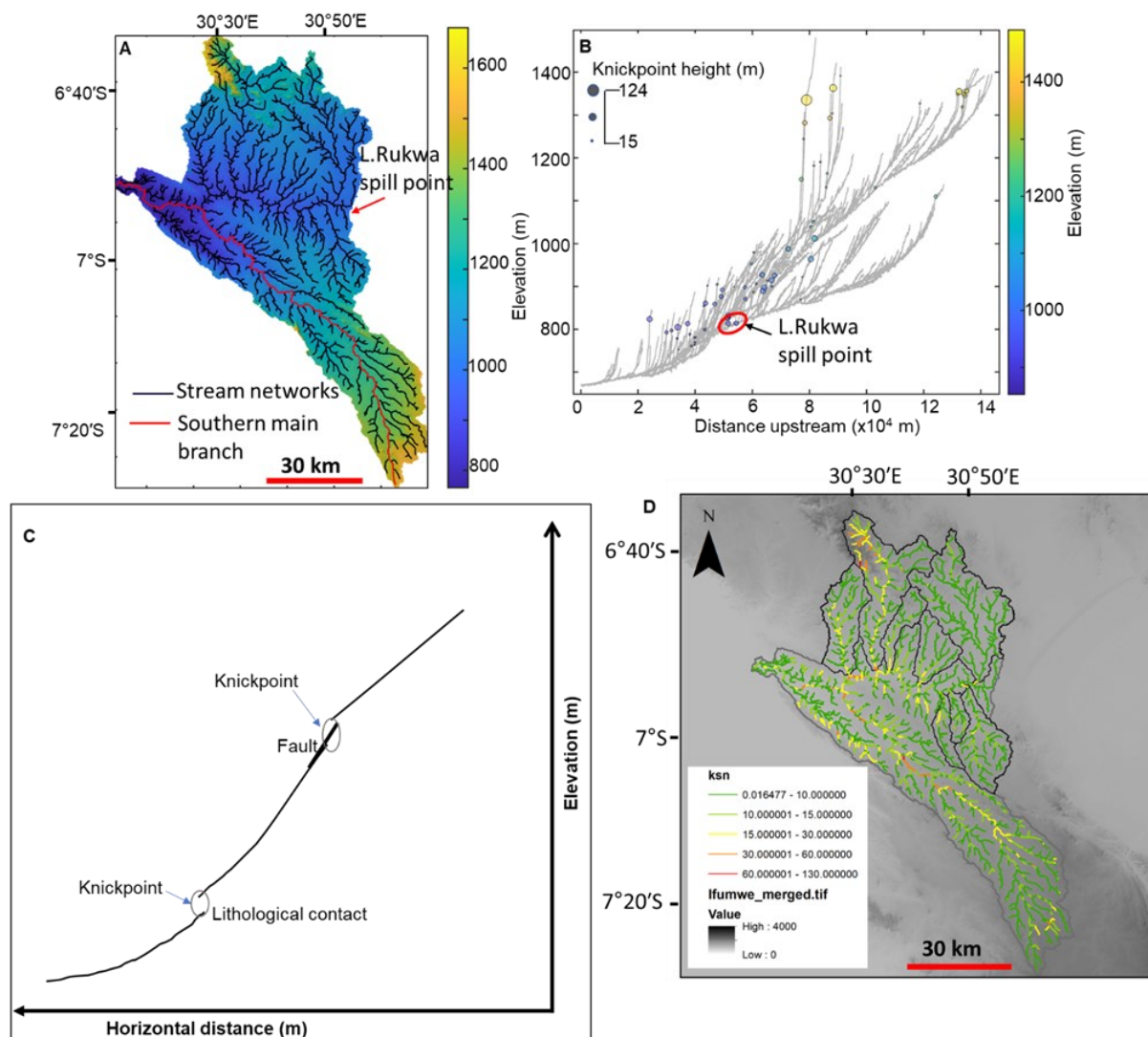


Figure S15: Analysis of knickpoints from the Ifumwe tributaries extracted from a 30m resolution SRTM. (A) Ifumwe catchment with northern and southern branches identified. Note that several tributaries join the northern branch nearly at a right angle. (B) Stream profiles extracted from the Ifumwe catchment using the Topographic Analysis Kit (TAK) for TopoToolbox (MATLAB) tools (Forte and Whipple, 2019). The upper part and lower part are the southern branch and northern branch respectively. Red oval represents the Lake Rukwa spill point. (C) A schematic diagram of a longitudinal profile showing the knickpoint formation along stream channels due to different factors modified after Ahmed et al. (2019). Note that faulting or uplift causes steep

knickpoints. (D) Steepness index (K_{sn}) for Ifumwe River tributaries, analysed tributaries in grey. K_{sn} of all tributaries increases at junction with North Branch.

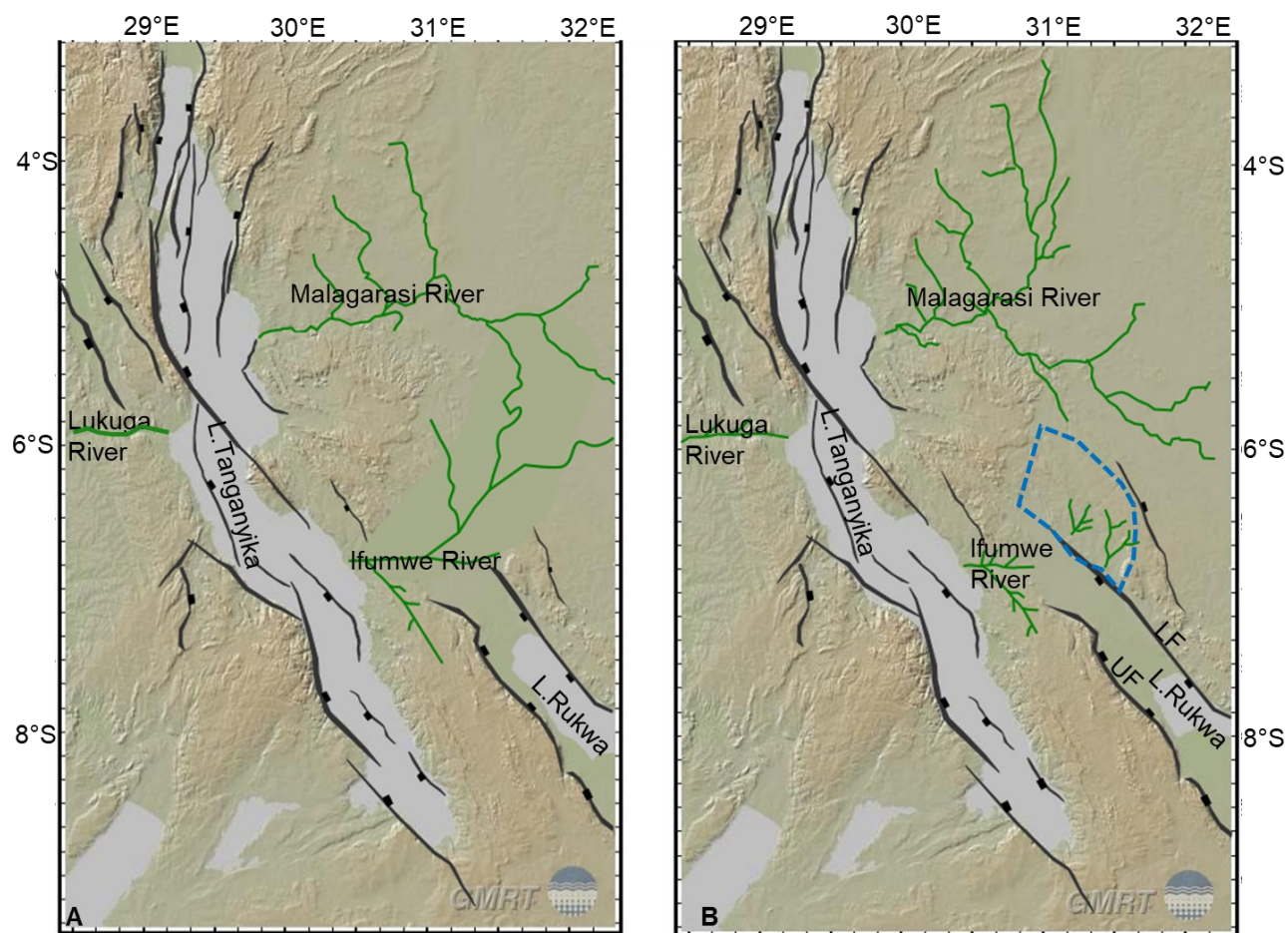


Figure S16: Conceptual illustration of the large paleo-Ifumwe River, an alternative explanation for the formation of the Karema deltaic deposits. (A) Paleogeography during the deposition of the Karema deltaic deposits. Note that during that time, the Malagarasi River was connected with the Ifumwe River causing larger drainage area for the Ifumwe River. It was during that time when the Karema delta was formed. (B) Late stage of the Ifumwe and Malagarasi Rivers. During that time, the continued north-westwards propagation of the Lupa fault caused the local uplift

(marked by blue dashed polygon) that also caused the disconnection of the Malagarasi River from the Ifumwe River. Consequently, the drainage area of the Ifumwe River shrunk as observed today. LF= Lupa Fault, UF = Ufipa Fault. Figure made with GeoMapApp (www.geomapapp.org) / CC BY (Ryan et al., 2009).

References

- Abbate, A., Papini, M. and Longoni, L., 2021. Extreme rainfall over complex terrain: An application of the linear model of orographic precipitation to a case study in the Italian pre-alps. *Geosciences*, 11(1), p.18.
- Ahmed, M.F. and Rogers, J.D., 2013, October. Thalweg profiles and knickpoints as useful discriminators of prehistoric landslide dams in Northern Pakistan. In 125th Annual meeting Geological Society of America, Denver Colorado, Oct (pp. 24-28).
- Ahmed, M.F., Ali, M.Z., Rogers, J.D. and Khan, M.S., 2019. A study of knickpoint surveys and their likely association with landslides along the Hunza River longitudinal profile. *Environmental earth sciences*, 78(5), pp.1-15.
- Ahmed, M.F., Rogers, J.D. and Ismail, E.H., 2018. Knickpoints along the upper Indus River, Pakistan: An exploratory survey of geomorphic processes. *Swiss Journal of Geosciences*, 111(1), pp.191-204.
- Al-Ibiari, M.G., Ismail, A.A., El-Khateef, A.A., Basheer, A.A., El-laban, A.M. and Tarek, Y., 2018. Analysis and interpretation of aeromagnetic data for Wadi Zeidun area, Central Eastern Desert, Egypt. *Egyptian journal of petroleum*, 27(3), pp.285-293.

- Alin, S.R. and Cohen, A.S., 2003. Lake-level history of Lake Tanganyika, East Africa, for the past 2500 years based on ostracode-inferred water-depth reconstruction. *Palaeogeography, Palaeoclimatology, Palaeoecology*, 199(1-2), pp.31-49. [https://doi.org/10.1016/S0031-0182\(03\)00484-X](https://doi.org/10.1016/S0031-0182(03)00484-X).
- Alken, P., Thébaud, E., Beggan, C.D., Amit, H., Aubert, J., Baerenzung, J., Bondar, T.N., Brown, W.J., Califf, S., Chambodut, A. and Chulliat, A., 2021. International geomagnetic reference field: the thirteenth generation. *Earth, Planets and Space*, 73(1), pp.1-25.
- Alpert, P. and Shafir, H., 1989. Mesoscale distribution of orographic precipitation: Numerical study and comparison with precipitation derived from radar measurements. *Journal of Applied Meteorology and Climatology*, 28(10), pp.1105-1117.
- Andersen, L.S. and Unrug, R., 1984. Geodynamic evolution of the Bangweulu Block, northern Zambia. *Precambrian Research*, 25(1-3), pp.187-212.
- Anderson, R.S. and Anderson, S.P., 2010. *Geomorphology: the mechanics and chemistry of landscapes*. Cambridge University Press.
- Arisoy, M.Ö. and Dikmen, Ü., 2013. Edge detection of magnetic sources using enhanced total horizontal derivative of the tilt angle. *Yerbilimleri*, 34(1), pp.73-82.
- Athy, L.F., 1930. Density, porosity, and compaction of sedimentary rocks. *AAGP Bulletin*, 14(1), pp.1-24.
- Bader, M.J. and Roach, W.T., 1977. Orographic rainfall in warm sectors of depressions. *Quarterly Journal of the Royal Meteorological Society*, 103(436), pp.269-280.

- Baker, B.H., 1971. Explanatory note on the structure of the southern part of the African rift system. *Tectonics of Africa*, 6, pp.543-548.
- Bardwell, K., Bagge, M., Archard, G., McMahon, A., Sutton, E., Keeley, M., Banks, N (Intern Information Technologies Ltd, Oxon, South-central England, UK). *The Petroleum Potential of the Luangwa Valley*, 1992. (unpublished)
- Barker, P. and Gasse, F., 2003. New evidence for a reduced water balance in East Africa during the Last Glacial Maximum: implication for model-data comparison. *Quaternary Science Reviews*, 22(8-9), pp.823-837.
- Barker, P., Telford, R., Gasse, F. and Thevenon, F., 2002. Late Pleistocene and Holocene palaeohydrology of Lake Rukwa, Tanzania, inferred from diatom analysis. *Palaeogeography, Palaeoclimatology, Palaeoecology*, 187(3-4), pp.295-305.
- Barstad, I. and Smith, R.B., 2005. Evaluation of an orographic precipitation model. *Journal of Hydrometeorology*, 6(1), pp.85-99.
- Barstad, I., Grabowski, W.W. and Smolarkiewicz, P.K., 2007. Characteristics of large-scale orographic precipitation: Evaluation of linear model in idealized problems. *Journal of Hydrology*, 340(1-2), pp.78-90.
- Batumike, J.M., Griffin, W.L., Belousova, E.A., Pearson, N.J., O'Reilly, S.Y. and Shee, S.R., 2008. LAM-ICPMS U–Pb dating of kimberlitic perovskite: Eocene–Oligocene kimberlites from the Kundelungu Plateau, DR Congo. *Earth and Planetary Science Letters*, 267(3-4), pp.609-619.
- Beacom, L.E., Holdsworth, R.E., McCaffrey, K.J.W. and Anderson, T.B., 2001. A quantitative study of the influence of pre-existing compositional and fabric

- heterogeneities upon fracture-zone development during basement reactivation. Geological Society, London, Special Publications, 186(1), pp.195-211.
- Becker, Alfred, and Harald Bugmann. "Global change and mountain regions—an IGBP initiative for collaborative research." *Global Change and Protected Areas*. Springer, Dordrecht, 2001. 3-9.
- Beiki, M., 2010. Analytic signals of gravity gradient tensor and their application to estimate source location. *Geophysics*, 75(6), pp.159-174.
- Bellahsen, N., Leroy, S., Autin, J., Razin, P., d'Acremont, E., Sloan, H., Pik, R., Ahmed, A. and Khanbari, K., 2013. Pre-existing oblique transfer zones and transfer/transform relationships in continental margins: new insights from the southeastern Gulf of Aden, Socotra Island, Yemen. *Tectonophysics*, 607, pp.32-50.
- Bergonzini, L., Richard, Y., Petit, L. and Camberlin, P., 2004. Zonal circulations over the Indian and Pacific Oceans and the level of Lakes Victoria and Tanganyika. *International Journal of Climatology: A Journal of the Royal Meteorological Society*, 24(13), pp.1613-1624.
- Bhuiyan, M.A.E., Nikolopoulos, E.I., Anagnostou, E.N., Quintana-Seguí, P. and Barella-Ortiz, A., 2018. A nonparametric statistical technique for combining global precipitation datasets: Development and hydrological evaluation over the Iberian Peninsula. *Hydrology and Earth System Sciences*, 22(2), pp.1371-1389.
- Biggs, J., Anthony, E.Y. and Ebinger, C.J., 2009. Multiple inflation and deflation events at Kenyan volcanoes, East African Rift. *Geology*, 37(11), pp.979-982. <https://doi.org/10.1130/G30133A.1>.

- Biggs, J., Anthony, E.Y. and Ebinger, C.J., 2009. Multiple inflation and deflation events at Kenyan volcanoes, East African Rift. *Geology*, 37(11), pp.979-982. <https://doi.org/10.1130/G30133A.1>.
- Blake, R., 1995. *Potential Theory in Gravity & Magnetic Application*.
- Boniface, N., Schenk, V. and Appel, P., 2012. Paleoproterozoic eclogites of MORB-type chemistry and three Proterozoic orogenic cycles in the Ubendian Belt (Tanzania): Evidence from monazite and zircon geochronology, and geochemistry. *Precambrian Research*, 192, pp.16-33.
- Borg, G. and Shackleton, R.M., 1997. The tanzania and ne-zaire cratons. *Oxford Monographs on Geology and Geophysics*, 35, pp.608-619.
- Borrego, D., Nyblade, A.A., Accardo, N.J., Gaherty, J.B., Ebinger, C.J., Shillington, D.J., Chindandali, P.R., Mbogoni, G., Ferdinand, R.W., Mulibo, G. and O'Donnell, J.P., 2018. Crustal structure surrounding the northern Malawi rift and beneath the Rungwe Volcanic Province, East Africa. *Geophysical Journal International*, 215(2), pp.1410-1426.
- Bosworth, W., 1992. Mesozoic and early Tertiary rift tectonics in East Africa. *Tectonophysics*, 209(1-4), pp.115-137.
- Bousquet, O. and Smull, B.F., 2003. Observations and impacts of upstream blocking during a widespread orographic precipitation event. *Quarterly Journal of the Royal Meteorological Society: A journal of the atmospheric sciences, applied meteorology and physical oceanography*, 129(588), pp.391-409.
- Braun, J., Willett, S.D., 2013. A very efficient $O(n)$, implicit and parallel method to solve the stream power equation governing fluvial incision and landscape evolution.

Geomorphology 180-181, 170–179.
<http://dx.doi.org/10.1016/j.geomorph.2012.10.008>.

Brooks, J.L., 1950. Speciation in ancient lakes (concluded). *The Quarterly Review of Biology*, 25(2), pp.131-176. <https://doi.org/10.1086/397539>.

Buck, W.R., Karner, G.D., Taylor, B., Driscoll, N.W. and Kohlstedt, D.L., 2004. Consequences of asthenospheric variability on continental rifting. *Rheology and deformation of the lithosphere at continental margins*, 62, pp.1-30. <https://doi.org/10.7312/karn12738-002>.

Bugmann, H., 2001. *Global change and mountain regions* (No. 363.73874 G562g). Stockholm, Sweden: IGBP.

Burgess, C.F., Rosendahl, B.R., Sander, S., Burgess, C.A., Lambiase, J., Derksen, S. and Meader, N., 1988. The structural and stratigraphic evolution of Lake Tanganyika: a case study of continental rifting. In *Developments in geotectonics* (Vol. 22, pp. 859-881). Elsevier. <https://doi.org/10.1016/b978-0-444-42903-2.50040-3>.

Butterworth, S., 1930. On the theory of filter amplifiers. *Wireless Engineer*, 7(6), pp.536-541.

Cahen, L., 1978. *Synthèse des connaissances relatives au Groupe (anciennement Série) de la Lukuga (Permien du Zaïre)*.

Cardillo, M., Orme, C.D.L. and Owens, I.P., 2005. Testing for latitudinal bias in diversification rates: an example using New World birds. *Ecology*, 86(9), pp.2278-2287.

- Caroletti, Giulio Nils, and Ida Barstad. "An assessment of future extreme precipitation in western Norway using a linear model." *Hydrology and Earth System Sciences* 14, no. 11 (2010): 2329-2341.
- Carroll, A.R. and Bohacs, K.M., 1999. Stratigraphic classification of ancient lakes: Balancing tectonic and climatic controls. *Geology*, 27(2), pp.99-102.
- Cartwright, J., Bouroullec, R., James, D. and Johnson, H., 1998. Polycyclic motion history of some Gulf Coast growth faults from high-resolution displacement analysis. *Geology*, 26(9), pp.819-822.
- Cartwright, J.A., Trudgill, B.D. and Mansfield, C.S., 1995. Fault growth by segment linkage: an explanation for scatter in maximum displacement and trace length data from the Canyonlands Grabens of SE Utah. *Journal of Structural Geology*, 17(9), pp.1319-1326.
- Chakravarthi, V. and Sundararajan, N., 2007. 3D gravity inversion of basement relief—A depth-dependent density approach. *Geophysics*, 72(2), pp.I23-I32.
- Childs, C., Watterson, J. and Walsh, J.J., 1995. Fault overlap zones within developing normal fault systems. *Journal of the Geological Society*, 152(3), pp.535-549.
- Chisenga, C., Kolawole, F., Rajaonarison, T., Atekwana, E.A., Yan, J. and Shemang, E.M., 2023. Localization of large intraplate earthquakes along faulted density-contrast boundaries: Insights from the 2017 Mw6.5 Botswana earthquake. *Journal of African Earth Sciences*, 197, p.104752.
- Chorowicz, J., 2005. The east African rift system. *Journal of African Earth Sciences*, 43(1-3), pp.379-410.

- Choubert, G., Faure-Muret, A. and Sougy, J., 1968. International tectonic map of Africa 1: 5,000,000, Sheet 1. Assoc. Afr. Geol. Surv., UNESCO, Paris.
- Cohen, A.S., Lezzar, K.E., Tiercelin, J.J. and Soreghan, M., 1997. New palaeogeographic and lake-level reconstructions of Lake Tanganyika: implications for tectonic, climatic and biological evolution in a rift lake. *Basin research*, 9(2), pp.107-132. <https://doi.org/10.1046/j.1365-2117.1997.00038.x>.
- Cohen, A.S., Palacios-Fest, M.R., Msaky, E.S., Alin, S.R., McKee, B., O'Reilly, C.M., Dettman, D.L., Nkotagu, H. and Lezzar, K.E., 2005. Paleolimnological investigations of anthropogenic environmental change in Lake Tanganyika: IX. Summary of paleorecords of environmental change and catchment deforestation at Lake Tanganyika and impacts on the Lake Tanganyika ecosystem. *Journal of Paleolimnology*, 34(1), pp.125-145. <https://doi.org/10.1007/s10933-005-2422-4>.
- Cohen, A.S., Soreghan, M.J. and Scholz, C.A., 1993. Estimating the age of formation of lakes: an example from Lake Tanganyika, East African Rift system. *Geology*, 21(6), pp.511-514. [https://doi.org/10.1130/0091-7613\(1993\)021%3C0511:etaofo%3E2.3.co;2](https://doi.org/10.1130/0091-7613(1993)021%3C0511:etaofo%3E2.3.co;2).
- Cohen, A.S., Van Bocxlaer, B., Todd, J.A., McGlue, M., Michel, E., Nkotagu, H.H., Grove, A.T. and Delvaux, D., 2013. Quaternary ostracodes and molluscs from the Rukwa Basin (Tanzania) and their evolutionary and paleobiogeographic implications. *Palaeogeography, Palaeoclimatology, Palaeoecology*, 392, pp.79-97. <https://doi.org/10.1016/j.palaeo.2013.09.007>.

- Coleman, J.M. and Roberts, H.H., 1989. Deltaic coastal wetlands. In Coastal Lowlands (pp. 1-24). Springer, Dordrecht. https://doi.org/10.1007/978-94-017-1064-0_1.
- Collier, C.G., 1975. A representation of the effects of topography on surface rainfall within moving baroclinic disturbances. Quarterly Journal of the Royal Meteorological Society, 101(429), pp.407-422.
- Cooper, G.R.J. and Cowan, D.R., 2006. Enhancing potential field data using filters based on the local phase. Computers & Geosciences, 32(10), pp.1585-1591.
- Costa, K.M., Russell, J.M., Vogel, H. and Bijaksana, S., 2015. Hydrological connectivity and mixing of Lake Towuti, Indonesia in response to paleoclimatic changes over the last 60,000 years. Palaeogeography, Palaeoclimatology, Palaeoecology, 417, pp.467-475.
- Coulter, G.W., Tiercelin, J.J., Mondegeur, A., Hecky, R.E. and Spigel, R.H., 1991. Lake Tanganyika and its life.
- Craig, H., 1974. Lake Tanganyika geochemical and hydrographic study: 1973 expedition.
- Crane, K. and Bonatti, E., 1987. The role of fracture zones during early Red Sea rifting: structural analysis using Space Shuttle radar and LANDSAT imagery. Journal of the Geological Society, 144(3), pp.407-420.
- Crochet, P., Jóhannesson, T., Jónsson, T., Sigurðsson, O., Björnsson, H., Pálsson, F. and Barstad, I., 2007. Estimating the spatial distribution of precipitation in Iceland using a linear model of orographic precipitation. Journal of Hydrometeorology, 8(6), pp.1285-1306.

- Croissant, T. and Braun, J., 2014. Constraining the stream power law: a novel approach combining a landscape evolution model and an inversion method. *Earth surface dynamics*, 2(1), pp.155-166.
- Dagang, Z., Xiangang, M., Xitao, Z., Zhaogang, S., Zufeng, X.U., Chaobin, Y.A.N.G., Zhibang, M.A., Zhonghai, W.U., Zhenhan, W.U. and Jianping, W.A.N.G., 2004. Evolution of an ancient large lake in the southeast of the northern Tibetan Plateau. *Acta Geologica Sinica-English Edition*, 78(4), pp.982-992.
- Daly, C., Neilson, R.P. and Phillips, D.L., 1994. A statistical-topographic model for mapping climatological precipitation over mountainous terrain. *Journal of Applied Meteorology and Climatology*, 33(2), pp.140-158.
- Daly, M.C., 1988. Crustal shear zones in Central Africa: a kinematic approach to Proterozoic tectonics. *Episodes Journal of International Geoscience*, 11(1), pp.5-11. doi:10.18814/epiiugs/1988/v11i1/003
- Daly, M.C., Chorowicz, J. and Fairhead, J.D., 1989. Rift basin evolution in Africa: the influence of reactivated steep basement shear zones. Geological Society, London, *Special Publications*, 44(1), pp.309-334.
- Day, J.J., Cotton, J.A. and Barraclough, T.G., 2008. Tempo and mode of diversification of Lake Tanganyika cichlid fishes. *PloS one*, 3(3), p.e1730. <https://doi.org/10.1371/journal.pone.0001730>.
- Degens, E.T., von Herzen, R.P., Wong, H.K., Deuser, W.G. and Jannasch, H.W., 1973. Lake Kivu: structure, chemistry and biology of an East African rift lake. *Geologische Rundschau*, 62(1), pp.245-277. <https://doi.org/10.1007/BF01826830>.

- Delvaux, D. and Barth, A., 2010. African stress pattern from formal inversion of focal mechanism data. *Tectonophysics*, 482(1-4), pp.105-128. <https://doi.org/10.1016/j.tecto.2009.05.009>.
- Delvaux, D. and Williamson, D., 2008. Interactions between Great Lakes level change, tectonics and volcanism in the Rungwe Volcanic Province, SW highlands of Tanzania. *Journal of African Earth Sciences*, 58(5), pp.764-777. <https://doi.org/10.1016/j.jafrearsci.2009.11.011>.
- Delvaux, D., 2001a. Karoo rifting in western Tanzania: precursor of Gondwana break-up. *Contributions to geology and paleontology of Gondwana in honor of Helmut Wopfner: Cologne, Geological Institute, University of Cologne*, pp.111-125.
- Delvaux, D., 2001b. Tectonic and palaeostress evolution of the Tanganyika-Rukwa-Malawi rift segment, East African rift System. *Peri-Tethys Memoir*, 6, pp.545-567.
- Delvaux, D., Kervyn, F., Macheyeke, A.S. and Temu, E.B., 2012. Geodynamic significance of the TRM segment in the East African Rift (W-Tanzania): Active tectonics and paleostress in the Ufipa plateau and Rukwa basin. *Journal of Structural Geology*, 37, pp.161-180. 37, 161–180. doi:10.1016/j.jsg.2012.01.008
- Dettman, D.L., Palacios-Fest, M.R., Nkotagu, H.H. and Cohen, A.S., 2005. Paleolimnological investigations of anthropogenic environmental change in Lake Tanganyika: VII. Carbonate isotope geochemistry as a record of riverine runoff. *Journal of Paleolimnology*, 34(1), pp.93-105. <https://doi.org/10.1007/s10933-005-2400-x>.

- Dickinson, J.L., Murphy, C.A. and Robinson, J.W. 2012 Interpretation of FTG data using Tensor Axis Realignment: ASEG 2012, Brisbane, Australia, Extended Abstract.
- Dickinson, W.R., 2013. Rejection of the lake spillover model for initial incision of the Grand Canyon, and discussion of alternatives. *Geosphere*, 9(1), pp.1-20.
- Drogue, G., Humbert, J., Deraisme, J., Mahr, N. and Freslon, N., 2002. A statistical–topographic model using an omnidirectional parameterization of the relief for mapping orographic rainfall. *International Journal of Climatology: A Journal of the Royal Meteorological Society*, 22(5), pp.599-613.
- Eberle, D., 1988. Basic geophysical aspects of gold prospection in Nyanzian greenstone belts of Tanzania. Open-fi2e Report, 86.
- Ebinger, C.J., 1989. Tectonic development of the western branch of the East African rift system. *Geological Society of America Bulletin*, 101(7), pp.885-903.
[https://doi.org/10.1130/0016-7606\(1989\)101%3C0885:tdotwb%3E2.3.co;2](https://doi.org/10.1130/0016-7606(1989)101%3C0885:tdotwb%3E2.3.co;2).
- Ebinger, C.J., Deino, A.L., Tesha, A.L., Becker, T. and Ring, U., 1993. Tectonic controls on rift basin morphology: evolution of the Northern Malawi (Nyasa) Rift. *Journal of Geophysical Research: Solid Earth*, 98(B10), pp.17821-17836.
- Ebinger, C.J., Keir, D., Bastow, I.D., Whaler, K., Hammond, J.O., Ayele, A., Miller, M.S., Tiberi, C. and Hautot, S., 2017. Crustal structure of active deformation zones in Africa: Implications for global crustal processes. *Tectonics*, 36(12), pp.3298-3332.
- Ebinger, C.J., Oliva, S.J., Pham, T.Q., Peterson, K., Chindandali, P., Illsley-Kemp, F., Drooff, C., Shillington, D.J., Accardo, N.J., Gallacher, R.J. and Gaherty, J., 2019. Kinematics

of active deformation in the Malawi rift and Rungwe Volcanic Province, Africa. *Geochemistry, Geophysics, Geosystems*, 20(8), pp.3928-3951.

Edmond, J.M., Stallard, R.F., Craig, H., Craig, V., Weiss, R.F. and Coulter, G.W., 1993. Nutrient chemistry of the water column of Lake Tanganyika. *Limnology and Oceanography*, 38(4), pp.725-738.

Ehsan Bhuiyan, M.A., Nikolopoulos, E.I. and Anagnostou, E.N., 2019a. Machine learning-based blending of satellite and reanalysis precipitation datasets: A multiregional tropical complex terrain evaluation. *Journal of Hydrometeorology*, 20(11), pp.2147-2161.

Ehsan Bhuiyan, M.A., Nikolopoulos, E.I., Anagnostou, E.N., Polcher, J., Albergel, C., Dutra, E., Fink, G., Martínez-de la Torre, A. and Munier, S., 2019b. Assessment of precipitation error propagation in multi-model global water resource reanalysis. *Hydrology and Earth System Sciences*, 23(4), pp.1973-1994.

Evjen, H.M., 1936. The place of the vertical gradient in gravitational interpretations. *Geophysics*, 1(1), pp.127-136.

Felton, A.A., Russell, J.M., Cohen, A.S., Baker, M.E., Chesley, J.T., Lezzar, K.E., McGlue, M.M., Pigati, J.S., Quade, J., Stager, J.C. and Tiercelin, J.J., 2007. Paleolimnological evidence for the onset and termination of glacial aridity from Lake Tanganyika, Tropical East Africa. *Palaeogeography, Palaeoclimatology, Palaeoecology*, 252(3-4), pp.405-423. <https://doi.org/10.1016/j.palaeo.2007.04.003>.

- Fernandez-Alonso, M. and Theunissen, K., 1998. Airborne geophysics and geochemistry provide new insights in the intracontinental evolution of the Mesoproterozoic Kibaran belt (Central Africa). *Geological Magazine*, 135(2), pp.203-216.
- Ferrier, K.L., Huppert, K.L. and Perron, J.T., 2013. Climatic control of bedrock river incision. *Nature*, 496(7444), pp.206-209.
- Florio, G., 2018. Mapping the depth to basement by iterative rescaling of gravity or magnetic data. *Journal of Geophysical Research: Solid Earth*, 123(10), pp.9101-9120.
- Fontijn, Karen, Damien Delvaux, Gerald GJ Ernst, Matthieu Kervyn, Evelyne Mbede, and Patric Jacobs. "Tectonic control over active volcanism at a range of scales: Case of the Rungwe Volcanic Province, SW Tanzania; and hazard implications." *Journal of African Earth Sciences* 58, no. 5 (2010): 764-777.
- Forte, A.M. and Whipple, K.X., 2019. Short communication: The Topographic Analysis Kit (TAK) for TopoToolbox, *Earth Surf. Dynam.*, 7, 87–95.
- Furman, T., 2007. Geochemistry of East African Rift basalts: an overview. *Journal of African Earth Sciences*, 48(2-3), pp.147-160. <https://doi.org/10.1016/j.jafrearsci.2006.06.009>.
- Garcia-Castellanos, D., Vergés, J., Gaspar-Escribano, J. and Cloetingh, S., 2003. Interplay between tectonics, climate, and fluvial transport during the Cenozoic evolution of the Ebro Basin (NE Iberia). *Journal of Geophysical Research: Solid Earth*, 108(B7).
- Gardner, T.W., 1983. Experimental study of knickpoint and longitudinal profile evolution in cohesive, homogeneous material. *Geological Society of America Bulletin*, 94(5), pp.664-672.

- Gawthorpe, R.L. and Leeder, M.R., 2000. Tectono-sedimentary evolution of active extensional basins. *Basin Research*, 12(3-4), pp.195-218.
- Gawthorpe, R.L., Leeder, M.R., Kranis, H., Skourtsos, E., Andrews, J.E., Henstra, G.A., Mack, G.H., Muravchik, M., Turner, J.A. and Stamatakis, M., 2018. Tectono-sedimentary evolution of the Plio-Pleistocene Corinth rift, Greece. *Basin Research*, 30(3), pp.448-479. <https://doi.org/10.1111/bre.12260>.
- Gawthorpe, R.L., Sharp, I., Underhill, J.R. and Gupta, S., 1997. Linked sequence stratigraphic and structural evolution of propagating normal faults. *Geology*, 25(9), pp.795-798. [https://doi.org/10.1130/0091-7613\(1997\)025%3C0795:lssase%3E2.3.co;2](https://doi.org/10.1130/0091-7613(1997)025%3C0795:lssase%3E2.3.co;2).
- George, R., Rogers, N. and Kelley, S., 1998. Earliest magmatism in Ethiopia: Evidence for two mantle plumes in one flood basalt province. *Geology*, 26(10), pp.923-926. [https://doi.org/10.1130/0091-7613\(1998\)026%3C0923:emieef%3E2.3.co;2](https://doi.org/10.1130/0091-7613(1998)026%3C0923:emieef%3E2.3.co;2).
- Georgis, J.F., Roux, F., Chong, M. and Pradier, S., 2003. Triple-Doppler radar analysis of the heavy rain event observed in the Lago Maggiore region during MAP IOP 2b. *Quarterly Journal of the Royal Meteorological Society: A journal of the atmospheric sciences, applied meteorology and physical oceanography*, 129(588), pp.495-522.
- Gillespie, P.A., Walsh, J.T. and Watterson, J., 1992. Limitations of dimension and displacement data from single faults and the consequences for data analysis and interpretation. *Journal of Structural Geology*, 14(10), pp.1157-1172.
- Gillman, C., 1933. The hydrology of Lake Tanganyika. Government printer. *Bull. Geol Surv. Dar-es-Salaam. Tanz.*, 5, pp.1-27.

- Granser, H., 1987. Three-dimensional interpretation of gravity data from sedimentary basins using an exponential density-depth function. *Geophysical Prospecting*, 35(9), pp.1030-1041.
- Grauch, V.J.S. and Hudson, M.R., 2011. Aeromagnetic anomalies over faulted strata. *The Leading Edge*, 30(11), pp.1242-1252.
- Guan, H., Wilson, J.L. and Makhnin, O., 2005. Geostatistical mapping of mountain precipitation incorporating autosearched effects of terrain and climatic characteristics. *Journal of Hydrometeorology*, 6(6), pp.1018-1031.
- Gupta, S., Collier, J.S., Garcia-Moreno, D., Oggioni, F., Trentesaux, A., Vanneste, K., De Batist, M., Camelbeeck, T., Potter, G., Vliet-Lanoë, V. and Arthur, J.C., 2017. Two-stage opening of the Dover Strait and the origin of island Britain. *Nature Communications*, 8(1), pp.1-12.
- Haberyan, K.A. and Hecky, R.E., 1987. The late Pleistocene and Holocene stratigraphy and paleolimnology of Lakes Kivu and Tanganyika. *Palaeogeography, palaeoclimatology, palaeoecology*, 61, pp.169-197. [https://doi.org/10.1016/0031-0182\(87\)90048-4](https://doi.org/10.1016/0031-0182(87)90048-4).
- Hack, J.T., 1957. *Studies of longitudinal stream profiles in Virginia and Maryland* (Vol. 294). US Government Printing Office.
- Hao, F., Zhou, X., Zhu, Y. and Yang, Y., 2009. Mechanisms for oil depletion and enrichment on the Shijiutuo uplift, Bohai Bay Basin, China. *AAPG bulletin*, 93(8), pp.1015-1037.
- Hecky, R.E. and Kling, H.J., 1981. The phytoplankton and protozooplankton of the euphotic zone of Lake Tanganyika: Species composition, biomass, chlorophyll content, and spatio-temporal distribution 1. *Limnology and Oceanography*, 26(3), pp.548-564.

- Heilman, E., Kolawole, F., Atekwana, E.A. and Mayle, M., 2019. Controls of basement fabric on the linkage of rift segments. *Tectonics*, 38(4), pp.1337-1366.
- Hergarten, S. and Robl, J., 2021. A simple and efficient model for orographic precipitation. *Geoscientific Model Development Discussions*, pp.1-28.
- Hinze, W.J., Von Frese, R.R., Von Frese, R. and Saad, A.H., 2013. Gravity and magnetic exploration: Principles, practices, and applications. Cambridge University Press.
- Hobbs, P.V., Easter, R.C. and Fraser, A.B., 1973. A theoretical study of the flow of air and fallout of solid precipitation over mountainous terrain: Part II. Microphysics. *Journal of Atmospheric Sciences*, 30(5), pp.813-823.
- Hokanson, K.J., Peterson, E.S., Devito, K.J. and Mendoza, C.A., 2020. Forestland-peatland hydrologic connectivity in water-limited environments: hydraulic gradients often oppose topography. *Environmental Research Letters*, 15(3), p.034021.
- Holtzschlag, D.J. and Koschik, J.A., 2002. Two-dimensional hydrodynamic model of the St. Clair-Detroit River Waterway in the Great Lakes basin (No. 1). US Department of the Interior, US Geological Survey.
- Huffman, G.J., E.F. Stocker, D.T. Bolvin, E.J. Nelkin, J.T., 2019. GPM IMERG Final Precipitation L3 1 month 0.1 degree x 0.1 degree V06, Greenbelt, MD, Goddard Earth Sciences Data and Information Services Center (GES DISC), Accessed: 01 April 2022, 10.5067/GPM/IMERG/3B-MONTH/06.
- Hussein, H.M., Marzouk, I., Moustafa, A.R. and Hurukawa, N., 2006. Preliminary seismicity and focal mechanisms in the southern Gulf of Suez: August 1994 through December 1997. *Journal of African Earth Sciences*, 45(1), pp.48-60.

- Hutchinson, M.F., 1998. Interpolation of rainfall data with thin plate smoothing splines. Part I: Two-dimensional smoothing of data with short range correlation. *Journal of Geographic Information and Decision Analysis*, 2(2), pp.139-151.
- Huziy, O. and Sushama, L., 2017. Impact of lake–river connectivity and interflow on the Canadian RCM simulated regional climate and hydrology for Northeast Canada. *Climate Dynamics*, 48(3), pp.709-725. <https://doi.org/10.1007/s00382-016-3104-9>.
- Ibraheem, I.M., Gurk, M., Tougiannidis, N. and Tezkan, B., 2018. Subsurface investigation of the Neogene Mygdonian Basin, Greece using magnetic data. *Pure and Applied Geophysics*, 175(8), pp.2955-2973.
- Ivanov, A.V., Rasskazov, S.V., Boven, A., Punzalan, L., Brandt, I.S., Brandt, S.B. and Fernandez-Alonso, M., 1999. Timing and Late Cenozoic volcanic activity and rift basin formations in the Rungwe province of Tanzania substantiated by K–Ar and $^{40}\text{Ar}/^{39}\text{Ar}$ dating. *Proceedings of Rifting in Intracontinental Setting: Baikal Rift System and other Continental Rifts, Irkutsk and Lake Baikal, Russia, August*, pp.22-30.
- Jackson, D., Helwig, J.H., Dinkelman, M.G., Silva, M. and Protacio, J.A.P., 2013, June. Integration of 2D Seismic, Gravity Gradiometry, and Magnetic Data on a Passive Margin-NE Greenland. In *75th EAGE Conference & Exhibition incorporating SPE EUROPEC 2013* (pp. cp-348). European Association of Geoscientists & Engineers.
- Jacobsen, B.H., 1987. A case for upward continuation as a standard separation filter for potential-field maps. *Geophysics*, 52(8), pp.1138-1148.

- Jaeger, K.L., Olden, J.D. and Pelland, N.A., 2014. Climate change poised to threaten hydrologic connectivity and endemic fishes in dryland streams. *Proceedings of the National Academy of Sciences*, 111(38), pp.13894-13899. <https://doi.org/10.1073/pnas.1320890111>.
- Jamaludin, S.N.F., Pubellier, M. and Sautter, B., 2021. Shallow vs. Deep Subsurface Structures of Central Luconia Province, Offshore Malaysia Reveal by Aeromagnetic, Airborne Gravity and Seismic Data. *Applied Sciences*, 11(11), p.5095.
- Jess, S., Koehn, D., Fox, M., Enkelmann, E., Sachau, T. and Aanyu, K., 2020. Paleogene initiation of the Western Branch of the East African Rift: The uplift history of the Rwenzori Mountains, Western Uganda. *Earth and Planetary Science Letters*, 552, p.116593. <https://doi.org/10.1016/j.epsl.2020.116593>.
- Johnson, A.I., 2019. *Limnology, climatology and paleoclimatology of the East African lakes*. Routledge.
- Katumwehe, A.B., Abdelsalam, M.G. and Atekwana, E.A., 2015. The role of pre-existing Precambrian structures in rift evolution: The Albertine and Rhino grabens, Uganda. *Tectonophysics*, 646, pp.117-129.
- Katz, B.J., 1990. Lacustrine basin exploration. *Case Studies and Modern Analogs: American Association of Petroleum Geologists, Memoir*, 50, p.340.
- Kebede, B. and Mammo, T., 2021. Processing and interpretation of full tensor gravity anomalies of Southern Main Ethiopian Rift. *Heliyon*, 7(4), p.e06872.
- Kelts, K., 1988. *Environments of deposition of lacustrine petroleum source rocks: an introduction*. Geological Society, London, Special Publications, 40(1), pp.3-26.

- Kennerley, J.B., 1962. Itaka. 1:125000 Map. Quarter Degree Sheet 243, with brief explanation. Geological Survey of Tanzania.
- Kilembe, E.A. and Rosendahl, B.R., 1992. Structure and stratigraphy of the Rukwa rift. *Tectonophysics*, 209(1-4), pp.143-158.
- Kinabo, B.D., Atekwana, E.A., Hogan, J.P., Modisi, M.P., Wheaton, D.D. and Kampunzu, A.B., 2007. Early structural development of the Okavango rift zone, NW Botswana. *Journal of African Earth Sciences*, 48(2-3), pp.125-136.
- King, G.C., Stein, R.S. and Rundle, J.B., 1988. The growth of geological structures by repeated earthquakes 1. Conceptual framework. *Journal of Geophysical research: solid Earth*, 93(B11), pp.13307-13318.
- Kirby, E. and Whipple, K., 2001. Quantifying differential rock-uplift rates via stream profile analysis. *Geology*, 29(5), pp.415-418. [https://doi.org/10.1130/0091-7613\(2001\)029%3C0415:QDRURV%3E2.0.CO;2](https://doi.org/10.1130/0091-7613(2001)029%3C0415:QDRURV%3E2.0.CO;2).
- Kirshbaum, D.J. and Smith, R.B., 2009. Orographic precipitation in the tropics: Large-eddy simulations and theory. *Journal of the Atmospheric Sciences*, 66(9), pp.2559-2578.
- Kjennerud, T., Lippard, S.J. and Vanhauwaert, P., 2001. Short term development of intracontinental rifts, with reference to the late Quaternary of the Rukwa Rift (East African Rift System). *Marine and petroleum geology*, 18(3), pp.307-317.
- Kolawole, F., Atekwana, E.A., Laó-Dávila, D.A., Abdelsalam, M.G., Chindandali, P.R., Salima, J. and Kalindekafe, L., 2018b. High-resolution electrical resistivity and aeromagnetic imaging reveal the causative fault of the 2009 M w 6.0 Karonga, Malawi earthquake. *Geophysical Journal International*, 213(2), pp.1412-1425.

- Kolawole, F., Atekwana, E.A., Laó-Dávila, D.A., Abdelsalam, M.G., Chindandali, P.R., Salima, J. and Kalindekafe, L., 2018a. Active deformation of Malawi rift's north basin Hinge zone modulated by reactivation of preexisting Precambrian Shear zone fabric. *Tectonics*, 37(3), pp.683-704.
- Kolawole, F., Atekwana, E.A., Laó-Dávila, D.A., Abdelsalam, M.G., Chindandali, P.R., Salima, J. and Kalindekafe, L., 2018b. Active deformation of Malawi rift's north basin Hinge zone modulated by reactivation of pre-existing Precambrian Shear zone fabric. *Tectonics*, 37(3), pp.683-704.
- Kolawole, F., Atekwana, E.A., Malloy, S., Stamps, D.S., Grandin, R., Abdelsalam, M.G., Leseane, K. and Shemang, E.M., 2017. Aeromagnetic, gravity, and Differential Interferometric Synthetic Aperture Radar analyses reveal the causative fault of the 3 April 2017 Mw 6.5 Moiyabana, Botswana, earthquake. *Geophysical Research Letters*, 44(17), pp.8837-8846.
- Kolawole, F., Firkins, M.C., Al Wahaibi, T.S., Atekwana, E.A. and Soreghan, M.J., 2021a. Rift interaction zones and the stages of rift linkage in active segmented continental rift systems. *Basin Research*, 33(6), pp.2984-3020.
- Kolawole, F., Phillips, T.B., Atekwana, E.A. and Jackson, C.A.L., 2021b. Structural inheritance controls strain distribution during early continental rifting, Rukwa rift. *Frontiers in Earth Science*, p.670.
- Kolawole, F., Vick, T., Atekwana, E.A., Laó-Dávila, D.A., Costa, A.G. and Carpenter, B.M., 2022. Strain localization and migration during the pulsed lateral propagation of the Shire Rift Zone, East Africa. *Tectonophysics*, 839, p.229499.

- Korup, O., Montgomery, D.R. and Hewitt, K., 2010. Glacier and landslide feedbacks to topographic relief in the Himalayan syntaxes. *Proceedings of the National Academy of Sciences*, 107(12), pp.5317-5322.
- Ku, C.C. and Sharp, J.A., 1983. Werner deconvolution for automated magnetic interpretation and its refinement using Marquardt's inverse modeling. *Geophysics*, 48(6), pp.754-774.
- Kyriakidis, P.C., Kim, J. and Miller, N.L., 2001. Geostatistical mapping of precipitation from rain gauge data using atmospheric and terrain characteristics. *Journal of Applied Meteorology*, 40(11), pp.1855-1877.
- Lamb, M.P., Finnegan, N.J., Scheingross, J.S. and Sklar, L.S., 2015. New insights into the mechanics of fluvial bedrock erosion through flume experiments and theory. *Geomorphology*, 244, pp.33-55.
- Lambiase, J.J. and Bosworth, W.P., 1995. Structural development and stratigraphy of the Kyokpo Pull-Apart Basin, South Korea and tectonic implications for inverted extensional basins. *Geological Society, London, Special Publications*, 88(1), pp.457-471. [https:// doi.org/10.1144/GSL.SP.1995.088.01.24](https://doi.org/10.1144/GSL.SP.1995.088.01.24).
- Lambiase, J.J., 1990. A model for tectonic control of lacustrine stratigraphic sequences in continental Rift Basins: Chapter 16, pp.265-276. <https://doi.org/10.1306/m50523c16>.
- Laó-Dávila, D.A., Al-Salmi, H.S., Abdelsalam, M.G. and Atekwana, E.A., 2015. Hierarchical segmentation of the Malawi Rift: The influence of inherited lithospheric heterogeneity and kinematics in the evolution of continental rifts. *Tectonics*, 34(12), pp.2399-2417.

- Lavayssière, A., Drooff, C., Ebinger, C., Gallacher, R., Illsley-Kemp, F., Oliva, S.J. and Keir, D., 2019. Depth extent and kinematics of faulting in the southern Tanganyika rift, Africa. *Tectonics*, 38(3), pp.842-862. <https://doi.org/10.1029/2018tc005379>.
- Lavers, D.A., Allan, R.P., Wood, E.F., Villarini, G., Brayshaw, D.J. and Wade, A.J., 2011. Winter floods in Britain are connected to atmospheric rivers. *Geophysical Research Letters*, 38(23).
- Leeder, M.R. and Gawthorpe, R.L., 1987. Sedimentary models for extensional tilt-block/half-graben basins. Geological Society, London, Special Publications, 28(1), pp.139-152. <https://doi.org/10.1144/GSL.SP.1987.028.01.11>.
- Lenoir, J.L., Liégeois, J.P., Theunissen, K. and Klerkx, J., 1994. The Palaeoproterozoic Ubendian shear belt in Tanzania: geochronology and structure. *Journal of African Earth Sciences*, 19(3), pp.169-184.
- Leopold, L.B. and Wolman, M.G., 1960. River meanders. *Geological Society of America Bulletin*, 71(6), pp.769-793.
- Lezzar, K.E., Tiercelin, J.J., Batist, M.D., Cohen, A.S., Bandora, T., Rensbergen, P.V., Turdu, C.L., Mifundu, W. and Klerkx, J., 1996. New seismic stratigraphy and Late Tertiary history of the North Tanganyika Basin, East African Rift system, deduced from multichannel and high-resolution reflection seismic data and piston core evidence. *Basin Research*, 8(1), pp.1-28. <https://doi.org/10.1111/j.1365-2117.1996.tb00112.x>.
- Lezzar, K.E., Tiercelin, J.J., Le Turdu, C., Cohen, A.S., Reynolds, D.J., Le Gall, B. and Scholz, C.A., 2002. Control of normal fault interaction on the distribution of major Neogene sedimentary depocenters, Lake Tanganyika, East African rift. *AAPG*

bulletin, 86(6), pp.1027-1059. <https://doi.org/10.1306/61eedc1a-173e-11d7-8645000102c1865d>.

Litinsky, V.A., 1989. Concept of effective density: Key to gravity depth determinations for sedimentary basins. *Geophysics*, 54(11), pp.1474-1482.

Livingstone, D.A., 1965. Sedimentation and the history of water level change in Lake Tanganyika. *Limnology and Oceanography*, 10(4), pp.607-610. <https://doi.org/10.4319/lo.1965.10.4.0607>.

Logatchev, N.A. and Zorin, Y.A., 1992. Baikal rift zone: structure and geodynamics. *Tectonophysics*, 208(1-3), pp.273-286. <https://doi.org/10.1016/B978-0-444-89912-5.50020-X>.

Lonergan, L., Cartwright, J. and Jolly, R., 1998. The geometry of polygonal fault systems in Tertiary mudrocks of the North Sea. *Journal of Structural Geology*, 20(5), pp.529-548.

Machlus, M., Enzel, Y., Goldstein, S.L., Marco, S. and Stein, M., 2000. Reconstructing low levels of Lake Lisan by correlating fan-delta and lacustrine deposits. *Quaternary International*, 73, pp.137-144.

Malin, K.H., 2017. Improved Constraint on Salt Geometry in the Southern Nordkapp Basin- Modeling salt geometry using potential field data integrated with traditional reflection seismic and well data (Master's thesis, NTNU).

Maniatis, G., Kurfeß, D., Hampel, A. and Heidbach, O., 2009. Slip acceleration on normal faults due to erosion and sedimentation—Results from a new three-dimensional

- numerical model coupling tectonics and landscape evolution. *Earth and Planetary Science Letters*, 284(3-4), pp.570-582.
- Manya, S. and Maboko, M.A., 2008. Geochemistry and geochronology of Neoproterozoic volcanic rocks of the Iramba–Sekenke greenstone belt, central Tanzania. *Precambrian Research*, 163(3-4), pp.265-278.
- Mataragio, J. and Kieley, J., 2009. Application of full tensor gradient invariants in detection of intrusion-hosted sulphide mineralization: Implications for deposition mechanisms. *First break*, 27(7).
- McGlue, M.M., Ivory, S.J., Stone, J.R., Cohen, A.S., Kamulali, T.M., Latimer, J.C., Brannon, M.A., Kimirei, I.A. and Soreghan, M.J., 2020. Solar irradiance and ENSO affect food security in Lake Tanganyika, a major African inland fishery. *Science advances*, 6(41), p.eabb2191. <https://doi.org/10.1126/sciadv.abb2191>.
- McGlue, M.M., Lezzar, K.E., Cohen, A.S., Russell, J.M., Tiercelin, J.J., Felton, A.A., Mbede, E. and Nkotagu, H.H., 2008. Seismic records of late Pleistocene aridity in Lake Tanganyika, tropical East Africa. *Journal of Paleolimnology*, 40(2), pp.635-653. <https://doi.org/10.1007/s10933-007-9187-x>.
- McGlue, M.M., Scholz, C.A., Karp, T., Ongodia, B. and Lezzar, K.E., 2006. Facies architecture of flexural margin lowstand delta deposits in Lake Edward, East African Rift: constraints from seismic reflection imaging. *Journal of Sedimentary Research*, 76(6), pp.942-958. <https://doi.org/10.2110/jsr.2006.068>.

- McKenzie, D., 1978. Some remarks on the development of sedimentary basins. *Earth and Planetary science letters*, 40(1), pp.25-32. [https://doi.org/10.1016/0012-821x\(78\)90071-7](https://doi.org/10.1016/0012-821x(78)90071-7).
- Menzies, M., Gallagher, K., Yelland, A. and Hurford, A.J., 1997. Volcanic and nonvolcanic rifted margins of the Red Sea and Gulf of Aden: crustal cooling and margin evolution in Yemen. *Geochimica et Cosmochimica Acta*, 61(12), pp.2511-2527.
- Meyer, A., 1993. Phylogenetic relationships and evolutionary processes in East African cichlid fishes. *Trends in ecology & evolution*, 8(8), pp.279-284.
- Mickus, K.L., Aiken, C.L. and Kennedy, W.D., 1991. Regional-residual gravity anomaly separation using the minimum-curvature technique. *Geophysics*, 56(2), pp.279-283.
- Mikhailov, V., Pajot, G., Diament, M. and Price, A., 2007. Tensor deconvolution: A method to locate equivalent sources from full tensor gravity data. *Geophysics*, 72(5), pp.I61-I69
- Miller, H.G. and Singh, V., 1994. Potential field tilt—a new concept for location of potential field sources. *Journal of applied Geophysics*, 32(2-3), pp.213-217.
- Milliman, J.D. and Syvitski, J.P., 1992. Geomorphic/tectonic control of sediment discharge to the ocean: the importance of small mountainous rivers. *The journal of Geology*, 100(5), pp.525-544. <https://doi.org/10.1086/629606>.
- Mohr, P.A. and Wood, C.A., 1976. Volcano spacings and lithospheric attenuation in the Eastern Rift of Africa. *Earth and Planetary Science Letters*, 33(1), pp.126-144. [https://doi.org/10.1016/0012-821X\(76\)90166-7](https://doi.org/10.1016/0012-821X(76)90166-7).

- Morales, A., Posselt, D.J. and Morrison, H., 2021. Which combinations of environmental conditions and microphysical parameter values produce a given orographic precipitation distribution? *Journal of the Atmospheric Sciences*, 78(2), pp.619-638.
- Morley, C.K. and Ngenoh, D.K., 1999. AAPG Studies in Geology# 44, Chapter 1: Introduction to the East African Rift System. *Geoscience of Rift Systems—Evolution of East Africa*, pp.1–18. <http://dx.doi.org/10.1306/st44623c1>.
- Morley, C.K., 1988. Variable extension in Lake Tanganyika. *Tectonics*, 7(4), pp.785-801. <https://doi.org/10.1029/tc007i004p00785>.
- Morley, C.K., 1989. Extension, detachments, and sedimentation in continental rifts (with particular reference to East Africa). *Tectonics*, 8(6), pp.1175-1192. <https://doi.org/10.1029/TC008i006p01175>.
- Morley, C.K., 1995. Developments in the structural geology of rifts over the last decade and their impact on hydrocarbon exploration. Geological Society, London, Special Publications, 80(1), pp.1-32.
- Morley, C.K., 2010. Stress re-orientation along zones of weak fabrics in rifts: An explanation for pure extension in ‘oblique’ rift segments? *Earth and Planetary Science Letters*, 297(3-4), pp.667-673.
- Morley, C.K., Cunningham, S.M., Harper, R.M. and Wescott, W.A., 1992. Geology and geophysics of the Rukwa rift, East Africa. *Tectonics*, 11(1), pp.69-81.
- Morley, C.K., Nelson, R.A., Patton, T.L. and Munn, S.G., 1990. Transfer zones in the East African rift system and their relevance to hydrocarbon exploration in rifts. *AAPG bulletin*, 74(8), pp.1234-1253. <https://doi.org/10.1306/0c9b2475-1710-11d7-8645000102c1865d>.

- Mtelela, C., 2018. Preliminary sedimentology and stratigraphy of the enigmatic middle lake beds succession (pleistocene?) in the Rukwa Rift Basin, Tanzania. *Tanzania Journal of Science*, 44(1), pp.75-96.
- Muirhead, J.D., Wright, L.J. and Scholz, C.A., 2019. Rift evolution in regions of low magma input in East Africa. *Earth and Planetary Science Letters*, 506, pp.332-346. <https://doi.org/10.1016/j.epsl.2018.11.004>.
- Murphy, C.A. and Dickinson, J.L., 2010, April. Geological mapping and targeting using invariant tensor analysis on full tensor gravity data. In *EGM 2010 International Workshop* (pp. cp-165). European Association of Geoscientists & Engineers.
- Murphy, C.A., 2004. The Air-FTG airborne gravity gradiometer system. *Airborne gravity*, pp.7-14.
- Murphy, C.A., Mumaw, G.R. and Zuidweg, K.A.R.E.L., 2005, June. Regional target prospecting in the Faroe-Shetland Basin area using 3D-FTG Gravity data. In *67th EAGE Conference & Exhibition* (pp. cp-1). European Association of Geoscientists & Engineers.
- Nabighian, M.N. and Hansen, R.O., 2001. Unification of Euler and Werner deconvolution in three dimensions via the generalized Hilbert transform. *Geophysics*, 66(6), pp.1805-1810.
- Neiman, P.J., Ralph, F.M., White, A.B., Kingsmill, D.E. and Persson, P.O.G., 2002. The statistical relationship between upslope flow and rainfall in California's coastal mountains: Observations during CALJET. *Monthly Weather Review*, 130(6), pp.1468-1492.

- Nelson, R.A., Patton, T.L. and Morley, C.K., 1992. Rift-segment interaction and its relation to hydrocarbon exploration in continental rift systems. *AAPG bulletin*, 76(8), pp.1153-1169.
- O'Connor, J.E. and Beebee, R.A., 2009. Floods from natural rock-material dams. *Megaflooding on Earth and Mars*, pp.128-171.
- O'Connor, J.E., Baker, V.R., Waitt, R.B., Smith, L.N., Cannon, C.M., George, D.L. and Denlinger, R.P., 2020. The Missoula and Bonneville floods—A review of ice-age megafloods in the Columbia River basin. *Earth-science reviews*, 208, p.103181.
- O'Connor, P.M., Sertich, J.J., Stevens, N.J., Roberts, E.M., Gottfried, M.D., Hieronymus, T.L., Jinnah, Z.A., Ridgely, R., Ngasala, S.E. and Temba, J., 2010. The evolution of mammal-like crocodyliforms in the Cretaceous Period of Gondwana. *Nature*, 466(7307), pp.748-751.
- O'Donnell, J.P., Adams, A., Nyblade, A.A., Mulibo, G.D. and Tugume, F., 2013. The uppermost mantle shear wave velocity structure of eastern Africa from Rayleigh wave tomography: Constraints on rift evolution. *Geophysical Journal International*, 194(2), pp.961-978. [https:// doi.org/10.1093/gji/ggt135](https://doi.org/10.1093/gji/ggt135).
- Olive, J.A., Behn, M.D. and Malatesta, L.C., 2014. Modes of extensional faulting controlled by surface processes. *Geophysical Research Letters*, 41(19), pp.6725-6733.
- Olive, J.A., Malatesta, L.C., Behn, M.D. and Buck, W.R., 2022. Sensitivity of rift tectonics to global variability in the efficiency of river erosion. *Proceedings of the National Academy of Sciences*, 119(13), p.e2115077119.

- Omar, G.I. and Steckler, M.S., 1996. Fission track evidence on the initial rifting of the Red Sea: two pulses, no propagation. *Oceanographic Literature Review*, 7(43), p.684.
- Pan, E., Amadei, B. and Savage, W.Z., 1995, April. Gravitational and tectonic stresses in anisotropic rock with irregular topography. In *International journal of rock mechanics and mining sciences & geomechanics abstracts* (Vol. 32, No. 3, pp. 201-214). Pergamon.
- Pasteels, P., Villeneuve, M., De Paepe, P. and Klerkx, J., 1989. Timing of the volcanism of the southern Kivu province: implications for the evolution of the western branch of the East African Rift system. *Earth and Planetary Science Letters*, 94(3-4), pp.353-363. [https://doi.org/10.1016/0012-821X\(89\)90152-0](https://doi.org/10.1016/0012-821X(89)90152-0).
- Peace, A.L., Welford, J.K., Geng, M., Sandeman, H., Gaetz, B.D. and Ryan, S.S., 2018. Rift-related magmatism on magma-poor margins: Structural and potential-field analyses of the Mesozoic Notre Dame Bay intrusions, Newfoundland, Canada and their link to North Atlantic Opening. *Tectonophysics*, 745, pp.24-45.
- Pechlivanidou, S., Cowie, P.A., Duclaux, G., Nixon, C.W., Gawthorpe, R.L. and Salles, T., 2019. Tipping the balance: Shifts in sediment production in an active rift setting. *Geology*, 47(3), pp.259-262.
- Pilkington, M. and Roest, W., 1992. Draping aeromagnetic data in areas of rugged topography. *Journal of Applied Geophysics*, 29(2), pp.135-142.
- Plasman, M., Tiberi, C., Ebinger, C., Gautier, S., Albaric, J., Peyrat, S., Déverchère, J., Le Gall, B., Tarits, P., Roecker, S. and Wambura, F., 2017. Lithospheric low-velocity zones associated with a magmatic segment of the Tanzanian Rift, East Africa. *Geophysical Journal International*, 210(1), pp.465-481.

- Plisnier, P.D., Chitamwebwa, D., Mwape, L., Tshibangu, K., Langenberg, V. and Coenen, E., 1999. Limnological annual cycle inferred from physical-chemical fluctuations at three stations of Lake Tanganyika. In *From limnology to fisheries: Lake Tanganyika and other large lakes* (pp. 45-58). Springer, Dordrecht.
- Rao, D.B., 1986. Modelling of sedimentary basins from gravity anomalies with variable density contrast. *Geophysical Journal International*, 84(1), pp.207-212.
- Reid, A.B., Allsop, J.M., Granser, H., Millett, A.T. and Somerton, I.W., 1990. Magnetic interpretation in three dimensions using Euler deconvolution. *Geophysics*, 55(1), pp.80-91.
- Rhea, J.O., 1977. Orographic precipitation model for hydrometeorological use (Doctoral dissertation, Colorado State University. Libraries).
- Richardson, N.J., Densmore, A.L., Seward, D., Fowler, A., Wipf, M., Ellis, M.A., Yong, L. and Zhang, Y., 2008. Extraordinary denudation in the Sichuan Basin: Insights from low-temperature thermochronology adjacent to the eastern margin of the Tibetan Plateau. *Journal of geophysical research: solid earth*, 113(B4).
- Ricklefs, R.E., 2003. Global diversification rates of passerine birds. *Proceedings of the Royal Society of London. Series B: Biological Sciences*, 270(1530), pp.2285-2291.
- Roberts, E.M., O'Connor, P.M., Stevens, N.J., Gottfried, M.D., Jinnah, Z.A., Ngasala, S., Choh, A.M. and Armstrong, R.A., 2010. Sedimentology and depositional environments of the Red Sandstone Group, Rukwa Rift Basin, southwestern Tanzania: New insight into Cretaceous and Paleogene terrestrial ecosystems and

- tectonics in sub-equatorial Africa. *Journal of African Earth Sciences*, 57(3), pp.179-212.
- Roberts, E.M., O'Connor, P.M., Gottfried, M.D., Stevens, N., Kapalima, S. and Ngasala, S., 2004. Revised stratigraphy and age of the Red Sandstone Group in the Rukwa Rift basin, Tanzania. *Cretaceous Research*, 25(5), pp.749-759.
- Roberts, E.M., Stevens, N.J., O'Connor, P.M., Dirks, P.H.G.M., Gottfried, M.D., Clyde, W.C., Armstrong, R.A., Kemp, A.I.S. and Hemming, S., 2012. Initiation of the western branch of the East African Rift coeval with the eastern branch. *Nature Geoscience*, 5(4), pp.289-294. [https:// doi.org/10.1038/ngeo1432](https://doi.org/10.1038/ngeo1432).
- Rosendahl, B.R. and Livingstone, D.A., 1983. Rift lakes of East Africa-new seismic data and implications for future research. *Episodes Journal of International Geoscience*, 6(1), pp.14-19.
- Rosendahl, B.R., 1987. Architecture of continental rifts with special reference to East Africa. *Annual Review of Earth and Planetary Sciences*, 15, p.445.
- Rosendahl, B.R., Reynolds, D.J., Lorber, P.M., Burgess, C.F., McGill, J., Scott, D., Lambiase, J.J. and Derksen, S.J., 1986. Structural expressions of rifting: lessons from Lake Tanganyika, Africa. *Geological Society, London, Special Publications*, 25(1), pp.29-43. <https://doi.org/10.1144/GSL.SP.1986.025.01.04>.
- Rosendahl, B.R., Versfelt, J.W., Scholz, C.A., Buck, J.E., and Woods, L.D., 1988. Seismic atlas of Lake Tanganyika, East Africa. Duke, Project PROBE, Duke University.
- Rotunno, R. and Ferretti, R., 2003. Orographic effects on rainfall in MAP cases IOP 2b and IOP 8. *Quarterly Journal of the Royal Meteorological Society: A journal of the*

atmospheric sciences, applied meteorology and physical oceanography, 129(588), pp.373-390.

- Russell, J.M., Barker, P., Cohen, A., Ivory, S., Kimirei, I., Lane, C., Leng, M., Maganza, N., McGlue, M., Msaky, E. and Noren, A., 2020. ICDP workshop on the Lake Tanganyika Scientific Drilling Project: a late Miocene–present record of climate, rifting, and ecosystem evolution from the world's oldest tropical lake. *Scientific Drilling*, 27, pp.53-60. <https://doi.org/10.5194/sd-27-53-2020>.
- Salem, A., Masterton, S., Campbell, S., Fairhead, J.D., Dickinson, J and Murphy, C. 2013. Interpretation of tensor gravity data using an adaptive tile angle method. *Geophysical Prospecting*, 61, 1065-1076.
- Salem, A., Williams, S., Fairhead, D., Smith, R. and Ravat, D., 2008. Interpretation of magnetic data using tilt-angle derivatives. *Geophysics*, 73(1), pp.L1-L10.
- Salem, A., Williams, S., Fairhead, J.D., Ravat, D. and Smith, R., 2007. Tilt-depth method: A simple depth estimation method using first-order magnetic derivatives. *The leading edge*, 26(12), pp.1502-1505.
- Salzburger, W., Meyer, A., Baric, S., Verheyen, E. and Sturmbauer, C., 2002. Phylogeny of the Lake Tanganyika cichlid species flock and its relationship to the Central and East African haplochromine cichlid fish faunas. *Systematic biology*, 51(1), pp.113-135.
- Sambridge, M., 1999. Geophysical inversion with a neighbourhood algorithm—I. Searching a parameter space. *Geophysical journal international*, 138(2), pp.479-494.
- Sander, S. and Rosendahl, B.R., 1989. The geometry of rifting in Lake Tanganyika, East Africa. *Journal of African Earth Sciences (and the Middle East)*, 8(2-4), pp.323-354.

- Saria, E., Calais, E., Stamps, D.S., Delvaux, D. and Hartnady, C.J.H., 2014. Present-day kinematics of the East African Rift. *Journal of Geophysical Research: Solid Earth*, 119(4), pp.3584-3600.
- Savijärvi, H. and Järvenoja, S., 2000. Aspects of the fine-scale climatology over Lake Tanganyika as resolved by a mesoscale model. *Meteorology and atmospheric physics*, 73(1), pp.77-88. <https://doi.org/10.1007/s007030050066>.
- Schluter, D., 2000. *The ecology of adaptive radiation*. OUP Oxford.
- Scholz, C.A. and Rosendahl, B.R., 1988. Low lake stands in Lakes Malawi and Tanganyika, East Africa, delineated with multifold seismic data. *Science*, 240(4859), pp.1645-1648. <https://doi.org/10.1126/science.240.4859.1645>.
- Scholz, C.A., 1995. Deltas of the Lake Malawi Rift, East Africa: seismic expression and exploration implications. *AAPG bulletin*, 79(11), pp.1679-1697. <https://doi.org/10.1306/7834DE54-1721-11D7-8645000102C1865D>.
- Scholz, C.A., Cohen, A.S., Johnson, T.C., King, J.W. and Moran, K., 2006. The 2005 Lake Malawi scientific drilling project. *Scientific Drilling*, 2, pp.17-19.
- Scholz, C.A., Johnson, T.C., Cohen, A.S., King, J.W., Peck, J.A., Overpeck, J.T., Talbot, M.R., Brown, E.T., Kalindekaffe, L., Amoako, P.Y. and Lyons, R.P., 2007. East African megadroughts between 135 and 75 thousand years ago and bearing on early-modern human origins. *Proceedings of the National Academy of Sciences*, 104(42), pp.16416-16421. <https://doi.org/10.1073/pnas.0703874104>.

- Scholz, C.A., King, J.W., Ellis, G.S., Swart, P.K., Stager, J.C. and Colman, S.M., 2003. Paleolimnology of Lake Tanganyika, East Africa, over the past 100 kyr. *Journal of Paleolimnology*, 30(2), pp.139-150.
- Scholz, C.A., Rosendahl, B.R. and Scott, D.L., 1990. Development of coarse-grained facies in lacustrine rift basins: Examples from East Africa. *Geology*, 18(2), pp.140-144.
- Scholz, C.A., Talbot, M.R., Brown, E.T. and Lyons, R.P., 2011. Lithostratigraphy, physical properties and organic matter variability in Lake Malawi Drillcore sediments over the past 145,000 years. *Palaeogeography, Palaeoclimatology, Palaeoecology*, 303(1-4), pp.38-50.
- Schumm, S.A., 1977. *The fluvial system*.
- Shaban, S.N., Scholz, C.A., Muirhead, J.D. and Wood, D.A., 2021. The stratigraphic evolution of the Lake Tanganyika Rift, East Africa: Facies distributions and paleo-environmental implications. *Palaeogeography, Palaeoclimatology, Palaeoecology*, 575, p.110474.
- Sheriff, R.E., 1977. Limitations on resolution of seismic reflections and geologic detail derivable from them: Section 1. Fundamentals of stratigraphic interpretation of seismic data.
- Sherman, S.I., 1992. Faults and tectonic stresses of the Baikal rift zone. *Tectonophysics*, 208(19921), pp.297-307.
- Shestakova, A.A. and Toropov, P.A., 2021. Orographic and lake effect on extreme precipitation on the Iranian coast of the Caspian Sea: a case study. *Meteorology and Atmospheric Physics*, 133(1), pp.69-84.

- Simpson, G.G., 1953. The major features of evolution. Columbia University Press.
- Sinclair, M.R., 1994. A diagnostic model for estimating orographic precipitation. *Journal of Applied Meteorology and Climatology*, 33(10), pp.1163-1175.
- Sklar, L.S. and Dietrich, W.E., 2006. The role of sediment in controlling steady-state bedrock channel slope: Implications of the saltation–abrasion incision model. *Geomorphology*, 82(1-2), pp.58-83.
- Small, E.E. and Anderson, R.S., 1998. Pleistocene relief production in Laramide Mountain ranges, western United States. *Geology*, 26(2), pp.123-126.
- Smith, B.L., Yuter, S.E., Neiman, P.J. and Kingsmill, D.E., 2010. Water vapor fluxes and orographic precipitation over northern California associated with a landfalling atmospheric river. *Monthly weather review*, 138(1), pp.74-100.
- Smith, R.B. and Barstad, I., 2004. A linear theory of orographic precipitation. *Journal of the Atmospheric Sciences*, 61(12), pp.1377-1391.
- Smith, R.B. and Evans, J.P., 2007. Orographic precipitation and water vapor fractionation over the southern Andes. *Journal of Hydrometeorology*, 8(1), pp.3-19.
- Smith, R.B., 1979. The influence of mountains on the atmosphere. In *Advances in geophysics* (Vol. 21, pp. 87-230). Elsevier.
- Smith, R.B., 2003. A linear upslope-time-delay model for orographic precipitation. *Journal of hydrology*, 282(1-4), pp.2-9.
- Smith, R.B., 2006. Progress on the theory of orographic precipitation. *Special Papers- Geological Society of America*, 398, p.1.

- Smith, R.B., Barstad, I. and Bonneau, L., 2005. Orographic precipitation and Oregon's climate transition. *Journal of the Atmospheric Sciences*, 62(1), pp.177-191.
- Smith, R.B., Jiang, Q., Fearon, M.G., Tabary, P., Dorninger, M., Doyle, J.D. and Benoit, R., 2003. Orographic precipitation and air mass transformation: An Alpine example. *Quarterly Journal of the Royal Meteorological Society: A journal of the atmospheric sciences, applied meteorology and physical oceanography*, 129(588), pp.433-454.
- Smith, R.B., Minder, J.R., Nugent, A.D., Storelvmo, T., Kirshbaum, D.J., Warren, R., Lareau, N., Palany, P., James, A. and French, J., 2012. Orographic precipitation in the tropics: The Dominica Experiment. *Bulletin of the American Meteorological Society*, 93(10), pp.1567-1579.
- Snyder, N.P., Whipple, K.X., Tucker, G.E. and Merritts, D.J., 2003. Importance of a stochastic distribution of floods and erosion thresholds in the bedrock river incision problem. *Journal of Geophysical Research: Solid Earth*, 108(B2).
- Sodemann, H. and Stohl, A., 2009. Asymmetries in the moisture origin of Antarctic precipitation. *Geophysical research letters*, 36(22).
- Stager, J.C., Cocquyt, C., Bonnefille, R., Weyhenmeyer, C. and Bowerman, N., 2009. A late holocene paleoclimatic history of Lake Tanganyika, East Africa. *Quaternary Research*, 72(1), pp.47-56.
- Stein, R.S. and Barrientos, S.E., 1985. Planar high-angle faulting in the Basin and Range: Geodetic analysis of the 1983 Borah Peak, Idaho, earthquake. *Journal of Geophysical Research: Solid Earth*, 90(B13), pp.11355-11366.

- Stevens, N.J., Gottfried, M.D., Roberts, E.M., Kapilima, S., Ngasala, S. and O'Connor, P.M., 2008. Paleontological exploration in Africa. In Elwyn Simons: a search for origins (pp. 159-180). Springer, New York, NY.
- Stock, J.D. and Montgomery, D.R., 1999. Geologic constraints on bedrock river incision using the stream power law. *Journal of Geophysical Research: Solid Earth*, 104(B3), pp.4983-4993.
- Stuckless, E., 2008. Celtic minerals assessment report discussing Geochemistry. Geophysics, and Diamond Drilling on the Budgell's Harbour Property, Central Newfoundland.
- Surdam, R.C. and Stanley, K.O., 1980. Effects of changes in drainage-basin boundaries on sedimentation in Eocene Lakes Gosiute and Uinta of Wyoming, Utah, and Colorado. *Geology*, 8(3), pp.135-139.
- Talling, J.F., 1991. Lake Tanganyika and its life, GW Coulter (Ed.) with contributions from J.-J. Tiercelin, A. Mondegver, RE Hecky and RH Spigel, British Museum (Natural History) Publications—Oxford University Press, 1991. 354 pp. Price: £ 60.00. <https://doi.org/10.1002/aqc.3270010210>.
- Tedla, G.E., Van Der Meijde, M., Nyblade, A.A. and Van der Meer, F.D., 2011. A crustal thickness map of Africa derived from a global gravity field model using Euler deconvolution. *Geophysical Journal International*, 187(1), pp.1-9.
- Theunissen, K., Klerkx, J., Melnikov, A. and Mruma, A., 1996. Mechanisms of inheritance of rift faulting in the western branch of the East African Rift, Tanzania. *Tectonics*, 15(4), pp.776-790. <https://doi.org/10.1029/95TC03685>.

- Thevenon, F., Williamson, D. and Taieb, M., 2002. A 22 kyr BP sedimentological record of Lake Rukwa (8 S, SW Tanzania): environmental, chronostratigraphic and climatic implications. *Palaeogeography, Palaeoclimatology, Palaeoecology*, 187(3-4), pp.285-294.
- Tiercelin, J.J., Chorowicz, J., Bellon, H., Richert, J.P., Mwanbene, J.T. and Walgenwitz, F., 1988. East African Rift System: offset, age and tectonic significance of the Tanganyika-Rukwa-Malawi intracontinental transcurrent fault zone. *Tectonophysics*, 148(3-4), pp.241-252. [https://doi.org/10.1016/0040-1951\(88\)90133-3](https://doi.org/10.1016/0040-1951(88)90133-3).
- Tiercelin, J.J., Soreghan, M., Cohen, A.S., Lezzar, K.E. and Bouroullec, J.L., 1992. Sedimentation in large rift lakes: example from the Middle Pleistocene—Modern deposits of the Tanganyika Trough, East African Rift System. *Bull. Centres Rech. Explor.-Prod. Elf Aquitaine*, 16, pp.83-111.
- Tierney, J.E., Russell, J.M., Huang, Y., Damsté, J.S.S., Hopmans, E.C. and Cohen, A.S., 2008. Northern hemisphere controls on tropical southeast African climate during the past 60,000 years. *science*, 322(5899), pp.252-255.
- Trudgill, B. and Cartwright, J., 1994. Relay-ramp forms and normal-fault linkages, Canyonlands National Park, Utah. *Geological Society of America Bulletin*, 106(9), pp.1143-1157.
- Van der Beek, P., Mbede, E., Andriessen, P. and Delvaux, D., 1998. Denudation history of the Malawi and Rukwa Rift flanks (East African Rift System) from apatite fission track thermochronology. *Journal of African Earth Sciences*, 26(3), pp.363-385.

- Vasuki, Y., Holden, E.J., Kovesi, P. and Micklethwaite, S., 2014. Semi-automatic mapping of geological Structures using UAV-based photogrammetric data: An image analysis approach. *Computers & Geosciences*, 69, pp.22-32. <https://doi.org/10.1016/j.cageo.2014.04.012>
- Vaucher, A., Barruol, G. and Tommasi, A., 1997. Why do continents break-up parallel to ancient orogenic belts? *Terra Nova*, 9(2), pp.62-66.
- Verduzco, B., Fairhead, J.D., Green, C.M. and MacKenzie, C., 2004. New insights into magnetic derivatives for structural mapping. *The leading edge*, 23(2), pp.116-119.
- Verner, S., 1953. Interpretation of magnetic anomalies at sheet-like bodies. *Gen.-stab: s lit. anst.(distr.)*.
- Versfelt J, Rosendahl BR. Relationships between pre-rift structure and rift architecture in Lakes Tanganyika and Malawi, East Africa. *Nature*. 1989 Jan;337(6205):354-7.
- Vincens, A., Buchet, G., Williamson, D. and Taieb, M., 2005. A 23,000 yr pollen record from Lake Rukwa (8 S, SW Tanzania): new data on vegetation dynamics and climate in Central Eastern Africa. *Review of Palaeobotany and Palynology*, 137(3-4), pp.147-162.
- Walsh, J.J. and Watterson, J., 1988. Analysis of the relationship between displacements and dimensions of faults. *Journal of Structural geology*, 10(3), pp.239-247.
- Walsh, J.J., Bailey, W.R., Childs, C., Nicol, A. and Bonson, C.G., 2003. Formation of segmented normal faults: a 3-D perspective. *Journal of Structural Geology*, 25(8), pp.1251-1262.
- Walsh, J.J., Nicol, A. and Childs, C., 2002. An alternative model for the growth of faults. *Journal of Structural Geology*, 24(11), pp.1669-1675.

- Walsh, L.S., Martin, A.J., Ojha, T.P. and Fedenczuk, T., 2012. Correlations of fluvial knickzones with landslide dams, lithologic contacts, and faults in the southwestern Annapurna Range, central Nepalese Himalaya. *Journal of Geophysical Research: Earth Surface*, 117(F1).
- Wedmore, L. N. J., Williams, J. N., Biggs, J., Fagereng, Å., Mphepo, F., Dulanya, Z., et al. (2020). Structural Inheritance and Border Fault Reactivation during Active Early-Stage Rifting along the Thyolo Fault, Malawi. *J. Struct. Geology*. 139, 104097.
- Weisse, A.K. and Bois, P., 2001. Topographic effects on statistical characteristics of heavy rainfall and mapping in the French Alps. *Journal of Applied Meteorology*, 40(4), pp.720-740.
- Wescott, W.A., Krebs, W.N., Engelhardt, D.W. and Cunningham, S.M., 1991. New biostratigraphic age dates from the Lake Rukwa rift basin in western Tanzania. *AAPG bulletin*, 75(7), pp.1255-1263. <https://doi.org/10.1306/0C9B2925-1710-11D7-8645000102C1865D>.
- Wheeler, W.H. and Karson, J.A., 1989. Structure and kinematics of the Livingstone Mountains border fault zone, Nyasa (Malawi) Rift, southwestern Tanzania. *Journal of African Earth Sciences (and the Middle East)*, 8(2-4), pp.393-413.
- Whipple, K.X. and Tucker, G.E., 1999. Dynamics of the stream-power river incision model: Implications for height limits of mountain ranges, landscape response timescales, and research needs. *Journal of Geophysical Research: Solid Earth*, 104(B8), pp.17661-17674.

- Whipple, K.X., 2004. Bedrock rivers and the geomorphology of active orogens. *Annu. Rev. Earth Planet. Sci.*, 32, pp.151-185.
- Wilson, R.W., Holdsworth, R.E., Wild, L.E., McCaffrey, K.J.W., England, R.W., Imber, J. and Strachan, R.A., 2010. Basement-influenced rifting and basin development: a reappraisal of post-Caledonian faulting patterns from the North Coast Transfer Zone, Scotland. *Geological Society, London, Special Publications*, 335(1), pp.795-826.
- Wolfenden, E., Ebinger, C., Yirgu, G., Renne, P.R. and Kelley, S.P., 2005. Evolution of a volcanic rifted margin: Southern Red Sea, Ethiopia. *Geological Society of America Bulletin*, 117(7-8), pp.846-864. [https:// doi.org/10.1130/B25516.1](https://doi.org/10.1130/B25516.1).
- Wright, L.J., Muirhead, J.D. and Scholz, C.A., 2020. Spatiotemporal Variations in Upper Crustal Extension Across the Different Basement Terranes of the Lake Tanganyika Rift, East Africa. *Tectonics*, 39(3), p.e2019TC006019. [https:// doi.org/10.1029/2019TC006019](https://doi.org/10.1029/2019TC006019).
- Xu, S., Hao, F., Xu, C., Wang, Y., Zou, H. and Gong, C., 2015. Differential compaction faults and their implications for fluid expulsion in the northern Bozhong Subbasin, Bohai Bay Basin, China. *Marine and Petroleum Geology*, 63, pp.1-16.
- Zhang, C., Mushayandebvu, M.F., Reid, A.B., Fairhead, J.D. and Odegard, M.E., 2000. Euler deconvolution of gravity tensor gradient data. *Geophysics*, 65(2), pp.512-520.

Vita (biographical data)

Shaidu Nuru Shaban, PhD.

Tanzania Petroleum Development Corporation, P.O.Box 2774, Dar es Salaam,

Mobile: +255787228916, Email: snuru@tpdc.co.tz

KEY SKILLS

- Use geophysical data and drill core data to study how the tectonic processes and hydroclimate variability control the rift basins development, and its oil and natural gas implications. This include using Petrel and DecisionSpace™ software to analyse the seismic data, as well as RStudio and MATLAB to perform statistical analyses.
- Use MapInfo and ArcGIS for geological mapping, drill planning and execution, and geophysical investigation planning in minerals, oil, and natural gas projects.
- Assess, risk and rank oil and gas exploration opportunities in Tanzania.
- Performed basin analysis for Ruvu, Tanga and Ruvuma basin in Tanzania. This enabled TPDC to de-risk most of the exploration projects located within these basins.
- Coordinate with natural gas reservoir engineers for optimal production to meet national natural gas demand.
- Participated in petroleum contract negotiations for three hydrocarbon exploration blocks in Tanzania.
- Used geostatistics software such as Vulcan MapTek and Supervisor to estimate the ounces of gold resources for the North Mara Gold Mine, Tanzania.

EDUCATION

PhD in Earth Sciences, Syracuse University, NY, USA 2018 – 2022

Dissertation: “Cenozoic Extension of the Lake Tanganyika Rift, East Africa: Structure, Tectonostratigraphy and Paleoenvironmental Reconstruction”

MSc. Petroleum Exploration Geosciences, the University of Manchester, UK 2014 - 2015

Project: “Hydrocarbon Potential of the East African Margin - Offshore Southern Tanzania, Mozambique and Comoros”

BSc. in Geology, the University of Dar es Salaam, Tanzania 2006 – 2010

Project: “Control of gold mineralization of the Nyabirama Pit- North Mara Gold Mine, Tanzania”.

PROFESSIONAL EXPERIENCE

- 2013 – Present: Working as a Petroleum Geologist at Tanzania Petroleum Development Corporation (TPDC), Tanzania.
- 2012 – March 2013: Working as a Resource Estimation Geologist at North Mara Gold Mine (African Barrick Gold), Tanzania.
- August 2010 – 2012: Working as a Junior Geotechnical Geologist at North Mara Gold Mine (African Barrick Gold), Tanzania.

AWARDS AND GRANTS

- 2021 – 2022: Research Excellence Doctoral Funding, Graduate Fellowship, Syracuse University.
- 2020 – 2021: Association of America Petroleum Geoscientists, Grant-in- Aid,
- 2020: Graduate Student Organization (Syracuse University).
- 2019 – 2020: Syracuse University Water Initiative Fellowship.
- 2018 – 2019: NRT-Empower programme, Professional Development Training Mini-Grant.
- 2019: International Students Academic Excellence Syracuse University, Phi Beta Delta.

PUBLICATIONS (PUBLISHED)

Shaban, S.N, Scholz, A.C, Muirhead, J.D, Wood, D.A (2021). The Stratigraphic Evolution of the Lake Tanganyika Rift: Facies Distributions and Paleoenvironmental Implications. *Paleogeography, Paleocology and Paleoclimatology.*

Russell, J. M., Barker, P., Cohen, A., Ivory, S., Kimirei, I., Lane, C., ... & **Nuru, S.** (2020). ICDP workshop on the Lake Tanganyika Scientific Drilling Project: a late Miocene–present record of climate, rifting, and ecosystem evolution from the world's oldest tropical lake. *Scientific Drilling*, 27, 53-60.

PUBLICATION (in review)

Shaban, S.N., Scholz, A.C, Xe, L (2022). The Paleo-Hydrologic Connectivity of Rift lakes Tanganyika and Rukwa, East Africa: Influence of Orographic Precipitation.

Shaban, S.N., Scholz, A.C, Kolawole, F (2022). The Deep Basin and Underlying Basement Structure of the Tanganyika Rift.

TEACHING EXPERIENCE

- 2018 – 2021: Teaching Assistant of Earth Sciences introductory courses, **Syracuse University, New York, USA.**
- 2013 – 2018: Mentoring university students during their intern and industrial attachments, **Tanzania Petroleum Development Corporation.**
- 2011 – 2012: Mentoring college students during their intern and industrial attachments, **North Mara Gold Mine, Tanzania.**
- 2008 – 2010: Part-Time Teacher of Mathematics and Physics, **Alfarouq High School, Tanzania.**

TECHNICAL REPORTS

- Revised Stratigraphy of Ruvuma Basin, Tanzania.
- Technical Review on Upper Cretaceous, Lower Cretaceous and Upper Jurassic hydrocarbon resources of Ruvu Block, Tanzania, 2016.
- The revised stratigraphy and hydrocarbon potential of Ruhuhu basin 2016.
- Hydrocarbon Potential and Petroleum Systems, Offshore Southern Tanzania, Comoros, Mozambique (MSc. Thesis), 2015.

- Structural control of gold mineralization in the North Mara Gold Mine, Tanzania, 2010.

TECHNICAL PRESENTATIONS

- Shaban. S and Scholz A. C, "Lacustrine Deltaic Deposits of Southern L. Tanganyika and Implications for Paleo-environmental Reconstructions". The East African Petroleum Conference & Exhibition (EAPCE'19), 2019 Mombasa, Kenya.
- Scholz A. C, Shaban. S, "The Stratigraphy of Lake Tanganyika". ICDP workshop on the Lake Tanganyika Scientific Drilling Project, 2019, Dar es Salaam, Tanzania
- Shaban. S, "The Petroleum Potential of Tanzania". The Petroleum Global Show, 2016 Calgary, Alberta, Canada.
- Duyverman. H, Shaban. S and, Msacky. E, "Shale Oil/Gas Potential of Tanzania" PESGB Conference on African Geology, 2016 Houston, USA.
- Shaban. S and Duyverman. H, "Shale Oil/Gas Potential of Tanzania" European Association of Geoscientists and Engineers Conference, 2015 Dar es Salaam, Tanzania.

EXTRACURRICULAR ACTIVITIES

- Member, Board Advisory Committee, Vocational Education Training Authority, Tanzania, 2018 – 2020.
- Member, Curriculum Review Team, Dar es Salaam Maritime Institute, 2017.
- Member, Tanzania Oil & Gas Local Content Regulations Review Team, 2017.
- Member, task force for establishment of Safety Training Centre and Oil and Gas Technical College, Tanzania Ports Authority College 2017.
- Member, Curriculum Review Team, Dar es Salaam Institute of Technology, 2017.
- Member, Review Team, The Petroleum (Local Content) Regulations, 2017.

PROFESSION MEMBERSHIPS

- Society of Exploration Geophysicists (SEG)
- Association of American Petroleum Geoscientists (AAPG)

- Tanzania Geological Society (TGS)

REFERENCES

1. Mr. Kelvin Komba

Director, Exploration, Production and Development,

TPDC, Azikiwe, 2774, Dar es Salaam, Tanzania

Email: komba@tpdc.co.tz

2. Prof. Christopher A Scholz

Syracuse University, Earth Sciences, 13244, Syracuse, NY

Email: cascholz@syr.edu